ORNL
Master Copy

Spatial Variability in Groundwater Chemistry in Fractured Rock: Nolichucky Shale, Oak Ridge, TN

by
Madeline Eve Schreiber

A thesis submitted in partial fulfillment of
the requirements for the degree of

Master of Science
(Geology)

at the
University of Wisconsin-Madison
1995

Abstract

A field study was conducted in the fractured Nolichucky Shale on the Oak Ridge Reservation, TN, to assess the degree of spatial variability of groundwater flow and chemistry and to identify the major factors contributing to variability. Results of the field investigation indicate a groundwater flow direction that is significantly affected by horizonal and vertical anisotropy resulting from discrete fracture zones in the shale. Hydraulic tests were conducted in open boreholes to identify and characterize the major flow zones. High flow zones were identified at the saprolite/bedrock interface in all three boreholes and at deeper intervals in two of the boreholes. These results were used to determine locations for packer samples, collected from the open borehole, and for sampling ports of multilevel wells.

Results of the discrete zone sampling indicate significant spatial variability in groundwater chemistry. Three major water types, Ca-HCO_3, Na-HCO_3, and Ca-Na-HCO_3, were identified. The water types correlate between the multilevel wells, forming hydrochemical facies. The orientation of these facies appears to be strongly influenced by the flow direction, if horizontal and vertical anisotropy are assumed. Although the origins of the Ca-HCO_3 and Na-HCO_3 water types have been examined in previous studies, the source of the Ca-Na-HCO_3 water type has not been evaluated. Three hypotheses of the origin of the Ca-Na-HCO_3 type were evaluated using geochemical models: 1) local water-rock reactions of the Ca-HCO_3 and Na-HCO_3 waters with minerals in the surrounding matrix and on fracture

surfaces, 2) conservative mixing of the Ca-HCO_3 and Na-HCO_3 waters, and 3) mixing with associated geochemical reactions. The modeling results suggest that the third hypothesis, mixing with water-rock interactions, is the most plausible source of the Ca-Na-HCO_3 water type. This mixing appears to be occurring locally in the discharge zone. It is clear from the observed spatial variability in groundwater chemistry that the zones that contain the Ca-HCO_3 and Na-HCO_3 waters are not well-connected along most of the flow path from the recharge to the discharge zone. If they were connected, the shallow groundwater in this discharge area would be well-mixed and would not retain distinct chemical signatures.

The results of this study indicate that carefully designed multilevel wells can yield detailed information on the spatial variability of groundwater chemistry. A sample collected from a 50' screened interval retains the chemical signature of one of the highest flow zones in the well. The advantage of such a sample is that it is useful in identifying the bulk characteristics of the screened formation. The disadvantage is that, due to the effects of dilution and mixing, vertically averaged samples will obscure the presence of different chemistries, or contaminants, from individual flow zones. Continued characterization of the temporal variability on flow and transport at the field site is aimed at collecting data that will assist in the development of sampling protocols in fractured media.

Acknowledgements

The initial idea for this project came from Drs. Geri Moline and Laura Toran of the Oak Ridge National Lab (ORNL). Geri designed the different components of the field project and supervised my field work during the summer of 1994. During this past year, she kept me up-to-date on the progress of ongoing field work, provided me with additional data, edited abstracts, and reviewed several drafts of this thesis. For her interest, thoughtfulness, and patience, I thank her. Other people at ORNL have contributed in various ways to this project, including W. Sanford, M. Brown, T. Zondlo, G. Jacobs, D. Taylor, S.Y. Lee, A. Halleran, and the pipefitters who repeatedly fixed the packer sampler.

Back in Madison, my advisor, Dr. Jean Bahr, helped me to sort out the various types of data that Geri and I collected. Her insight and knowledge helped me to better understand the hydrogeology and geochemistry of the field site and also greatly improved the multiple thesis drafts she reviewed. My committee members, Drs. Carl Bowser and Jill Banfield, shared much of their expertise in geochemical modeling and mineralogy, respectively, and posed thought-provoking questions at my thesis defense.

Thanks goes out to the hydro students, who have provided me with personal and academic support beyond the call of duty, from countless coffee breaks to late night discussions in the hydro lab. Friends from college and home have brought me

news from the emergency room, the courtroom, and the literary world, reminding me that there is life outside of graduate school. I owe thanks to my family for always encouraging me to push ahead. Their endless support is much appreciated.

Financial support for this research came from the Department of Energy's Environmental Restoration and Waste Management Fellowship, a Weeks Research Assistantship, and a fellowship from the American Groundwater Scientists and Engineers.

Table of Contents

Abstract ii

Acknowledgements iv

Table of Contents vi

List of Figures ix

List of Tables x

1. Introduction 1
    1.1 Purpose 1
    1.2 Physical Setting 3
        Physiographic setting 3
        Geologic setting 3
        Hydrogeologic setting 6

2. Field Investigation 8
    2.1 Introduction 8
    2.2 Site Location 8
    2.3 Initial Site Characterization 8
        Hydraulic heads 12
        Hydraulic gradients 14
        Helium tracer test 19
        Bromide tracer test 25
        Core descriptions 30
    2.4 Hydraulic Tests 35
        Downhole camera 36
        Electromagnetic flowmeter tests 36
        Point dilution tests 46
    2.5 Multilevel Well Installation 50
    2.6 Summary 51

3. Geochemical Characterization 55
    3.1 Introduction 55
    3.2 Sampling Methods 56
        Pore water sampling 56
        Packer sampling 58
        Multilevel well sampling 59
    3.3 Analytical Methods 59
    3.4 Data Quality 61

3.5 Results 63
Pore water samples 63
Packer samples 66
Multilevel well samples 66
3.6 Discussion 74
Major Ion Trends 74
Multilevel well samples 74
Packer samples 80
Pore water samples 82
Minor Ion Trends 84
Multilevel well samples 84
Packer samples 89
Comparison of discrete zone samples 90
Comparison of multilevel and long-screened well samples 91
Hydrochemical facies 92
3.7 Summary 97

4. Mineralogical Characterization 100
4.1 Introduction 100
4.2 Lithology 102
4.3 Mineralogy 102
Previous Studies 102
4.4 Sample Preparation 105
4.5 Analytical Methods 105
4.6 Results 109
Thin section 109
XRD 109
EDS 115
4.7 Summary 119

5. Sources of Vertical Variability in Groundwater Chemistry 121
5.1 Introduction 121
Hypothesis 1: Water-Rock Interactions 122
Hypothesis 2: Conservative Mixing 125
Hypothesis 3: Mixing with Water-Rock Interactions 125
5.2 Methods for Testing Hypotheses 125
Speciation-solubility models 126
Mass balance models 127
Reaction path models 128
Model input data 128
Sensitivity analyses 129
5.3 Results and Discussion 130
Speciation-solubility models 130

Mass balance and reaction path models 133
Hypothesis 1: Water-Rock Interactions 133
Evolution of Type 1 to Type 2 133
Evolution of Type 1 to Type 3 137
Evolution of Type 2 to Type 3 139
Hypothesis 2: Conservative Mixing 140
Hypothesis 3: Mixing with Water-Rock Interactions 141
Site hydrogeologic framework 146
5.4 Summary 148

6. Conclusions and Suggestions for Further Work 152
6.1 Conclusions 152
6.2 Suggestions for Further Work 154
Field studies 154
Mineralogical and geochemical studies 155
Modeling studies 157

7. References cited 158

Appendix A: Monitoring well construction 164
Appendix B: Water elevation and precipitation data 169
Appendix C: Gradient and flow direction calculations 179
Appendix D: Helium data 192
Appendix E: Bromide data 193
Appendix F: Core logs 194
Appendix G: Flowmeter data 209
Appendix H: Point dilution data 212
Appendix I: Geochemistry data 225
Appendix J: Packer sample concentration profiles 236
Appendix K: PHREEQE input files 242
Appendix L: U.W. and field sample numbers 248

List of Figures

Page

1-1: Map of the U.S., Tennessee, and the Oak Ridge Reservation (ORR) 4
1-2: Stratigraphic section of Bear Creek Valley, ORR 5
2-1: Map showing location of the field site on the ORR 9
2-2: Locations of monitoring wells at the field site 11
2-3: Water levels and precipitation versus time 13
2-4: Rose diagrams of shallow and deep gradient and flow directions 16
2-5: Bar graphs of the magnitude of the horizontal gradients 17
2-6: Bar graphs of the magnitude of the vertical gradients 18
2-7: Helium concentrations in the source well 21
2-8: Helium concentrations versus time for the well pairs 22
2-9: Bromide decay in the source well 27
2-10: Core logs of the GW821, GW822, and GW823 boreholes 31
2-11: Pictures of the core 33
2-12: Fence diagram 34
2-13: Pictures of electromagnetic flowmeter and point dilution set-up 38
2-14: Hydraulic test results for GW821 41
2-15: Hydraulic test results for GW822 42
2-16: Hydraulic test results for GW823 43
3-1: Locations of pore water, packer, and multilevel well samples 57
3-2: GW821 multilevel major ion concentration profiles 75
3-3: GW822 multilevel major ion concentration profiles 76
3-4: GW823 multilevel major ion concentration profiles 77
3-5: Trilinear diagram of multilevel well samples 79
3-6: Stiff diagrams of multilevel well samples 81
3-7: Trilinear diagram of packer samples 83
3-8: Trilinear diagram of pore water samples 85
3-9: GW821 multilevel minor ion concentration profiles 86
3-10: GW822 multilevel minor ion concentration profiles 87
3-11: GW823 multilevel minor ion concentration profiles 88
3-12: Stiff diagrams plotted on fence diagram 93
3-13: Cross-section along the average of the shallow and deep flow directions . 94
4-1: Pictures of hand samples 106
4-2: X-ray diffraction (XRD) scans of matrix 110
4-3: X-ray diffraction (XRD) scans of red-orange fracture coatings 111
4-4: X-ray diffraction (XRD) scans of other fracture coatings 112
4-5: Back-scattered electron (BSE) image and x-ray scan of illite 116
4-6: Back-scattered electron (BSE) image and x-ray scan of kaolinite 117
4-7: Back-scattered electron (BSE) image and x-ray scan of illite with oxides . 118
5-1: Saturation indices (SI=IAP/K) versus depth 131
5-2: Mass balance modeling results for creation of Type 2 from Type 1 water . 134
5-3: Mass balance modeling results for creation of Type 3 from Type 1 water . 138

List of Figures (con't) **Page**

5-4: NETPATH modeling results for the mixing Type 1 and Type 2 waters. . . . 144
5-5: Fence/Stiff diagram with mixing percentages of the multilevel well samples 145
5-6: Schematic cross-section along dip 147

List of Tables

2-1: Borehole camera observations 37
3-1: Summary of sample collection and analytical methods 60
3-2: Pore water sample results summary 64
3-3: Pore water charge balance calculations 65
3-4: Packer sample results summary 67
3-5: Packer charge balance calculations 69
3-6: Multilevel well and GW462 sample results summary 71
3-7: Multilevel well and GW462 sample charge balance calculations 73
4-1: Mineralogical composition of the Nolichucky Shale and saprolite 104
4-2: Mineralogical analysis results 113
5-1: Conservative mixing of Type 1 and Type 2 waters. 142

1. Introduction

1.1 Purpose

The complexity of flow systems in fractured rocks such as those found on the Oak Ridge Reservation (ORR) raises concerns about the representativeness of samples obtained utilizing standard monitoring wells. Within these fractured shales and carbonate rocks, the majority of groundwater flows through a network of fractures that comprise a small percentage of the pore volume (Solomon et al., 1992). These fractures provide pathways for groundwater flow, while flow through the low permeability matrix is orders of magnitudes lower. Monitoring wells are generally constructed using long screened intervals that may not intersect any active fracture zones or that may intersect multiple fracture zones representing very different flow paths. Thus, standard well construction can mask the vertical distribution of groundwater chemistry and prevent discrimination of relative contributions from the matrix and from distinct fracture zones.

In order to evaluate the effect of monitoring well construction on the representativeness of groundwater samples collected from fractured rock, variations in hydraulic properties of the rock and in groundwater chemistry must first be examined. The major goal of this project is to evaluate the degree of spatial variability in groundwater chemistry in a fractured shale. Some of the factors that may contribute to such variability, including water-rock interactions and mixing of

different water types, were examined to identify the spatial pattern of groundwater flow and geochemical transport in a discharge area. A field experiment in the fractured Nolichucky Shale on the Oak Ridge Reservation in eastern Tennessee was designed to address some of these issues.

The field investigation (Chapter 2) consisted of an initial site characterization and site instrumentation. The site characterization included water level monitoring, initiation of two tracer tests to establish flow dynamics, and hydraulic testing to quantify fracture zone characteristics. The site instrumentation included installation of multilevel wells adjacent to standard screened well pairs. The geochemical characterization (Chapter 3) consisted of pore water sampling, groundwater sampling from discrete zones, and groundwater sampling from a long-screened well to assess the spatial geochemical variability in the shallow groundwater system. Core samples from the Nolichucky Shale and overlying saprolite were collected as part of a mineralogical characterization aimed at identifying the types and phases of minerals present as coatings on fracture surfaces (Chapter 4). All specimens referenced in this thesis are in the collections of the Department of Geology and Geophysics, University of Wisconsin-Madison, under file number U.W. 1786. Geochemical models, in conjunction with results from the tracer tests, hydraulic tests, mineralogical characterization, and discrete zone sampling, were used to assess the spatial patterns of groundwater flow and chemistry in the shallow system (Chapter 5).

1.2 Physical Setting

Physiographic setting

The Oak Ridge Reservation (ORR) is located in eastern Tennessee, approximately 32 km west of Knoxville (**Figure 1-1**). The ORR is situated in the western portion of the Valley and Ridge physiographic province, within the Appalachian thrust belt of eastern Tennessee. The Tennessee portion of the Appalachian Valley and Ridge is characterized by the presence of a number of southeast-dipping imbricate thrust sheets; the major thrust faults traceable through the ORR are the Copper Creek and the White Oak Mountain thrust faults (Hatcher et al., 1992). The parallel ridges (average 1.8 km apart) and valleys are a result of differential erosion induced by the underlying structure of folds and faults.

Geologic setting

The bedrock geology exposed in the ORR is composed of sedimentary rocks that range in age from early Cambrian to early Mississippian (**Figure 1-2**). The strike of the beds is typically N55E; the dip varies between 30 and 60 degrees SE. The main geologic units are the Cambrian Rome Formation and Conasauga Group, the Cambro-Ordovician Knox Group, and the Ordovician Chickamauga Group. The Conasauga Group, which includes the Nolichucky Shale, has served as the principal unit for the disposal of radioactive waste in the ORR (Hatcher et al., 1992).

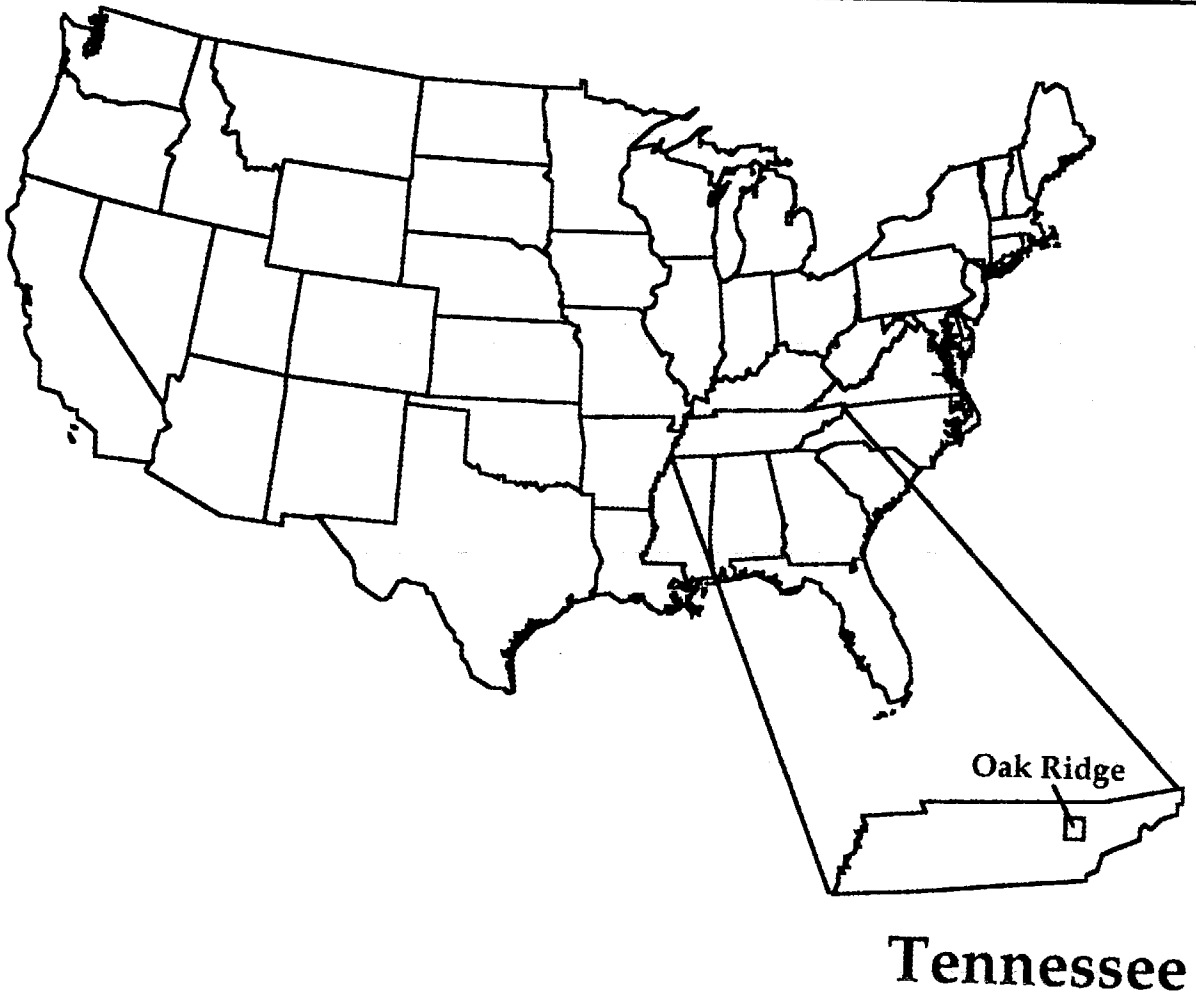

Figure 1-1: Map of the United States and Tennessee showing general location of the Oak Ridge Reservation (ORR).

			Thickness (m)	Formation	Hydrogeologic Unit
ORDOVICIAN	LOWER	Knox Group (Ock)	75-150	Mascot Dolomite	KNOX AQUIFER
			90-150	Kingsport Formation	
			40-60	Longview Dolomite	
			152-213	Chepultepec Dolomite	
CAMBRIAN	UPPER		244-335	Copper Ridge Dolomite	
		Conasauga Group (Cc)	100-110	Maynardville Limestone	
			150-180	**NOLICHUCKY SHALE**	ORR AQUITARDS
	MIDDLE		98-125	Dismal Gap Formation	
			25-34	Rogersville Shale	
			31-37	Friendship Formation	
			56-70	Pumpkin Valley Shale	
	LOWER		122-183	Rome Formation	

Figure 1-2: Stratigraphic section of Bear Creek Valley, ORR. Nolichucky Shale is highlighted in bold. From Hatcher et al., 1992.

Hydrogeologic setting

The geologic units on the ORR site have been divided into two hydrologic groups by Solomon et al. (1992). The first is the Knox Aquifer, which consists of the Knox Group and the Maynardville Limestone. Flow in the Knox Aquifer is dominated by solution conduits, resulting in the capacity for storing and transmitting large volumes of water. The second group is the ORR aquitards, which consist of all other units, including the Nolichucky Shale. Flow in this hydrologic group is controlled primarily by fractures. The ORR aquitards consist mostly of fractured shale, siltstone, sandstone, and thinly bedded limestone.

Solomon et al. (1992) divide the two hydrologic groups into four zones of differing hydrologic characteristics: the stormflow zone, the vadose zone, the groundwater zone, and the aquiclude. The uppermost zone is the stormflow zone, occurring near the top of the regolith, through which flow is transient and precipitation-generated. The stormflow zone is estimated to account for approximately 90% of all subsurface flow. During rain events, the stormflow zone partially or completely saturates and transmits water laterally to streams. The vadose zone, a mostly unsaturated zone above the water table, consists of clay and silt saprolite. Most of the recharge through the vadose zone occurs along discrete permeable features that may become saturated during rain events. Only three to seven cm of water annually percolates through the vadose zone to enter the saturated zone (Hatcher et al., 1992).

Beneath the vadose zone is the groundwater zone, continuously saturated, through which the remaining 10% of subsurface water is estimated to flow. The water table is associated with a transition zone between the saprolite (weathered bedrock) and unweathered bedrock. The high permeability of this zone is likely due to less advanced weathering relative to the upper saprolite but greater fracture density than the underlying bedrock. The transition zone has been loosely described from other drilling activities on the ORR as the zone below auger refusal but above competent bedrock. A similar transition zone has been described above fractured bedrock in the North Carolina Piedmont (Harned and Daniel, 1989), with higher transmissivity than either the overlying saprolite or underlying fractured crystalline rock. Groundwater flow below the water table interval occurs through permeable fractures which are poorly connected in three dimensions (Solomon et al., 1992). The lowermost zone of interest is the aquiclude, in which groundwater flow is on a geologic time scale .

In the ORR aquitards, groundwater flow paths in the saturated zone are primarily controlled by fractures. Bedding plane and strike parallel fractures are observed to be more permeable than dip parallel fractures (Solomon et al., 1992) and therefore transmit much of the flow along strike towards cross-cutting tributaries. The remainder flows down-dip, following the regional gradient, and seeps upward to discharge locations in main-valley streams.

2. Field Investigation

2.1 Introduction

This chapter describes the field investigation, which consisted of an initial site characterization and site instrumentation. The site characterization included water level monitoring, two tracer tests to establish flow dynamics, and borehole hydraulic tests to quantify fracture zone characteristics. The site instrumentation included installation of multilevel wells adjacent to standard screened well pairs.

2.2 Site Location

The field site chosen for this project is located in West Bear Creek Valley, near the intersection of Highway 95 and Bear Creek Valley Road (**Figure 2-1**). The site is underlain by the middle unit of the Nolichucky Shale. Bedding in this area dips approximately 45º to the south with respect to the ORR administrative coordinate system. All maps presented in this thesis are relative to administrative grid north, which is 34º 12' 51" W of true north.

2.3 Initial Site Characterization

The initial site characterization was designed to examine the temporal and spatial flow characteristics of the shallow groundwater system. Temporal variability in water quality may be related to seasonal or storm-related changes in recharge.

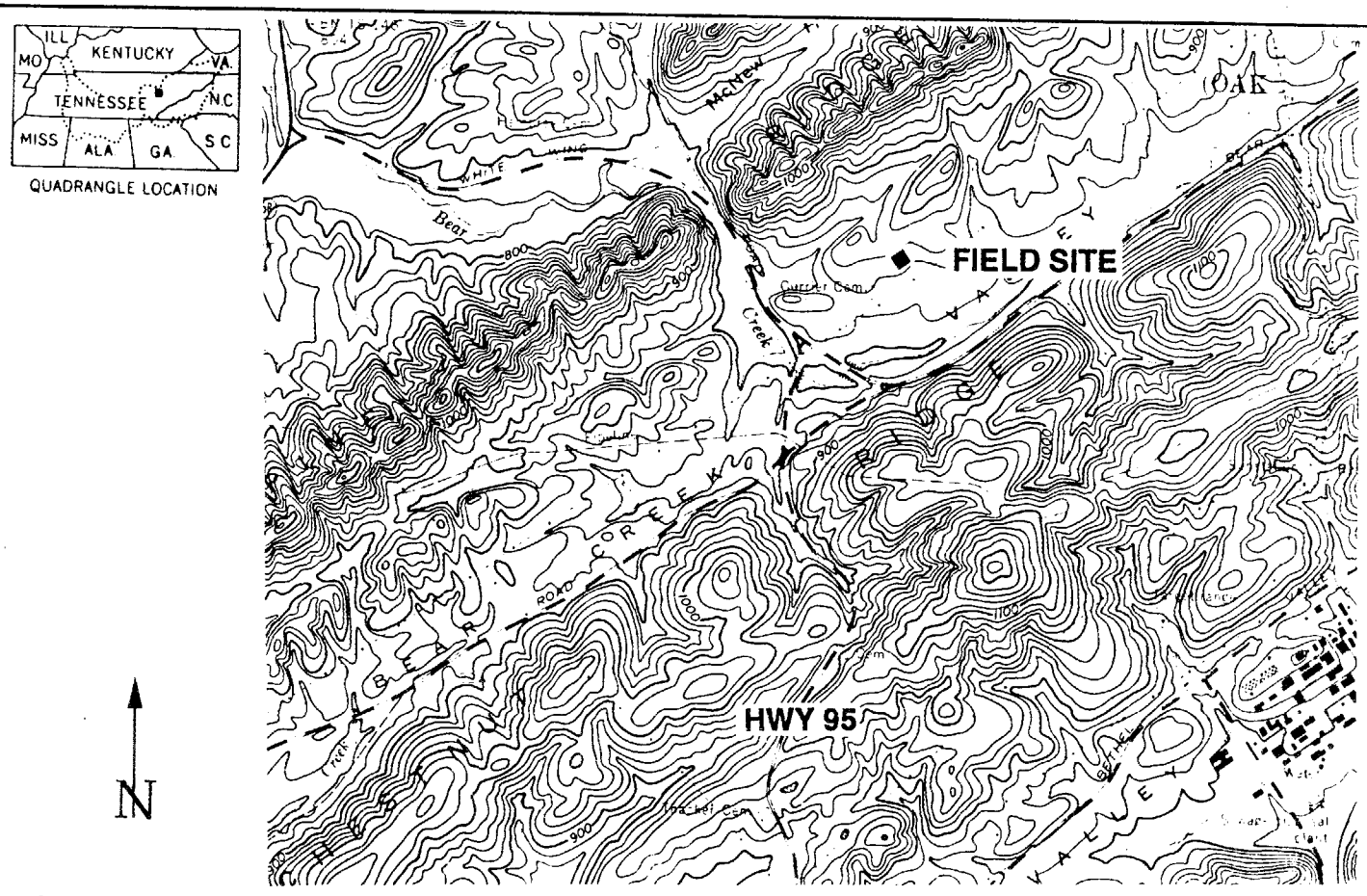

Figure 2-1: Map showing location of the field site on the ORR. From Bethel Valley Quadrangle, 7.5' series, U.S. Geological Survey, 1968.

Understanding the degree and causes of temporal variability is necessary to design an appropriate sampling schedule. The spatial variability of groundwater quality within fractured rocks is likely to be enhanced by the discrete nature of the fracture flow paths. An evaluation of the heterogeneous characteristics of the fractured formation is critical to establishing an appropriate spatial distribution of monitoring points, both vertically and laterally.

A network of wells was installed in 1987 for the purpose of conducting pump tests as part of a valley-wide site characterization (Gierke et al., 1988). This network, shown in **Figure 2-2**, consists of a source well, screened from depths of 20-70 ft, and three well pairs located updip, downdip, and along strike of the source well. For each well pair, the shallow well is screened from 15-25 ft and the deep well is screened from 60-70 ft. All depths are referenced to land surface. Details of the well construction are provided in **Appendix A.**

Results of the pump test and data analysis by Gierke et al. (1988) showed anisotropic drawdown with elongation parallel to strike. Bulk hydraulic conductivity values over the 54-ft saturated thickness of the pumping well ranged from 2.5E-03 cm/s to 5.5E-05 cm/s, with a geometric mean of 3.4E-04 cm/s. An analysis of directional hydraulic conductivities yielded a Kx (along-strike) value of 8.5E-03 cm/sec, a Ky (along-dip) value of 1.1E-03 cm/sec, and a Kz value of 5.6E-03 cm/sec.

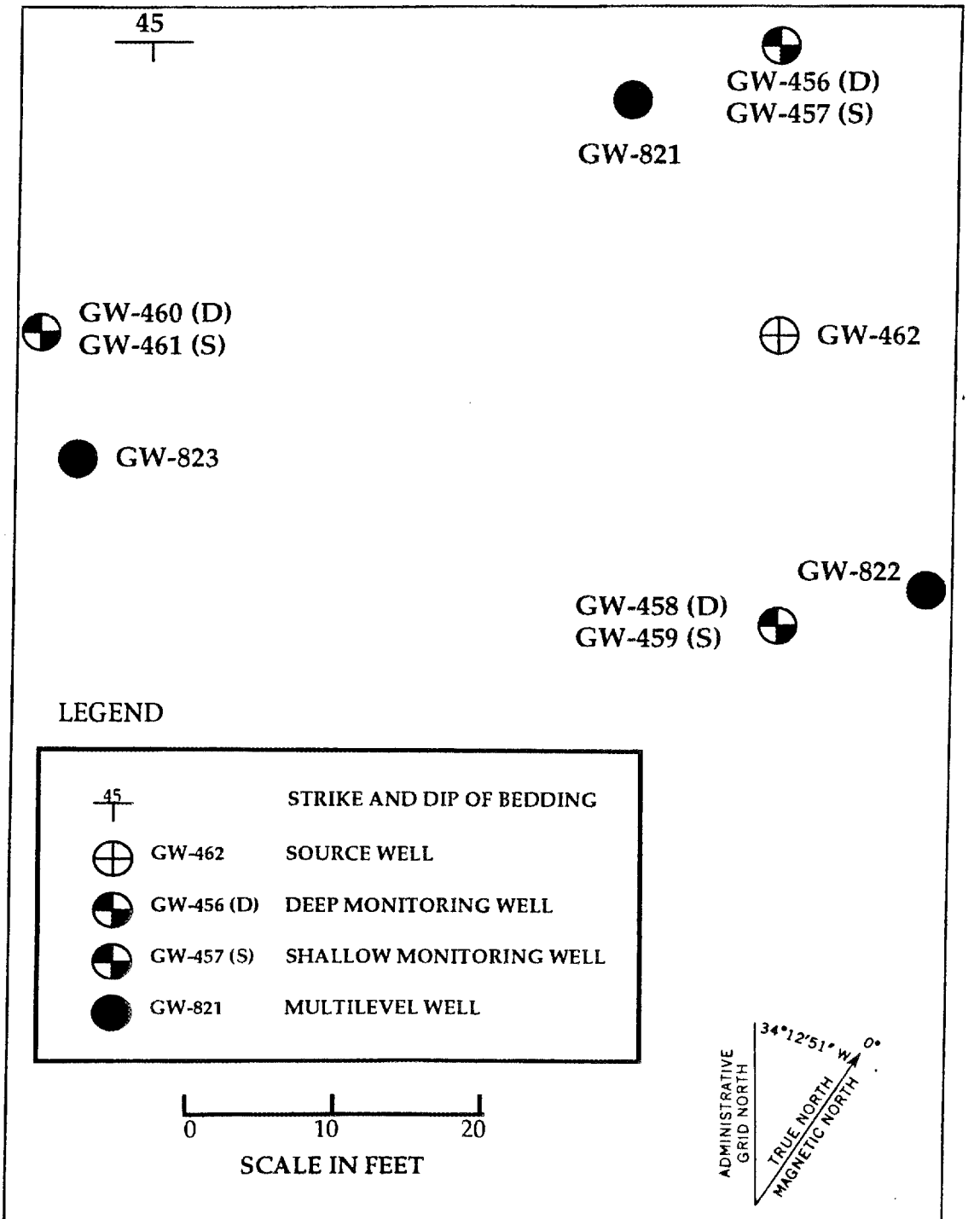

Figure 2-2: Locations of monitoring wells at the field site. Note that the map is oriented with respect to the ORR administrative grid, which is 34° 12' 51" W of true/magnetic north.

These values result in a strike to dip horizontal anisotropy ratio of approximately 8:1 and a vertical (Kx:Kz) anisotropy ratio of 1.5:1. Lee et al. (1992) report the results of other pump tests conducted on the ORR that estimate horizontal anisotropy ratios of 2:1 to 30:1. Rizk (1990) conducted pump tests in the Maryville Limestone (now called Dismal Gap Formation); these results yielded a strike to dip horizontal anisotropy ratio of 40:1. The anisotropy ratios estimated by Gierke et al. (1988), Lee et al. (1992), and Rizk (1990) indicate that anisotropy is a significant influence in the flow system and must be considered in any analysis of the flow and transport properties of the fractured formations on the ORR.

The existing network of wells provided the means for conducting preliminary tracer experiments prior to the start of intensive field activities. Beginning in March of 1994, helium and bromide tracers were injected into the source well for the purposes of establishing flow dynamics and generating tracer plumes that could then be used to identify active transport pathways. In addition, water levels were measured for each sampling event.

Hydraulic heads

Water level and precipitation data for the time period of March 1994 to May 1995 are summarized in **Figure 2-3** and in **Appendix B**. The well hydrographs show both seasonal and precipitation related variations. For example, a steep decline in water levels beginning in April of both 1994 and 1995 is due to evapotranspiration.

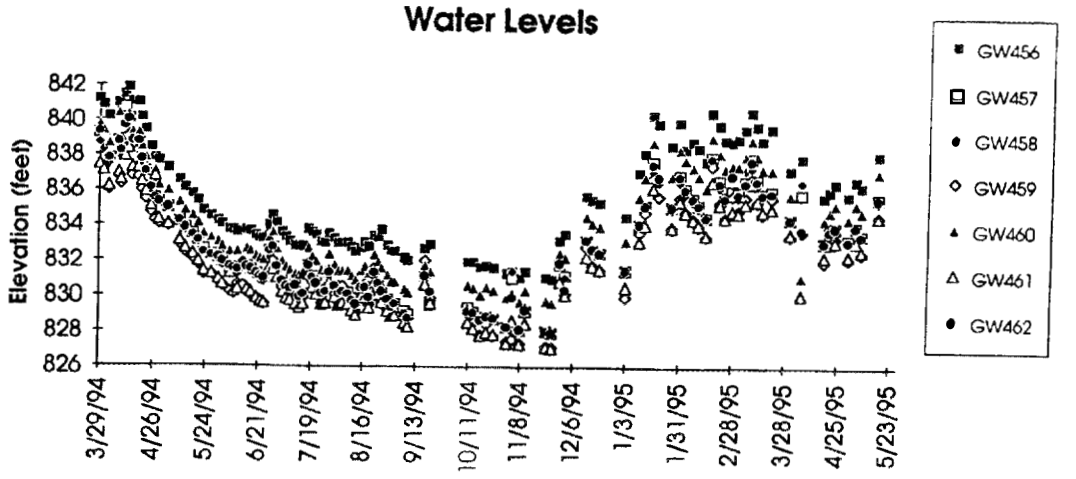

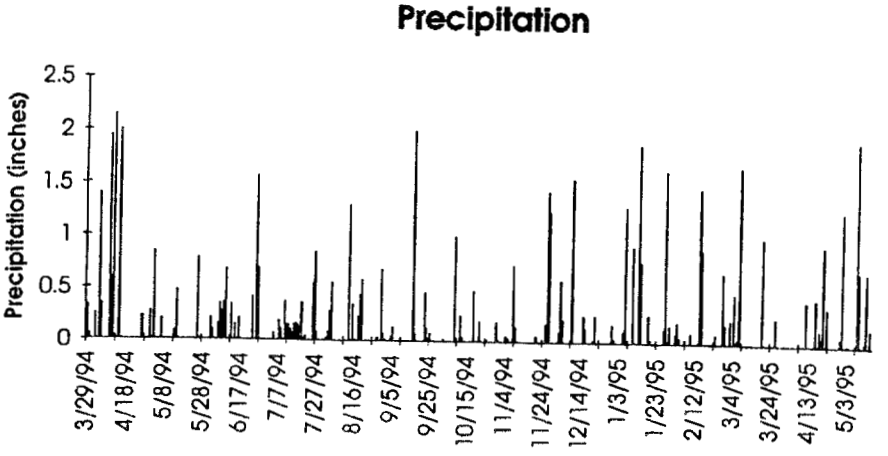

Figure 2-3: Hydrograph (water levels vs. time) of all well pairs and GW462 and precipitation (from adjacent site in West Bear Creek Valley) for the period of 3/29/94 to 5/17/95.

Large responses, shown as sharp peaks on the hydrograph, are observed in conjunction with storm events. The highest water levels are observed in GW456 (deep, updip well) and the lowest are seen in GW461 (shallow, along-strike well). Hydraulic heads within GW457, GW462, and GW458 are identical over most of the time of record, reflecting the good hydraulic connection seen in the pump test results reported by Gierke et al. (1988). This hydraulic connection is consistent with the geometry of the well locations relative to the geologic dip. A bed-parallel fracture zone intersecting the shallow updip well (GW457) would pass through the injection well (GW462) and intersect the screened interval of the deep downdip well (GW458).

Water levels in the shallow wells (**Appendix B**) appear to be very sensitive to precipitation events. The water levels of GW459 and GW461 are generally very similar. During precipitation events, however, the water level in GW459 changes significantly over a small time period, often up to a few feet in two days. In general, water level variations in the deep wells (**Appendix B**) show similar seasonal and precipitation related trends.

Hydraulic gradients

Horizontal hydraulic gradients were calculated for both the shallow (15-25') and deep (60-70') systems. All gradient calculations are shown in **Appendix C.** From an estimated anisotropy ratio of 8:1 (strike:dip), flow directions for both the shallow

and deep systems were also calculated. The orientations of the gradient and estimated flow direction for the shallow and deep systems are presented on a Rose diagram in **Figure 2-4.** The shallow gradient is generally oriented SSW (vector mean of 201 degrees), with fewer orientations WSW. With an 8:1 strike to dip anisotropy ratio, the shallow flow direction shifts to the west, with a vector mean of 249 degrees. The deep hydraulic horizontal gradient is generally oriented due south, with fewer south-southeast and south-southwest orientations (**Figure 2-4**). The orientation of the deep flow direction varies from south-southwest and to the south-southeast, although the vector mean remains similar to the gradient at 180 degrees. The average magnitude is 0.02 for the shallow horizontal gradient and 0.07 for the deep horizontal gradient (**Figure 2-5**).

The vertical gradients were calculated using the difference between the heads of the shallow and deep wells and dividing by the distance between the center of the well screens (45 ft). The magnitude of the vertical gradient versus time for each well pair is shown in **Figure 2-6**. In the along-strike well pair, the shallow and deep water levels show similar trends, although the shallow water level appears to be more responsive to recharge events than the deep water level. During the growing season, evapotranspiration increases the magnitude of the upward gradient, due to a decrease in the shallow water levels. The updip well pair reacts similarly to the along-strike pair, with correlated trends between shallow and deep but a more responsive shallow water level.

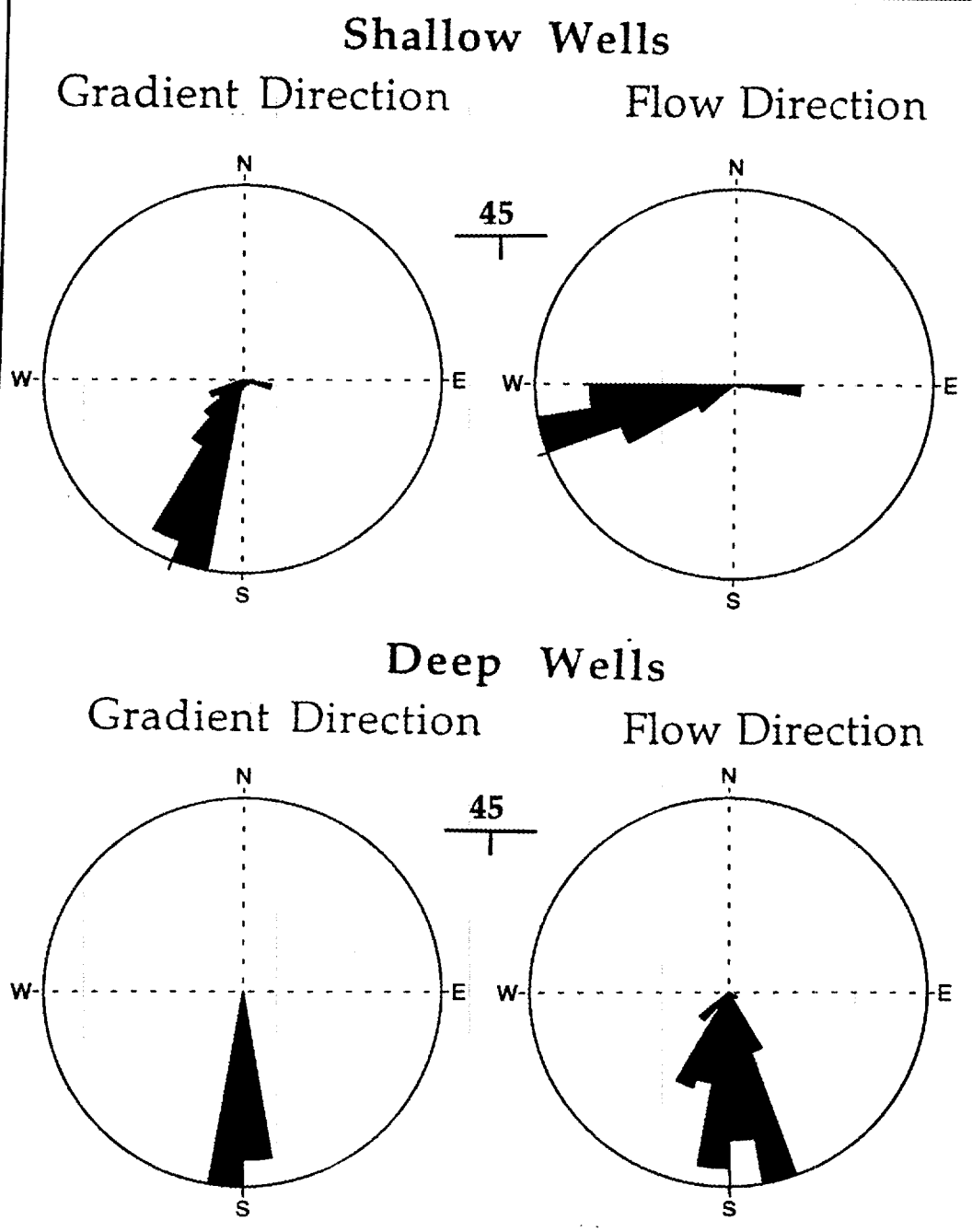

Figure 2-4: Rose diagrams of shallow and deep horizontal gradient and flow directions over the period of 3/29/94 to 5/17/95. Flow directions were calculated using an assumption of 8:1 (strike:dip) anisotropy. The radii lengths correspond to the number of measurements for a particular orientation.

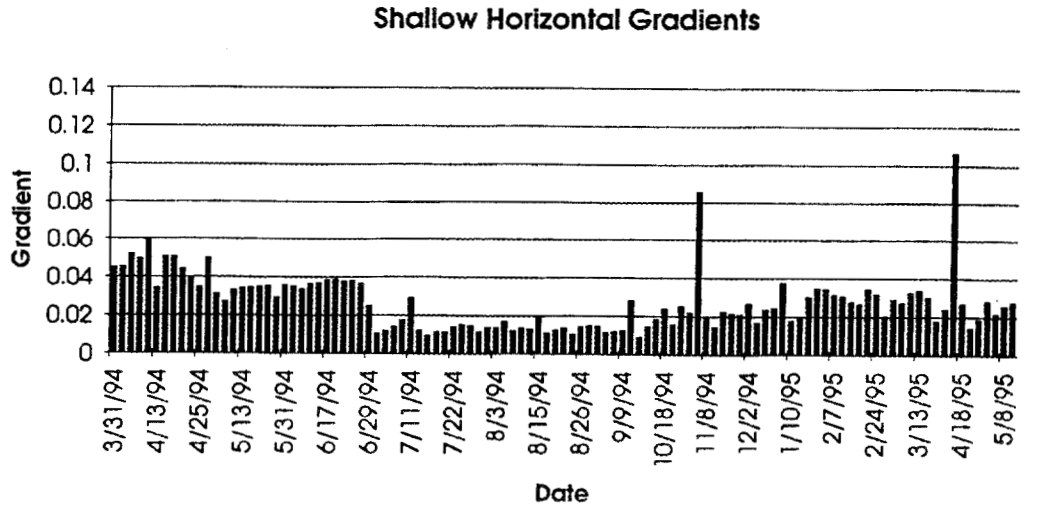

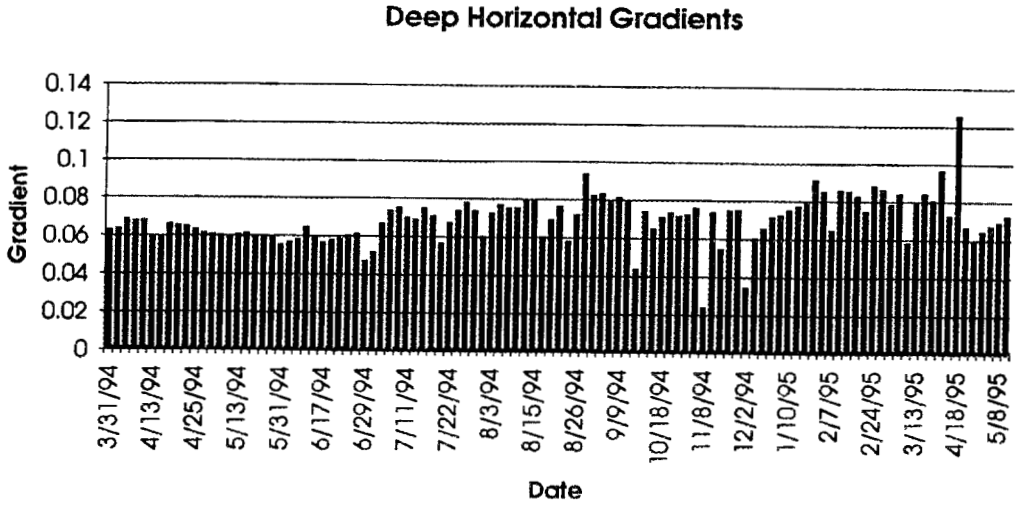

Figure 2-5: Bar graphs of the magnitude of the shallow and deep horizontal gradients.

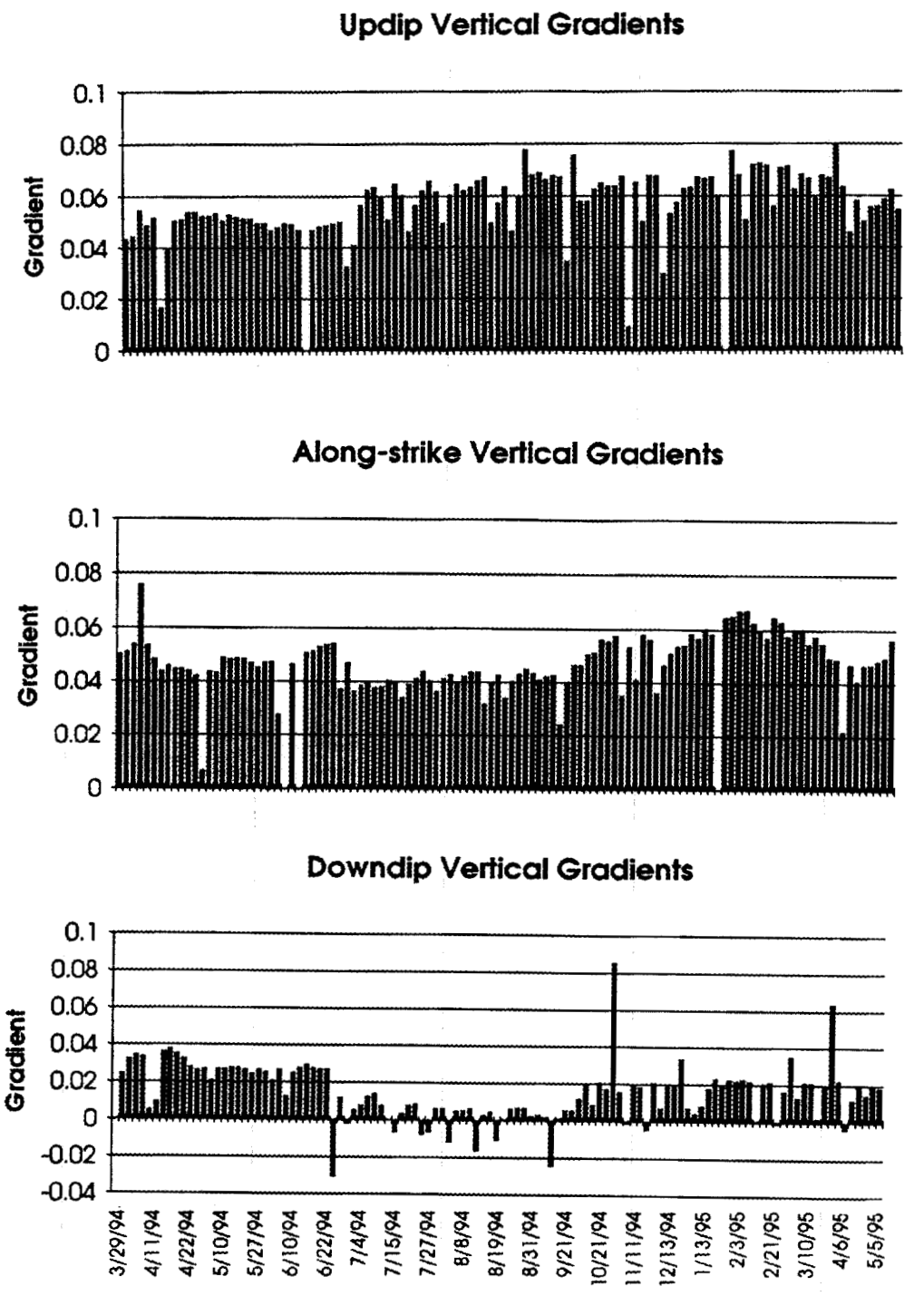

Figure 2-6: Bar graphs of the magnitude of the vertical gradients in each well pair.

The difference in water levels in the downdip pair is not as significant as in the other two pairs. The shallow water level is very sensitive and fluctuates up to a few feet over 2 days. The water level change is often significant enough to reverse the vertical gradient from upward to downward on a few of the measurement dates.

Helium tracer test

The purpose of the helium gas tracer test was to provide a means for studying the natural gradient dynamics at the field site prior to the start of other field activities and to provide an indication of the impact of those activities on flow and transport. Helium injection began on March 25, 1994 and continued until December 12, 1994. This study includes data from the beginning of the tracer test to early September, 1994. The gas injection system consisted of a compressed helium source connected to 400 ft of 1/16" O.D. Teflon tubing that was wrapped around 1" diameter PVC screen and placed in the source well. The tubing, which extends from 20-60 ft depths, provides a high surface area for diffusion of gas into the groundwater. Filter wrap was placed over the tubing-wrapped portion of the PVC to prevent any gas bubbles that might form on the outside of the tube from blocking the well screen and reducing permeability. Moderate flow of gas through the injection tubing should result in diffusion to saturation levels which are governed by the temperature of the groundwater.

Helium concentrations in the source well and the six observation wells were then

measured three times weekly using specially designed gas samplers (Sanford et al., 1994). These samplers consist of two parts: a length of copper tube sealed at one end and silver-soldered to a tire valve stem at the other; and a length of silicon tubing filled with clean sand that is sealed at one end and contains a valve stem cap at the other that has been drilled to allow the passage of gas. When the two portions of the sampler are attached, dissolved gases diffuse through the silicon tubing, coming to equilibrium with groundwater concentrations within 1.5 to 2 days. The valve stem is held open by a small ball bearing in the valve cap. When the sampler is extracted from the well, the silicon tube is disconnected, allowing the valve to close and preventing loss of the gas from the copper tube. Gas is then injected directly from the copper tube into a gas chromatograph for analysis. For this study, samplers were suspended in the middle of the screened intervals and allowed to equilibrate over a minimum of two days.

Helium concentrations in the source and observation wells are summarized in **Figures 2-7, 2-8,** and **Appendix D**. Concentrations are recorded as area counts rather than as absolute concentrations; however, because these area counts are linearly related to absolute concentration, C/C_0 can be calculated by dividing the area counts from an observation well sample by the area counts in a source well sample. **Figure 2-7** shows the time-averaged concentration of helium in the source well as area counts.

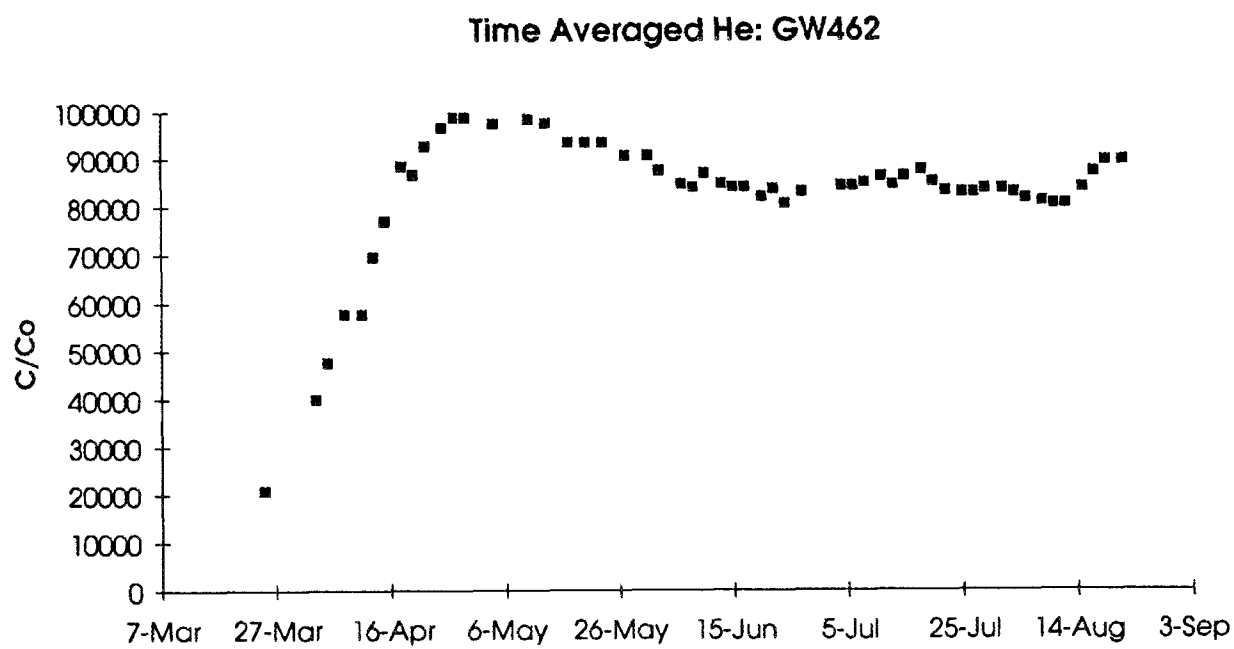

Figure 2-7: Helium concentrations in the source well, presented as time-averaged C/Co versus time. Averages were determined at any given time by including all previous measurements. Saturation (peak concentration) occurred approximately six weeks after initiation of the injection.

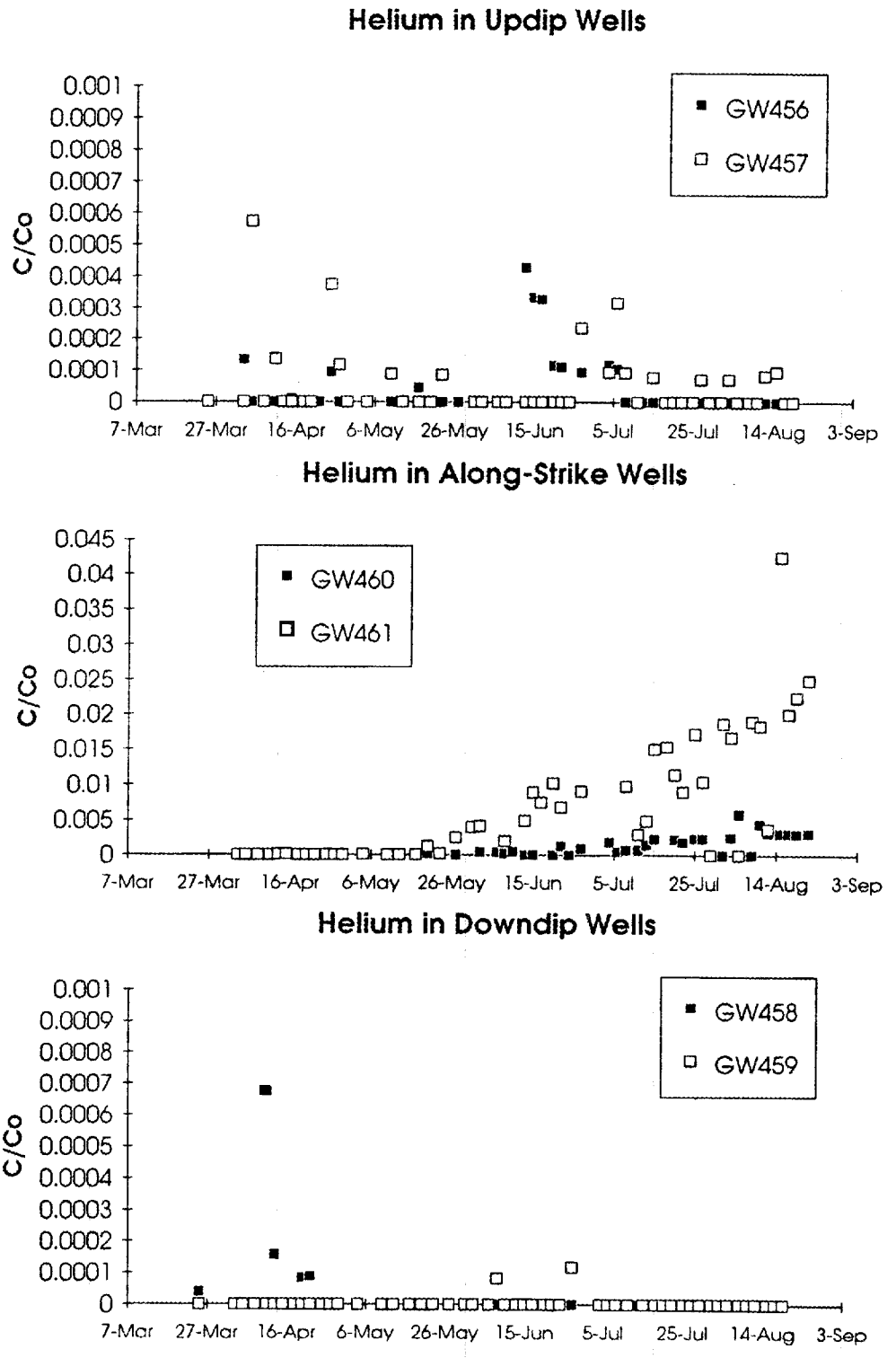

Figure 2-8: Helium concentrations versus time for the well pairs.

Cumulative averaging results in considerable smoothing of the concentration curve and masks the actual fluctuations in the data. The majority of these fluctuations can be attributed to sampling and not analytical error. In most cases the samples were analyzed within 24 hours of removal from the wells; however, analysis of some samples was delayed by as much as four days, resulting in potential leakage through the valve stems. Apparent leakage occurred on occasion even when the analyses were completed by the following day, evidenced by a very low concentration in the source well or by the absence of background gases such as argon. Additional sources of fluctuation are variations in the flow rate of helium and groundwater flux into the injection well. The flow of helium is controlled only by the low pressure gauge on the regulator, which required frequent adjustment to ensure that the gas bubbled at a rate sufficient to maintain saturation but low enough to prevent excessive waste of the helium. In some cases, bubbling had stopped between site visits for an unknown period of time. Flushing of the well during heavy rains could also have contributed to variations in the level of saturation. For these reasons it was felt that the cumulative averages were a better reflection of the source concentration "seen" by the observation wells than the measured concentration at any given point in time, and these were used for the calculation of C/C_0. Although the analytical error cannot be quantified, the errors related to sampler leakage and the presence of water vapor in some of the samples are likely to greatly exceed the errors from the helium analysis.

Helium concentrations in the observation wells are shown in **Figure 2-8**. Low but detectable concentrations of helium were seen in all six observation wells within a few days after the injection began, primarily in conjunction with storm events, although there was no consistent pattern to the wells in which it was observed. The majority of helium transport occurred closer to the direction of strike than the direction of dip. The large variations in C/C_0 are most likely due in part to the measurement error previously described. Helium was first detected in both along-strike wells on May 15, 1994, corresponding to a first arrival velocity of 0.28 m/d in the direction of strike. Concentrations in the along-strike wells five months after the start of injection were still orders of magnitude lower than the source concentration in spite of very early breakthrough via fracture flow paths, indicating either extremely low average advective velocity, continuous dilution by dispersive mixing, or retardation due to matrix diffusion.

While the majority of helium transport is observed parallel to strike, the occurrence of helium both up and down dip (**Figure 2-8**) suggests that flow system dynamics are very complex, perhaps varying with seasonal precipitation patterns. The presence of helium in the updip wells may be a result of short-term reversals in the horizontal hydraulic gradient during storm events that were not identified due to sampling frequency. In addition, a deeper source of helium brought to the shallow system from the upward vertical gradients may be the source of the sporadic detections in the updip wells. The occurrence of helium in the deep downdip well

may be a result of transport along a fracture zone that extends to the source well. This hydraulic connection was observed in the pump test conducted by Gierke et al. (1988).

Bromide tracer test

The purpose of the bromide tracer test was to chemically tag the active flow zones and to establish a tracer cloud for testing sampling methodologies. Bromide was introduced into the source well as a single slug injection on April 11, 1994. In order to minimize the impact of head and temperature changes, a concentrated bromide solution was created by removing several bailers of water from the source well, mixing with $MgBr_2 \cdot (H_2O)_6$, and reinjecting the solution into the well. The water within the well casing was then circulated by slowly raising and lowering a bailer to ensure adequate mixing and minimize density flow, and a grab sample was obtained for measurement of source concentration. All samples were collected by taking a bailer grab from the screened interval. No purging was done prior to sampling, and all water left in the bailer after obtaining a small volume for sampling was reintroduced into the well in order to minimize disturbances to the flow system. Samples were analyzed using an Orion A290 specific ion probe with a detection limit of 5 ppm. For each round of analyses, the probe was calibrated using known standards and was periodically rechecked during the analyses.

Analytical results for the source well are listed in **Appendix E**. Although the

detection limit of the bromide probe is 5 ppm, concentrations below this level are reported since they do indicate significant (although unquantifiable) concentrations. In all but one of the observation wells, no bromide was detected. In the shallow along strike well (GW461), low concentrations of bromide were first observed on June 15, 1994. These data would indicate a first arrival velocity of 0.23 m/d, which is consistent with the results obtained from the helium data given the more limited sensitivity of analytical methods for bromide detection as compared to helium. Because of mixing and dilution that are likely to occur within the well casing, the lack of detection of bromide in most of the observation wells is not necessarily an indication that the bromide is not present. One possible explanation for the low concentrations of bromide observed is that the well pairs intercept the fringe and not the center of the bromide plume. None of the well pairs is located along either the southwest direction of the hydraulic gradient and or the estimated west-southwest direction of flow (assuming horizontal anisotropy).

The decay of the source concentration of bromide is shown in **Figure 2-9**, plotted as log C/C_0 versus time. The curve shows an initial rapid decay, followed by a more linear decrease. The initial rapid decrease is most likely due to diffusion into the matrix driven by a high concentration gradient. The subsequent linear decrease is consistent with advective transport from the well and represents a specific discharge of approximately 1 cm/d through the cross-sectional area of the screened interval.

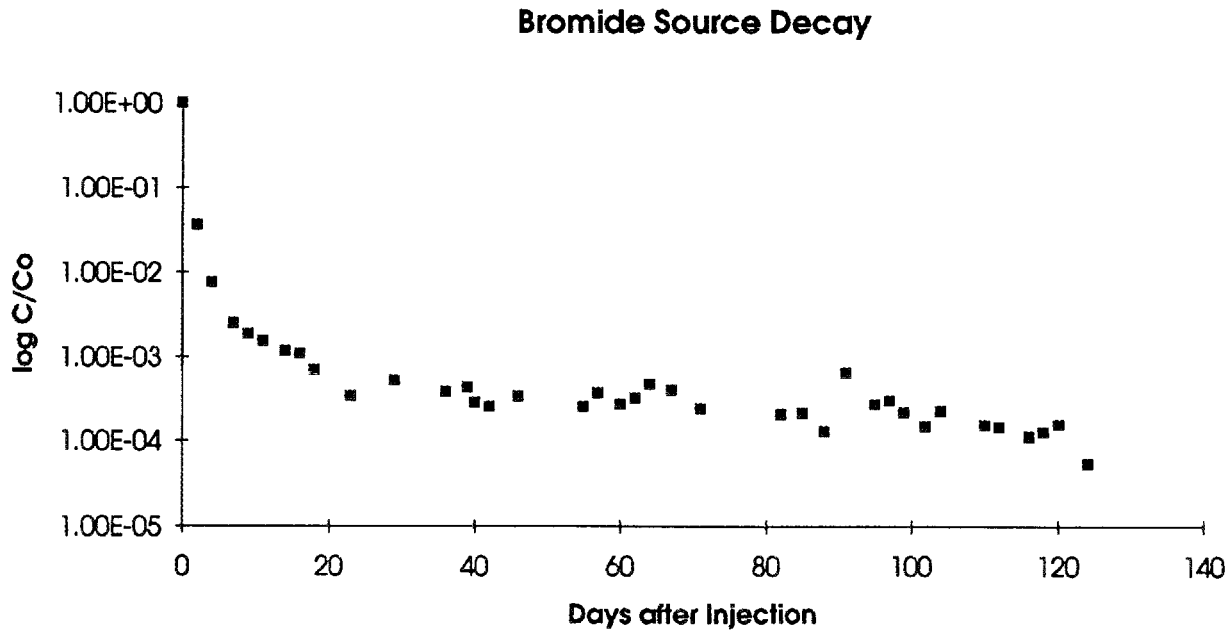

Figure 2-9: Bromide decay in the source well, presented as log C/Co versus time.

Rotasonic drilling

On June 28-30, 1994, three boreholes (GW821, GW822, GW823) were drilled and cored at the site using Rotasonic drilling. Rotasonic drilling is an acoustic method that utilizes high frequency vibration combined with slow rotation. It has many advantages over conventional rotary drilling, including drilling speed, waste minimization, continuous core recovery, and use of minimal drilling fluid (Barrow, 1994; Dustman et al., 1992). The Rotasonic technique used cuts a 3.75" diameter core, leaving a 4.5" diameter borehole. This technology was chosen primarily because of the potential for obtaining nearly continuous recovery of core without the use of drilling fluids. The interface between saprolite and bedrock corresponds to the permeable water table interval described previously, and is a high flow zone. Although it is one of the most significant flow zones in the ORR aquitards, the transition zone has been loosely described from other drilling activities on the ORR as the zone below auger refusal but above competent bedrock and has not been well characterized in the past due to the difficulty in recovering core. Obtaining a lithologic description of this zone was therefore a major goal of the Rotasonic drilling.

Dry coring through the saprolite and transition zone was very successful, resulting in nearly complete recovery of undisturbed core. However, once the competent shale was encountered, penetration became very slow and difficult and the core that was recovered was quite shattered. Because of the poor condition of the core, all

drilling below the top of bedrock was done using water. Drilling water was used below 25' in GW821, 31' in GW822, and 27' in GW823. These depths correspond approximately with the depth to competent bedrock; the exception is GW821, in which five feet of core was obtained from competent bedrock before dry drilling was abandoned. Competent bedrock is defined here as beginning with the first dark grey shale layer encountered, and is coincident with the onset of slower penetration during dry drilling.

Problems with borehole collapse were encountered where very wet, highly fractured zones occurred above bedrock. Extremely wet silty sand intervals were encountered from 18-19.5' in GW821, from 17-19' and 24-271' in GW822, and from 11-14' and at 17' in GW823. The borehole testing needed for the identification of multilevel sampler locations required that the boreholes remain open and uncased for two months after drilling. For this reason, temporary steel casing was installed in each of the boreholes from the ground surface through the transition zone to the top of bedrock after the holes were reamed out to a six-inch diameter. Unfortunately, this rendered the zones above bedrock inaccessible for borehole testing. Numerous problems were encountered during the drilling of GW823, primarily due to a heavily fractured zone from 46-49'. Core recovery through this zone was hampered by the inability to obtain a competent plug at the base of the core barrel, and significant washout and sloughing resulted in infilling of the bottom ten feet of the borehole.

Once extruded, the cores were measured, labelled, photographed, and briefly described in the field. Each core was then tightly wrapped in plastic sheeting to prevent desiccation. After surveying for organic and radioactive contamination by health physics personnel, the cores were transported to the core barn for more detailed logging.

Core descriptions

Core logging was conducted during drilling activities and later on in the summer of 1994. The depths of the described intervals are approximate, because the cores were often compacted and/or there was not full recovery. Core logs describing the characteristics of the soil, saprolite, transition zone, and bedrock are presented in **Figure 2-10** and **Appendix F**. Cores were held in the core barrel by dry drilling several inches at the bottom of each interval to obtain a tight plug. Because the depth of this core plug at the bottom of each interval was known, all compaction occurred above that point and depths were assigned relative to the bottom of each interval without accounting for compaction. Thus the core logs overestimate the amount of incomplete recovery and assign all loss to the top of each cored interval.

In general, the topsoil, characterized by a dark brown color and organic matter, was observed to be approximately 6 inches thick. The saprolite ranges in thickness from approximately 20' to 30' and is composed of olive to reddish-brown silty sand and clay, with shaly bedding and weathered greenish-grey shale fragments.

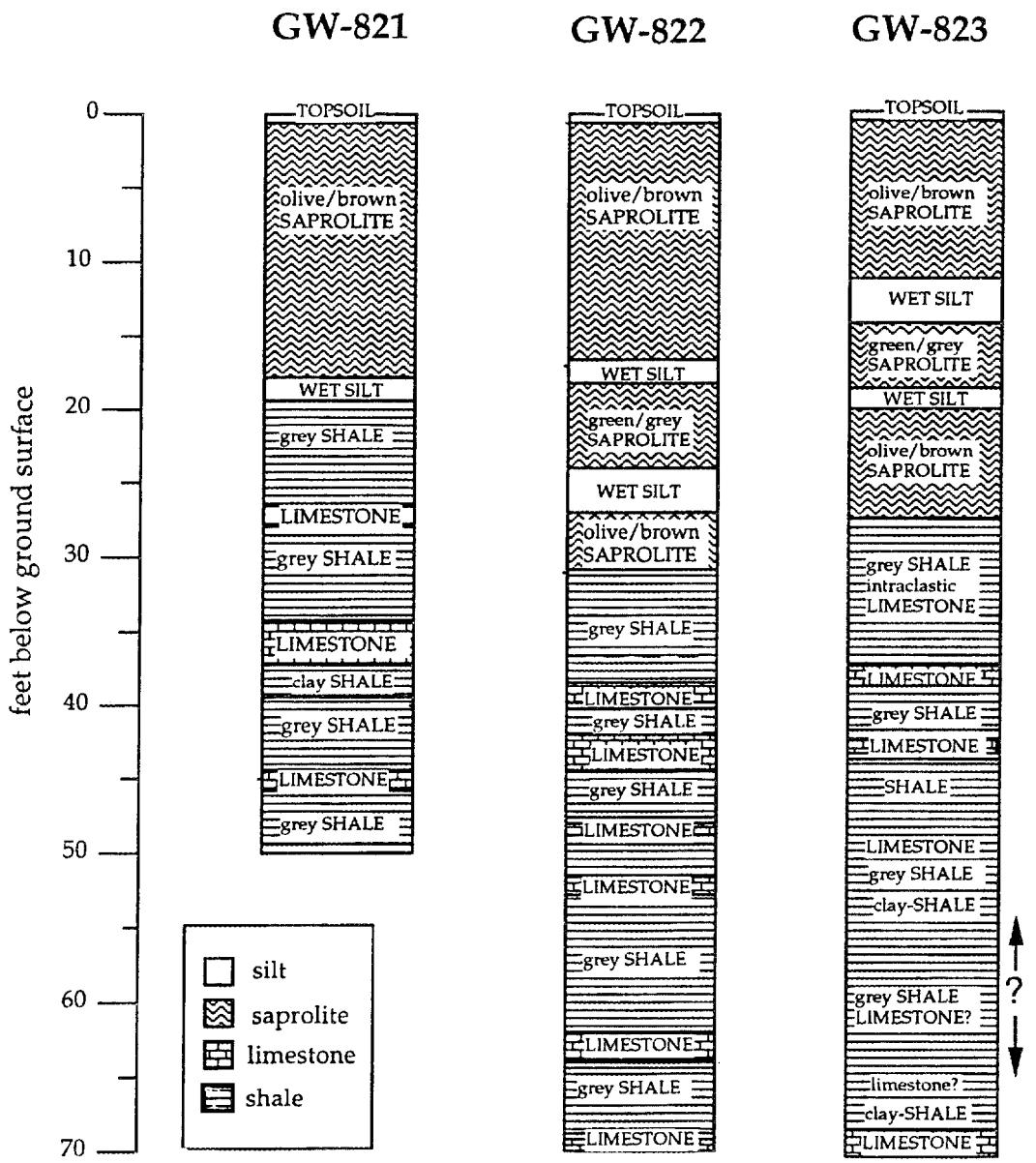

Figure 2-10: Core logs of the GW821, GW822, and GW823 boreholes.

Fragments in the less weathered portions of the saprolite are coated with black or reddish-brown oxides/hydroxides. This description of the saprolite correlates with the description of Hatcher et al. (1992).

The bedrock underlying the site, part of the middle unit of the Nolichucky Shale, is dark grey with lesser greenish-grey and reddish-grey shale containing thin carbonate interlayers and calcite veins. The carbonate was observed to be more competent and less weathered than the shale. The shale was very weathered and fissile (described as "clay-rich shale" in core logs) in many parts of the core.

Zones of competent shale were heavily oxidized on some surfaces. These red and orange stainings are evidence of groundwater flow through the fractures because dissolved oxygen in groundwater causes iron in solution to precipitate as hydroxides. Some of the oxide coatings were thick and covered an entire fracture surface while others were thin and covered only portions of a surface. Different micromorphologies, including discrete grains and finely crystalline coatings, were observed.

Pictures of the wet silty saprolite and an oxidized fracture surface in the shale are shown in **Figure 2-11**. A fence diagram (**Figure 2-12**), representing the subsurface geology at the site, shows that individual shale and carbonate units, numbered S-1 through S-7 and C-1 through C-6, can be traced between the boreholes.

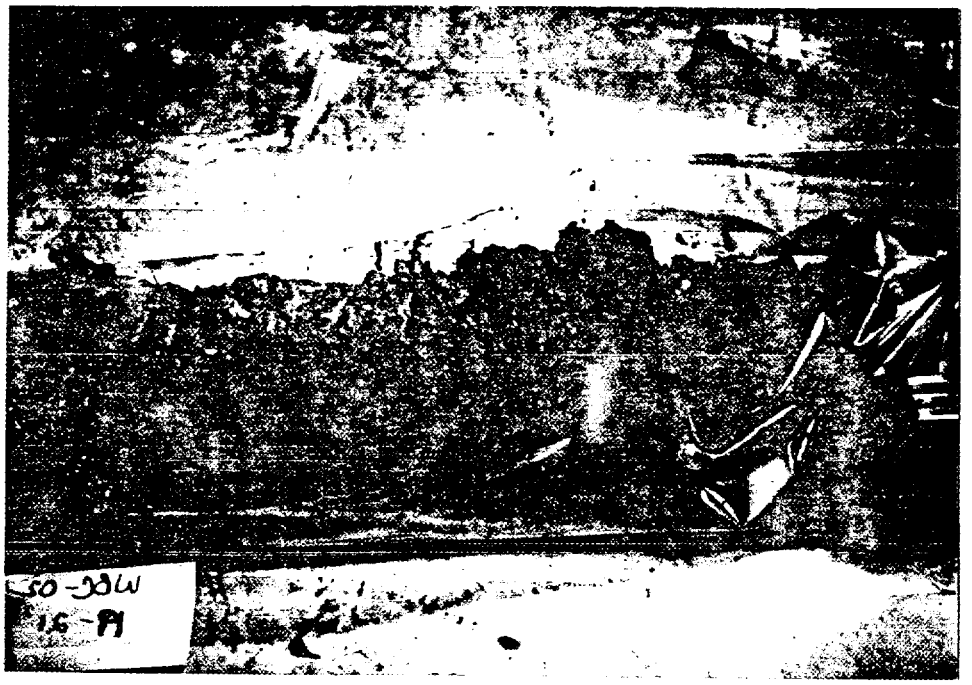

Figure 2-11: Pictures of core. Top - wet silty saprolite (from GW822 19-21'). Bottom- oxidized surface on shale (from GW823 40-45').

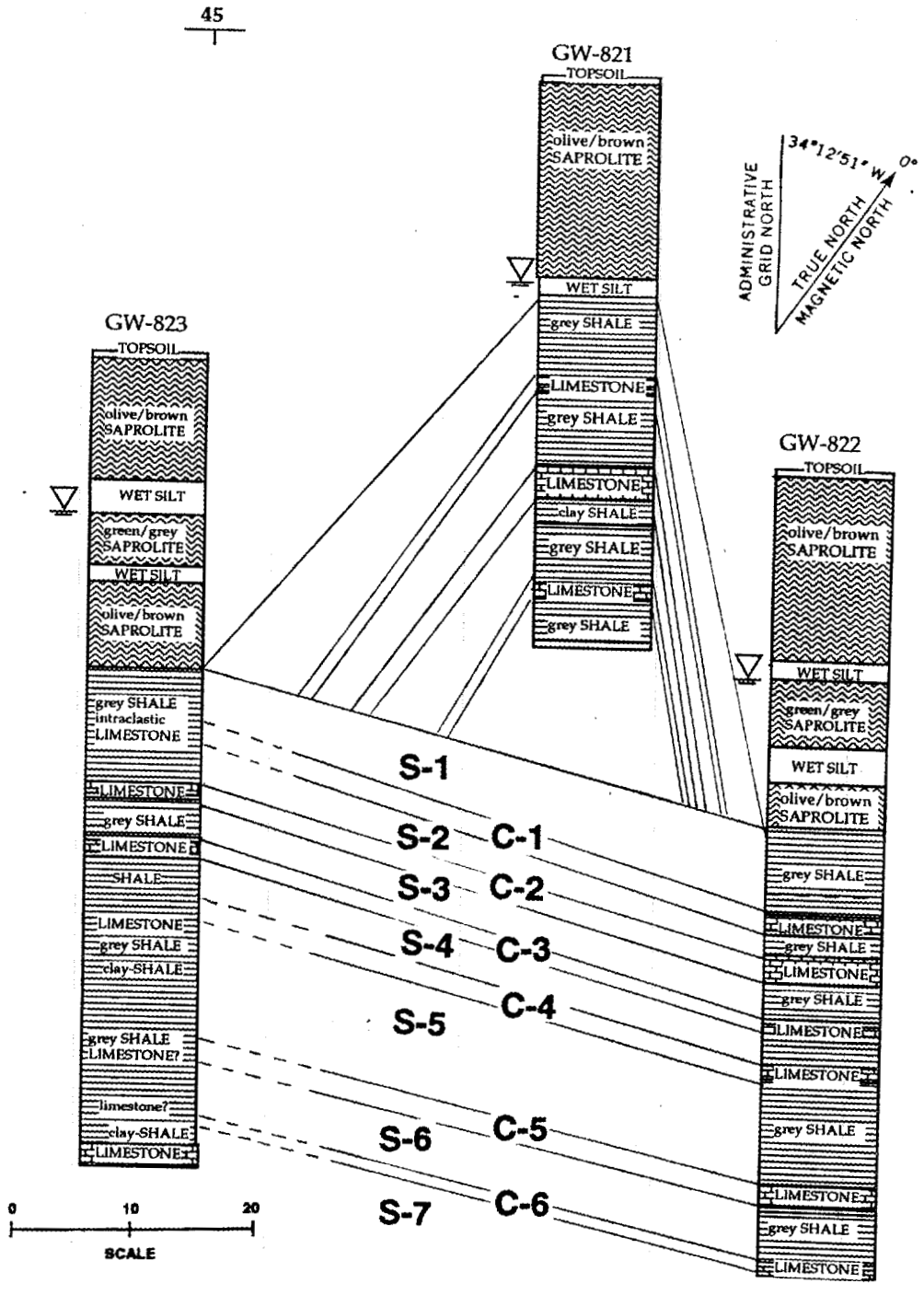

Figure 2-12: Fence diagram showing lithologic correlation between the three boreholes. Shale and carbonate intervals are numbered S1-S7 and C1-C6.

Because the shale in the core samples does not exist as full competent core pieces, but mostly as fragments or small pieces, it was difficult to determine any strike and dip orientations of bedding or fracture zones. However, the correlations of units between the boreholes indicate a 45º dip of the bedding, which is supported by the estimates of Gierke et al. (1988).

2.4 Hydraulic Tests

One of the main problems faced in field investigations in fractured media is developing techniques to identify and characterize spatial heterogeneity of hydraulic properties of fractured rock (Shapiro and Hsieh, 1991). Because hydraulic properties of fractured rock can vary over many orders of magnitude due to different permeabilities of open fractures, infilled fractures, and matrix, and are subject to abrupt spatial changes, the identification and characterization of permeable fractures are important features in the design of any field experiment in fractured media. Recent experiments in fractured rock (Shapiro and Hsieh, 1991; Williams and Conger, 1990; Paillet et al., 1990), have focused on conducting investigations using various field techniques to identify and characterize spatial variability in hydraulic properties of rock. These techniques include surface and borehole geophysics, seismic and electromagnetic tomographic imaging, geochemical analyses, hydraulic testing, and tracer testing, in conjunction with geologic, lithologic, and fracture mapping data. Employing a combination of techniques allows for a more thorough understanding of the complex nature of a fractured rock

system, including fracture orientation and aperture, fracture hydraulic conductivity, interconnectedness of fracture networks, and degree of fracture infilling.

Two types of borehole tests, electromagnetic flowmeter and point dilution tests, were conducted in the uncased portions of the boreholes following drilling and coring. The purpose of these tests was to identify and characterize the active flow zones and to combine this information with core observations to determine where to locate the sampling ports for the multilevel wells. In addition, a downhole camera was used to observe the condition of the borehole and to identify any major fracture or washout zones.

Downhole camera

A downhole video camera was used to obtain a visual picture of the condition of the borehole (**Table 2-1**). In general, the boreholes were competent, except for a few significant washout zones observed in GW-822 and GW-823. Other features observed in the borehole camera include steeply dipping (likely to be bed parallel) fractures and calcite veins.

Electromagnetic flowmeter tests

An electromagnetic (EM) borehole flowmeter (**Figure 2-13**) was used in the open interval below the temporary casing to identify the location and relative flow rate of individual fracture zones contributing groundwater flux into or out of the boreholes.

Table 2-1: Borehole Camera Observations

GW-821: camera zeroed approx. 0.5-1' BGS

camera depth	actual depth (ft. BGS)	observations
9988	13'	water
9979	22'	bottom of casing
9969	32'	ratty hole
9966	35'	ratty hole
9959	41'	mud (obscured view)

GW-822: zeroed at surface

camera depth	actual depth (ft BGS)	observations
9988	12'	water
9969	31'	bottom of casing
9968	32'	dipping fracture
9967	33'	dipping fracture
9966	34'	ratty hole
9965	35'	larger hole
9963	37'	larger hole
9961-60	39-40'	slight rattiness
9958	42'	slight rattiness
9957	43'	dipping fractures
9956	44'	dipping fracture
9952	48'	slight rattiness
9947	53'	fracture
9946-45	54-55'	very ratty hole
9945	55'	dipping fracture
9944-43	56-57'	larger hole
9941-40	59-60'	larger hole
9932	68'	bottom of borehole

GW-823: zeroed at surface

camera depth	actual depth (ft. BGS)	observations
9994	6'	water
9975	25'	bottom of casing
9971	29'	larger hole
9969	31'	larger hole
9963-62	37-38'	dipping fracture
9952-50	48-50'	ratty hole
9947-46	53-54'	ratty hole
9939	61'	bottom of borehole

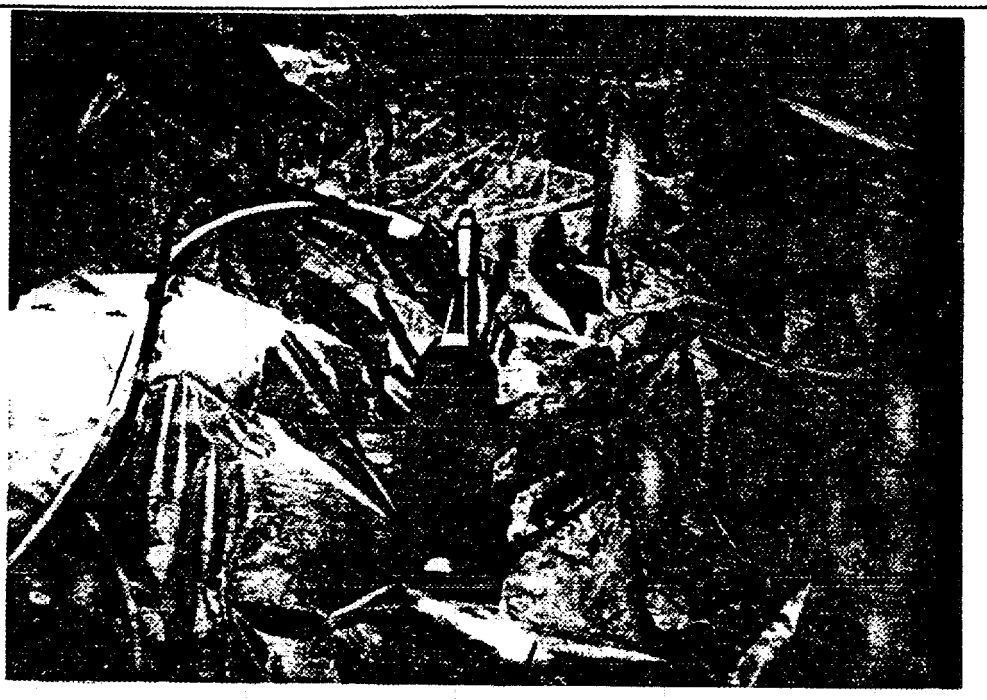

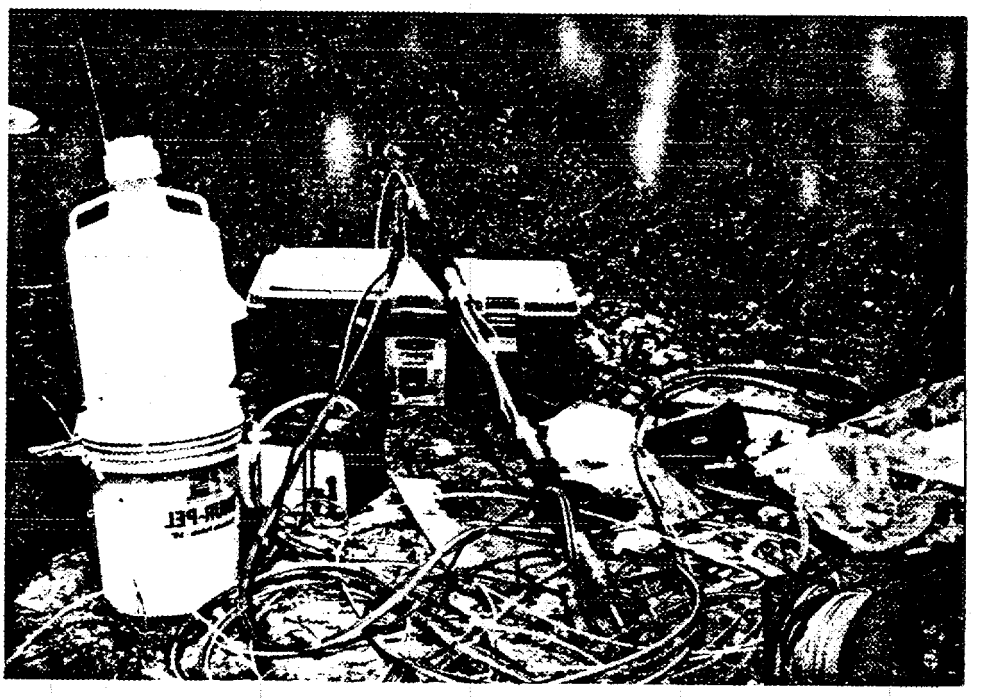

Figure 2-13: Pictures of electromagnetic flowmeter (top) and double packer system for point dilution testing (bottom).

The EM flowmeter measures the voltage induced by the movement of ions carried by groundwater as it flows through a metal cylinder containing a magnetic coil (Moore and Young, 1992). The cylinder is surrounded by a packer that can be inflated using compressed nitrogen in order to prevent flow from circumventing the cylinder. As the position of the flowmeter is changed, the flow zones are identified by a change in the flow rate between adjacent intervals. Flow can be either ambient or induced by pumping or injection. For this study, both ambient and injection tests were performed.

To conduct the flowmeter test, the equilibrium water level was first measured using a pressure transducer and water level meter prior to insertion of the flowmeter into the well. The pressure transducer allowed continuous monitoring of the static water level, in the case of ambient tests, and constant head, in the case of injection tests. The flowmeter equipment is powered by a 120 volt generator. Pressure and voltage readings are fed directly into a portable computer with a printer attachment, and a specialized software package is used to analyze and record field data in both electronic and hard copy form. At each borehole interval, the voltage was sampled at five-second intervals for a total of 60 seconds. The mean and standard deviation of the voltage was calculated for each 60-second period and recorded along with the flow in L/min (negative for downward, positive for upward) and the transducer reading. If the standard deviation was too high (> 0.005 v), the test was aborted or repeated. Occasionally, a test was accepted if the standard deviation exceeded the

acceptance criteria but was small relative to the measured voltage for that test. Periodic high level noise was experienced due, most likely, to the close proximity of the field site to high voltage power lines. Often, testing had to be postponed until the noise level dropped and the equipment once again stabilized.

The procedure followed for ambient tests was to first inflate the packer within the cased interval, where no flow occurs, to obtain the zero offset voltage. Tests were then conducted at two-foot intervals starting at the bottom of the borehole. The zero offset was then remeasured at the end of the test in order to adjust for instrument drift. In the case of injection tests, the zero offset was measured either immediately before injection within the cased interval or after injection at the bottom of the borehole. Identical depths were measured for both the ambient and injection tests. A peristaltic pump was used to inject tap water into the borehole to raise the water level elevation. Ideally, a five to ten foot change in head is desirable, but the most that was obtained for these boreholes was 0.6 to 0.7 ft even at the highest pump rate due to the high hydraulic conductivity within these boreholes. The flow rate was adjusted as needed to maintain a constant head throughout the test.

The flowmeter results are contained in **Appendix G** and are summarized graphically in **Figures 2-14** through **2-16.** Data were reduced by first removing the zero offset and instrument drift, assuming a linear change over time from beginning and final zero measurements.

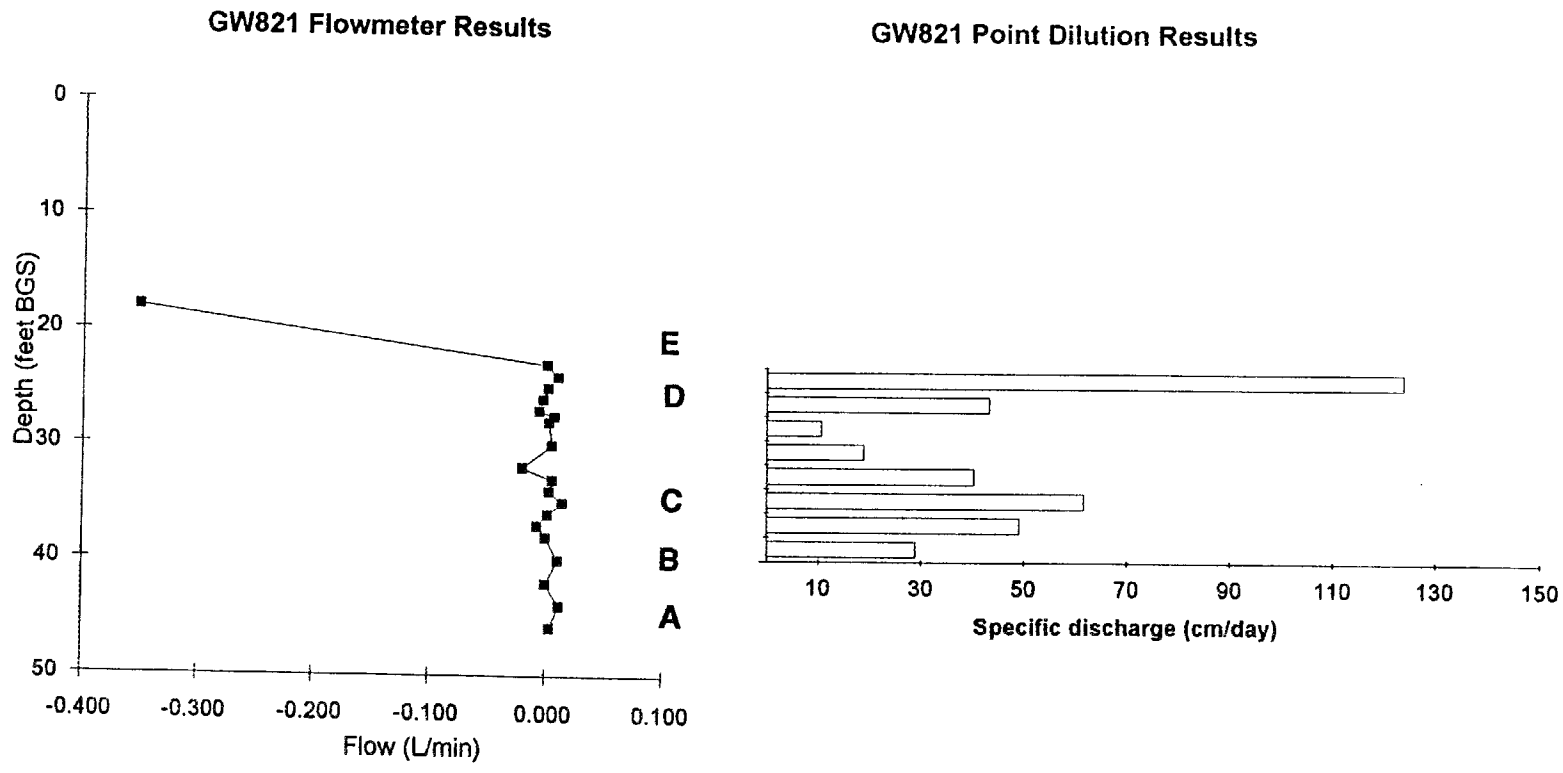

Figure 2-14: Hydraulic test results for GW821. The base of temporary casing is at 22.5'. Sampling ports (A-E) of the multilevel well are shown.

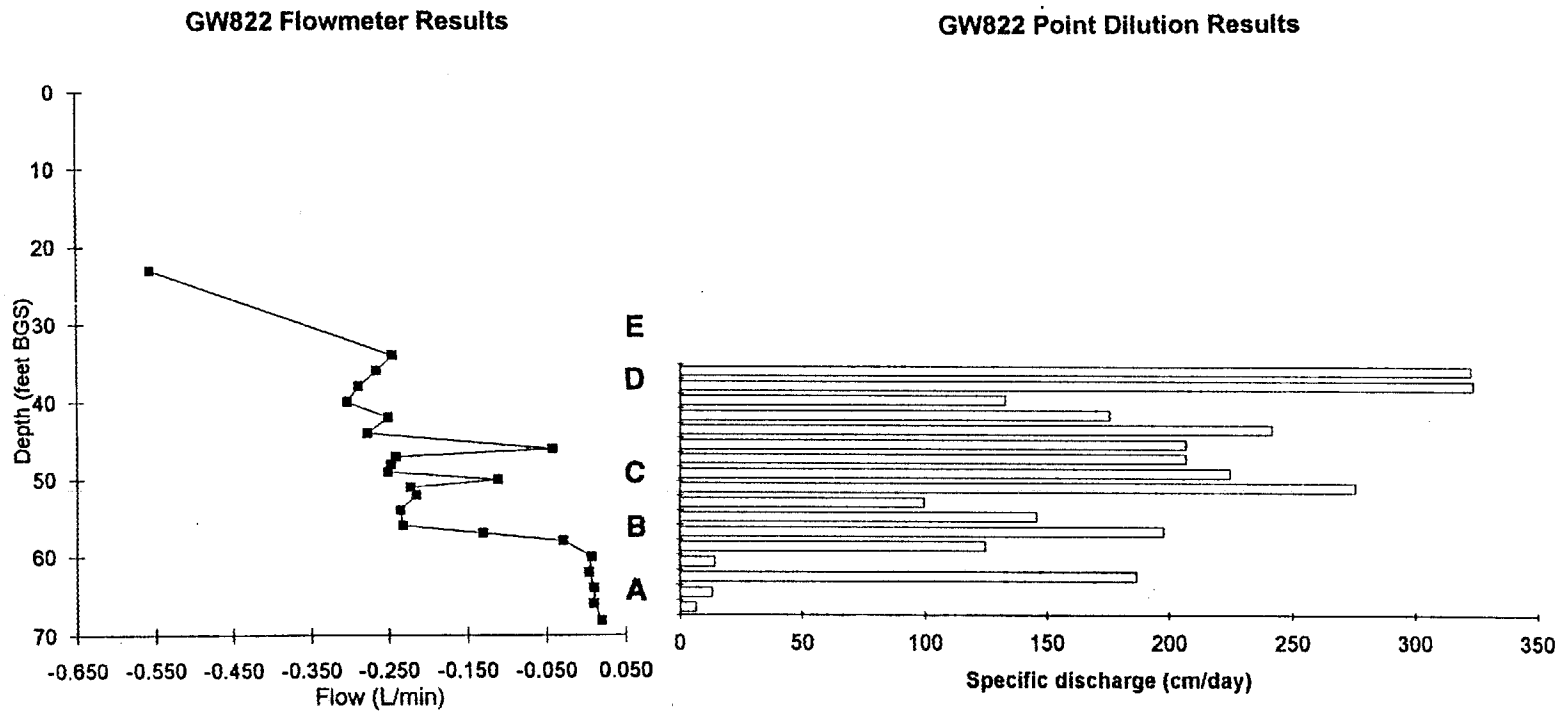

Figure 2-15: Hydraulic test results for GW822. The base of temporary casing is at 32'. Sampling ports (A-E) of the multilevel well are shown.

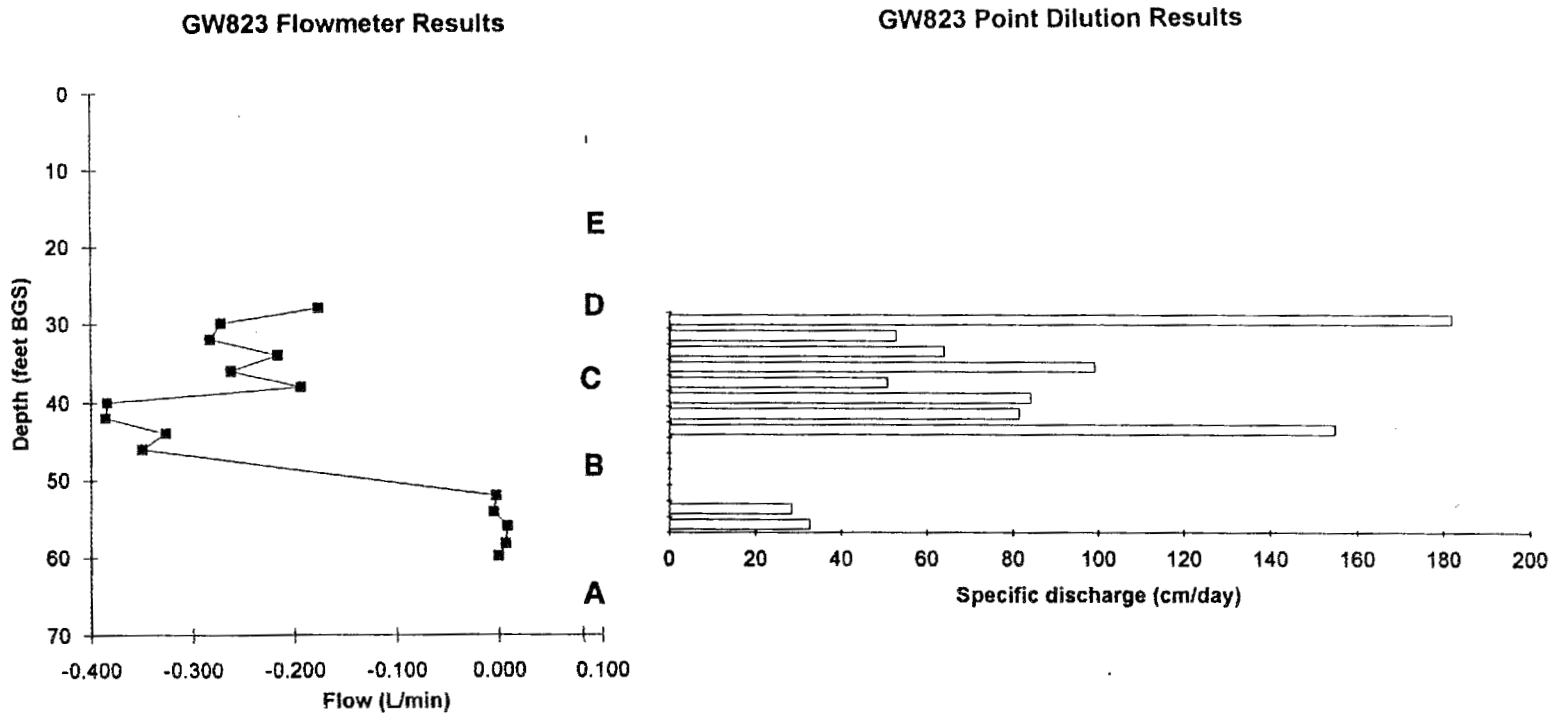

Figure 2-16: Hydraulic test results for GW823. The base of temporary casing is at 25'. Sampling ports (A-E) of the multilevel well are shown.

Injection data were further adjusted by removing the ambient flow measurement for the same interval. In this way, the flow profile for the injection test should reflect a true partitioning of the injection flow rate over the length of the borehole. However, the injection tests for GW823 and, to a lesser extent, GW821 were confounded by intermittent rain during testing that most likely resulted in non-steady-state conditions. Thus, the ambient tests for these boreholes were probably not reflective of ambient conditions at the time of the injection tests. However, a constant head was maintained by frequent adjustment of the flow rate during testing so that the total flow into the well should have been constant over the duration of the tests.

Ideally, one would expect the flowmeter test to produce a series of steps or ramps, increasing from zero at the bottom of the borehole to the total flow at the top. For injection tests, this total flow should be equal to the injection rate. Ramps would coincide with wider zones with dispersed fractures and steps would indicate the presence of discrete fractures or narrow zones. However, the flowmeter data obtained from these boreholes were much more complex, with ambient flow entering and exiting the borehole at different depths. Flow characteristics varied considerably from hole to hole. GW821 (**Figure 2-14**) showed very little flow within the uncased interval in either the ambient or injection tests. Because the casing was simply set in place to prevent collapse in the transition zone, there was nothing to prevent water from flowing under the casing and into the very transmissive zone near the base. If most of the flow during the injection test were pirated at the base

of the casing, then that would explain why the data nearly mirror those from the ambient test. However, both the borehole video and the core log indicate that fracturing within this borehole is minor compared to the other two boreholes.

GW822 (**Figure 2-15**) contains several stepped increases, the most notable from 57' - 58'. As in GW821, more than half of the injected flow entered the formation at the base of the casing. Steps in the ambient flow rate coincided well with fracture zones identified from the borehole video and by iron staining in the core. Two very sharp reversals at depths of 46' and 50' coincide with ratty, washed out zones noted in the borehole video. These reversals could be due to poor packer seating.

The flow profile for GW823 (**Figure 2-16**) was the most difficult to interpret. The tests results are confounded by the impact of rain showers during the time of the test, by having to conduct the test over multiple days due to severe background electrical interference, and because of the presence of an enormous washout zone that prevented seating of the packer within that interval. The dramatic shift between 46' and 52' indicates that a large amount of flow is moving out of the borehole through the washout zone. This zone is completely bypassed by the adjacent monitoring well pair, which is screened well above and below the zone, emphasizing the need to customize the monitoring well construction at the individual location rather than conforming to a predetermined design.

Point dilution tests

Point dilution is a method that provides an estimate of the specific discharge of groundwater through specified intervals. The basic field technique involves the injection of a tracer into borehole segments that have been isolated by packers and the subsequent measurement of the change in concentration over time. A picture of the double packer is shown in **Figure 2-13**. Point dilution tests were performed in the GW821, GW822, and GW823 boreholes to further identify the major flow zones and to quantify the specific discharge from each of the zones. The results of these tests were used to decide sampling intervals for the packer sampler and the locations of the sampling ports for the multilevel wells.

Distilled water was used as a tracer and changes in concentration were measured by monitoring the specific conductance (SC). The basic procedure is briefly described as follows. First, the initial specific conductance of the formation groundwater within the packed interval was measured. Distilled water was then circulated through this zone until a suitable minimum conductance was achieved (for these tests, ~ 1/2 of the initial SC measurement). Once this level was reached, the well water was recirculated and the change in the specific conductance during recovery was monitored. Careful monitoring of the hydraulic head within the packed interval was done to ensure that gradients were not induced during circulation of the distilled water.

The recovery of the specific conductance over time was analyzed using the following equation (Freeze and Cherry, 1979):

$$\frac{VdC}{\partial t} = qA(C_f - C) \tag{2-1}$$

which, when rearranged, becomes:

$$\int_{C_o}^{C_b} \frac{dC}{C_f - C} = qA\int_0^t dt \tag{2-2}$$

and simplified to:

$$-\ln\frac{C - C_b}{C_f - C_0} = \frac{qA}{V}t \tag{2-3}$$

where:

q = specific discharge of interval

V = volume of interval

A = cross-sectional area of interval

t = time

C_f = specific conductance of formation water

C_b = specific conductance in well water at time, t

C_0 = initial specific conductance after injection of distilled water

By plotting the "ln term", $-\ln[(C_f-C_b)/(C_f-C_0)]$, versus recovery time, the data can be fit with a regression line (units 1/t), the slope of which is equal to qA/V. For most of the intervals tested, the data became linear after 10 to 15 minutes. For this reason, the tests were stopped before the recovery was complete but after a linear increase was sufficiently demonstrated. The first interval tested (66-68.5' in GW822) was allowed to recover for 120 minutes to see when the data reached linearity and if the slope changed significantly over time after linearity was reached. After 120 minutes, recovery was still not complete; however, the data became linear after approximately 20 minutes and remained consistent. All subsequent tests were run for a minimum of 30 minutes, longer if necessary until linearity was achieved.

The specific conductance of the formation water (C_f) within any given interval was highest at the beginning of the day. The C_f decreased during each series of tests, because the isolated flow zones were not allowed to recover completely before deflating the packers and moving to the next interval. This allowed a gradual mixing of distilled water within the borehole. For calculating the fraction of recovery (the "ln term"), the original C_f for each series was used for all intervals within the series, because this C_f is a measure of the true formation water without the influence of the injected distilled water.

In all cases, the specific conductance continued to drop for a few to several minutes after the start of the test, due to the addition of distilled water in the intake line.

Many of the recovery plots were undulating; however, they all converged around the best-fit line. In the case where a slope change occurred during recovery, regressions were applied to late-time data.

The results of the point dilution tests are summarized in **Figures 2-14** through **2-16**. Data and the recovery plots are included in **Appendix H.** Tests were conducted at two foot intervals starting at the bottom of casing (22.5' in GW821, 32' in GW822, 26' in GW823) and extending to the bottom of borehole. Zones that were excluded from testing were the washout zones (46-51') in GW823 and in zones of extremely turbid water (42.5-48') in GW821.

The results for GW821 (**Figure 2-14**) show relatively low specific discharge values, with most less than 50 cm/d. The highest value measured (124 cm/d) was in the 24-26.5' interval; however, because the bottom of casing is at 22', zones above 24' could not be tested. These results are consistent with the flowmeter and core data that indicate the absence of some of the higher flow zones seen in the other two boreholes. Several attempts that were made to test the zones below 40' in GW821 were unsuccessful. These zones contained extremely silty water that repeatedly clogged the sample tubing. When the silty water was pumped up into the flow-through cell, the SC readings would not stabilize, possibly due to the abundance of clay particles in the water.

The results for GW822 (**Figure 2-15**) show much higher specific discharge values than in GW821. Three zones in the interval from 60-70' have values less than 20 cm/d; however, all of the other zones have specific discharge in excess of 100 cm/d. In five out of six of the zones from 40-50', specific discharge exceeds 200 cm/d, corresponding with higher flow noted in the flowmeter tests and the observations of highly fractured and weathered rock from the core and the downhole video. The zones immediately below the casing, 34-38.5', have the highest specific discharge measured in the hole, at ~320 cm/d. These observations are also supported by flowmeter data and the video observations. While the core from these intervals did not contain heavy oxide staining, the shale was extremely clay-rich, weathered, and fissile. The flow in the cased intervals is likely to be even higher, judging from flowmeter data and core observations.

The results for GW823 (**Figure 2-16**) are misleading. The specific discharge appears to be low, below 100 cm/d. However, the zone of highest flow as indicated by flowmeter data is the washout interval at 46-51'. An attempt was made to place a five foot separation between the packers to test this zone. However, the packers did not seat properly and so the test could not be conducted. A second major zone was identified immediately below the casing (155 cm/d from 28-30.5').

2.5 Multilevel Well Installation

The results from all borehole tests were combined with observations from the core

logs to identify the major flow zones within each borehole. In general, the data from all of these tests were consistent. This information was then used to determine the locations for groundwater sampling using the packer sampler and the locations for installation of the multilevel sampling ports. Solinst multilevel wells with five sampling ports per well were installed in GW821, 822, and 823 in the fall of 1994. A general description of multilevel well design is included in Pickens et al. (1981). A site specific description of the multilevel well installation is provided in Moline and Schreiber (1995). The casing that was installed during drilling had to be pulled during installation; this procedure was difficult and led to the partial collapse of GW823. Much of the borehole needed to be reaugered before the multilevel device could be installed. The multilevel well configurations are shown in **Appendix A.**

2.6 Summary

In summary, the site characterization was designed to assess the flow characteristics of the shallow groundwater system at the field site. The well hydrographs show both seasonal and precipitation related variations in both the shallow and deep well pairs. The horizontal gradients are oriented to the southwest in the shallow wells and to the south in the deep wells. If a horizontal anisotropy ratio of 8:1 (strike:dip) is assumed, the shallow flow direction has a more westward orientation than the gradient and the orientation of the deep flow direction varies from south-southwest and to the south-southeast, although the vector mean remains similar to the gradient at 180 degrees. The upward vertical gradients have similar

magnitude to the shallow horizontal gradients, which supports the assumption that the field site is in a discharge zone.

The helium and bromide tracer tests were designed to characterize the ambient flow dynamics at the field site. The majority of helium and bromide transport was observed in the along-strike well pairs. The Rhodamine WT tracer test conducted by Lee et al. (1992) and the noble gas tracer test of Sanford et al. (1994) both show preferential tracer transport in the direction of strike. This preferential transport direction can be explained by the west-southwest orientation of the shallow horizontal flow direction when an anisotropy ratio of 8:1 (strike:dip) is assumed.

The bromide test showed the influence of matrix diffusion; although 15,200 ppm of bromide was present in the source well at the start of the test, no more than 5 ppm of bromide was ever detected in any of the wells, suggesting that bromide may have diffused into the matrix. Other studies on the ORR have identified matrix diffusion as a significant process in controlling groundwater chemistry in fractured sedimentary rocks (e.g. Toran et al., 1991). One explanation for the lack of significant bromide detection is that the bromide traveled through fractures that did not intersect the monitoring wells. None of the well pairs is located along the direction of the shallow gradient or flow direction from the source well. Therefore, it is likely that the well pairs are intercepting the fringes, and not the center, of the tracer plumes.

Three new boreholes were drilled at the field site. The core recovery was excellent in the saprolite and transition zone, but was not as good in the more competent shale. Soil cover was observed to be very thin, less than 6 inches thick. The saprolite recovered in core consists of silty sand and clay and is heavily stained and weathered. Wet silty zones were encountered in all three boreholes. The bedrock, part of the middle unit of the Nolichucky Shale, is interlayered shale and carbonate. Oxidized surfaces were observed in many sections of the core; these are interpreted to be fracture surfaces. The shale and carbonate units were correlated between the boreholes. These correlations support the 45º dip estimated by Gierke et al. (1988).

Two types of borehole tests, electromagnetic flowmeter and point dilution, were conducted to identify and characterize the active flow zones. The advantage of the flowmeter test is that it is less time-consuming than the point dilution and provides useful information about the relative permeability of the various flow intervals. However, it is subject to interference due to electrical noise and can be misleading if a single high permeability zone is able to handle all of the injected flow at the expense of any underlying zones. Point dilution tests provide definitive information about absolute flow rates and are not as susceptible to noise. They are, however, subject to uncertainty due to indeterminate packer seating.

The results of the hydraulic tests were generally consistent. The highest flow zone

in each of the boreholes is approximately at the saprolite/bedrock interface, termed the transition zone. No other significant flow zones were identified in GW821. A number of very high flow zones were identified in GW822, one distinct zone at approximately 58-60', a wider zone from approximately 40-50', and the zone at the top of bedrock. In addition to the high flow at the bedrock surface in GW823, a major flow zone which extends from approximately 45-52' was identified by the flowmeter and the borehole camera.

The combined information from the core descriptions and the hydraulic tests was then used to determine the locations for groundwater sampling using the packer sampler and the locations for installation of the multilevel sampling ports.

3. Geochemical Characterization

3.1 Introduction

The purpose of this chapter is to characterize the major geochemical processes and spatial trends in the shallow groundwater system at the field site. Examining the degree of spatial variability will aid in assessing the pattern of flow and chemical transport in this discharge zone. In addition, the sampling of spatial intervals on a small scale using the multilevel wells will provide more detailed information on the groundwater geochemistry than was possible in previous studies that relied on geochemical data from long-screened wells.

Pore water samples were collected from several intervals in the saprolite in an attempt to evaluate the chemical characteristics of matrix water. Two types of discrete zone samples, packer and multilevel well samples, were collected to assess the degree of vertical variability of groundwater chemistry. A sample from GW462, which is screened from 20 to 70', was collected to compare with discrete zone samples. The geochemical results are combined with results of the hydraulic tests to differentiate the major water types in the shallow groundwater system and to examine the relationship between groundwater flow and chemical transport in the shallow system.

3.2 Sampling Methods

Pore water sampling

Pore water samples were collected from saturated zones that were drilled without the use of water. Some were collected from the core at the time of drilling and others later during subsequent detailed core logging. A more thorough pore water sampling program was planned; however, the use of water during coring within the competent bedrock precluded pore water sampling below the saprolite.

Locations of pore water samples are shown in **Figure 3-1**. For this study, only the samples with sufficient moisture were prepared for analysis. Although PW82202/03 and PW82204/05 were collected from the same zones, they cannot be considered duplicate samples because they were collected at different times. One set was put into sample bottles in the field after the cores were extruded from the core barrel while the other set was sampled two months later during core logging. The cores were wrapped in plastic to minimize desiccation; however, a certain degree of gas diffusion likely occurred. All of the samples were centrifuged at the same time in 250 ml bottles until the minimum volume required for analysis was obtained. The supernatant was removed for analysis and the remaining sediment was discarded. The pore water samples were clear after centrifuging and were not filtered prior to analysis.

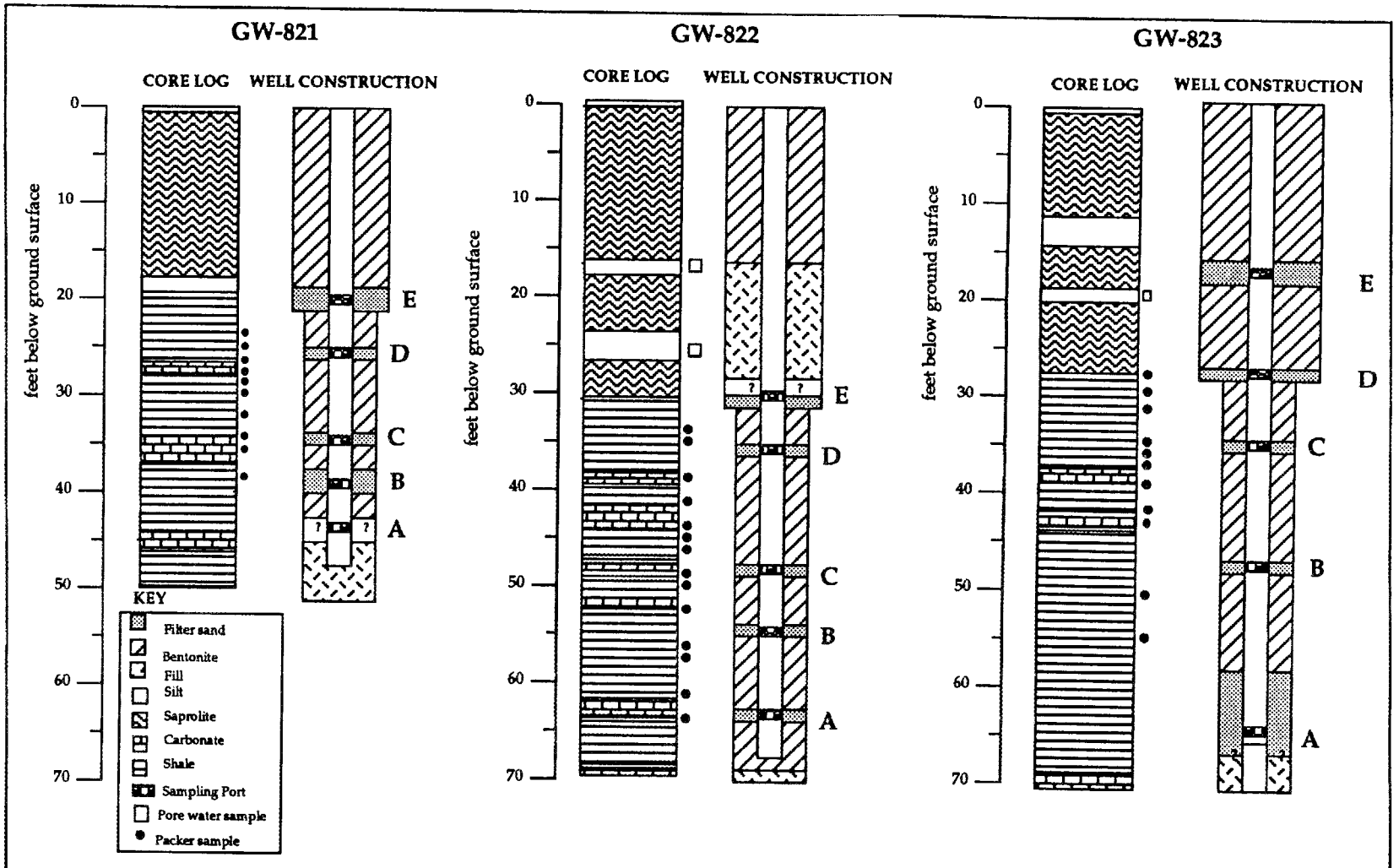

Figure 3-1: Locations of pore water, packer, and multilevel well samples.

Packer sampling

Discrete fracture zones identified from the combined information of flowmeter testing, point dilution testing, core log descriptions, and borehole camera observations were sampled using a packer sampler in the open boreholes, prior to the installation of multilevel wells. These zones are shown in **Figure 3-1**. The packer sampler, designed by Kent Novakowski at the National Water Research Institute, Ontario, allows sampling from discrete fracture zones. A six-inch grooved plate with a sampling port at the center is attached along the side of a packer. Sample tubing (1/8" O.D.) connects the sampling port through the inside of the packer to the surface. As the packer is inflated, the plate is pressed against the side of the borehole allowing water to be channeled along the groove in the plate and into the sampling port. A scaled-up version was built for this project that allowed samples to be obtained from larger diameter boreholes.

To sample discrete zones, the packer sampler was lowered into the borehole with the center of the sampling port at the center of the sampling interval and was inflated with nitrogen gas so that it contacted the borehole wall at approximately 20 psi. The volume of water in the sampling tube (approximately 100 ml) was then purged with a peristaltic pump prior to collecting the sample. All samples were placed in a cooler immediately upon collection and were refrigerated after they were brought in from the field.

Multilevel well sampling

The locations of the sampling ports in the multilevel wells are shown in **Figure 3-1**. The wells were purged and sampled using a peristaltic pump. One well volume was generally purged prior to sampling. The multilevel port GW822E was blocked and was not available for sampling. That port has since been cleared. GW462, screened from 20 to 70', was sampled using the same procedures as the multilevels. Purge water was monitored for pH, temperature, specific conductance, and turbidity using a Horiba U7 meter. Samples were filtered in the field using 0.45 micron filters and were then preserved if necessary. Preservation methods are presented in **Table 3-1**. All samples were placed in a cooler immediately upon collection and were refrigerated after they were brought in from the field.

3.3 Analytical Methods

The multilevel well and GW462 samples were analyzed for pH, temperature, specific conductance, and turbidity in the field. Specific conductance was temperature-corrected by the meter and was measured in umhos/cm (equivalent to uS/cm). The packer samples were analyzed only for specific conductance in the field. In the laboratory, all of the samples were analyzed for pH, anions (SO_4, Cl, NO_3, Br, F, PO_4), cations (Ca, Mg, Na, K, Al, Ag, B, Ba, Be, Cd, Co, Cr, Cu, Fe, Li, Mg, Mn, Mo, Ni, P, Pb, Se, Si, Se, V, Zn), alkalinity, and total organic carbon (TOC). A summary of sample collection and analytical methods is shown in **Table 3-1**.

Table 3-1: Summary of Sample Collection and Analytical Methods

Sample Type	Analytes	Volume (ml)	Filtered?	Preservation	Analytical	
					Method	Location
Pore water	cations	10	N	HCl pH<2	ICP	ACD
Groundwater (packer)	anions	5	N	none	IC	ESD
	alkalinity	10	N	none	Gran titration	ESD
	total organic C	5	N	HCl pH 2-3	High-T combustion	ESD
Groundwater (multilevel)	cations	10	Y	HNO3 pH<2	ICP	ACD
	anions	5	Y	none	IC	ESD
	alkalinity	10	N	none	Gran titration	ESD
	total organic C	5	N	HCl pH<2	High-T combustion	ESD

Notes:
HCl = hydrochloric acid
HNO3 = nitric acid
ICP = inductively coupled plasma spectroscopy
IC = ion chromotography
AA = atomic absorption
ACD = Analytical Chemistry Division, ORNL
ESD = Environmental Sciences Division, ORNL

3.4 Data Quality

The accuracy of the analytical methods was evaluated by comparing results of replicate analyses of the same sample for cations and anions. The accuracy of the sampling method was evaluated by comparing the results of analysis of duplicate samples collected at the same location under the same conditions. Duplicate samples were collected for multilevel well samples only. Charge-balance calculations were performed to evaluate both analytical and sampling methods. The percent charge balance error (% CBE) was calculated using the following equation:

$$\%CBE = \frac{\sum(z_c m_c) - \sum(z_a m_a)}{\sum(z_c m_c) + \sum(z_a m_a)} * 100 \qquad (3\text{-}1)$$

where:

z = valence of ion

m_c = molal concentrations of cations (Ca^{2+}, Fe^{2+}/Fe^{3+}, Mg^{2+}, K^+, Na^+)

m_a = molal concentrations of anions (HCO_3^-, Br^-, Cl^-, F^-, NO_3^-, PO_4^{3-}, SO_4^{2-}).

Because the ionic strength was low enough that the density of water could be assumed equal to 1 g/cm^3, molar concentrations were assumed to be equal to molal concentrations and were therefore used in the above equation. A charge imbalance of greater than 5% signifies poor sampling or analytical methods resulting in low quality data that should not be used for interpretation.

The presence of particulates and colloids in the samples was also evaluated. Unfiltered samples likely contain particulates. Filtered samples will not contain large particles but may contain colloids. Preservation of these samples with acid for cation analysis can dissolve these particles or strips sorbed ions, leading to results that are not representative of the dissolved species in groundwater. One technique used to evaluate the presence of particulates and/or colloids that contain iron is to calculate the charge balance error with and without iron. If the charge balance error has excess positive charge that is reduced to an acceptable level when iron is not included in the balance, then it is likely that particles containing iron are present in the sample. Iron is often not included in charge balance calculations due to the common occurrence of fine-grained iron oxides in groundwater samples (Dr. C.J. Bowser, personal communication). The solubility limits for certain ions in natural waters can also be used to determine if particles are contributing to high ion concentrations. For example, the solubility limit for aluminum is 0.02 to 0.04 mg/l (nearly neutral pH). Under oxidizing conditions, the solubility limit is 1 mg/l for manganese and 0.3 mg/l for iron (Hem, 1985). If groundwater of pH close to 7 has significantly higher concentrations of these types of ions, then colloidal contamination is likely. Evaluating the presence of colloids using this method is complicated by the formation of organic and inorganic complexes that will increase the total ion analytical concentrations.

3.5 Results

Pore water samples

A summary of results of the pore water sampling program is presented in **Table 3-2**. The complete chemical data are shown in **Appendix I**. The replicate analyses are often significantly different, especially with respect to chloride, sulfate, and aluminum. Duplicate samples could not be collected due to the difficulty in extracting sufficient volumes for analysis, so the sampling method cannot be evaluated. With the exception of PW82306, the results for the pore water analyses show very high concentrations of both cations and anions (TDS up to 850 mg/l).

Charge balance calculations with and without iron are shown in **Table 3-3**. The pore waters have significant charge balances errors. All samples with the exception of PW82306 have excess positive charge. The errors are reduced slightly if iron is not included in the balance, suggesting that iron may be contributing to the charge imbalance. Recognizing that particulates could contribute not only iron but also other cations to samples preserved with acid, these results suggest that the positive charge imbalances may be due to the presence of particulates or colloids as a result of not filtering the samples. This hypothesis is supported by concentrations of aluminum, iron, manganese, chromium, nickel, and silver are all significantly above their respective solubility limits.

Table 3-2: Pore Water Sample Results Summary

			Major Anions			Minor Anions		
Sample	depth ft	Lab pH	HCO3 (mg/L)	SO4 (mg/L)	Cl (mg/L)	Br (mg/L)	NO3 (mg/L)	PO4 (mg/L)
PW82202	16.00	8	353.33	102.78	72.76	0.8852	0	0.1175
PW82202R	16.00	8	353.33	97.31	68.27	0.8402	0	0.1159
PW82203	16.00	8	185.56	64.16	65.24	0.7926	0	0.1325
PW82203R	16.00	8	185.56	65.44	66.96	0.8088	0	0.0685
PW82204	25.00	8	177.27	20.08	8.79	0.1166	0	0
PW82204R	25.00	8	177.27	20.34	9.52	0.1123	0	0.1386
PW82205	25.00	8	161.67	20.92	9.61	0.1086	0	0.0438
PW82205R	25.00	8	161.67	20.97	9.57	0.1157	0	0.2326
PW82306	18.00	6	3.41	18.91	83.50	0.3909	0.2173	0.0821
PW82306R	18.00	6	3.41	13.22	21.18	0.1452	0.1919	0.0629

		Major Cations				Minor Cations				
Sample	depth	Ca (mg/L)	Mg (mg/L)	Na (mg/L)	K (mg/L)	Al (mg/L)	Fe (mg/L)	Mn (mg/L)	Si (mg/L)	Sr (mg/L)
PW82202	16.00	260	12.0	21.0	7.4	6.8	11	3	15	0.52
PW82202R	16.00	260	12.0	21.0	7.4	7.8	11	3	15	0.52
PW82203	16.00	99	8.6	17.0	6.5	2.5	3.3	1.4	6.8	0.19
PW82203R	16.00	99	8.6	17.0	6.5	3.5	3.3	1.4	6.8	0.19
PW82204	25.00	68	5.0	3.5	4.0	7.9	11	1.6	17	0.13
PW82204R	25.00	68	5.0	3.5	4.0	8.9	11	1.6	17	0.13
PW82205	25.00	65	8.2	3.3	5.4	17	23	2.9	32	0.13
PW82205R	25.00	65	8.2	3.3	5.4	18	23	2.9	32	0.13
PW82306	18.00	2	0.3	1.2	<2	0.53	0.83	0.12	5.6	0.0053
PW82306R	18.00	2	0.3	1.2	<3	1.53	0.83	0.12	5.6	0.0053

Notes:
Not all data shown due to non-detection or very low concentrations. Full data set included in Appendix I.
R = replicate analysis

Table 3-3: Pore Water Sample Charge Balance Calculations

		with Fe			without Fe		
		Cations	Anions		Cations	Anions	
Sample	%CBE	meq/L	meq/L	%CBE	meq/L	meq/L	%CBE
PW82202	22.05	15.65	10.00	22.05	15.06	10.00	20.21
PW82202R	23.21	15.65	9.76	23.21	15.06	9.76	21.38
PW82203	3.85	6.73	6.23	3.85	6.55	6.23	2.52
PW82203R	3.26	6.73	6.30	3.26	6.55	6.30	1.93
PW82204	13.10	4.65	3.57	13.10	4.06	3.57	6.37
PW82204R	12.68	4.65	3.60	12.68	4.06	3.60	5.95
PW82205	23.61	5.43	3.36	23.61	4.20	3.36	11.12
PW82205R	23.52	5.43	3.36	23.52	4.20	3.36	11.03
PW82306	-85.53	0.22	2.82	-85.53	0.17	2.82	-88.30
PW82306R	-61.99	0.22	0.94	-61.99	0.22	0.94	-61.99

Notes:
R = replicate analysis

Packer samples

A summary of results for the packer samples is presented in **Table 3-4**. The complete chemical data, are shown in **Appendix I**. In general, the replicate analyses deviated less than 5%. The exceptions were for chloride for the GW82116 and GW82121 replicates, which deviated 12% and 18%, respectively, and potassium concentrations for the replicate samples GW82325 and GW82335, which deviated 16% and 19%, respectively. No duplicate packer samples were collected.

Charge balance calculations are shown in **Table 3-5**. When the charge balance error calculations include iron, almost one-half (16) of the sample analyses, not including replicates, have charge balance errors of greater than 5%. When iron was taken out of the charge balance calculations, only 12 samples had errors greater than 5%. As discussed previously, particulates that can contribute iron to solution may also contribute other cations to samples preserved with acid. These results suggest that the positive charge imbalances in the packer samples may be due to presence of particulates as a result of not filtering the samples.

Multilevel well samples

A summary of results for the multilevel well and GW462 samples is presented in **Table 3-6**. Replicate analyses were generally consistent with the exception of aluminum concentrations of the replicates for GW822A and GW823D.

Table 3-4: Packer Sample Results Summary

				Major Anions			Minor Anions		
Well/sample#	depth ft	Lab pH	Spec. Cond. (uS/cm)	HCO3 (mg/L)	SO4 (mg/L)	Cl (mg/L)	Br (mg/L)	NO3 (mg/L)	PO4 (mg/L)
GW82115	24	8.27	339.0	210.8	5.8526	0.7652	0.0152	0	0
GW82115RC	24	8.27		210.8	5.8526	0.7652	0.0152	0	0
GW82116	25.5	8.16	340.0	209.5	6.1116	0.7825	0	0.0366	0
GW82116RA	25.5	8.16		209.5	6.0908	0.8877	0.061	0	0
GW82117	27.4	7.99	344.0	209.2	6.203	0.8357	0	0	0
GW82118	28.6	8.02	345.0	211.0	6.1366	1.0019	0	0	0
GW82119	30.2	8.02	346.0	215.7	6.2116	0.9688	0	0	0
GW82120	32.2	8.08	345.0	212.9	6.105	1.2764	0	0	0
GW82121	33	8.00	347.0	214.9	6.0776	1.2896	0	0	0
GW82121RA	33	8.00		214.9	6.0712	0.9195	0	0	0
GW82122	35.2	8.09	345.0	210.8	6.3012	0.8794	0	0	0
GW82123	37	8.04		210.2	6.1738	0.9488	0	0	0.0784
GW82124	39	7.93	347.0	220.8	6.1685	0.9615	0	0	0
GW82214	33.3	8.01	348.0	211.5	6.6351	1.243	0.3518	0	0
GW82201	34.6	8.00	311.0	219.6	6.7757	1.1144	0.376	0.0271	0
GW82201RA	34.6	8.00		219.6	6.69	1.0673	0.335	0	0
GW82202	37.7	7.97	344.0	219.5	6.5156	0.9512	0.3409	0.0453	0
GW82203	41	8.01	341.0	224.9	6.5718	1.0148	0.3495	0.0852	0
GW82204	42.7	8.21	315.0	216.2	6.5511	0.889	0.3388	0.0524	0
GW82205	45	8.18	342.0	213.5	6.4592	1.1765	0.3458	0	0
GW82205RC	45	8.18		213.5	6.4592	1.1765	0.3458	0	0
GW82206	47	8.17	342.0	220.1	6.5468	0.929	0.3452	0.0667	0
GW82206RA	47	8.17		220.1	6.605	0.9777	0.3358	0.0695	0
GW82207	48.7	8.14	341.0	247.1	6.5068	1.0262	0.3278	0.0388	0
GW82208	51.3	8.26	339.0	210.9	6.511	0.9421	0.3235	0.0814	0
GW82209	53	8.04	334.0	212.1	6.5209	0.9434	0.2998	0.0546	0
GW82213	55.5	8.10	338.0	212.3	6.7633	0.9691	0.3081	0.0832	0
GW82210	57.2	7.98	336.0	214.8	6.4854	0.9064	0.2844	0.0422	0
GW82211	61	8.02	328.0	218.7	6.5418	1.0001	0.2329	0.0537	0
GW82211RA	61	8.02		218.7	6.2463	1.0034	0.2209	0.0475	0
GW82212	63.2	7.99	344.0	215.9	6.3498	1.0017	0.2041	0.0443	0
GW82325	27.7	7.84	326.0	210.7	6.3313	1.0593	1.44	0	0
GW82325RC	27.7	7.84		210.7	6.3313	1.0593	1.44	0	0
GW82326	29	7.78	350.0	217.8	6.2774	1.0658	1.4543	0	0
GW82326RA	29	7.78		217.8	6.2538	1.1039	1.4406	0	0
GW82327	32	7.85	315.0	272.0	6.3227	1.1194	1.4133	0	0
GW82328	34.9	7.82	349.0	217.9	5.9935	0.973	1.4279	0	0
GW82329	36	7.82	349.0	218.5	6.0924	1.0609	1.4004	0	0
GW82330	37	7.89	352.0	219.5	5.939	1.3097	1.398	0	0
GW82331	39	7.84	350.0	210.3	5.9272	0.8923	1.3913	0	0
GW82331RA	39	7.84		210.3	6.1177	0.9835	1.4265	0	0
GW82332	42	8.00	335	210.2	6.0838	0.9303	1.4385	0.0078	0
GW82333	43.1	7.98	332	213.5	6.0892	0.948	1.408	0	0
GW82335	51.2	8.02	345	216.5	6.1291	0.9865	1.2923	0	0.1188
GW82335RC	51.2	8.02		216.5	6.1291	0.9865	1.2923	0	0.1188
GW82334	55.1	7.99	339	218.8	6.1788	0.908	1.1672	0.0284	0

Not all data shown due to non-detection or low concentrations. Full data set included in Appendix I.

RC = replicate cation analysis

RA = replicate anion analysis

Table 3-4: Packer Sample Results Summary (con't)

		Major Cations					Minor Cations				
	depth	Ca	Mg	Na		K	Al	Fe	Mn	Si	Sr
Well/sample#	ft	(mg/L)	(mg/L)	(mg/L)		(mg/L)	(mg/L)	(mg/L)	(mg/L)	(mg/L)	(mg/L)
GW82115	24	58	8.3	6.3	<	2	0.95	2.2	0.25	9.2	0.37
GW82115RC	24	58	8.2	6.2		2.2	0.94	2.2	0.25	9.1	0.37
GW82116	25.5	55	8.2	6.5	<	2	0.58	2.3	0.32	8.6	0.41
GW82116RA	25.5	55	8.2	6.5	<	3	1.58	2.3	0.32	8.6	0.41
GW82117	27.4	55	8.4	6.8		2.3	0.47	1.6	0.32	8.6	0.43
GW82118	28.6	56	8.5	6.8		2.2	0.52	2.1	0.35	8.7	0.44
GW82119	30.2	55	8.5	7	<	2	0.49	1.7	0.36	8.6	0.45
GW82120	32.2	58	9	7.2	<	2	1.1	3.6	0.48	9.4	0.47
GW82121	33	67	10	7.1		3.1	3.3	7.8	0.87	12	0.5
GW82121RA	33	67	10	7.1		3.1	4.3	7.8	0.87	12	0.5
GW82122	35.2	62	9.8	7.1		2.5	2.6	9.8	1	11	0.5
GW82123	37	60	9.7	7.3		2.5	2.1	6.7	0.78	11	0.51
GW82124	39	58	9.6	7.9		2.7	1.4	4.1	0.66	9.8	0.53
GW82214	33.3	65	9	6.6		2	1.3	5.9	0.28	10	0.46
GW82201	34.6	60	8	6.5	<	2	0.49	2.1	0.16	9.8	0.45
GW82201RA	34.6	60	8	6.5	<	3	1.49	2.1	0.16	9.8	0.45
GW82202	37.7	58	7.7	6.5	<	2	0.17	0.96	0.14	9.2	0.45
GW82203	41	60	8	6.7	<	2	0.61	2.3	0.16	9.8	0.45
GW82204	42.7	48	7.1	6.1	<	2	0.09	0.58	0.12	8.6	0.41
GW82205	45	60	7.8	6.5	<	2	0.33	1.6	0.15	9.4	0.45
GW82205RC	45	60	7.7	6.5	<	2	0.33	1.6	0.15	9.4	0.45
GW82206	47	58	7.6	6.6	<	2	0.17	0.91	0.14	9.2	0.45
GW82206RA	47	58	7.6	6.6	<	3	1.17	0.91	0.14	9.2	0.45
GW82207	48.7	58	7.7	6.6	<	2	0.27	0.9	0.15	9.3	0.44
GW82208	51.3	50	7.6	6.9	<	2	0.05	0.2	0.13	9.2	0.48
GW82209	53	50	7.6	6.9	<	2	0.074	0.47	0.13	8.8	0.47
GW82213	55.5	61	8.9	7	<	2	0.98	2.5	0.19	10	0.5
GW82210	57.2	57	8.1	7		2.1	0.37	1.3	0.15	9	0.53
GW82211	61	73	10	8.2		2.7	2.5	6.1	0.34	11	0.66
GW82211RA	61	73	10	8.2		2.7	3.5	6.1	0.34	11	0.66
GW82212	63.2	61	10	8.9		2.3	1.6	3.5	0.22	11	0.68
GW82325	27.7	110	8.7	6.4		3.1	1.7	6.8	1.2	9.6	0.45
GW82325RC	27.7	110	8.6	6		2.6	1.6	6.7	1.2	9.5	0.44
GW82326	29	76	9.9	6.2		2.4	4.5	11	0.8	14	0.39
GW82326RA	29	76	9.9	6.2		2.4	5.5	11	0.8	14	0.39
GW82327	32	59	7.6	6.3	<	2	0.72	3.4	0.49	8.8	0.37
GW82328	34.9	59	7.4	6.4	<	2	0.32	2.2	0.44	8.8	0.37
GW82329	36	59	7.5	6.2	<	2	0.55	2.6	0.45	9	0.37
GW82330	37	59	7.5	6.4	<	2	0.71	6.2	0.48	9.3	0.37
GW82331	39	62	7.8	6.7	<	2	0.45	2.9	0.45	9.3	0.39
GW82331RA	39	62	7.8	6.7	<	3	1.45	2.9	0.45	9.3	0.39
GW82332	42	62	7.9	6.9	<	2	0.64	3.7	0.48	9.6	0.4
GW82333	43.1	61	7.7	6.9	<	2	0.37	202	0.45	9.1	0.39
GW82335	51.2	70	9.5	7.9		2.5	3.4	16	1.6	14	0.45
GW82335RC	51.2	71	9.6	7.8		3.1	3.4	16	1.6	14	0.45
GW82334	55.1	74	10	9.1		3.1	3.6	14	2.3	14	0.49

Not all data shown due to non-detection or low concentrations. Full data set included in Appendix I.

RC = replicate cation analysis

RA = replicate anion analysis

Table 3-5: Packer Sample Charge Balance Calculations

		with Fe			without Fe		
Sample	depth ft	Cations meq/L	Anions meq/L	CBE %	Cations meq/L	Anions meq/L	CBE %
GW82115	24.0	3.97	3.60	4.90	3.85	3.60	3.39
GW82115RC	24.0	4.01	3.60	5.44	3.89	3.60	3.95
GW82116	25.5	3.83	3.58	3.27	3.70	3.58	1.63
GW82116RA	25.5	3.83	3.59	3.23	3.70	3.59	1.59
GW82117	27.4	3.88	3.58	3.95	3.79	3.58	2.83
GW82118	28.6	3.96	3.61	4.53	3.85	3.61	3.09
GW82119	30.2	3.84	3.69	1.96	3.75	3.69	0.76
GW82120	32.2	4.14	3.65	6.27	3.95	3.65	3.89
GW82121	33.0	4.97	3.69	14.87	4.55	3.69	10.54
GW82121RA	33.0	4.97	3.68	15.01	4.55	3.68	10.68
GW82122	35.2	4.80	3.61	14.13	4.27	3.61	8.39
GW82123	37.0	4.53	3.60	11.44	4.17	3.60	7.34
GW82124	39.0	4.32	3.77	6.70	4.10	3.77	4.09
GW82214	33.3	4.64	3.64	12.00	4.32	3.64	8.50
GW82201	34.6	4.05	3.81	2.99	3.93	3.81	1.58
GW82201RA	34.6	4.05	3.81	3.04	3.93	3.81	1.63
GW82202	37.7	3.86	3.76	1.28	3.81	3.76	0.61
GW82203	41.0	4.07	3.86	2.64	3.94	3.86	1.10
GW82204	42.7	3.28	3.71	-6.21	3.24	3.71	-6.69
GW82205	45.0	4.00	3.67	4.34	3.92	3.67	3.26
GW82205RC	45.0	4.00	3.67	4.24	3.91	3.67	3.16
GW82206	47.0	3.86	3.77	1.06	3.81	3.77	0.42
GW82206RA	47.0	3.86	3.78	1.02	3.81	3.78	0.38
GW82207	48.7	3.86	4.22	-4.41	3.81	4.22	-5.04
GW82208	51.3	3.43	3.62	-2.74	3.42	3.62	-2.90
GW82209	53.0	3.45	3.64	-2.80	3.42	3.64	-3.17
GW82213	55.5	4.21	3.65	7.15	4.08	3.65	5.54
GW82210	57.2	3.94	3.69	3.32	3.87	3.69	2.42
GW82211	61.0	5.22	3.75	16.34	4.89	3.75	13.16
GW82211RA	61.0	5.22	3.75	16.42	4.89	3.75	13.25
GW82212	63.2	4.50	3.70	9.73	4.31	3.70	7.61
GW82325	27.7	6.93	3.63	31.20	6.56	3.63	28.74
GW82325DC	27.7	6.88	3.63	30.92	6.52	3.63	28.47
GW82326	29.0	5.53	3.75	19.20	4.94	3.75	13.70
GW82326RA	29.0	5.53	3.75	19.19	4.94	3.75	13.70
GW82327	32.0	4.03	4.64	-7.08	3.84	4.64	-9.38
GW82328	34.9	3.95	3.74	2.71	3.83	3.74	1.19
GW82329	36.0	3.97	3.75	2.79	3.83	3.75	1.00
GW82330	37.0	4.17	3.77	5.00	3.84	3.77	0.85
GW82331	39.0	4.18	3.61	7.31	4.03	3.61	5.42
GW82331RA	39.0	4.18	3.62	7.21	4.03	3.62	5.32
GW82332	42.0	4.24	3.62	7.97	4.04	3.62	5.58
GW82333	43.1	14.83	3.67	60.32	3.98	3.67	4.02
GW82335	51.2	5.54	3.72	19.61	4.68	3.72	11.39
GW82335RC	51.2	5.61	3.72	20.21	4.75	3.72	12.12
GW82334	55.1	5.74	3.76	20.91	4.99	3.76	14.11

Notes: RA = replicate anion analysis, RC = replicate cation analysis

Duplicate samples were also collected and analyzed. The duplicates for GW821D and GW823A are significantly different (>90%) from the original sample with respect to aluminum and iron concentrations. Although these percent differences are high, it is important to remember that the concentrations are very low and that small absolute differences generate large percentage changes. The most probable cause of these inconsistencies is minor colloidal contamination. Because the multilevel well samples were filtered prior to analysis, the presence of particles in the samples was minimized, however, colloids, including iron and aluminum hydroxides, can pass through 0.45 micron filters (Appelo and Postma, 1993). The presence of colloids is supported by concentrations of aluminum, iron, and manganese that exceed the solubility limits. The complete chemical data are shown in **Appendix I**.

The results of the charge balance calculations for the multilevel well and GW462 samples are presented in **Table 3-7**. The charge balances for the multilevel well samples are excellent. With one exception, the charge balance errors are all below 5%. Charge balance errors were also calculated without iron. The results show no significant decrease in the errors, suggesting that iron is not a major source of error in the multilevel well samples. The positive and negative charge balance errors are balanced, indicating that the errors are random and are not systematic (Fritz, 1994). The charge imbalance for the GW462 sample was -1%.

Table 3-6: Multilevel Well and GW462 Sample Results Summary

Well/sample	depth ft	Purge vol (ml)	Lab pH	Field pH	TOC (ppm)	Temp (deg C)	Turb. (ppm)	Major Anions HCO3 (mg/L)	SO4 (mg/L)	Cl (mg/L)	Minor Anions Br (mg/L)	F (mg/L)	NO3 (mg/L)	PO4 (mg/L)
GW462	20-70	11000	7.58	7.5	0.194	11.9	172	226.77	6.8	0.85	0.35	< 0.1	< 0.1	< 0.5
GW821E	20.0	250	7.86	7.7	0.445	5.6	140	184.35	6.9	0.94	< 0.1	< 0.1	0.55	< 0.5
GW821ERC	20.0		7.86	7.7		5.6	140	184.35	6.9	0.94	< 0.1	< 0.1	0.55	< 0.5
GW821D	25.5	1000	7.82	7.6	0.254	5.6	330	214.09	7.3	1.1	< 0.1	0.12	< 0.1	< 0.5
GW821DD	25.5		7.82	7.6		5.6	330	211.29	6.6	0.92	< 0.1	< 0.1	0.32	< 0.5
GW821C	34.0	1250	7.99	7.5	0.836	6.9	400	238.48	31	1.5	< 0.1	< 0.1	1.3	< 0.5
GW821CRA	34.0		7.99	7.5		6.9	400	238.48	31	1.4	< 0.1	< 0.1	1.2	< 0.5
GW821B	38.5	1500	8.12	7.6	1.082	7.2	100	244.57	45	1.5	< 0.1	< 0.1	1.9	< 0.5
GW821A	45.5	1750	8.37	7.9	4.681	7.7	140	231.77	30	3.1	< 0.1	0.1	1.6	< 0.5
GW822E	29.5	1150	8.28	7.4	0.727	11.2	60	223.48	6.9	1	4.7	< 0.1	0.32	< 0.5
GW822D	34.0	1350	7.85	7.4	2.005	4.9	130	249.33	41	1.5	< 0.1	< 0.1	0.57	< 0.5
GW822DRA	34.0		7.85	7.4		4.9	130	249.33	41	1.4	< 0.1	< 0.1	0.58	< 0.5
GW822C	48.5	0.12	8.04	7.5	4.851	3.6	200	263.84	110	3.7	0.14	< 0.1	0.9	< 0.5
GW822B	54.0	2050	7.77	7.3	0.537	7.5	190	233.36	20	1	< 0.1	< 0.1	0.51	< 0.5
GW822A	65.0	2500	7.76	7.5	0.646	10	210	218.48	11	0.82	< 0.1	< 0.1	< 0.1	< 0.5
GW822ARC	65.0		7.76	7.5		10	210	218.48	11	0.82	< 0.1	< 0.1	< 0.1	< 0.5
GW822AD	65.0		7.71	7.5		10	210	223.48	10	0.83	< 0.1	< 0.1	< 0.1	< 0.5
GW823D	27.0	1075	7.71	7.2	3.543	10.1	330	329.55	170	5.5	1.8	< 0.1	< 0.1	< 0.5
GW823DRC	27.0		7.76	7.2		10.1	330	329.55	170	5.5	1.8	< 0.1	< 0.1	< 0.5
GW823C	35.5	1400	7.86	7.3	1.183	9.7	270	275.05	28	2.9	0.42	< 0.1	0.56	< 0.5
GW823CRA	35.5		7.86	7.3		9.7	270	275.05	28	2.9	0.41	< 0.1	0.56	< 0.5
GW823B	48.0	1900	7.75	7.4	0.289	10.9	195	226.29	11	1	0.34	0.1	0.33	< 0.5
GW823A	65.5	2500		8.1	2.076	5.7	310	241.53	11	1.3	< 0.1	0.17	0.36	< 0.5
GW823AD	65.5		8.01	8.1		5.7	310	241.53	11	1.3	< 0.1	0.17	0.37	< 0.5

Note: Not all data are shown due to non-detects or very low concentrations. Full data set included in Appendix I.

RC = replicate cation analysis

RA = replicate anion analysis

D = duplicate sample

Table 3-6: Multilevel Well and GW462 Sample Results Summary (con't)

		Major Cations					Minor Cations				
Well/sample	depth ft	Ca (mg/L)	Mg (mg/L)	Na (mg/L)		K (mg/L)	Al (mg/L)	Fe (mg/L)	Mn (mg/L)	Si (mg/L)	Sr (mg/L)
GW462	20-70	52	9.4	8.5		2.4	< 0.05	0.21	0.28	9.4	0.67
GW821E	20.0	47	5.9	6.8	<	2	< 0.05	< 0.05	0.36	7.3	0.21
GW821ERC	20.0	47	5.9	6.8	<	2	< 0.05	< 0.05	0.36	7.3	0.21
GW821D	25.5	56	7.1	7.4	<	2	0.73	0.43	0.35	9.3	0.65
GW821DD	25.5	55	7	7.4	<	2	< 0.05	< 0.05	0.31	7.8	0.56
GW821C	34.0	41	7.6	47	<	2	3.8	1.5	0.84	17	1
GW821CRA	34.0	41	7.6	47	<	2	3.8	1.5	0.84	17	1
GW821B	38.5	29	7	68		2.2	1.8	0.62	0.51	13	0.98
GW821A	45.5	28	6.5	60		3.1	2.5	1.2	0.85	13	1.2
GW822E	29.5	62	6.1	5	<	2	< 0.05	< 0.05	0.021	7.1	0.36
GW822D	34.0	58	9.4	33		2.4	0.19	0.19	0.17	10	0.57
GW822DRA	34.0	58	9.4	33		2.4	0.19	0.19	0.17	10	0.57
GW822C	48.5	49	7.7	82		3.2	0.053	0.07	0.63	7.7	0.94
GW822B	54.0	51	9	21	<	2	0.053	< 0.05	0.1	8.9	0.67
GW822A	65.0	43	9.6	18		2.9	0.16	0.31	0.16	9.6	0.82
GW822ARC	65.0	43	9.6	18		2.8	1.7	0.32	0.16	9.6	0.82
GW822AD	65.0	43	9.5	18		2.8	0.15	0.31	0.16	9.5	0.81
GW823D	27.0	61	7.1	120	<	2	0.96	0.76	5.8	8.2	1.7
GW823DRC	27.0	59	7.1	120		2.4	1.3	0.9	5.8	9	1.7
GW823C	35.5	55	6.8	46		2.2	1.9	0.84	0.54	11	1.3
GW823CRA	35.5	55	6.8	46		2.2	1.9	0.84	0.54	11	1.3
GW823B	48.0	51	6.2	19	<	2	< 0.05	< 0.05	0.3	7.6	0.46
GW823A	65.5	38	6.1	24	<	2	0.76	0.43	1.8	6.9	1.1
GW823AD	65.5	46	7.3	29	<	2	< 0.05	< 0.05	2.1	6.7	0.53

Note: Not all data are shown due to non-detects or very low concentrations. Full data set included in Appendix I.

RC = replicate cation analysis

RA = replicate anion analysis

D = duplicate sample

Table 3-7: Multilevel Well and GW462 Sample Charge Balance Calculations

		with Fe			without Fe		
Well/sample	depth ft	Cations meq/l	Anions meq/l	CBE %	Cations meq/l	Anions meq/l	CBE %
GW462	20-70	3.81	3.89	-0.99	3.80	3.89	-1.14
GW821E	20.0	3.13	3.20	-1.17	3.13	3.20	-1.17
GW821ERC	20.0	3.13	3.20	-1.17	3.13	3.20	-1.17
GW821D	25.5	3.72	3.70	0.34	3.70	3.70	0.03
GW821DD	25.5	3.64	3.63	0.15	3.64	3.63	0.15
GW821C	34.0	4.80	4.62	1.89	4.71	4.62	1.05
GW821CRA	34.0	4.80	4.61	1.94	4.71	4.61	1.09
GW821B	38.5	5.07	5.02	0.51	5.04	5.02	0.18
GW821A	45.5	4.68	4.54	1.55	4.62	4.54	0.86
GW822E	29.5	3.81	3.90	-1.11	3.81	3.90	-1.11
GW822D	34.0	5.17	4.99	1.80	5.16	4.99	1.70
GW822DRA	34.0	5.17	4.99	1.82	5.16	4.99	1.72
GW822C	48.5	6.73	6.73	-0.04	6.73	6.73	-0.07
GW822B	54.0	4.20	4.28	-0.93	4.20	4.28	-0.93
GW822A	65.0	3.81	3.83	-0.32	3.79	3.83	-0.53
GW822ARC	65.0	3.81	3.83	-0.34	3.79	3.83	-0.57
GW822AD	65.0	3.80	3.89	-1.25	3.78	3.89	-1.47
GW823D	27.0	8.89	9.12	-1.29	8.85	9.12	-1.52
GW823DRC	27.0	8.86	9.12	-1.46	8.81	9.12	-1.73
GW823C	35.5	5.41	5.19	2.06	5.36	5.19	1.64
GW823CRA	35.5	5.41	5.19	2.06	5.36	5.19	1.65
GW823B	48.0	3.88	3.98	-1.27	3.88	3.98	-1.27
GW823A	65.5	3.46	4.24	-10.05	3.44	4.24	-10.38
GW823AD	65.5	4.16	4.24	-0.98	4.16	4.24	-0.98

Notes:
RC = replicate cation analyses
RA = replicate anion analyses
D = duplicate sample

3.6 Discussion

The results of the sampling program indicate that the shallow groundwater in the Nolichucky Shale at the field site is neutral to slightly alkaline (pH 7-8). Precipitation in the ORR has a pH of approximately 4.5 (NADP, 1994). The pH changes after infiltration can be explained by the reaction of infiltrating water with carbonate minerals in saprolite and bedrock underlying the field site. The major anions follow this general order of decreasing concentration: $HCO_3^- >> SO_4^{2-} > Cl^-$. The major cations follow this general order of decreasing concentration: $Ca^{2+} > Na^+ > Mg^{2+} >> K^+$, although there are exceptions.

In order to evaluate the general chemical characteristics of the shallow groundwater, different graphical presentations of the chemical data are used, including major and minor ion concentration profiles to examine spatial geochemical variability and trilinear and Stiff diagrams to evaluate the relative proportions of the major ions. A common way to group waters is to classify them by the dominant cation and anion (meq/L), e.g., a calcium bicarbonate type water has calcium as the dominant cation and bicarbonate as the dominant anion (Hem, 1985).

Major Ion Trends

Multilevel well samples

Concentration profiles of the major ions for the multilevel well samples are shown in **Figures 3-2** through **3-4**. **Figure 3-2** shows the major ion profiles in GW821.

GW821 Multilevel Major Ions

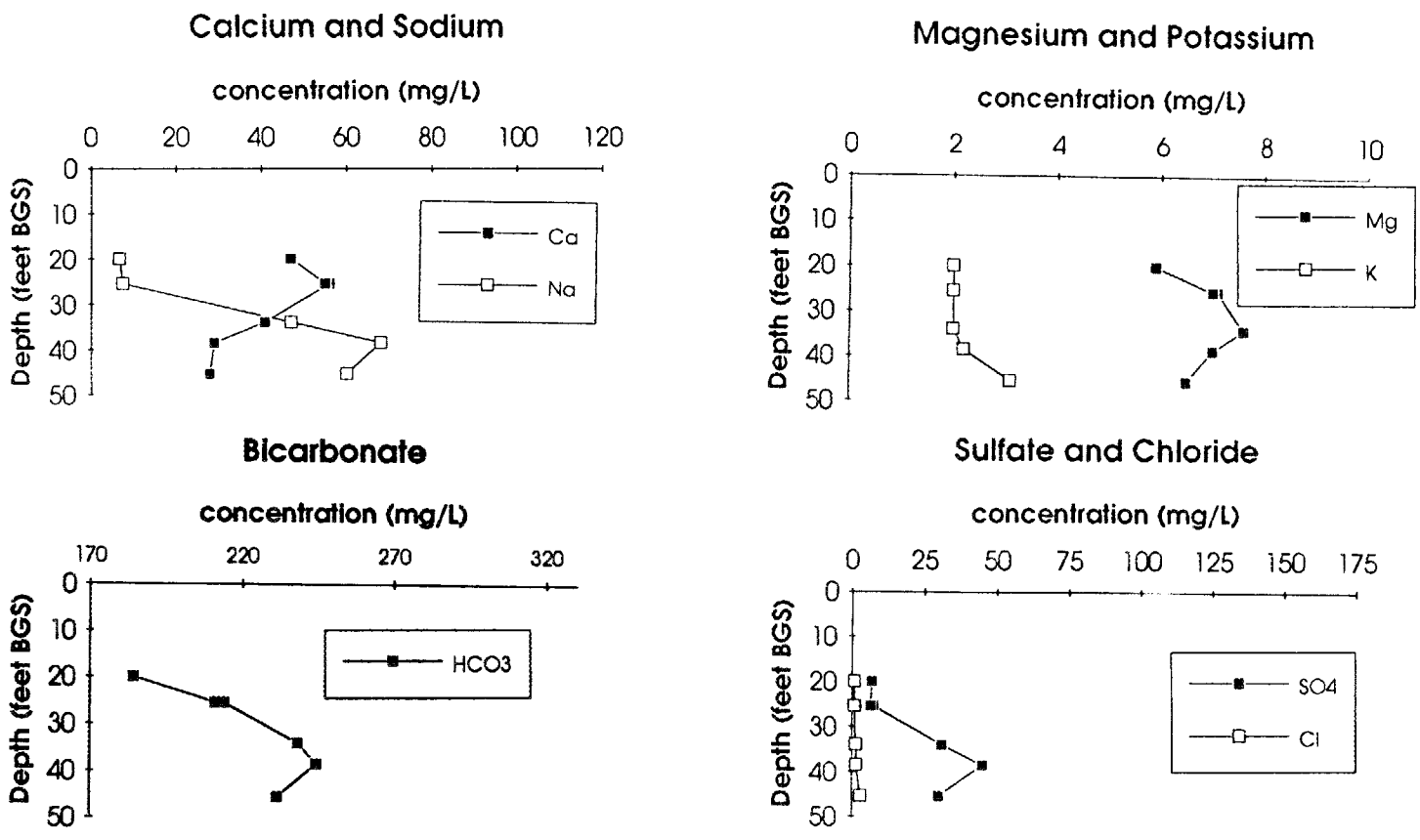

Figure 3-2: GW821 multilevel major ion concentration profiles.

GW822 Multilevel Major Ions

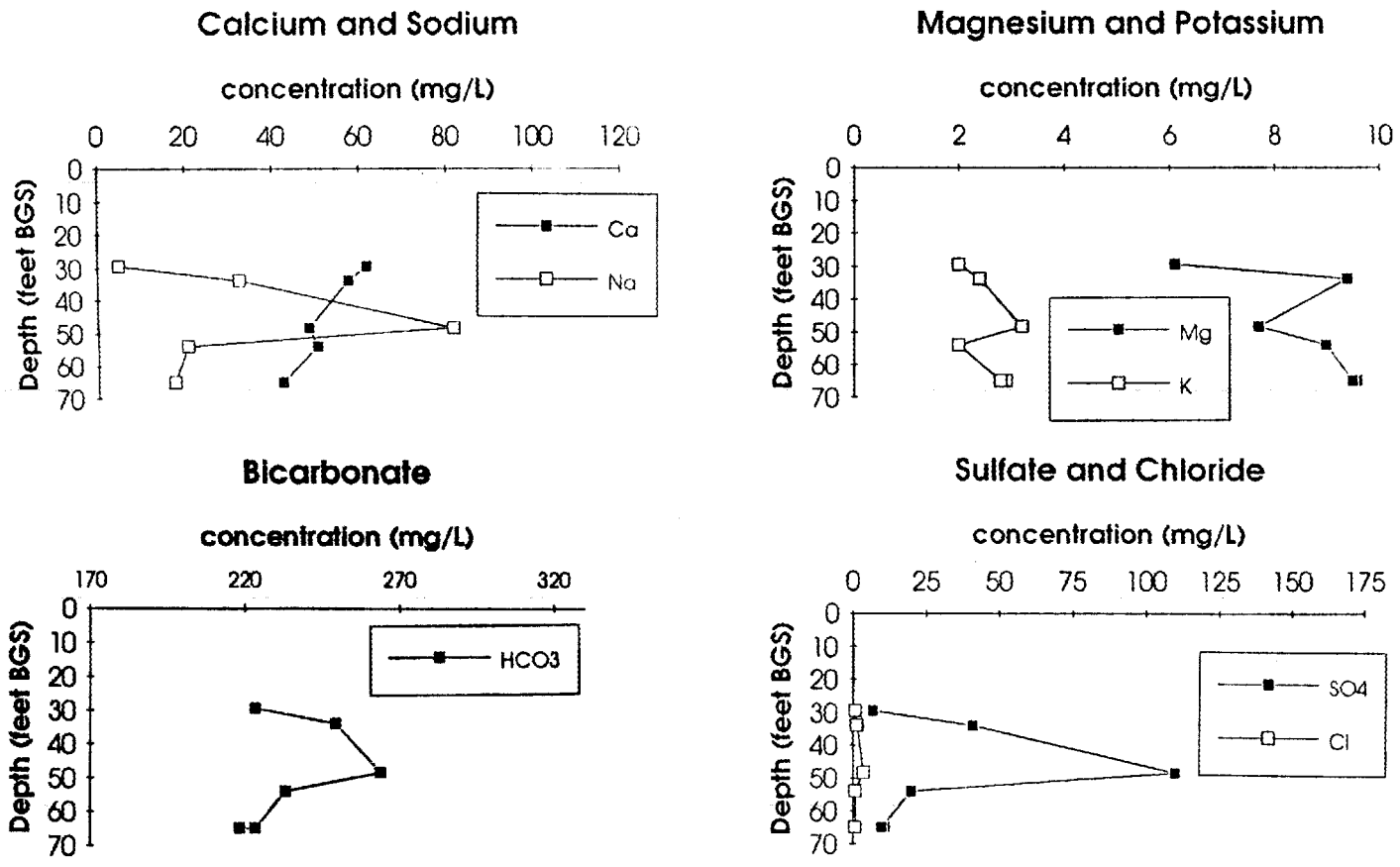

Figure 3-3: GW822 multilevel major ion concentration profiles.

GW823 Multilevel Major Ions

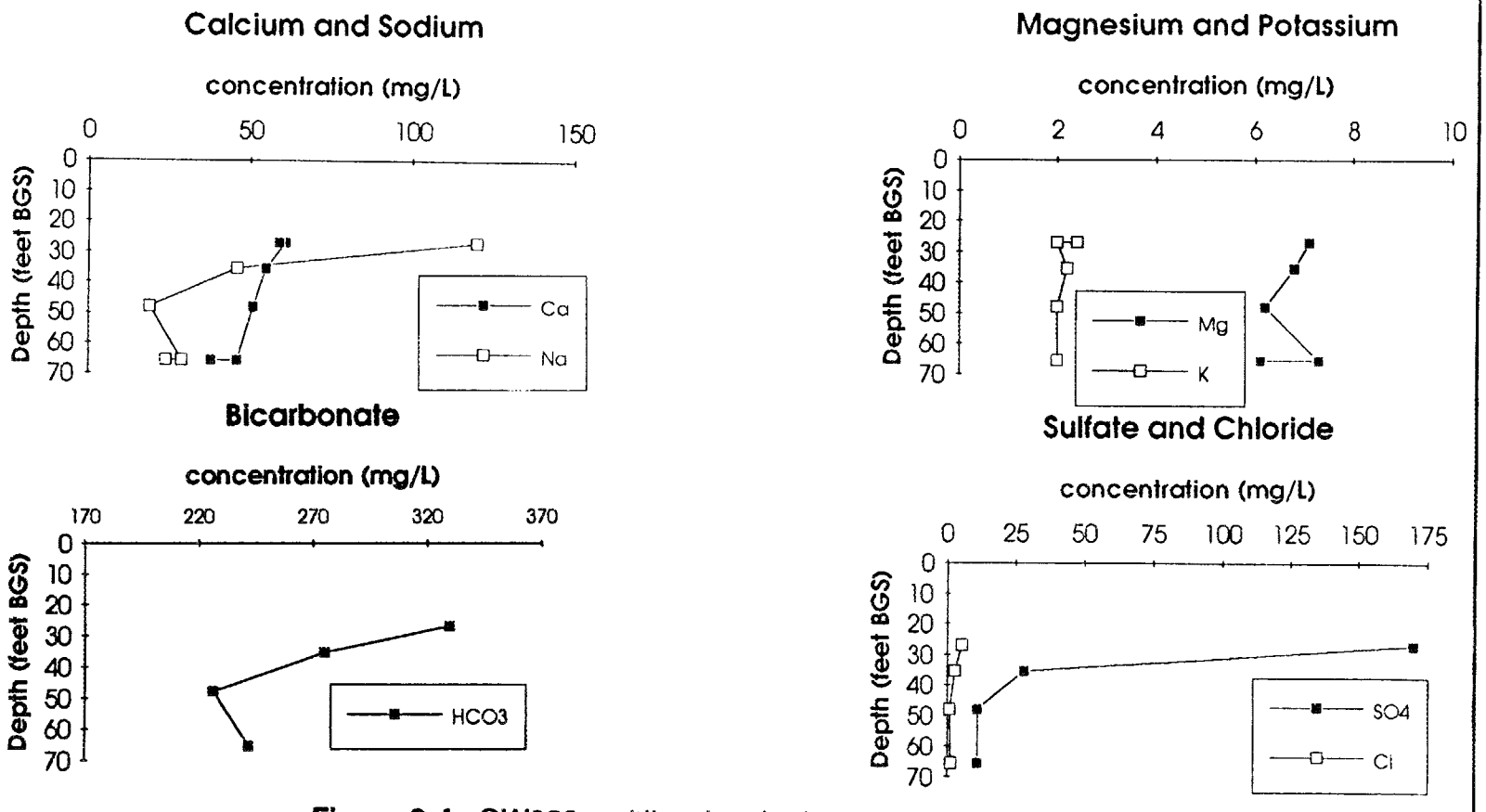

Figure 3-4: GW823 multilevel major ion concentration profiles.

The cation profiles show an increase in sodium with depth and a concomitant decrease in calcium. Similar to sodium, bicarbonate and sulfate concentrations increase with depth until 38.5' and then slightly decrease in the deepest sample at 45.5'. **Figure 3-3** shows concentrations of the major ions with depth in GW822. Similar to GW821, sodium increases and calcium decreases with depth until 48.5'. Below this, however, both sodium and calcium decrease with depth. Also similar to GW821, the bicarbonate and sulfate profiles mimic the sodium profile. The major ion concentration profiles of GW823 are shown in **Figure 3-4**. Like the other wells, calcium concentrations decrease with depth. The bicarbonate and sulfate trends are also similar in that they mimic the sodium. Unlike the other wells, however, the sodium, bicarbonate, and sulfate are in the highest concentrations in the shallow zone and then decrease dramatically with depth. These observations suggest that the concentrations of sodium, calcium, bicarbonate, and sulfate are controlled by related geochemical processes. These processes appear to have a lateral variability in addition to a vertical variability, as evidenced by the similarities between GW821 and GW822, and the differences between those wells and GW823.

A trilinear diagram shows the percentage composition of the major cations and anions for the multilevel well samples and GW462 (**Figure 3-5**). Each apex of a ternary plot represents a 100% concentration of one of the three ions. The points on the ternary plots are projected to one point in the diamond-shaped field.

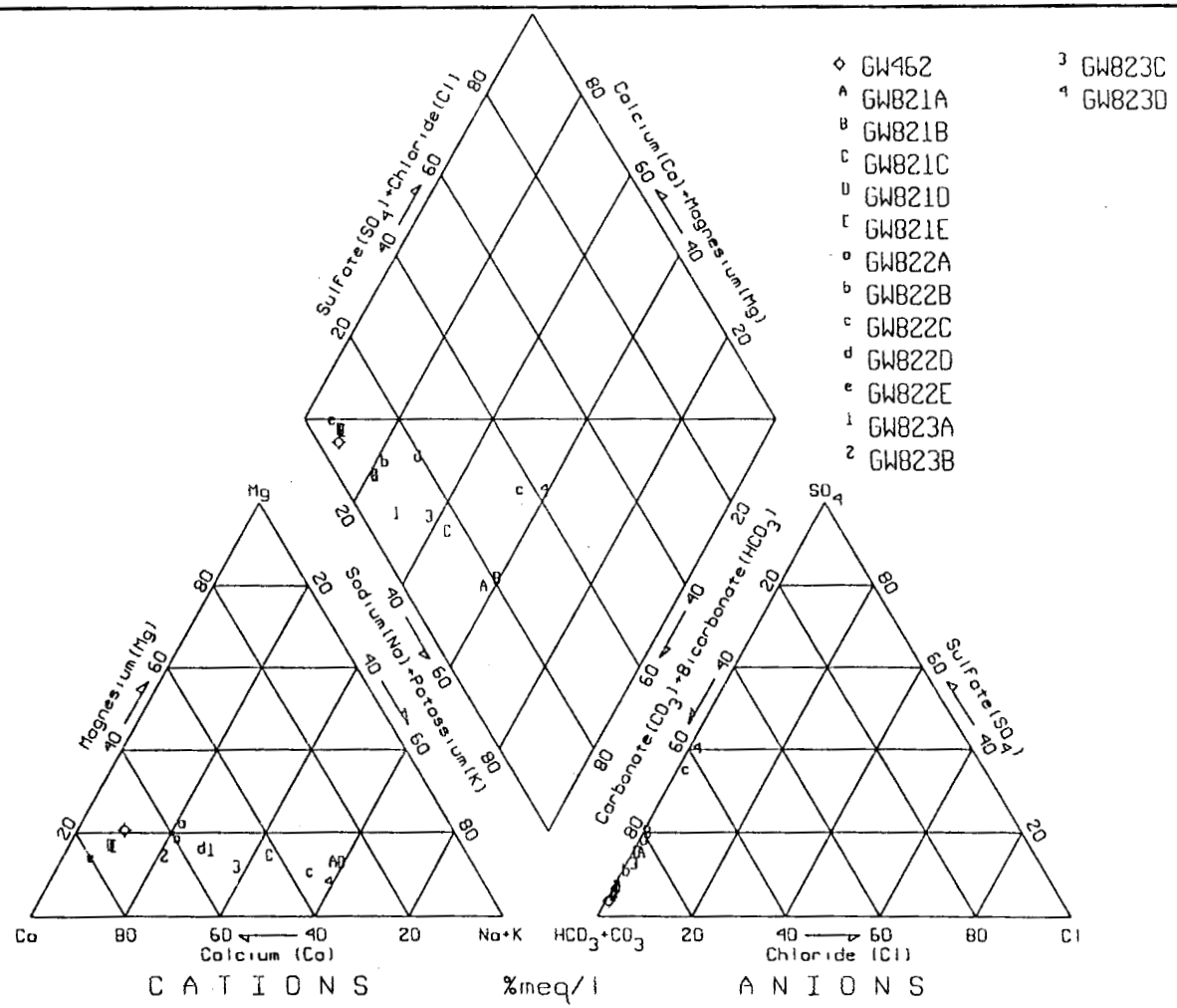

Figure 3-5: Trilinear diagram of multilevel well samples.

There is considerable variation between samples, both within the same well and between wells. Within each well, most of the variation is due to changes in the calcium to sodium ratio. In general, calcium is the dominant cation; however, four of the samples have sodium as the dominant cation. The anion variations, which are less subtle than the cation variations, are due to changes in the bicarbonate to sulfate ratio. Bicarbonate is the dominant anion in all of the samples, although sulfate is a major anion in two of the samples (823D, 822C). Three major water types can be identified in this diagram: Ca-HCO_3, Na-HCO_3, and Ca-Na-HCO_3.

Stiff diagrams were constructed to show the dominant cations and anions (equivalents) in each multilevel well sample. These diagrams are useful in providing a rapid visual comparison of samples (**Figure 3-6**). The three water types can be distinguished by three distinct shapes: Ca-HCO_3 (e.g. 821E, 822E), Na-HCO_3 (e.g. 823D, 822C) and Ca-Na-HCO_3 (e.g. 823A, 821C). The deepest samples in GW821 have a Na-HCO_3 signature but have lower sulfate concentrations than the Na-HCO_3 samples in GW822 and GW823.

Packer samples

The results of the packer samples are significantly different from the results of the multilevels. In the multilevel samples, sodium and sulfate can reach concentrations up to 120 mg/l and 170 mg/l, respectively, while in the packer samples, sodium and sulfate concentrations do not exceed 9 mg/l and 7 mg/l, respectively.

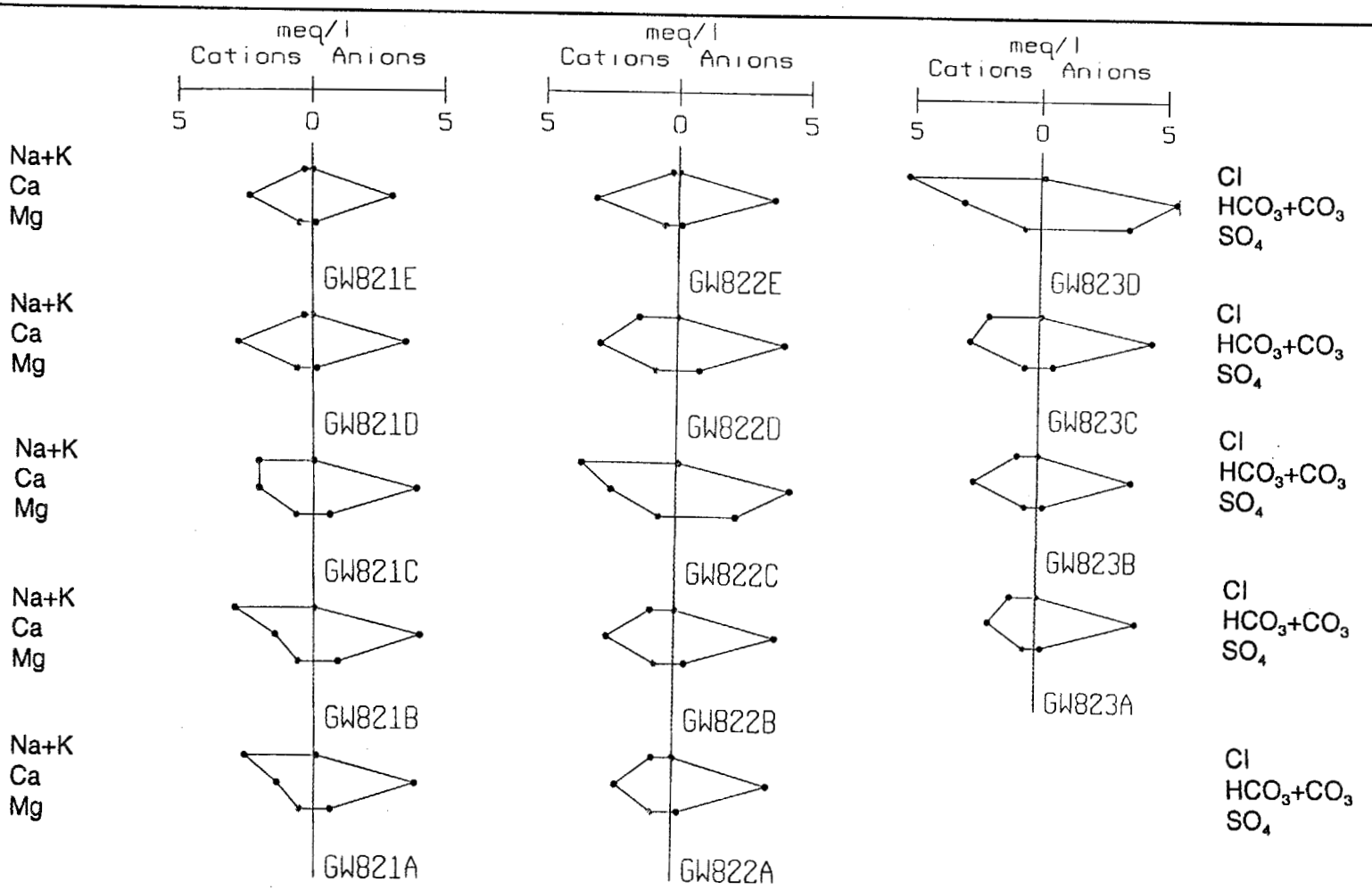

Figure 3-6: Stiff diagrams of multilevel well samples.

Major ion concentration versus depth profiles of the packer samples are shown in **Appendix J.** The packer profiles show very different trends than the multilevel well profiles. In all of the profiles, sodium does not vary at all with depth. The calcium variations in the packer samples do not follow the variations in the multilevel well samples. The bicarbonate and sulfate profiles vary much more subtly than the multilevel samples and do not mimic sodium. The only similarity between the packer and multilevel well trends are in the bicarbonate concentrations, which do not always show a similar profile, but have peak concentrations at the same depths. The random variability and the lack of correlation between profiles in the packer samples suggest that these samples are not accurate representations of the discrete flow zones.

The packer samples all have calcium as the dominant cation and bicarbonate as the dominant anion (**Figure 3-7**). The overlapping of points on the trilinear diagram shows the homogeneity of chemical composition of the packer samples. The GW462 sample is also plotted on this diagram, showing the similarity of a sample of mixed borehole water (20-70') to the packer samples. Due to the homogeneity of the packer samples, Stiff diagrams were not constructed.

Pore water samples

The pore water samples show a concentration increase an order of magnitude than the groundwater samples, with respect to chloride and calcium concentrations.

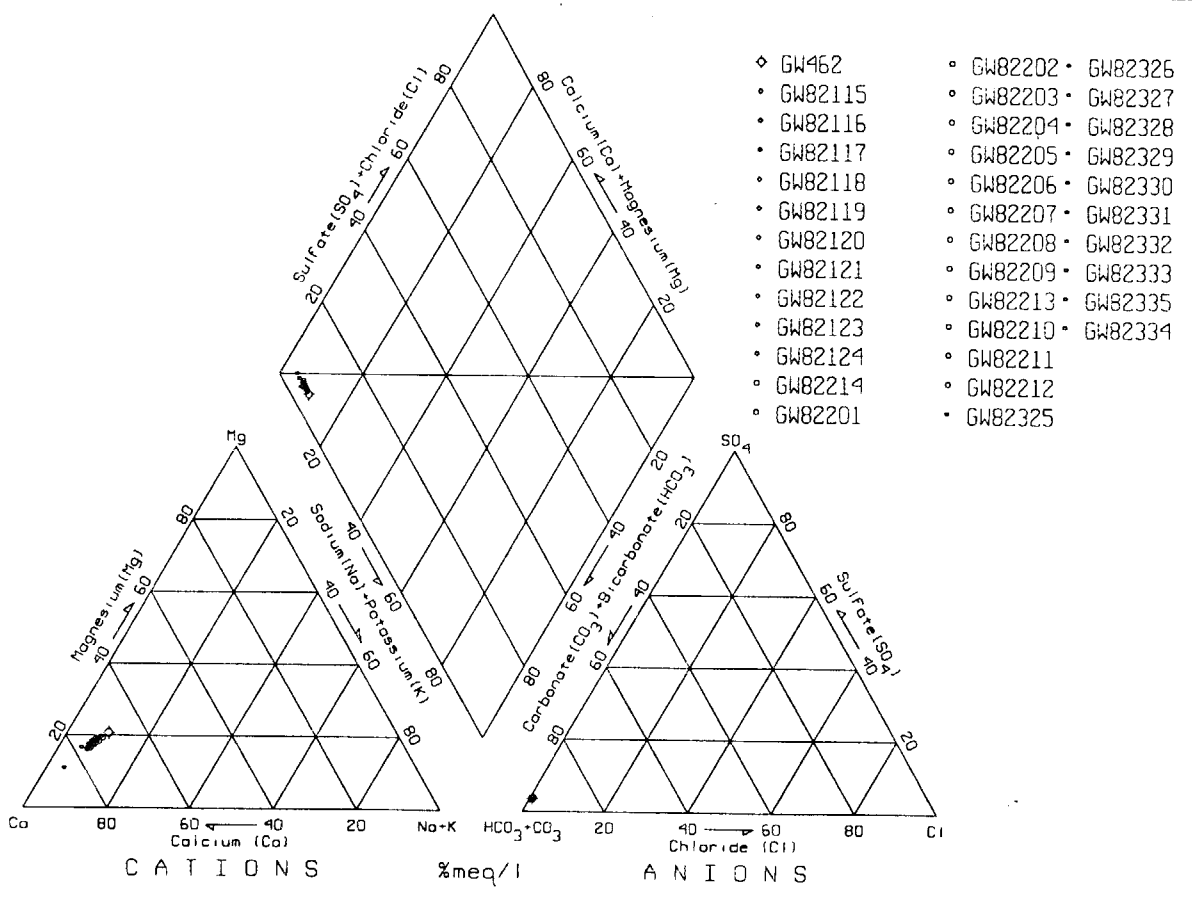

Figure 3-7: Trilinear diagram of packer samples.

The pore water samples are a wide range of types, from Ca-HCO_3 to Ca-SO_4-Cl (**Figure 3-8**). The high negative excess charge in PW82306 and general anomalous concentrations of ions are difficult to understand. The alkalinity in this sample was extremely low, as were the calcium, magnesium, and sodium concentrations, while the chloride concentration was extremely high. The pH of this sample is 5.54, which is lower than any of the other pore water and groundwater samples. The inconsistent concentrations between the sample and its replicate suggest that this sample cannot be considered to be representative of *in situ* conditions.

Minor Ion Trends

Multilevel well samples

Iron, manganese, and aluminum show significant variations with depth in all three multilevel wells (**Figures 3-9** through **3-11**). In GW821 (**Figure 3-9**), the three profiles are correlated, with the highest concentrations at 34,' but do not resemble the major ion trends. The bromide tracer was not detected. In GW822, the iron and aluminum, but not manganese, profiles are correlated (**Figure 3-10**). The bromide tracer was detected in highest concentrations in the shallowest sample (29.5'). In GW823 (**Figure 3-11**), the highest concentrations of iron, aluminum, and manganese are in the shallowest sample, consistent with the major ion profiles. The bromide tracer was detected in all but the deepest sample.

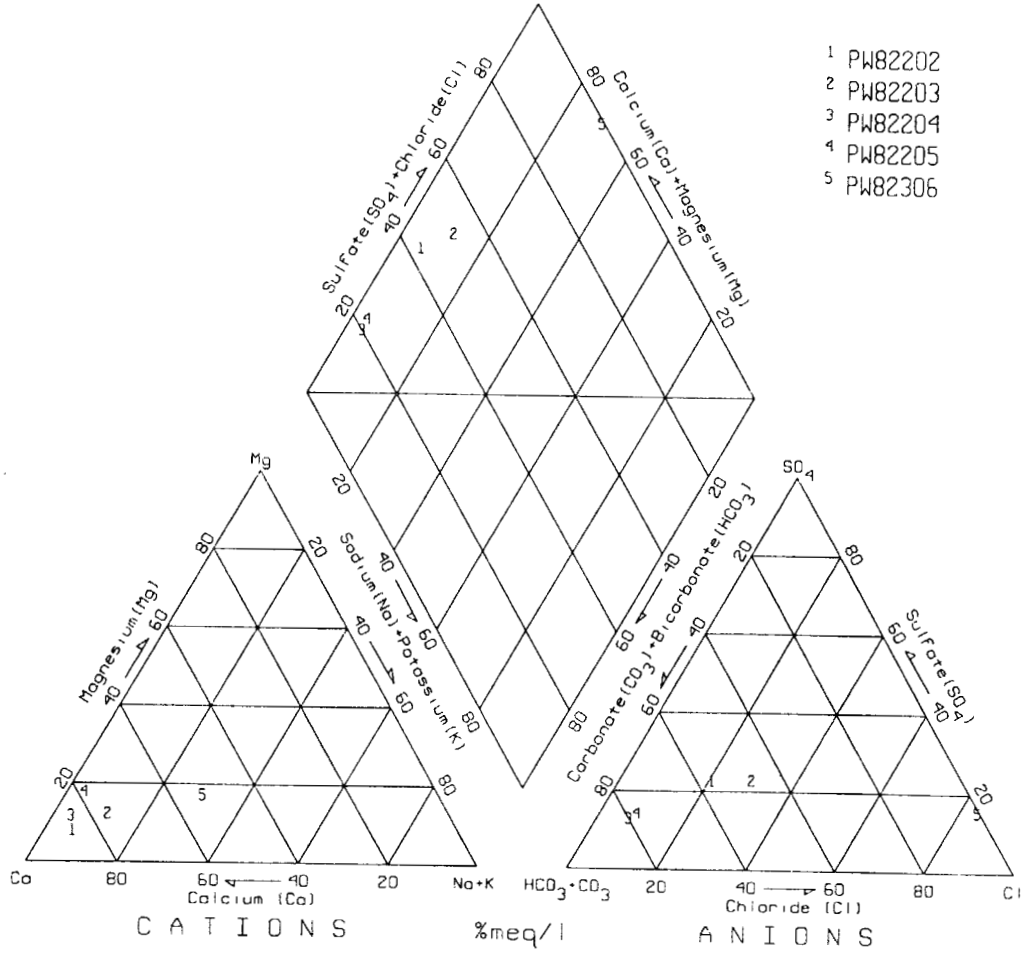

Figure 3-8: Trilinear diagram of pore water samples.

GW821 Multilevel Minor Ions

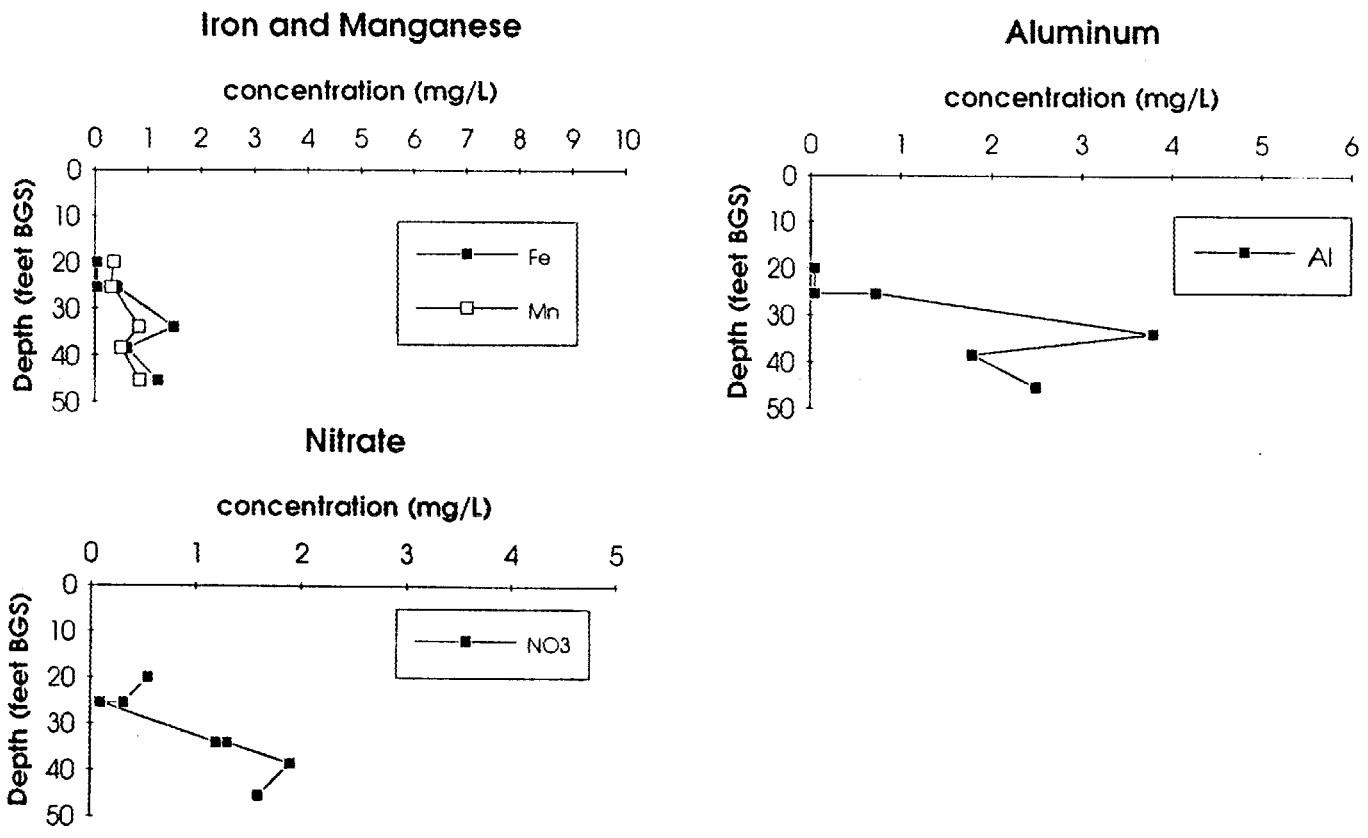

Figure 3-9: GW821 multilevel minor ion concentration profiles.

GW822 Multilevel Minor Ions

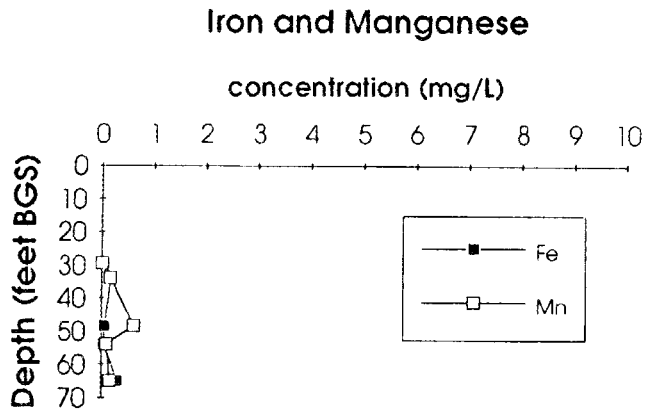

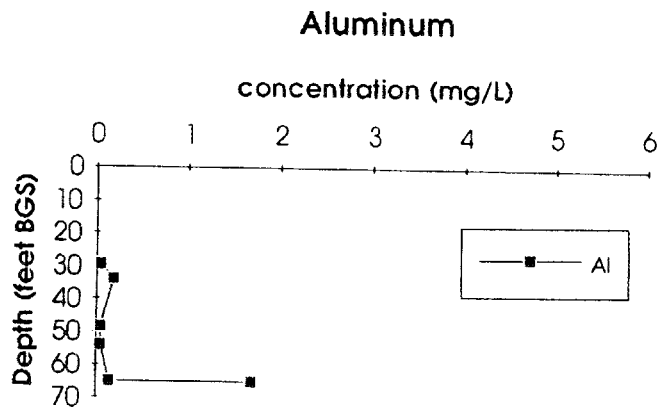

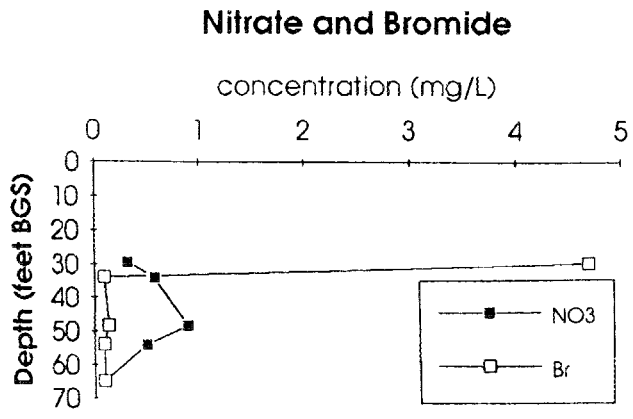

Figure 3-10: GW822 multilevel minor ion concentration profiles.

GW823 Multilevel Minor Ions

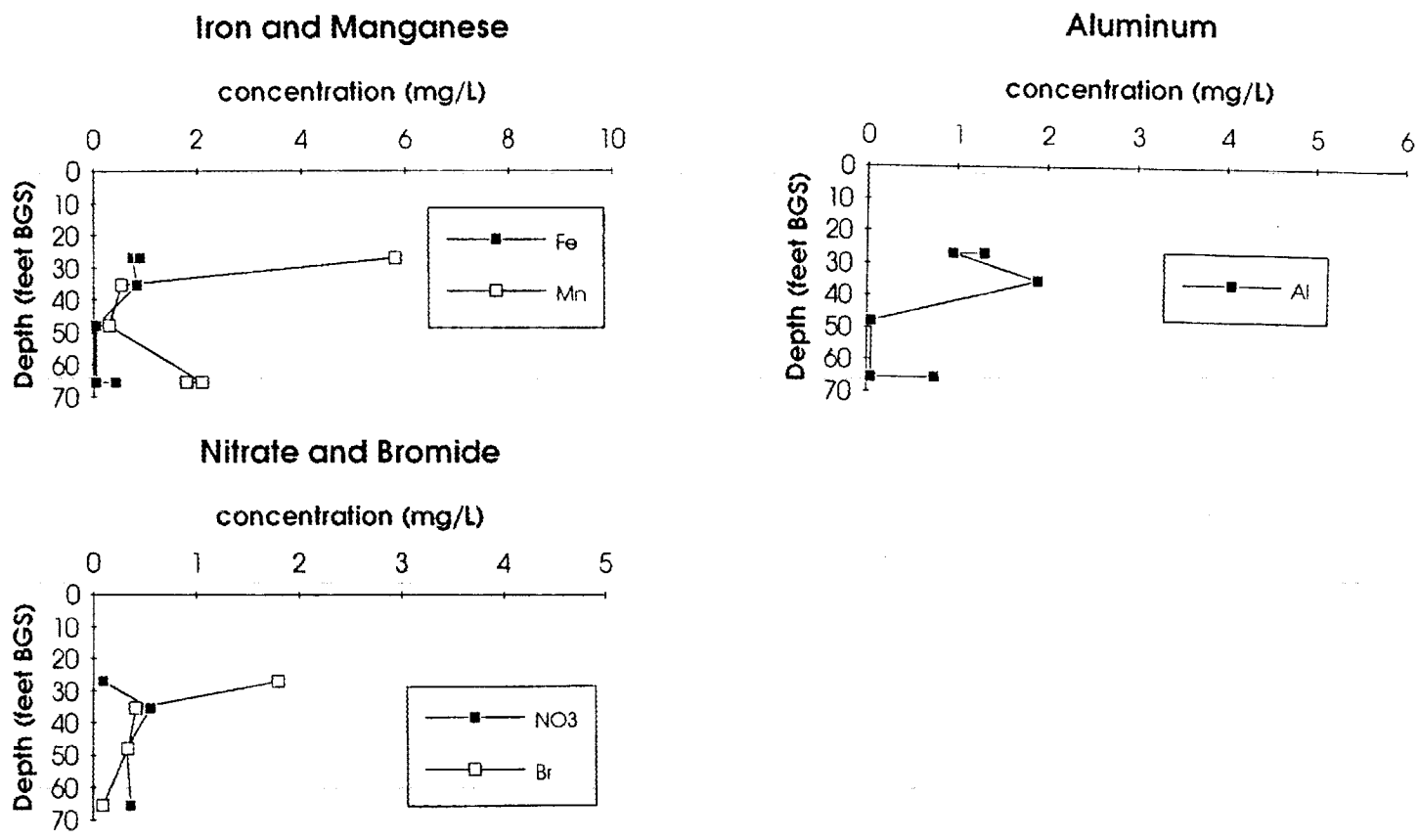

Figure 3-11: GW823 multilevel minor ion concentration profiles.

As discussed previously, the metal ion concentrations in the multilevels are likely influenced by colloids, and as such, interpretations of trends are difficult to make. The bromide concentrations, however, correlate with the earlier results of the tracer test, showing the majority of transport along the flow direction and lesser transport along the regional gradient, which follows the direction of dip.

Packer samples

The minor ion concentrations profiles are shown in **Appendix J**. In the GW821 packer samples, iron and aluminum are correlated and show similar trends with the multilevels. The bromide tracer was detected in low concentrations (<0.1 mg/l), as a result of lower detection limits than in the multilevel samples. In the GW822 packer samples, iron and aluminum trends are correlated but are not similar to the multilevel trends. The bromide tracer was detected in all of the samples at low (<0.5 mg/l) concentrations and decreases with depth, similar to the multilevel trend. The packer samples from GW823 show higher concentrations of iron and aluminum than the multilevel samples. The trends of the metal ions do not correlate with each other or with the multilevel well results. The bromide trend is similar to the multilevel, with the highest concentration in the shallow zones and decreasing concentrations with depth.

For the metal ions, the packer samples have higher concentrations than the multilevel samples, especially with respect to iron, have greater variability, and

show trends that do not correlate with each other or with the major ions. The most likely explanation for the second observation is that the samples contain particulate matter as a result of not filtering the samples.

Comparison of discrete zone samples

Two types of discrete zone sample, packer samples and samples from multilevel wells, were collected in this study to evaluate the spatial variability in groundwater chemistry in the shallow groundwater system. As previously discussed, the results of these two sample types are different, both with respect to trends and with respect to concentrations. For the major ions, the packer samples are much less variable with depth than the multilevels and are more chemically homogeneous. Two possible explanations for this observed homogeneity are 1) the packer sampler was not adequately isolating the fracture intervals or 2) there was not sufficient purging prior to sampling. It would be difficult to assess if the sampler was sufficiently isolating the fracture zones. Due to strong vertical gradients in the shallow system, borehole mixing is likely and sufficiently large volumes of this mixed water could be stored in the fracture zones of the open borehole. For this reason, the purging of only the volume of tubing is likely to be insufficient for the collection of samples that are representative of the discrete fracture zones.

Despite the problems with the packer sample data, the sampler is a very useful tool for collecting discrete zone samples. Many of the problems with the data can be

attributed to insufficient purging prior to sampling and to not filtering the samples, as opposed to flaws in the design of the packer sampler itself. The advantage of the packer sampler over the multilevel wells is that the sampler is easy to use and samples can be collected from an open borehole. In addition, the packer sampler is much less expensive than installing multilevel wells. However, it is clear from the previous discussion that multilevel wells provide samples that are most representative of the discrete flow zones in the saprolite and in the fractured bedrock.

Comparison of multilevel and long-screened well samples

The long-screened interval of GW462 allows groundwater from many flow zones to enter the well. Because these flow zones have different flow rates and chemical characteristics, the chemical composition of a mixed sample will be vertically averaged, which will be most heavily weighted by the high flow zones in the well. The sample of GW462 is a Ca-HCO_3 type, indicating that high flow zones intercepting the well are Ca-HCO_3 waters. The advantage of sampling from a long-screened well is that it is useful for identifying the bulk chemical characteristics of the screened formation. The disadvantage is that due the effects of dilution and mixing, vertically averaged samples will obscure the presence of different groundwater chemical compositions, for example, the Na-HCO_3 water type. In fractured rocks, contaminated groundwater can flow through discrete zones that may not be well-connected to other zones. If a contaminated zone were to intersect

a long-screened well, the contaminant concentrations could be mixed and diluted so that they were no longer detectable. In this situation, there is a distinct advantage of collecting groundwater samples from multilevel wells which screen discrete flow zones.

Hydrochemical facies

The multilevel well samples can be separated into three basic chemistry types: Ca-HCO_3 (Type 1), Na-HCO_3 (Type 2), and Ca-Na-HCO_3 (Type 3). The different water types observed in the multilevel wells were plotted on a three-dimensional fence diagram to show the general orientation of the hydrochemical facies (**Figure 3-12**). The diagram shows that the water types can be connected between the boreholes. The Type 1 water is observed in the shallowest two samples of GW821 and the shallowest sample of GW822. The Type 2 water is present at the saprolite/bedrock surface in GW823. In GW821 and GW822, this water type is observed almost 25 ft and 20 ft below that surface, respectively. The Type 3 water is observed in all of the other samples, which have varying proportions of calcium and sodium.

A cross-section (**Figure 3-13**) was constructed to relate the orientation of the hydrochemical facies with stratigraphy and flow direction. The section runs along the direction that corresponds to the average of the shallow and deep flow directions (assuming an 8:1 horizontal anisotropy ratio). It extends from GW821 (B') to an interpolated point (B) between GW822 and GW823.

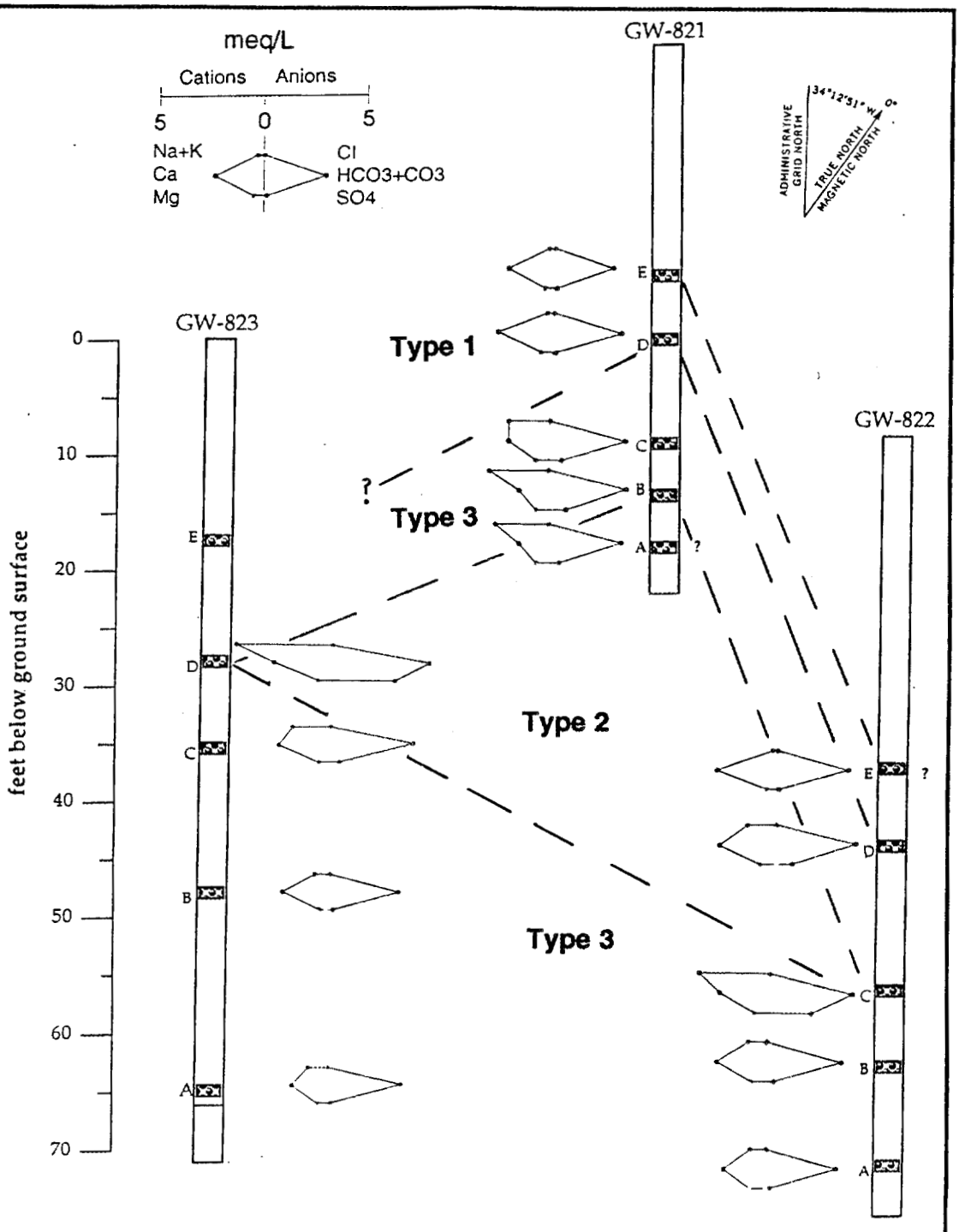

Figure 3-12: Stiff diagrams plotted on fence diagram, showing orientation of the hydrochemical facies.

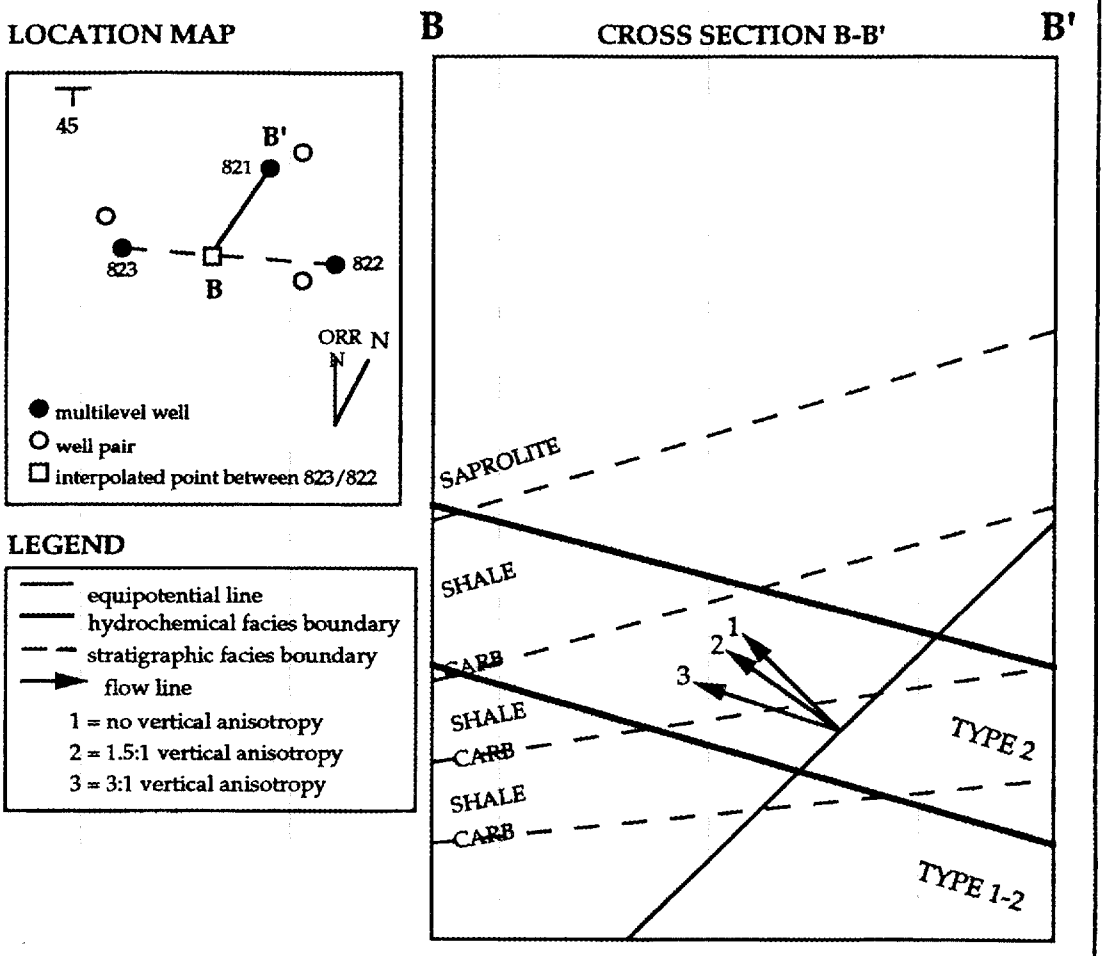

Figure 3-13: Cross-section along the line of the average of the shallow and deep flow directions showing lithologic correlations, hydrochemical facies, equipotential lines, and flow direction with different degrees of vertical anisotropy.

The shallow and deep heads at B and B' were interpolated from known heads in the well pairs that were averaged over the time period of March 1994 to May 1995. The boundaries of the stratigraphic and hydrochemical facies at B were interpolated from known points in GW822 and GW823.

Three flow lines are drawn on the cross-section. One is the flow line drawn perpendicular to the equipotential line, which assumes vertically isotropic conditions. The second flow line was drawn with a vertical anisotropy ratio of 1.5:1, which was the maximum calculated from directional hydraulic conductivity measurements made by Gierke et al. (1988). This anisotropy ratio shifts the flow direction downward by 11°. Using a vertical anisotropy ratio of 3:1, the flow lines are parallel to the projected boundary of the hydrochemical facies. This ratio is conceivable, considering that shales often have a high vertical anisotropy by virtue of the orientation of bedding. The value from Gierke et al. (1988) was approximate, based on only two values of the maximum horizontal conductivity and a single measure of vertical conductivity. If a 3:1 ratio can be assumed, the orientation of the hydrochemical facies appears to be controlled by gradients that are strongly affected by both horizontal and vertical anisotropy.

Another interesting observation is that the Type 2 water is constrained on both top and bottom by Type 3 waters. There are a few possible explanations for this. The first is that the Type 2 water is contained in a discrete flow zone that is coming up

from depth to discharge. Another explanation is that remnant Na-HCO_3 waters in the pores of the low permeability shale matrix have not been flushed out by more recent water. This explanation is not as plausible as the first, because in GW823, the Type 2 water was observed at the saprolite/bedrock interface, which is a zone of high flow.

Previous studies on the ORR (Haase, 1992: Solomon et al., 1992; Moore and Toran, 1992) have correlated these Type 1 and Type 2 waters with different depths in the regional groundwater system. The Type 1 water has been observed in the shallow system, to a depth of approximately 30 to 60 m. The Type 2 water has been identified at intermediate depths, below 30 to 60 m. A study conducted by Haase (1992) on shale groundwater on the ORR concluded that the interface between the shallow Type 1 and intermediate Type 2 groundwater is nearly horizontal, cuts across bedding, and is very abrupt, suggesting that it represents a boundary between groundwater flow systems which interact minimally with each other. The boundary between the Type 1 and Type 2 hydrochemical facies on the cross-section is steeply dipping and is also diffuse, as evidenced by Type 3 hydrochemical facies which occur between the Type 1 and Type 2 facies. These results do not appear to agree with the results of Haase (1992); however, many of the differences can be explained by the location of the field site and the spatial resolution of sampling points. The steeply dipping nature of the hydrochemical facies observed in this study may be due to the location of the site in a discharge

zone, where groundwater flows upward from depth. The conclusion of Haase (1992) that the boundary is abrupt may be due to large vertical spacing of groundwater samples. In this study, the multilevel wells provide samples with much smaller vertical spacing (less than 10 ft), allowing for more detailed chemical resolution.

One potential source of the Type 2 waters is bentonite that was used in the installation of the multilevel wells. Bentonite that contains Na-montmorillonite and gypsum could provide an additional source of sodium and sulfate to the groundwater samples. There are several reasons why bentonite contamination is unlikely. First, the orientation of the Type 2 hydrochemical facies correlates with the orientation of the other hydrochemical facies. Second, two of the samples with a Type 2 signature are from high flow zones; if the sampling ports were contaminated with bentonite, they would likely have been flushed out during the three months between the well installation and sampling.

3.7 Summary

The results of the groundwater sampling show that the shallow groundwater at the field site is neutral to slightly alkaline (pH 7-8) and can be divided into three major water types: Ca-HCO_3 (Type 1), Na-HCO_3 (Type 2), and Ca-Na-HCO_3 (Type 3). The results of the multilevel well sampling clearly show that there is significant vertical variability in shallow groundwater chemistry at the field site. The trends of

the major cations show a strong inverse relationship between calcium and sodium in GW821 and GW822. In all three wells, the bicarbonate and sulfate concentration profiles mimic the sodium profile. Trends in the minor ions were more difficult to distinguish due to possible colloid contamination, which is likely to be affecting the concentrations of aluminum, iron, manganese, and silica.

The three major water types can be correlated between the wells, forming hydrochemical facies. The orientation of the hydrochemical facies is steeply dipping from a high in GW823 to lower depths in GW821 and GW822. Both the hydrochemical facies and groundwater flow cut obliquely across bedding. These relationships suggest that the orientation of the hydrochemical facies is largely controlled by the groundwater flow direction, which is offset from the gradient due to both horizontal and vertical anisotropy. The influence of the anisotropy on the direction of flow observed in this field study has also been observed in other studies on the ORR (e.g. Sanford et al., 1994).

The wedge of Type 2 water vhich is constrained on top and bottom by Type 3 waters may be a result of deeper waters that are discharging though a discrete flow zone. Strong upward gradients exist at the site, indicating a probable mechanism, an upward flow direction, that could account for the presence of deeper waters in the shallow system. Remnant water from pore fluids of the shale could also have this type of signature and could be the source of the Type 2 wedge. In order for this

water to remain and not be flushed out by fresher water, the Type 2 water would have to be present in low permeability zones. The presence of this water at the saprolite/bedrock interface in GW823, a zone of known high flow, weakens this argument. Another possible source of the Type 2 water is interaction of bentonite with Type 1 water, although there are several reasons why bentonite contamination is unlikely. First, the orientation of the Type 2 hydrochemical facies correlates with the orientation of the other hydrochemical facies. Second, two of the samples with a Type 2 signature are from high flow zones; if the sampling ports were contaminated with bentonite, they would likely have been flushed out during the three months between the well installation and sampling.

The Ca-HCO_3 (Type 1) and Na-HCO_3 (Type 2) water types described in previous studies were also observed in this study. However, the smaller vertical spacing of sampling points provided by the multilevel wells yielded greater resolution which resulted in the identification of a third water type in the shallow groundwater system: Ca-Na-HCO_3 (Type 3). The next step is to look at the possible sources of the Type 3 water. The geochemical trends discussed in this chapter suggest two possible sources: 1) water-rock interactions between the Type 1 and Type 2 waters and the surrounding rock and 2) mixing of Types 1 and 2 waters. In order to examine water-rock interactions, the mineralogy of the rock must first be characterized, which is the focus of the next chapter.

4. Mineralogical Characterization

4.1 Introduction

In studying the effects of water-rock interactions on the spatial variability of groundwater chemistry, it is important to examine the different mineralogies encountered by groundwater in the surrounding matrix and along fracture surfaces. The focus of this chapter is a characterization of the matrix and fracture coating mineralogy of samples collected from core.

Mineralogical characteristics that may play important roles in controlling groundwater chemistry are the relative content of calcite, clays, oxides, sulfides, and organic matter (Von Damm and VandenBrook, 1989). Due to its high solubility and rapid dissolution rate, calcite plays a vital role in controlling the groundwater chemistry, particularly with respect to alkalinity. Clays and oxides are important because their large surface areas have more sites available for surface- and biologically-mediated processes. Cation exchange, which occurs primarily on clays, can significantly affect the concentrations of the major cations in groundwater, including calcium, sodium, potassium, and magnesium. The mobility of heavy metals is largely controlled by biological and chemical reactions which take place at the hydrous oxide/water interface; ions can be adsorbed onto surfaces or incorporated into the oxide structure. Sulfide minerals, such as pyrite, will change the redox conditions of groundwater which will have a significant effect on what

types of species are dominant in solution.

Reactions between water and host materials occur most rapidly at low pH. In soil pores, the level of carbon dioxide in soil pores can be up to 100 times the atmospheric levels (Matthess, 1982), resulting in higher concentrations of carbonic acid and thus, lower pH. As a result, the most intense weathering of both silicate and carbonate minerals occurs in soils. In fractured low-permeability rock, such as shale, weathering reactions will be concentrated in fracture zones, because the permeability of the matrix is orders of magnitude lower than the fractures. Physical and chemical weathering of the primary silicate minerals results in formation of secondary minerals, such as clays and oxides, in fracture zones. Some common clay minerals formed by weathering are vermiculite, kaolinite, and smectite, which are all important sources of exchangeable cations (McBride, 1994). Due to the low solubility of iron in normal pH ranges, iron in solution is precipitated as oxides or hydroxides (Schwertmann and Taylor, 1977) and as a result, iron oxides, such as goethite and hematite, are abundant in soil and saprolite systems. Manganese oxides, such as birnessite, are less abundant in most soils but are important for providing essential nutrients to plants and animals and also have a high sorption capacity for heavy metals (McKenzie, 1977).

The results of the mineralogical characterization of Lee et al. (1987) are presented in **Table 4-1**. The dominant minerals identified were illite and quartz. Other identified minerals include kaolinite, chlorite, and calcite. A feldspar phase was identified but Lee et al. (1987) did not distinguish between potassium and plagioclase feldspar. Pyrite and organic matter were identified in trace amounts (less than 2 weight percent). The major portion of carbonate was observed as fracture-filling secondary calcite; however, detrital dolomite and calcite were also identified. Petrographic studies indicated the presence of clay minerals observed to be preferentially oriented along bedding planes. Several microfractures, up to 0.3 mm size, were filled with calcite and secondary silica.

Phillips (1988) analyzed the soils and saprolites of the Nolichucky Shale and the underlying Maryville Limestone (now called the Dismal Gap Formation). Results indicated low organic carbon values which generally decrease with depth. Values of pH of the soil samples varied from 4.5 to 7.3. Minerals were identified using XRD and DCS (differential scanning calorimetry). In the clay-size fraction, kaolinite, hydroxy-interlayered vermiculite, and illite were identified, with lesser organics and Fe/Mn oxides. The micromorphology of the oxides was also examined. At least six different types of iron and manganese oxides were observed, present as individual nodules, crystals, and infillings as well as coatings on pores and weathered bedrock. Iron and manganese intermixing in oxides was also observed. The results of Phillips (1988) are summarized in **Table 4-1**.

Table 4-1: Mineralogical Composition of the Nolichucky Shale and Saprolite

Minerals	Shale* Weight %	Saprolite** Weight %
Illite	43	30-50
Chlorite+kaolinite	14	--
Kaolinite	(see above)	30-50
Vermiculite	--	10-20
Quartz+feldspar	29	--
Carbonates	11	--
Oxides	NA	<10
Pyrite	<2	NA
Total organic carbon	<2	<1

Notes:

* from Lee et al. (1987), sample from Joy-2 well, 181-181.5 m.

** from Phillips (1988), sample of intelayered Nolichucky Shale and Maryville Limestone, clay-size fraction

NA= not analyzed

4.4 Sample Preparation

Sixty-one samples were collected from the Nolichucky Shale drill core for examination. Pictures of hand samples are shown in **Figure 4-1**. The samples designated for analysis were chosen to represent the different shale and carbonate lithologies encountered as well the areas of heaviest weathering and oxidation. Samples for XRD analysis were scraped with a scalpel, powdered in a quartz mortar and pestle, suspended in deionized water, and dropped on a quartz slab.

Samples for SEM/EDS analysis were chosen by the presence of relatively thick oxide coverings on fracture surfaces to ensure that the coatings could be detected. Some of the samples were prepared by cutting small pieces and securing them in a 1" I.D. ring with epoxy. Other samples were powdered and mounted onto double-sided tape. One powdered sample was mounted onto epoxy. All of the samples were carbon coated prior to analysis.

4.5 Analytical Methods

The analytical methods chosen for mineralogic analysis were x-ray diffraction (XRD) and scanning electron microscopy (SEM). A thorough discussion of the XRD method is provided by Wilson (1987). The SEM method is described in detail by Goldstein et al. (1992). Initially, the mineralogical study was designed to include electron microprobe analysis; however, due to the highly weathered nature of the shale, preparing thin sections of weathered and oxidized areas was not feasible.

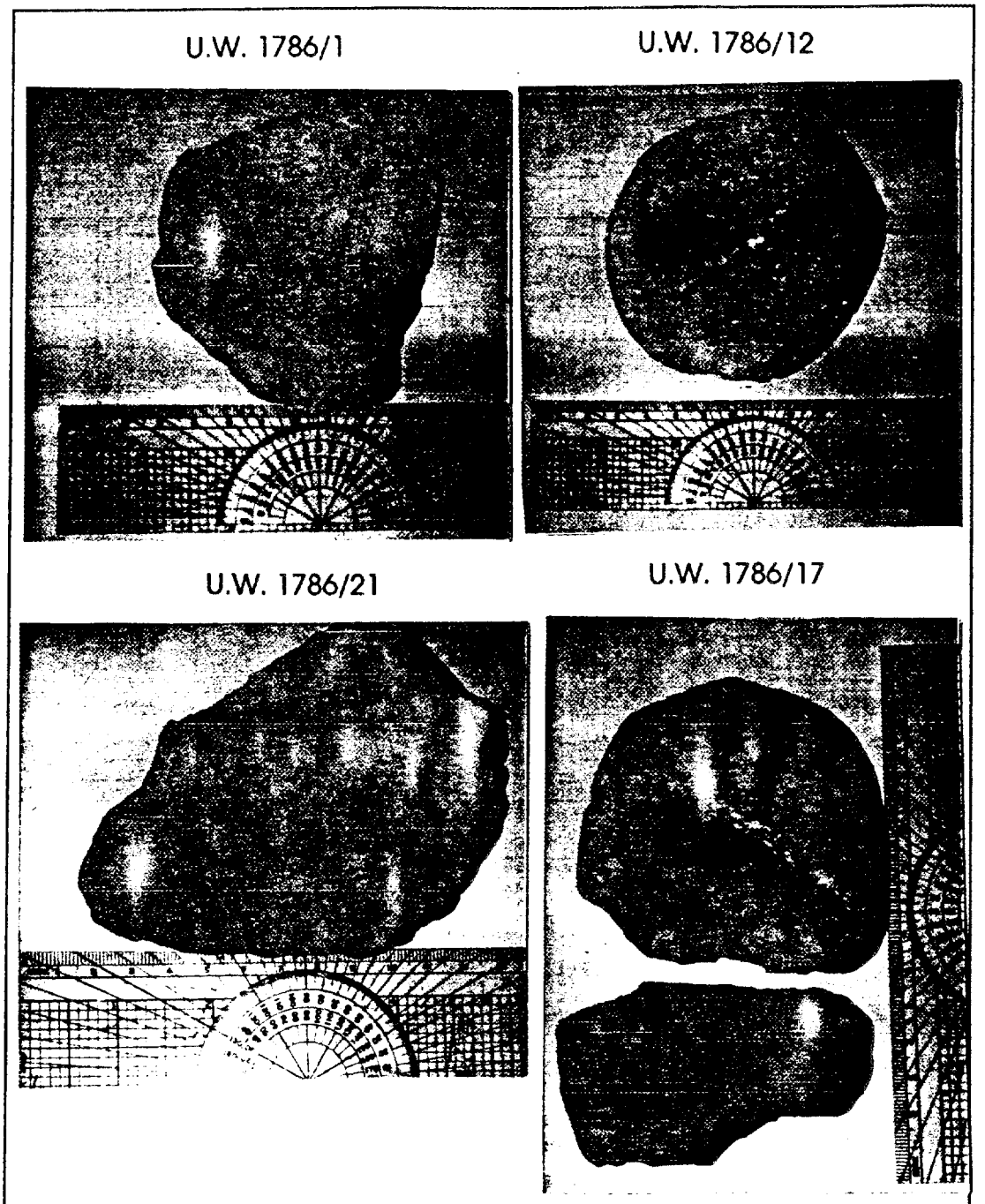

Figure 4-1: Pictures of hand samples, showing types of oxides that were sampled.

The thin, rough surfaces of the mineral coatings were repeatedly ground off during section preparation. For this reason, only one thin section was prepared.

XRD and SEM are not the ideal techniques for identification of weathering products, especially fine-grained oxides. Using XRD to identify oxides is often extremely difficult because the fine-grained nature of oxide crystallites tends to reduce coherent stacking of x-rays, leading to broad, diffuse XRD patterns (e.g. McKenzie, 1977). Iron oxides have tremendous pigmenting power, so although orange-red surface staining may indicate the presence of an Fe oxide/hydroxide, the concentration may be too low to be detected by XRD. Manganese oxides and hydroxides are even more difficult to identify using XRD because they are usually present in even lower concentrations than the iron oxides. More appropriate techniques for the identification of Mn oxides are high-resolution transmission electron microscopy (HRTEM), x-ray fluorescence spectroscopy (XRF), extended x-ray absorption fine structure (EXAFS), or infrared (IR) spectroscopy.

X-ray diffraction analyses were performed on a Seifert-3000 diffractometer connected to a Scintag computer software system. The radiation was CuKα generated (λ=1.5406) at 45 kV and 30 mA. Diffraction scans were completed at a degree interval of 0.15-0.5 at a preset time (second/step) of between 1.0 and 12.0. Scans were collected between the 2θ range of 2 and between 70 and 90°. Slit sizes used were 0.5/1.0 on the collection detector and 2.0/3.0 on the generation

source. The scans were analyzed using Scintag software, were background corrected, and were compared to JCPDS (Joint Center for Powder Diffraction Studies) cards. The quartz plate used for sample mounting was scanned at a continuous rate from 2θ of 10 to 90° to identify the presence of background quartz peaks, of which there were none.

Particle sizes of crystals that caused peak broadening were analyzed using the Scherrer method. This method involves fitting the profiles and then measuring the height of columns of the crystals that are normal to the beam. This technique is good for cubic or spherical particles less than 1000 Å in diameter. An external silica standard (NBS Standard Reference Material 640b) was run with the same slit sizes used for the sample analyses. The particle size, or "c-size", is calculated as a volume-weighted average:

$$c-size = \frac{\sum(n_i d_i^4)}{\sum(n_i d_i^3)} \qquad (4\text{-}1)$$

where:

n = number of crystals

d_i = diameter of crystal (Å)

Scanning electron microscopic (SEM) analyses were performed on a Cameca model SX50/51 electron microprobe. Qualitative elemental compositions were

determined by energy dispersive spectrometry (EDS) using a PGT IMIX system which consisted of a Si/Li detector with a standard beryllium window. Back-scattered electron (BSE) imaging was used to identify "brighter" oxide grains. Wavelength-dispersive spectra (WDS) x-ray mapping was also used to scan the powdered samples for elements of interest (i.e., Mn). Column conditions were 15 kV and 20 nA.

4.6 Results

Thin section

Identification of minerals in the thin section (U.W. 1786/20) was difficult due to the extreme fine-grained matrix; however, elongated, platy clay minerals and dark, opaque oxides were apparent. The oxides occurred as discrete grains in the matrix and as concentrated fillings in microfractures parallel to bedding.

XRD

XRD scans of the samples are shown in **Figures 4-2** through **4-4**. Results of the XRD peak interpretations are presented in **Table 4-2**, along with a description of the sample, the shale or carbonate unit in which the sample was collected, and the multilevel sampling well port that is closest to the depth of the sample.

Certain minerals, such as quartz and calcite, were easily identified due to their high concentrations in the samples and their strong, sharp peaks on the XRD scans.

XRD Scans: Matrix Minerals

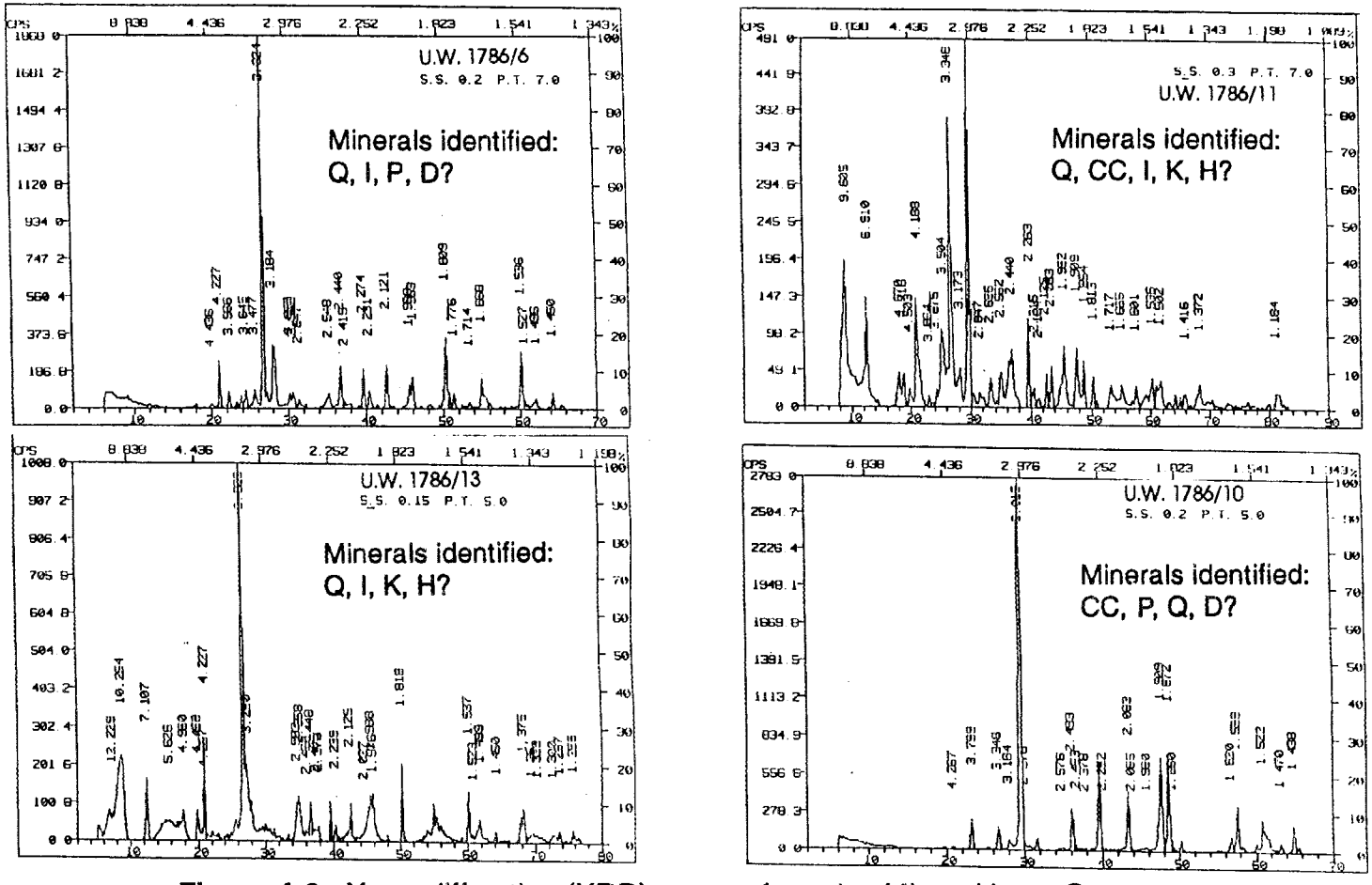

Figure 4-2: X-ray diffraction (XRD) scans of matrix. Mineral key: Q=quartz, CC=calcite, P=plagioclase, I=illite, K=kaolinite, G=goethite, H=hematite, D= dolomite.

XRD Scans: Orange-Red Fracture Coatings

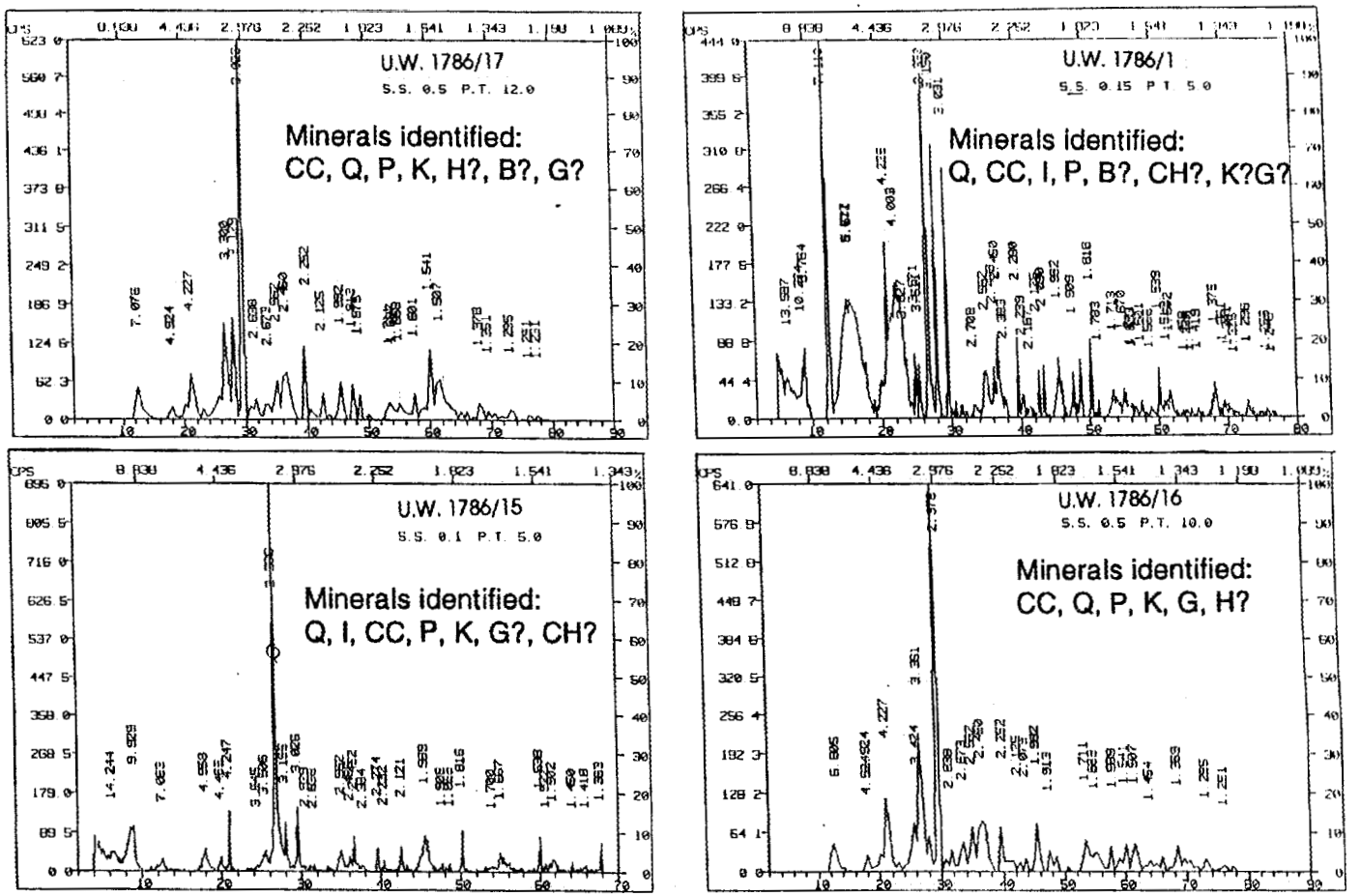

Figure 4-3: X-ray diffraction (XRD) scans of red-orange fracture coatings. Mineral key: Q=quartz, CC=calcite, P=plagioclase, I=illite, K=kaolinite, G=goethite, H=hematite, D=dolomite, CH=chlorite, B=birnessite.

XRD Scans: Other Fracture Coatings

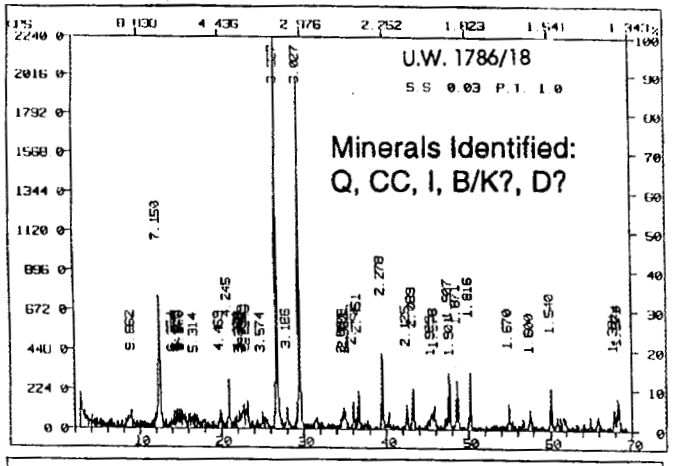

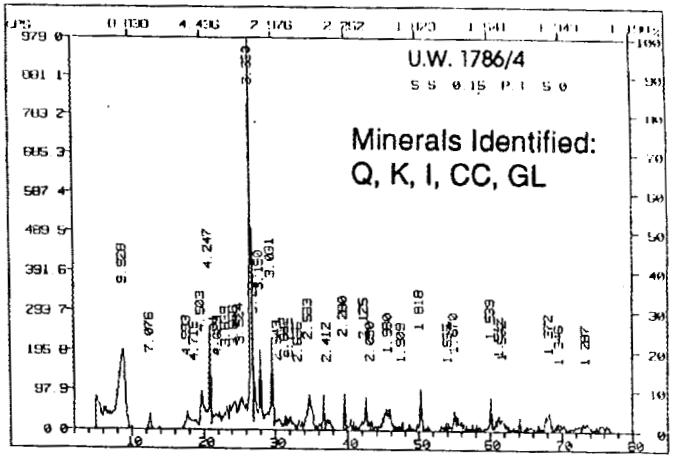

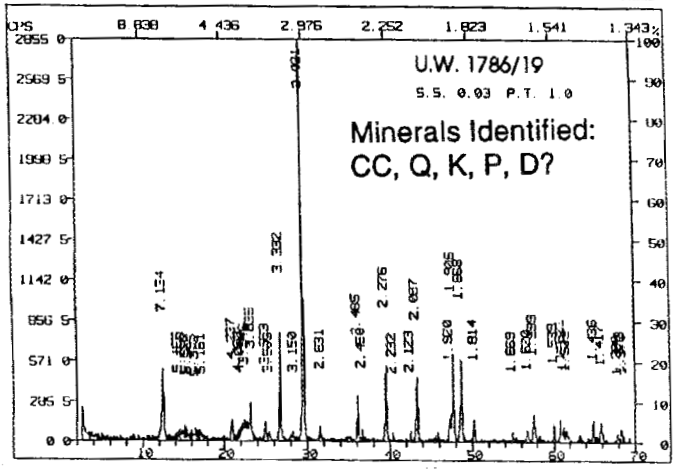

Figure 4-4: X-ray diffraction (XRD) scans of other fracture coatings. Mineral key: Q=quartz, CC=calcite, P=plagioclase, I=illite, K=kaolinite, G=goethite, H=hematite, D= dolomite, CH=chlorite, B=birnessite, GL=glauconite.

Table 4-2: Mineralogical Analysis Results

Well#	U.W. Sample#	Field Sample#	Depth	Shale Unit#	Carb Unit#	ML Port*	Sample Description	XRD Analysis Identified	XRD Analysis Tentatively Identified	EDS Analysis
GW821	U.W.1786/1	821-14	19'			E	red-orange staining on shale/sap	Q, CC, P, I	G? CH? K? B?	
GW821	U.W.1786/2	821-10	24'	S-4		D	red-orange staining on shale/sap			
GW821	U.W.1786/3	821-2red	32'	S-4		C	red-orange staining on shale/calc	Q, I, K, CC, GL		Q, I, CH?
GW821	U.W.1786/4	821-2grn	32'	S-4			green weathered mineral	Q, CC, K, I, G		I, GL?
GW821	U.W.1786/5	821-5	37.5'		C-4	B	red-orange staining on carbonate	C, Q, I, G	H?	
GW822	U.W.1786/6	822-14	29.5'			E	weathered shale	Q, P, I	D?	
GW822	U.W.1786/7	822-18	31'	S-1		E	red-orange stained shale/clay	CC, Q, P, I, K	G? CH?	
GW822	U.W.1786/8	822-1	48.5'		C-3	C	red-orange stained carbonate	CC, Q	K? B?	
GW822	U.W.1786/9	822-3gry	52'		C-4		carbonate matrix	CC, Q, P	D?	
GW822	U.W.1786/10	822-3 blk	52'		C-4		black layer on carbonate	CC, Q, P, K, I		CC, Q, Al-silicates, apatite
GW822	U.W.1786/11	822-13	55-60'	S-5		B	stained shale	CC, Q, I, K, P	H?	
GW822	U.W.1786/12	822-2	60-65'		C-5	A	mineralized calcite vein			CC, I, Q, K, Al-oxide
GW823	U.W.1786/13	823-7	18-19'			E	weathered shale	Q, I, K	H?	
GW823	U.W.1786/14	823-6	22-22.5'				red-orange staining on shale/sap			Al-silicates, Mn/Fe-oxides, CH?
GW823	U.W.1786/15	823-23	26.5'			D	red-orange staining on shale/sap	Q, CC, I, K	G? CH?	
GW823	U.W.1786/16	823-9	38'	S-3		C	red-orange staining on shale	CC, Q, K, G, P	H?	K, Fe-oxide, Mg/Fe/Al-silicates
GW823	U.W.1786/17	823-20	43-44'	S-4			red-orange staining on shale	CC, Q, K, P	H? B? G?	
GW823	U.W.1786/18	823-22a	48-49'	S-4			black crust on shale surface	Q, CC, I	B? D? P?	
GW823	U.W.1786/19	823-22b	48-49'	S-4		B	white crust on shale surface	CC, Q, K, P	D?	
GW823	U.W.1786/20	823-1	65-70'	S-7		A	red-orange staining on shale/clay			I, CH, P? Mn-oxide, biotite?

Notes:
* ML Port = Multilevel well sampling port
Mineral key: Q=quartz, CC=calcite, P=plagioclase, K=kaolinite, I=illite
G=goethite, H=hematite, CH=chlorite, D=dolomite, B=birnessite, GL=glauconite

The clay minerals (illite, kaolinite, chlorite, glauconite) were more difficult to identify due to often diffuse peaks and overlapping of diagnostic peaks. The oxides were extremely difficult to identify; only goethite was positively identified. Dolomite may be present in some of the samples but the diagnostic dolomite peak overlaps with calcite and was hard to distinguish in all but a few samples. There is a plagioclase phase present but because albite and anorthite have such similar peaks, a distinction between the two could not be made.

Figure 4-2 shows the XRD scans for matrix materials. The shale matrix samples were all collected from weathered intervals so they are not representative of competent shale. The primary minerals identified in the weathered shale are quartz, calcite, illite, kaolinite, and plagioclase. Tentatively identified minerals are goethite, hematite, and dolomite. The carbonate matrix consists of calcite and quartz; a tiny peak at around 2.88 Å suggests the presence of trace amounts of dolomite.

Figure 4-3 shows the XRD scans for the red-orange coatings that were scraped from rock surfaces. The samples were not always scanned under exactly the same conditions, leading to the different degrees of scattering of peaks. The primary minerals identified were quartz, calcite, illite, kaolinite, plagioclase, and goethite. Tentatively identified minerals are chlorite, hematite, and birnessite. A broad, diffuse peak is present in U.W. 1786/1 at a 2θ of 15.5 degrees. Particle size

analysis yielded a particle size of 40 Å. A similar peak was observed in U.W. 1786/8; particle size analysis also indicates a particle size diameter of 40 Å.

Figure 4-4 shows the XRD scans for other types of fracture coatings, including a white coating from the surface of weathered shale, a black coating from the same sample, and a green, soft mineral from a shale sample. The white sample (U.W. 1786/19) was found to contain calcite, quartz, kaolinite, plagioclase, and possibly dolomite. The black coating (U.W. 1786/18) consists of quartz, calcite, illite, and tentatively birnessite and dolomite (trace). The primary mineral of the green sample (U.W. 1786/4) was difficult to identify. A single grain was analyzed by Dr. S.W. Bailey using a Debye-Scherrer x-ray diffraction camera. The result indicated that the mineral had a 10 Å basal spacing. Three minerals with 10 Å 001 basal spacing are biotite, illite, and glauconite. The green color of the mineral suggested glauconite. This identification is supported by Foreman (1991) who observed glauconite in many of the carbonate lithologies and in enriched layers in the shale.

EDS

Pictures of back-scattered electron (BSE) images and the x-ray scans are presented in **Figures 4-5** through **4-7**. Minerals were identified by comparison of the x-ray scans included in Welton (1984). Minerals qualitatively identified using EDS were quartz, calcite, illite (**Figure 4-5**), kaolinite (**Figure 4-6**), and chlorite. Minor minerals include iron, manganese, and mixed iron-manganese oxide/hydroxides.

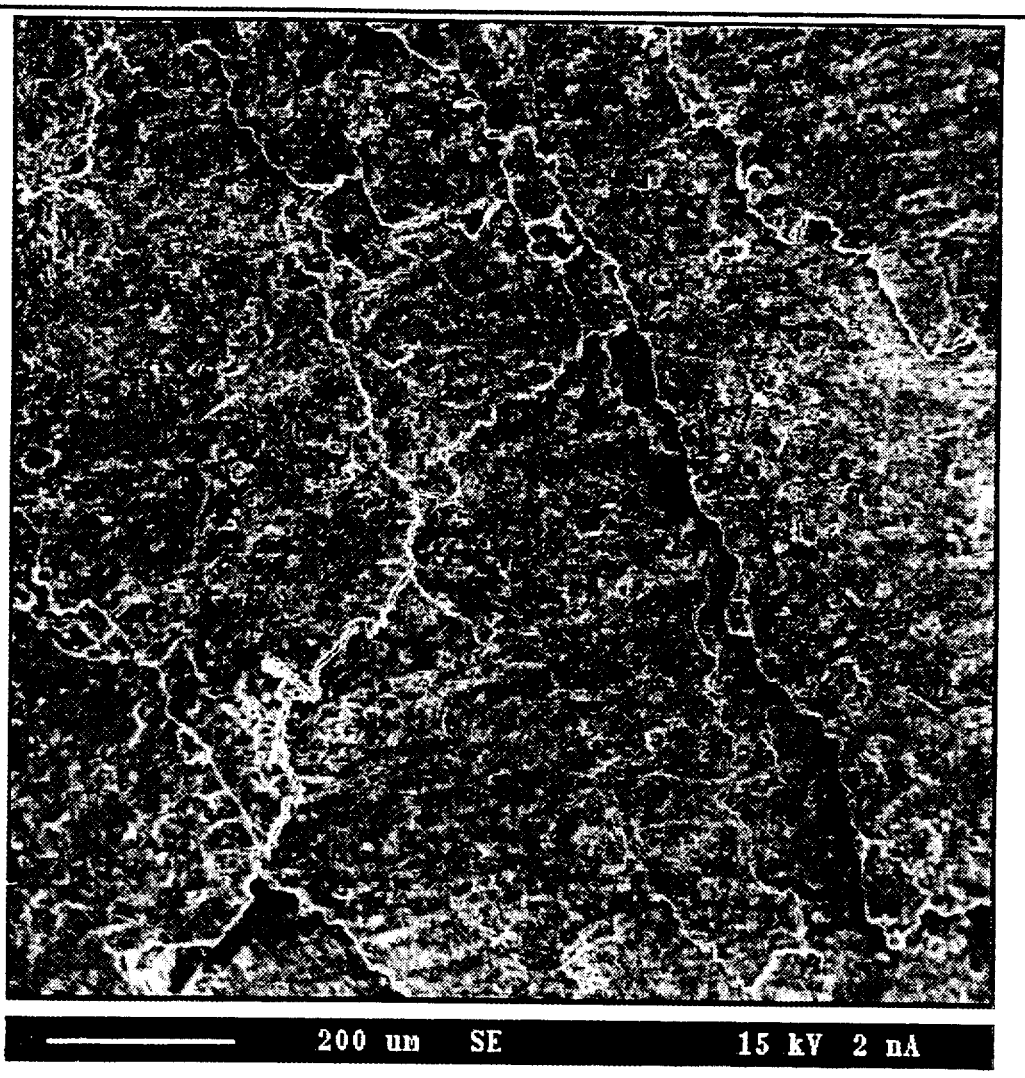

— ✓ test044 U.W. 1786/20

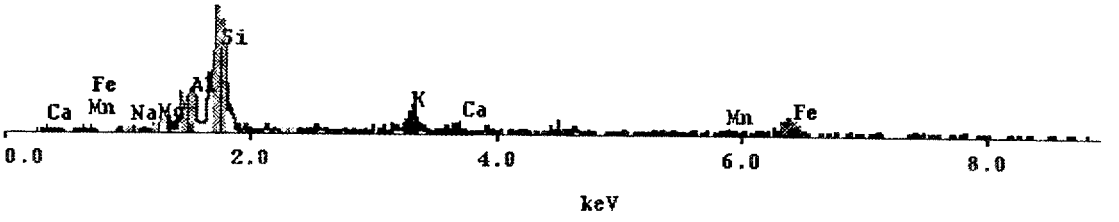

Figure 4-5: Back-scattered electron (BSE) image and x-ray scan of illite, the primary mineral of the shale matrix (U.W. 1786/20).

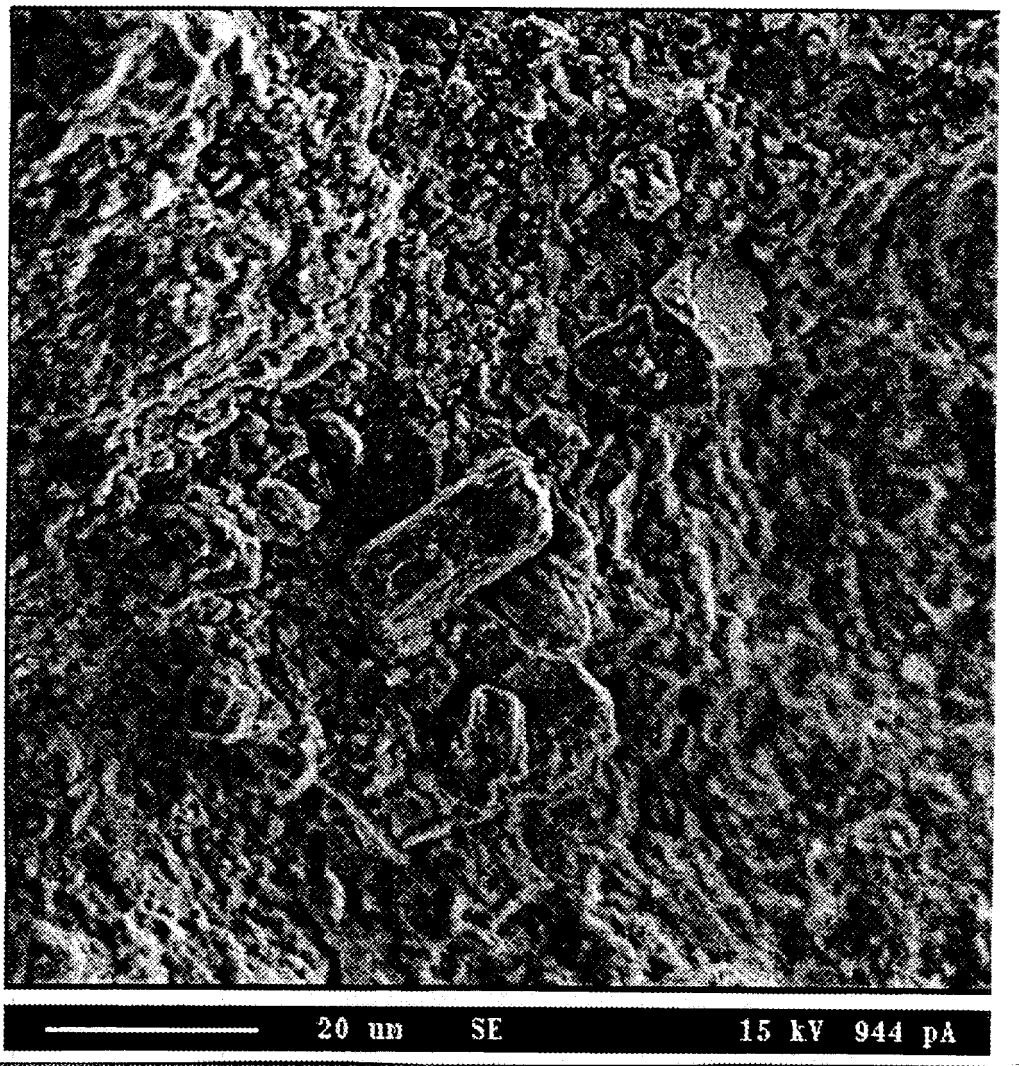

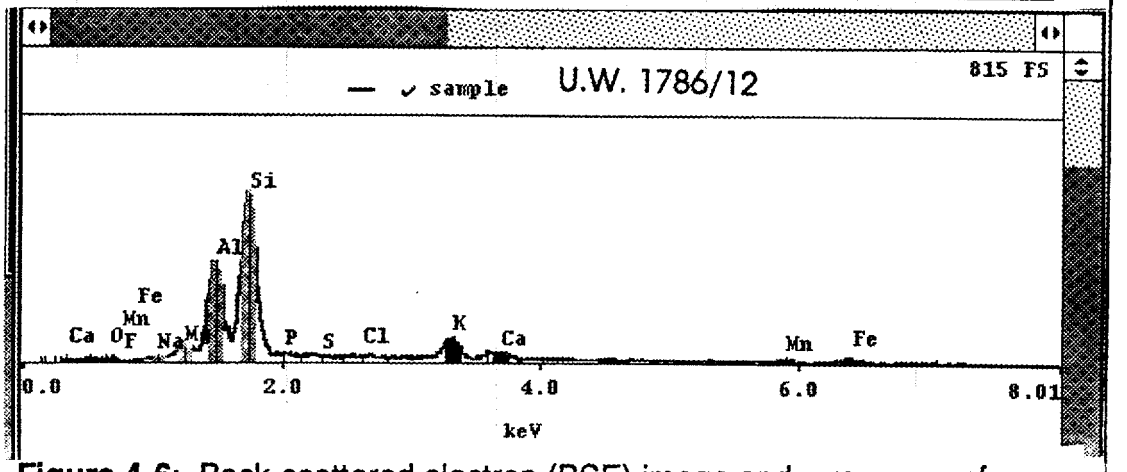

Figure 4-6: Back-scattered electron (BSE) image and x-ray scan of kaolinite, a mineral found both in the shale matrix and on fracture coatings (U.W. 1786/12).

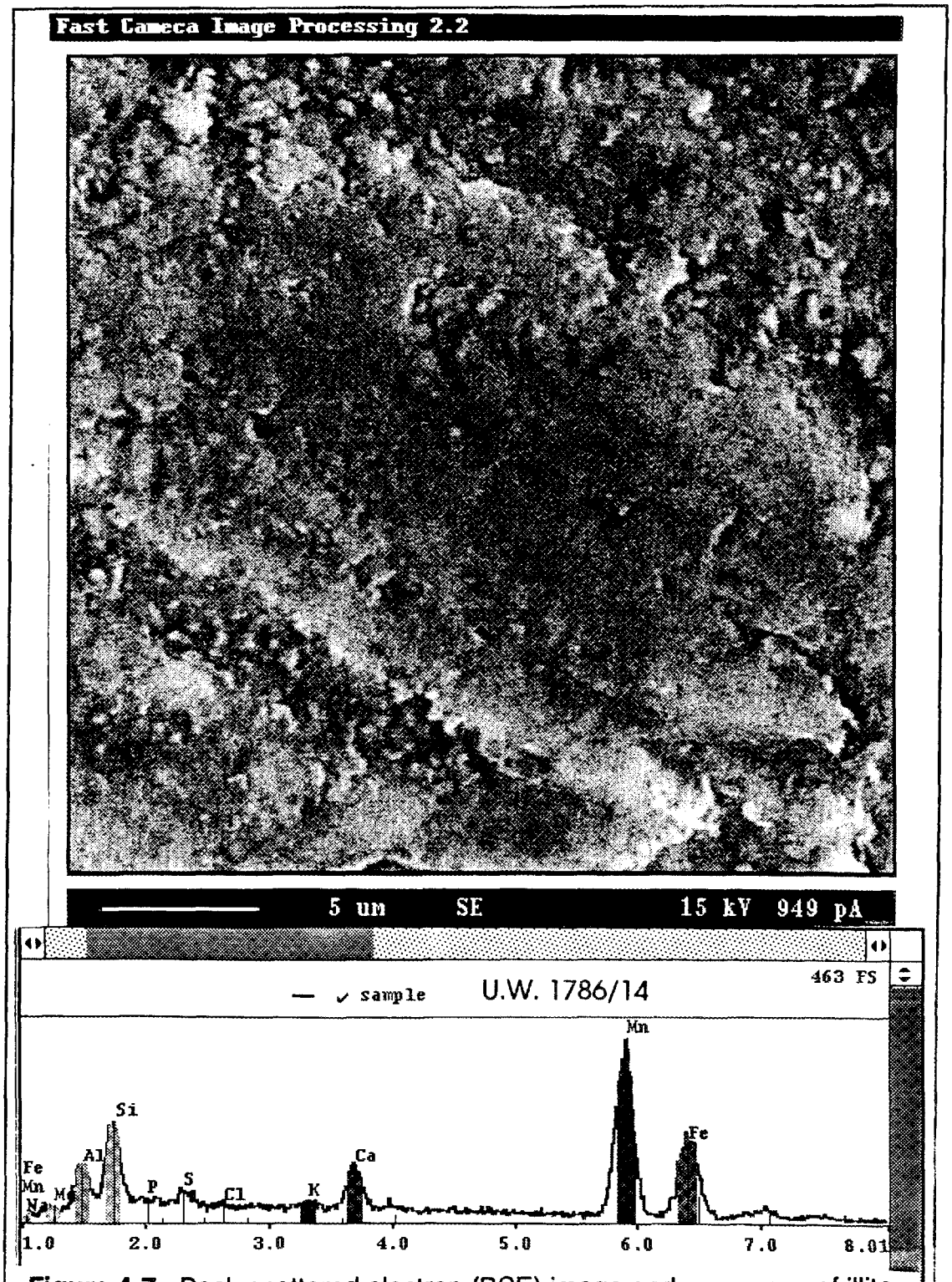

Figure 4-7: Back-scattered electron (BSE) image and x-ray scan of illite coated with iron and manganese oxides found on a fracture surface (U.W. 1786/14).

EDS analysis of oxide-coated matrix revealed high iron, manganese, aluminum, silicon, and lesser magnesium, potassium, calcium, and titanium. This may be due to the presence of very thin, fine-grained iron and manganese oxides on the surfaces of the clays and mica minerals (**Figure 4-7**). Mixed iron and manganese oxides have been observed in saprolite (Phillips, 1988).

4.7 Summary

The lithologic observations of core collected during drilling, described in Chapter 2, are consistent with descriptions of the middle unit of the Nolichucky Shale by Foreman (1991), in which the dominant carbonate lithology is an oolitic limestone. The shale is very fine-grained, and has both competent and highly weathered zones in core. Calcite veins are both cross-cutting and parallel to bedding. The shale and carbonate units correlated well between the boreholes; the correlations confirm an approximate 45 degree dip of bedrock to the southeast, estimated by Gierke et al. (1988).

Because drilling severely broke-up the shale, especially when drilling was done without fluids, fracture surfaces could not be identified as simply a break in core. Instead, they were inferred by oxide coatings. These surfaces were assumed to be in contact with groundwater which would oxidize any iron in the matrix and precipitate iron oxides and hydroxides. Although locating fractures was hindered by incomplete core recovery and/or compaction, many of these zones correlate with

zones of high flow identified by the borehole tests.

The results of the mineralogical study corroborate with the results of Lee et al. (1987). The major minerals identified in the shale bedrock are illite, quartz, calcite, chlorite, and kaolinite. Minor minerals include plagioclase, goethite, glauconite, and possible dolomite and birnessite. The feldspar phase was identified as plagioclase but the distinction between albite and anorthite could not be made. The carbonate interlayers in the shale consist primarily of calcite. The minerals in the Nolichucky that will likely play an important role in controlling the groundwater chemistry are calcite, which dissolves readily, clay minerals (illite, kaolinite, chlorite), which provide cation exchange sites, and oxides, which provide exchange sites and also have high sorptive capacities.

The mineral coatings on the fracture surfaces were tentatively identified as iron and manganese hydroxides. As mentioned above, oxides and clays, which commonly precipitate on fracture surfaces from water, have high sorptive capacities and are likely the largest influence on heavy metal transport in fractured rock. Knowledge of the types and phases of minerals that precipitate on fracture surfaces is essential to understanding the processes that control trace metal concentrations in groundwater. The techniques applied in this study were not sufficient to identify such poorly crystalline material. In order to properly investigate the nature of these coatings, techniques such as HRTEM or IR spectroscopy should be applied.

5. Sources of Vertical Variability in Groundwater Chemistry

5.1 Introduction

Three types of waters have been identified in the shallow groundwater system at the field site based on major ion predominance, Ca-HCO_3 (Type 1), Na-HCO_3 (Type 2), and Ca-Na-HCO_3 (Type 3). The origins of the Types 1 and 2 waters have been addressed in previous studies (Solomon et al., 1992; Moore and Toran, 1992; Haase, 1992). The modeling results of Haase (1992) conclude that the Type 1 water evolved under water-dominated conditions (low rock/water ratios) consistent with a shallow groundwater flow system and short flow paths (several 10s of meters). The Type 2 water has been observed in intermediate and deeper shale waters (below ~30-60 m depth). This water evolved under more rock-dominated conditions (higher rock/water ratios) which is consistent with a deeper flow system and long (several 100s to 1000s of meters) flow paths (Haase, 1992). It is presently thought that the Type 2 water originates from local recharge areas (i.e. ridges) (Moore and Toran, 1992) rather than from a regional system of groundwater that underflows the ridge.

Although the origins of the Types 1 and 2 waters have been examined, the source of the Type 3 water has not been previously addressed. Interactions between Types 1 and 2 waters and the surrounding rock may provide a possible source of the Type 3 water. The fence diagram of the hydrochemical facies (**see Figure 3-12**)

shows that the Type 3 waters are positioned vertically between the Types 1 and 2 waters, suggesting that mixing may contribute to the evolution of this type. This chapter describes the methods used to test three hypotheses of the possible sources of the Type 3 water: 1) water-rock reactions between Type 1 and Type 2 waters with the shale and carbonate rocks, 2) mixing of the Type 1 and Type 2 waters, and 3) mixing with associated water-rock interactions. The three hypotheses are tested using different types of geochemical models to look at speciation-solubility characteristics and probable geochemical mechanisms that could result in the Type 3 water.

Hypothesis 1: Water-Rock Interactions

Mass balance models were used to look at the possible water-rock reactions that could occur to account for 1) the evolution of Type 2 from Type 1 waters along the flow path from Pine Ridge to the field site and 2) the evolution of the Type 3 water from Types 1 and 2 waters in the discharge zone.

From the results of the mineralogical study and the geochemical characterization, in which high calcium, bicarbonate, and sulfate concentrations and an inverse correlation between calcium and sodium were observed, the water-rock reactions that could be important in controlling the groundwater chemistry at the field site are calcite dissolution and precipitation, cation exchange, silicate dissolution and precipitation, and dissolution of a sulfur-containing mineral.

The composition of Ca-HCO_3 water results from the reaction of recently recharged water with calcite:

$$CaCO_3 + H^+ <=> Ca^{2+} + HCO_3^- \quad (5\text{-}1)$$

In addition, calcite was identified on fracture surfaces, indicating that calcite is also precipitating in the shallow groundwater system and is acting as a sink for calcium and bicarbonate.

Changes in the ratios of calcium and sodium in natural waters have been typically attributed to cation exchange of calcium for sodium on clay exchange sites (e.g. Foster, 1950):

$$Ca^{2+} + 2Na\text{-}X <=> Ca\text{-}X_2 + 2Na^+ \quad (5\text{-}2)$$

The result of cation exchange is to increase the sodium and decrease the calcium in solution, creating Na-HCO_3 waters. In order for cation exchange processes to occur, there must be a sufficient volume of solids with high cation exchange capacities (CEC). The cation exchange capacity of materials is defined as the excess of counter ions in the zone adjacent to the charged surface or layer which can be exchanged for other cations (Freeze and Cherry, 1979). Solids with high CEC have large surface areas and are generally clay-size particles. Exchange capacity is therefore often linked to clay content of the material, percent organic matter, and oxide or hydroxide content. The presence of kaolinite (CEC = 3-15 meq/100g), illite (20-50), goethite (up to 100), chlorite (10-40), glauconite (5-40) in the shale and vermiculite (100-200) in the saprolite means that there are sufficient

sites available for exchange. Cation exchange will proceed until equilibrium is reached, after which additional Ca-HCO_3 that infiltrates through the exchange material will no longer evolve to Na-HCO_3 waters.

The weathering of silicate minerals affects the groundwater chemistry, although dissolution of most silicate minerals is relatively slow. Silicate weathering can also contribute to changes in chemical composition of water with respect to sodium and calcium. For example, Na-feldspar (albite) weathers to kaolinite, releasing sodium and silicic acid into solution:

$$2NaAlSi_3O_8 + 2H^+ + 9H_2O \Leftrightarrow Al_2Si_2O_5(OH)_4 + 2Na^+ + 4H_4SiO_4 \qquad (5\text{-}3)$$

Albite may be present in the shale and kaolinite has been identified on fracture surfaces, suggesting that this process may be an additional source of sodium to groundwater. Clay alteration and formation can also lead to changes in the chemical composition of groundwater. For instance, illite and albite can weather to montmorillonite. This series of reactions would also yield a decrease in calcium and an increase in sodium (Solomon et al., 1992). However, because montmorillonite was not identified in the matrix or on fractures, these reactions are not considered.

The dissolution of sulfur-containing minerals such as pyrite can provide sulfate to groundwater, as shown in the following reaction:

$$4FeS_2 + 15O_2 + 14H_2O \Leftrightarrow 4Fe(OH)_3 + 8SO_4^{2-} + 16H^+ \qquad (5\text{-}4)$$

Pyrite has been identified in trace amounts (<2 weight percent) by Lee et al. (1987).

Gypsum has not previously been identified in the Nolichucky but it may be present in underlying formations.

Hypothesis 2: Conservative Mixing

A second hypothesis is that conservative mixing of the Types 1 and 2 waters is the source of the Type 3 water. To examine this hypothesis, the Type 1 and Type 2 waters were mixed using geochemical models to determine if the mixtures approximate the varying calcium to sodium ratios observed in the Type 3 multilevel well samples.

Hypothesis 3: Mixing with Water-Rock Interactions

A third hypothesis is that the Type 1 and Type 2 waters are undergoing both mixing and associated water-rock reactions in the discharge zone to produce the Type 3 waters. This hypothesis was tested using a mass balance model that allows for both mixing and mass transfer.

5.2 Methods for Testing Hypotheses

The geochemical models used to evaluate the possible sources of the Type 3 waters are 1) speciation-solubility models to evaluate degree of saturation of waters with respect to key minerals, 2) reaction path models to simulate conservative mixing of different percentages of Types 1 and 2 waters, and 3) mass balance models to predict mixing reactions and to identify possible geochemical reactions

that may explain differences in water chemistry along a flow path. PHREEQE (Parkhurst et al., 1980) was used as both a speciation-solubility and a reaction path model, although its reaction path capabilities are limited. The mass balance models used were a spreadsheet mass balance model by Bowser and Jones (1990) and NETPATH (Plummer et al., 1991).

Speciation-solubility models

Speciation-solubility codes solve simultaneous equations describing the saturation state of water with respect to the minerals and gases of interest. From an input of solution analyses, the programs compute the activities of the complexed and free ionic species, and ion pairs. The models then calculate the ion activity product (IAP) and compare the IAP to the solubility products (K), resulting in the saturation index (SI = IAP/K). Because these codes do not consider rates of reaction, the actual precipitation or dissolution of minerals may not follow the predictions of the SI. If the input data contain charge balance errors, it is possible to choose a species with which to balance the charge. However, the geochemical data used in the modeling have charge balance errors less than 5%, so this option was not utilized.

Each speciation-solubility model uses a different thermodynamic database. The thoroughness and consistency of a database heavily influences the quality of the modeling results. The thermodynamic database used in NETPATH (Plummer et al.,

1991) is from the WATEQF model (Plummer et al., 1976). The thermodynamic database utilized by PHREEQE (Parkhurst et al., 1980) is user-defined, which allows for greater flexibility but also creates the potential for inconsistency. The results of the iron oxide/hydroxide saturation states using either of these databases are likely to be inaccurate because iron complexes with organic matter and the thermodynamic data for organic species are limited. In addition, the thermodynamic and solubility data on iron in its many possible forms are incomplete at this time. Particle size effects are probably the main cause of solubility variations of the crystalline oxyhydroxides (Macalady et al., 1990). As discussed in Chapter 4, the particle sizes of many of the oxide coatings are extremely small; therefore, the solubility and speciation calculations for the secondary oxides (i.e., goethite) can only be considered to be approximations.

Mass balance models

Mass balance models are useful in identifying possible reactions that may explain differences in water chemistry along a flow path. These models predict the amounts of assumed mineral or gas reactants and products that must dissolve and/or precipitate between an initial and a final point in a system. The biggest limitation of mass balance models is the lack of thermodynamic constraints, leading to predictions of impossible reactions. Another limitation is that the solutions of mass balance equations are not necessarily unique. The use of a mass balance model requires common sense and enough geochemical knowledge to know if predicted

reactions are possible, thermodynamically and kinetically, within the given geologic setting. A mass balance spreadsheet created by Bowser and Jones (1990) was used to identify sets of dissolution and precipitation reactions that might occur to account for water chemistry changes observed. NETPATH (Plummer et al., 1991) was used to compute mixing proportions of two initial waters and the geochemical reactions that can account for the observed composition of a final water.

Reaction path models

Reaction path models can predict the chemical composition of an aqueous solution and the amounts of minerals dissolved and precipitated if a particular set of hypothetical reactions and thermodynamic constraints are input. The major advantage of the more advanced reaction path models is that they can simulate systems in partial equilibrium. Although PHREEQE (Parkhurst et al., 1980) does not have the capability to simulate partial equilibrium, it can simulate several types of reactions, including mixing of two solutions.

Model input data

Input data for the all of the models include the chemical composition of a starting water. The speciation-solubility require temperature and redox state data. The reaction path and mass balance models require reacting phases. The minerals identified by this study (Chapter 4) and by Lee et al. (1987) were used for reacting phases in the shale. Although the bulk mineralogies are well-constrained, the

presence of trace minerals such as pyrite and soluble salts is not well known for samples collected during this study. The presence of gypsum in the Conasauga Group has been postulated (Solomon et al., 1992) but not substantiated. Pyrite was identified in the Nolichucky in trace amounts by Lee et al. (1987). The dominant feldspar phase is also not well-constrained. The XRD results show a minor amount of plagioclase feldspar, but do not distinguish between albite and anorthite.

Sensitivity analyses

Sensitivity analyses were conducted to examine the effect of different values of pH and dissolved oxygen (D.O.) on saturation indices of GW821A. Values of pH differed between field and laboratory measurements. The lab measurements are higher than the field measurements, some by a few tenths of a pH unit. This is likely due to degassing of CO_2 between the field and the lab which would increase the pH of solution (Roberson et al., 1963). The effects of pH on the saturation state of calcite and pCO_2 are significant. The field pH value resulted in a lower calculated value of the calcite SI and higher calculated pCO_2. Quartz saturation is not affected by changes in pH. Although the field pH values are less precise, they are more representative of the actual conditions in the groundwater system and therefore were used in the speciation-solubility modeling. Four measurements of D.O. from GW462 were taken in 1988-1989. The values range from 1.6 to 4.7 mg/l, with an average of 3 mg/l (S. Winters, written communication). Sensitivity analyses were conducted to examine the changes in speciation and solubility using the maximum,

the average, and the minimum D.O. values. The results of the D.O. sensitivity analyses showed changes in the speciation of the waters but no changes with respect to saturation indices.

5.3 Results and Discussion

Speciation-solubility models

Figure 5-1 presents the variations of saturation indices with depth for each of the multilevel wells calculated using PHREEQE (Parkhurst et al., 1980). The input files for the model calculations are shown in **Appendix K**. These saturation indices were calculated using field pH values and a D.O. value of 3 mg/l. A positive SI indicates that the water is theoretically oversaturated with respect to the mineral; therefore, if that mineral is in contact with the water, it should precipitate. If the SI equals zero, the water is in equilibrium with the mineral. A negative SI indicates that the water is undersaturated with respect to the mineral; therefore, if that mineral is in contact with the water, it should dissolve. These indices are not precise measures of equilibrium due to uncertainties in the analytical data and in the thermodynamic data used to calculate the equilibrium constants. Therefore, any SI near zero may represent equilibrium. Saturation indices within 5% of the log K of the solid are often estimated to represent the range of saturation (Jenne et al., 1980). Calcite is often interpreted to be in equilibrium when the SI is +/- 0.2 (Appelo and Postma, 1993).

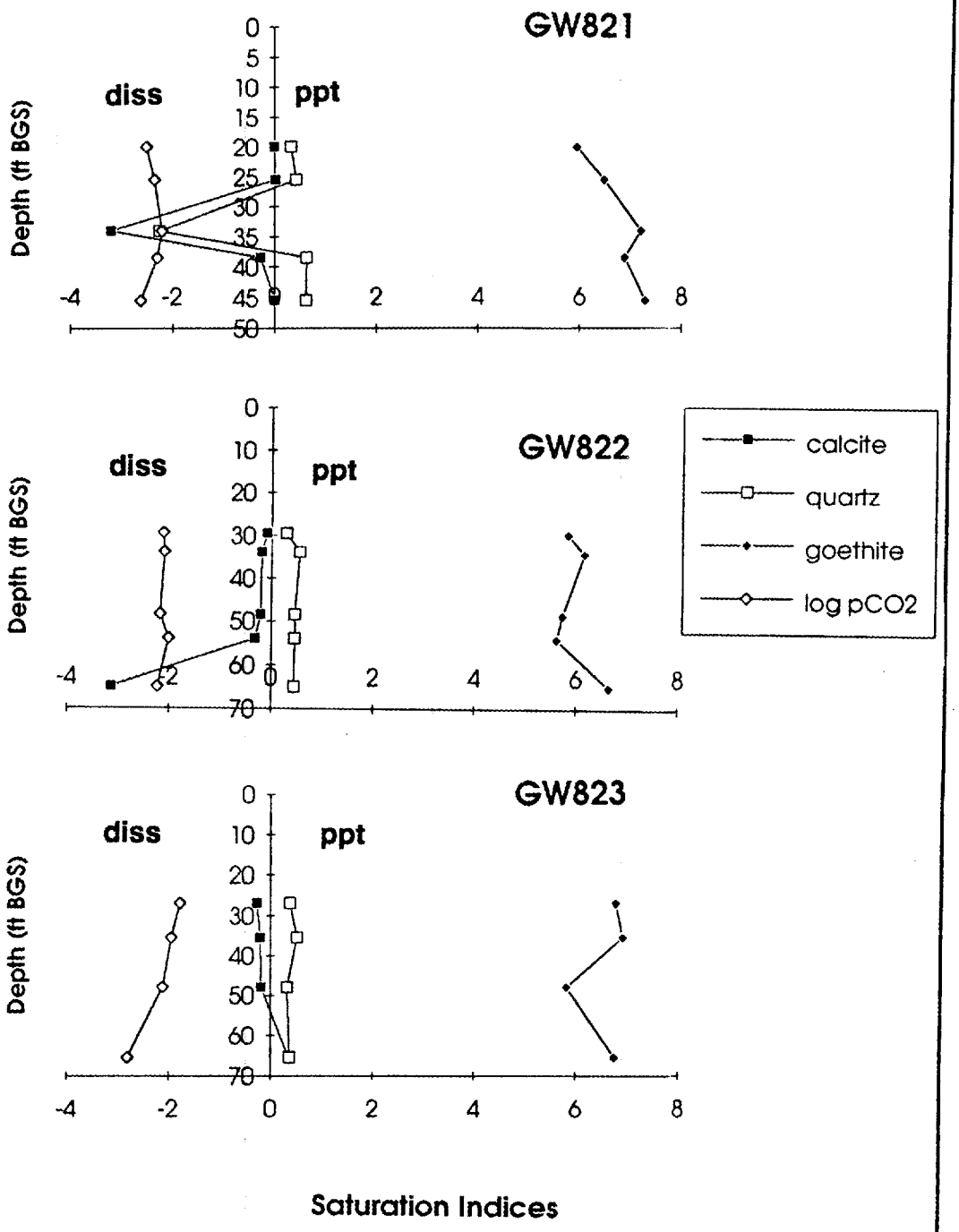

Figure 5-1: Saturation indices (SI=IAP/K) versus depth. SI calculated by PHREEQE, using field pH values and D.O. of 3 mg/l.

In general, the shallow groundwater at the field site is calculated to be slightly oversaturated with quartz and significantly oversaturated with iron oxides/hydroxides (goethite, hematite, amorphous $Fe(OH)_3$). Calculations show that the groundwater is generally in equilibrium with calcite. High negative calcite saturation indices (-3) in samples GW822A (65') and GW821C (34') may be a result of waters that have recently mixed and have not had time to reach equilibrium with respect to calcite (Mazor, 1992). The SI of iron oxides shows that in the presence of oxygen, iron will precipitate as oxides or oxyhydroxides, resulting in the iron oxide coatings observed on fracture surfaces discussed in Chapter 4.

The pCO_2 values calculated by PHREEQE (Parkhurst et al., 1980) (approximately 10^{-2} to $10^{-2.5}$ atm) are higher than atmospheric ($10^{-3.5}$ atm) which is to be expected in water which has equilibrated with calcite and has open gas exchange with the soil. The relatively constant values of the calculated pCO_2, as well as the pH, and concentrations of calcium and bicarbonate, strongly suggest that the system is open to the atmosphere. For groundwater that is saturated with calcite and in contact with an atmospheric pCO_2 of 10^{-3} atm, the pH is approximately 8, the concentration of calcium is approximately 10^{-3} M and the concentration of bicarbonate is approximately $10^{-2.8}$ M. These calculations are very close to the concentrations observed in the Type 1 samples.

Mass balance and reaction path models

The mass balance and reaction path models were used to evaluate the three hypotheses of the evolution of the Type 3 water.

Hypothesis 1: Water-Rock Interactions

Mass balance models were used to look at the possible water-rock reactions that could occur to account for 1) the evolution of the Type 2 from the Type 1 water along the flow path from Pine Ridge to the field site and 2) the evolution of the Type 3 water from Types 1 and 2 waters in the discharge zone. The phases considered in the model were the shale and carbonate matrix minerals (illite, kaolinite, chlorite, calcite, silica, plagioclase) and secondary weathering products identified on fracture surfaces (goethite, silica, kaolinite, calcite). Albite was included as the plagioclase phase to provide a source of sodium, although it was not positively identified in the mineralogical characterization. Pyrite was included as the source of sulfate. The mass balance model calculates mass transfer of phases in (dissolution) and out (precipitation) of an initial water to yield a final water. Positive mass transfer indicates dissolution and negative mass transfer indicates precipitation.

Evolution of Type 1 to Type 2

Two scenarios were able to account for the evolution of Type 1 to Type 2 water (**Figure 5-2**). The first scenario predicts exchange of calcium for sodium, dissolution of albite, pyrite, and calcite, and precipitation of silica and kaolinite.

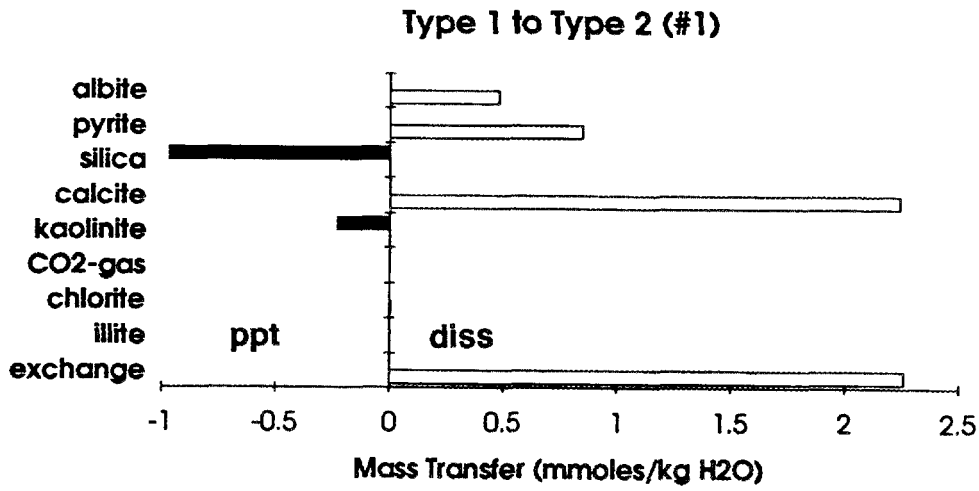

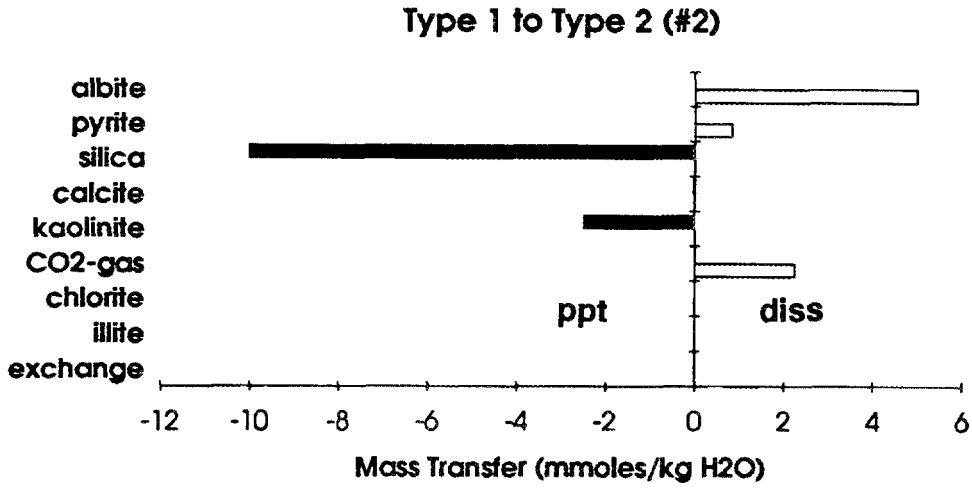

Figure 5-2: Mass balance modeling results for creation of Type 2 (Na-HCO_3) from Type 1 (Ca-HCO_3) water. A positive mass transfer value indicates dissolution of mineral phase; a negative value indicates precipitation.

The second scenario predicts dissolution of albite and pyrite and precipitation of silica and kaolinite. To evaluate if either of these reaction scenarios could take place along the local flow path from Pine Ridge to the field site, the residence times required for the predicted mass transfer can be estimated. First, the time it takes for groundwater to flow from Pine Ridge to the field site was calculated. Travel times were calculated using the following data taken from Table 1 of Moore and Toran (1992, p. 38-39). Average hydraulic conductivities in the aquitards are 8.8E-08 m/d in the unfractured rock matrix, 4.0E-04 m/d in low permeability intervals, and 6.6E-02 m/d in the permeable intervals. The matrix porosity is estimated to be 9.6E-03 and the fracture porosity is estimated to be 5.0E-04. The average hydraulic gradient in the aquitards is 0.05. With a distance from Pine Ridge and the field site of approximately 700 m, the time it would take for groundwater originating at Pine Ridge to reach the field site varies from 103 days in the permeable intervals to 48 years in the low permeability intervals to 10^6 years in the unfractured rock matrix. Groundwater in the water table interval flows through well-connected fractures and will reach the field site in the least amount of time. In the deeper intervals, where flow is dominated by fractures which may or may not be well-connected, groundwater will take a longer time to reach the field site.

To evaluate if evolution of Type 1 to Type 2 water is feasible along flow paths from Pine Ridge to the field site, mineral dissolution rates can be used to compare the time required to yield observed sodium concentrations in the Type 2 water to the

groundwater travel times. Because cation exchange reaction rates are not well known, the dissolution rate of albite is used. Using an albite dissolution rate of 1.19E-15 mol/cm^2/sec (Holdren and Berner, 1979; Lasaga, 1984), an average fracture aperture of 0.12 mm (Moore and Toran, 1992), and assuming that albite covers 10% of the fracture surface, the time it would take for 0.48 mmoles of albite/kg H_2O (predicted for the first scenario) to dissolve is 280 days. The second mineral assemblage predicts dissolution of 5 mmol of albite/kg H_2O, which would take eight years. These calculations show that the origin of the sodium in Type 2 from reactions of the Type 1 water with albite is feasible along flow paths from Pine Ridge to the field site, and that groundwater underflow is not required to account for the sodium concentrations in the Type 2 water.

Albite dissolution yields predicted precipitation of silica, which is a much slower reaction. The first scenario predicts 0.97 mmoles of silica/kg H_2O. The residence time required to precipitate this amount of silica on 50% of the fracture surface, based on the dissolution rate of quartz of 4E-18 mol/cm^2/sec (Rimstidt and Barnes, 1980; Lasaga, 1984), and assuming a reversible reaction, is approximately 90 years. The second scenario predicts precipitation of 10 mmoles of silica/kg H_2O. The residence time required to precipitate this amount of quartz is approximately 932 years, which exceeds the groundwater travel times in both the high and low permeability zones. Because the silica that is precipitated is likely to be an amorphous phase and not quartz, and recognizing that the precipitation rate of

amorphous silica will be higher than the one used, these calculated residence times must be viewed as estimates. However, they do provide a relative idea of the length of time required to dissolve and precipitate minerals according to the predictions of the mass balance models. These estimated residence times indicate that the first scenario is more likely than the second scenario to account for the evolution of Type 1 to Type 2 water.

The sulfate concentrations in the Type 2 water are assumed to result from pyrite dissolution because pyrite has been observed in the shale. The dissolution rate of pyrite is highly dependent on pH, the concentrations of electron acceptors such as oxygen and Fe^{3+}, temperature, and the specific surface areas of the pyrite crystals (Nicholson et al., 1988; 1990; Moses et al., 1987). Dissolution experiments conducted by Moses et al. (1987) indicate that pyrite dissolution rates are limited by the oxidation of sulfide to sulfate, which is controlled by the concentrations of dissolved oxygen and Fe^{3+}. Because the groundwater at the field site has relatively low D.O. (approximately 3 mg/l), the concentrations of Fe^{3+} are likely also to be low, and therefore, pyrite dissolution rates in this groundwater are assumed to be slow.

Evolution of Type 1 to Type 3

The mass balance model of evolution of Type 1 to Type 3 generated two scenarios of possible reactions (**Figure 5-3**). The first scenario predicts dissolution of calcite, illite, chlorite, and pyrite, Ca-Na exchange, and precipitation of kaolinite and silica.

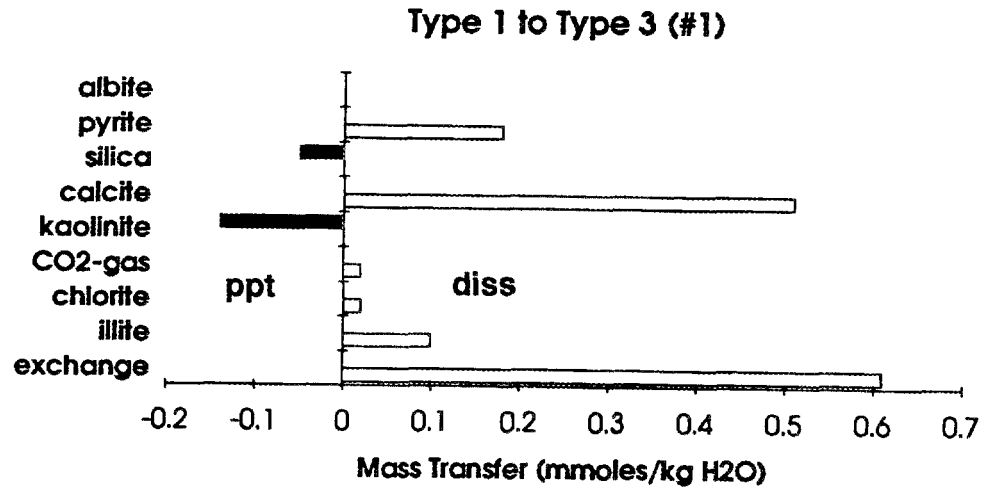

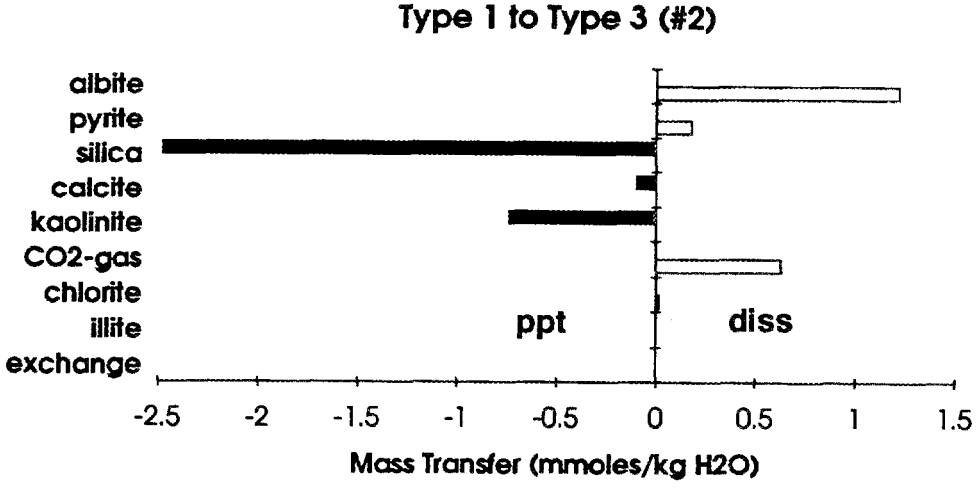

Figure 5-3: Mass balance modeling results for creation of Type 3 (Ca-Na-HCO_3) water from Type 1 (Ca-HCO_3) water. A positive mass transfer value indicates dissolution of mineral phase; a negative value indicates precipitation.

Groundwater was calculated to range from being in equilibrium to being undersaturated with calcite; calcite dissolution can therefore be expected. Ca-Na exchange is feasible due to the presence of clay minerals in the shale with high cation exchange capacities. Dissolution of illite and chlorite is plausible since these minerals are both present in the shale matrix. Precipitation of small amounts of the secondary minerals kaolinite and silica is expected because these minerals were identified on fracture surfaces. As previously discussed, the dissolution rate of pyrite in the absence of significant concentrations of dissolved oxygen and Fe^{3+} is assumed to be slow. Therefore, it is unlikely that Type 1 water, which is observed in permeable zones, would be present in the discharge zone for a long enough time for pyrite dissolution to account for the sulfate concentrations in the Type 3 water.

The second mass balance scenario of Type 1 to Type 3 evolution predicts dissolution of albite and precipitation of silica, calcite, pyrite, and kaolinite. Calculations of the residence time required to precipitate 2.5 mmoles of silica/kg of H_2O, based on the dissolution rate of quartz of 4E-18 mol/cm^2/sec (Rimstidt and Barnes, 1980; Lasaga, 1984), and assuming a reversible reaction, is 115 years. This would be feasible along a longer flow path, but not for reactions occurring locally in the discharge zone.

Evolution of Type 2 to Type 3

The mass balance model of evolution of the Type 2 to the Type 3 water did not yield

any plausible sets of reactions. Three models were obtained, two of which predicted exchange of sodium for calcium. This reaction is not favored unless brine-level concentrations of sodium are present because calcium is the preferred ion on the exchange site. The third model predicted albite precipitation as an alternative sink for sodium. This reaction is also highly unlikely, both thermodynamically and kinetically.

The results of the mass balance modeling indicate that water-rock interactions can account for the evolution of the Type 2 from the Type 1 water along the flow path from Pine Ridge to the field site. Water-rock interactions can also account for most of the evolution of Type 3 from Type 1 water through exchange of calcium for sodium, calcite dissolution, dissolution of illite, chlorite, and albite, and minor precipitation of kaolinite, goethite, and silica. One limitation of attributing the changes in concentrations between Types 1 and 3 solely to water-rock interactions is that pyrite dissolution alone cannot account for the sulfate concentrations in the Type 3 water. Another process that contributes sulfur to the Type 3 water, therefore, must be considered.

Hypothesis 2: Conservative mixing

Using NETPATH (Plummer et al., 1991), mixing ratios of Type 1 and 2 waters were calculated to result in Type 3 waters. These mixing ratios were determined by the sulfate concentrations in each of the waters. Using the ratios, PHREEQE

(Parkhurst et al., 1980) calculated the concentrations of the major and minor ions resulting from conservative mixing based on sulfate.

To evaluate if conservative mixing is a source of the Type 3 waters, the major ion concentrations calculated by PHREEQE (Parkhurst et al., 1980) were compared to the major ion concentrations in the Type 3 samples. This comparison shows that conservative mixing, based on sulfur, does not account for the compositions of other ions in the Type 3 waters (**Table 5-1**). For most of the samples, the conservative mixing ratio yielded calcium concentrations that are in excess of concentrations in the Type 3 waters and concentrations that are deficient with respect to sodium. The bicarbonate concentrations predicted by conservative mixing are not significantly different (<10%) from the Type 3 waters. These observations suggest that cation exchange may be an important influence on this system; this reaction would decrease the calcium and increase the sodium concentrations.

Hypothesis 3: Mixing and water-rock interactions

Using NETPATH (Plummer et al., 1991), mixing and geochemical reactions between initial waters of Types 1 and 2 and final waters of Type 3 were simulated. The mineral assemblage included all of the matrix and secondary minerals, except for goethite and pyrite; the mixing ratio was determined by sulfur. Goethite was not included because of probable colloidal contamination in the groundwater samples which can overestimate the dissolved iron concentration in solution.

Table 5-1: Conservative mixing of Type 1 and Type 2 water

PHREEQE (Parkhurst et al., 1980) mixing ratios determined by sulfur

Type 1 822E
Type 2 823D

	mix	822C	mix excess	mix deficient
Type 1 %	37			
Type 2 %	63			
Ca mmol/L	1.53	1.22	X	
Na mmol/L	3.37	3.57		X
HCO3 mmol/L	3.91	4.33		X
		822B		
Type 1 %	92			
Type 2 %	8			
Ca mmol/L	1.55	1.27	X	
Na mmol/L	0.62	0.92		X
HCO3 mmol/L	4.01	3.83	--	--
		822A		
Type 1 %	98			
Type 2 %	8			
Ca mmol/L	1.55	1.07	X	
Na mmol/L	0.32	0.78		X
HCO3 mmol/L	4.03	3.58	X	
		822D		
Type 1 %	79			
Type 2 %	21			
Ca mmol/L	1.54	1.45		
Na mmol/L	1.26	1.43		
HCO3 mmol/L	4	4.09	--	--

Notes: -- less than 5% difference

	mix	823A	mix excess	mix deficient
Type 1 %	98			
Type 2 %	2			
Ca mmol/L	1.55	0.95	X	
Na mmol/L	0.32	1.04		X
HCO3 mmol/L	4.03	3.96	--	--
		821C		
Type 1 %	85			
Type 2 %	15			
Ca mmol/L	1.54	1.02	X	
Na mmol/L	0.97	2.04		X
HCO3 mmol/L	4.00	3.91	--	--
		823B		
Type 1 %	97			
Type 2 %	3			
Ca mmol/L	1.55	1.27	X	
Na mmol/L	0.37	0.83		X
HCO3 mmol/L	4.03	3.71	X	
		821D		
Type 1 %	100			
Type 2 %	0			
Ca mmol/L	1.55	1.40	X	
Na mmol/L	0.22	0.32		X
HCO3 mmol/L	3.66	3.51	--	--

Sulfate was accounted for by mixing only. As discussed previously, it is unlikely that Type 1 water, which is observed in permeable zones, would be present in the discharge zone for a long enough time for pyrite dissolution to account for the sulfate concentrations in the Type 3 water.

Results of the mixing plus mass transfer scenarios obtained from NETPATH (Plummer et al., 1991) are summarized in **Figure 5-4**. These results show that the reactions induced by mixing that have the most influence on the formation of the Type 3 waters are calcite precipitation, Ca-Na exchange, and possibly albite dissolution. The silicate minerals (illite, chlorite, kaolinite) are important in controlling the chemistry with respect to potassium, magnesium, aluminum, and silica; however, these species (with the exception of aluminum), do not vary considerably in solution and as a result, very little silicate mass transfer is required. In all reactions, carbon dioxide is consumed.

The predicted mixing percentages are shown on the fence/Stiff diagram from Chapter 3 (**Figure 5-5**). Samples from GW821E, GW821D, and GW822E are 100% Type 1 water. GW823D is 100% Type 2 water. The other samples are shown as mixing percentages of the end-member waters. The calculated ratios for the mixtures correlate with the position of the mixture with respect to the Type 1 and Type 2 waters, giving support to the mixing hypothesis.

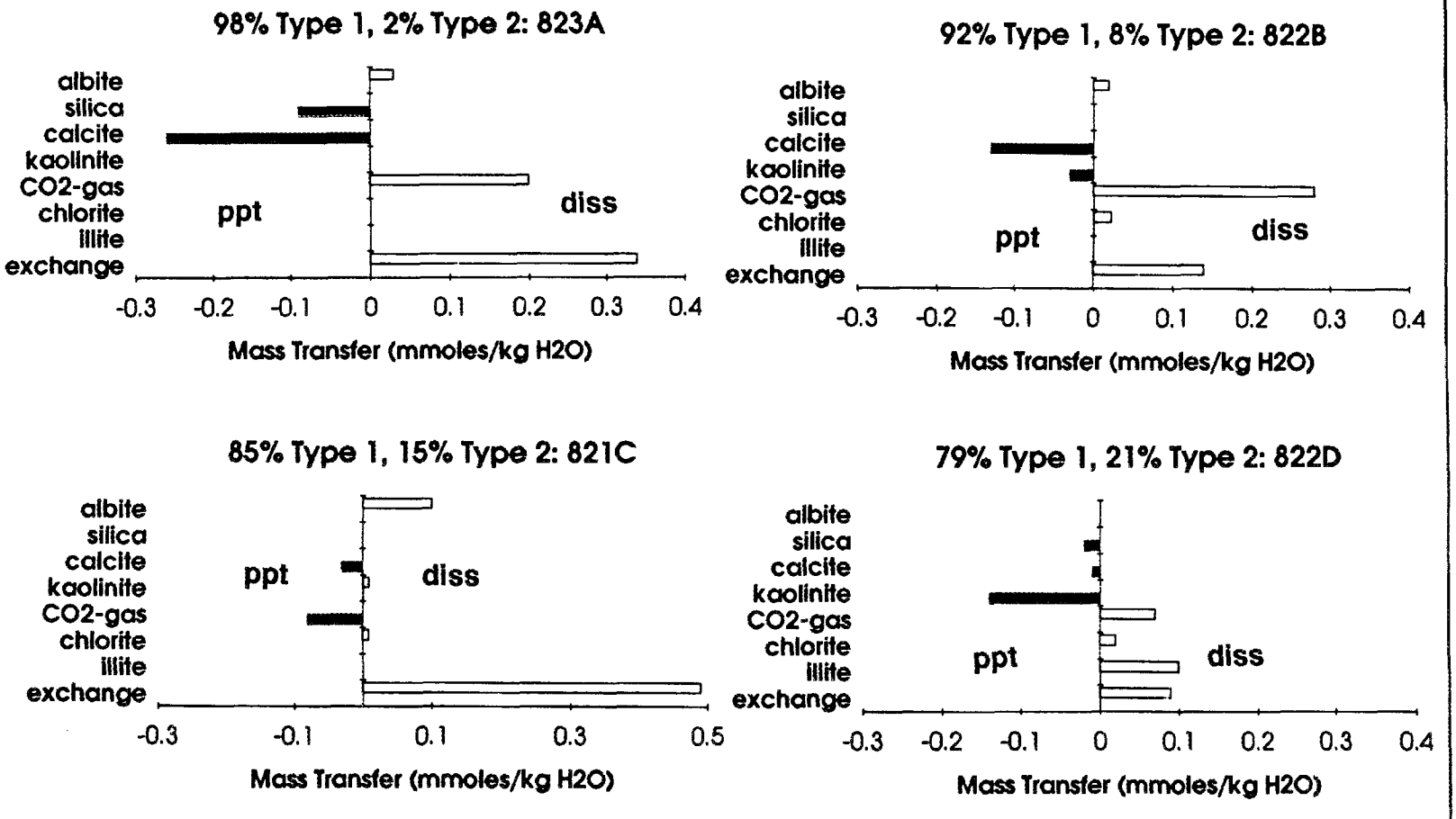

Figure 5-4: NETPATH modeling results for the mixing Type 1 ($Ca\text{-}HCO_3$) and Type 2 ($Na\text{-}HCO_3$) waters. The mixing ratios were determined by sulfate. A positive mass transfer value indicates dissolution of mineral phase; a negative value indicates precipitation.

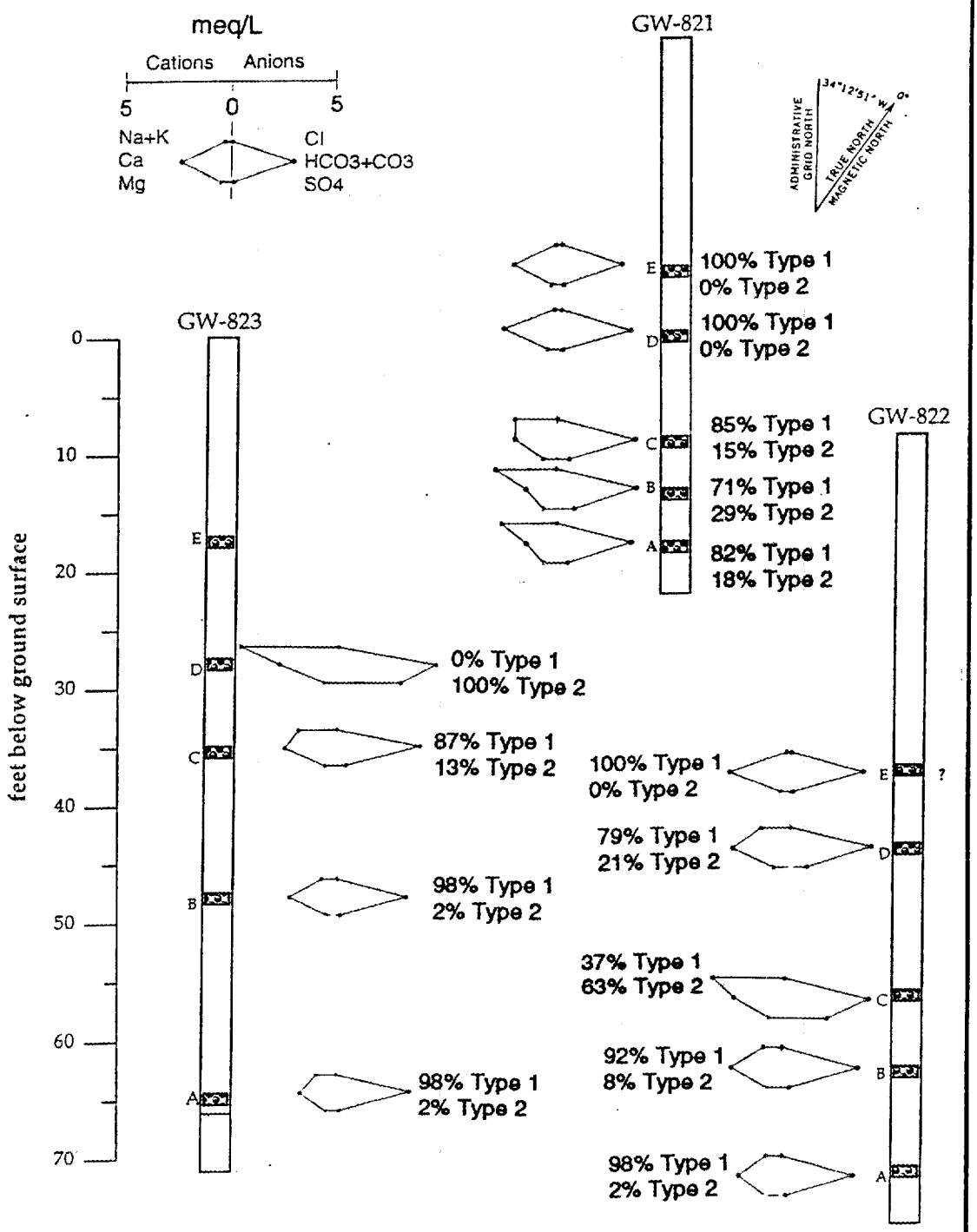

Figure 5-5: Fence/Stiff diagram showing mixing percentages of the multilevel well samples.

Due to the non-uniqueness of mass balance solutions, some caution should be used when examining the results of these simulations. For each model, at least one set of plausible reactions was obtained. The user must be aware of thermodynamically or kinetically impossible reactions, and must also have a sense of the relative proportions of phases in the rock. Despite these limitations, the results of the modeling show that mixing, combined with cation exchange, calcite dissolution and precipitation, silicate dissolution, and secondary mineral precipitation, are a plausible source of the Type 3 waters.

Site hydrogeologic framework

The local flow system along the direction of dip, as inferred from the results of this study and the conceptual model, is shown in **Figure 5-6**. The Type 1 water observed in some of the shallow multilevel well samples is thought to originate from recharge that infiltrates to the permeable water table interval, which approximates the saprolite/bedrock interface, and flows along short paths to the discharge zone. These paths are controlled by hydraulic gradients that are affected by both horizontal and vertical anisotropy. The Type 2 water has been observed in the intermediate groundwater zone, through which flow occurs primarily along permeable fractures. In discharge areas, these waters flow upward through less permeable zones. Calculations of residence time using predicted mass transfer and reaction rates indicate that Type 2 water can originate from Pine Ridge.

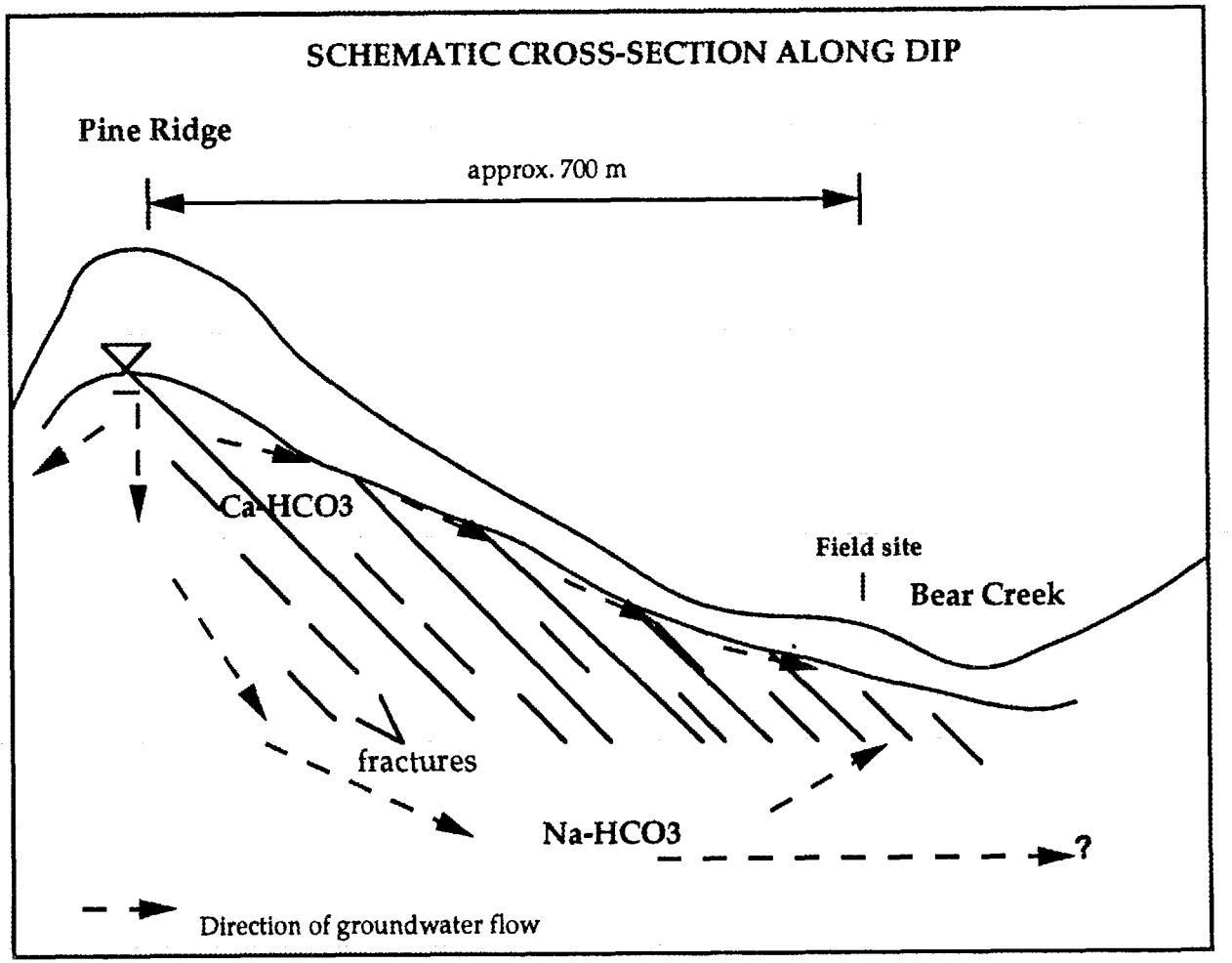

Figure 5-6: Schematic cross-section along dip showing generalized flow paths (Modified from Solomon et al., 1992).

Recharge can also infiltrate downward into the intermediate groundwater zone, through which flow is much more sluggish. These slower and longer flow paths allow for more time for water-rock interactions.

It is clear from the observed spatial variability in groundwater chemistry that the zones that contain the Type 1 and Type 2 waters are not well-connected along the flow path. If they were connected, the shallow groundwater in the discharge zone would be well-mixed and would not retain the observed chemical signatures. In the discharge zone, however, there appears to be mixing of the two waters as they converge, creating the Type 3 waters. This mixing induces water-rock reactions which result in water compositions that are different from a conservative mixture.

5.4 Summary

The results of the speciation-solubility calculations show that shallow groundwater is generally slightly oversaturated with quartz and significantly oversaturated with the iron oxides/hydroxides (goethite, hematite, amorphous $Fe(OH)_3$). The groundwater appears to be in equilibrium with calcite, although two samples are moderately undersaturated with calcite. These samples may represent recently mixed waters that have not had time to equilibrate with calcite. The presence of colloids in the multilevel well samples is supported by oversaturation with respect to the iron oxides. pCO_2 values are calculated to be slightly higher than atmospheric and do not vary significantly with depth, suggesting that most of the flow zones are

open to the atmosphere. Lower partial pressures of CO_2 calculated in the deep portion of GW823 indicate that some of the deeper zones, with lower flow rates, may be more isolated from the atmosphere.

The origin of the Type 2 water can be attributed to water-rock interactions between the Type 1 water and minerals in the shale and carbonate matrix. The time required for mineral dissolution and precipitation to account for this evolution is in the range of groundwater travel times in the lower permeability intervals from Pine Ridge to the field site.

Three hypotheses for the origin of the Type 3 waters are explored: 1) local reactions of Types 1 and 2 waters with surrounding rock, 2) conservative mixing of Types 1 and 2 waters, and 3) mixing with associated water-rock interactions. These hypotheses were tested using reaction path and mass balance models. The results of testing of the first hypothesis show that water-rock interactions can account for most of the concentration changes between the Type 1 and Type 3 waters, except for changes in the sulfate concentration. The time required to dissolve enough pyrite to account for the sulfate concentrations in the Type 3 waters exceeds the time that Type 1 water (which is observed in permeable intervals) resides in the discharge zone.

Conservative mixing of Types 1 and 2 was simulated using sulfur to determine the

mixing ratios. Results of reaction path modeling with these mixing ratios show differences in the calculated concentrations of the other major ions, when compared to the Type 3 samples. In general, the mixing yielded excesses of calcium and deficiencies in sodium. The third hypothesis, mixing and water-rock interactions, yielded the most plausible results, with appropriate predictions of phase precipitation and dissolution. The results of the calculated mixing percentages of the Type 3 waters correlate with the position of the samples relative to the Types and 2 waters. This systematic variation in mixing percentages gives further support to the mixing/geochemical reactions hypothesis. Due to the non-uniqueness of mass balance solutions, some caution should be used when examining the results of these predicted scenarios. The user must be aware of thermodynamically or kinetically impossible reactions, and must also have a sense of the relative proportions of phases in the rock.

The local flow system inferred from the results of this study correlates with the site conceptual model (Solomon et al., 1992; Moore and Toran, 1992). The Ca-HCO_3 (Type 1) water observed in the shallow groundwater samples in GW821 and GW822 is thought to originate from recharge that infiltrates to the permeable water table interval, which approximates the saprolite/bedrock interface, and flows along short paths to the discharge zone. These paths are controlled by hydraulic gradients that are affected by both horizontal and vertical anisotropy. The Na-HCO_3 (Type 2) water has been observed in the intermediate groundwater zone, through

which flow occurs primarily along permeable fractures. In discharge areas, these waters flow upward through less permeable zones. Calculations of residence time using predicted mass transfer and reaction rates indicate that it is plausible that the Na-HCO_3 (Type 2) water originates from Pine Ridge. Recharge at Pine Ridge which does not enter the water table interval infiltrates into the intermediate groundwater zone, through which flow is much more sluggish. These slower and longer flow paths allow for mnre time for water-rock interactions.

6. Conclusions and Suggestions for Further Work

6.1 Conclusions

This field experiment was designed to assess the flow and chemical characteristics of shallow groundwater in a fractured rock. Tracer tests and hydrochemical facies orientation show that the shallow groundwater flow direction is significantly affected by horizontal and vertical anisotropy. This anisotropy is likely related to the orientation of permeable fracture sets and to vertical heterogeneities in permeability as indicated by hydraulic tests.

Significant spatial variability in groundwater chemistry is observed. Groundwater in this discharge zone retains the chemical signatures of three water types, Ca-HCO_3, Ca- Na-HCO_3, and Na-HCO_3, which indicates the groundwater is flowing through discrete zones along most of the flow path. In the discharge zone, however, groundwater from deeper intervals is flowing upward, as evidenced by upward vertical gradients and by the presence of groundwater with a deeper signature (Na-HCO_3) in the shallow system. As these waters are flowing upward to discharge, they are mixing with the shallow Ca-HCO_3 groundwater to form a third, Ca-Na-HCO_3, water type.

The spatial variability in both flow and chemical properties of the shallow groundwater system has implications for standard sampling practices in fractured

rock. Standard screened wells allow groundwater from many flow zones to enter the well. Because these flow zones have different flow rates and groundwater chemistries, the composition of a groundwater sample will be vertically averaged, and will be most heavily weighted by the highest flow zones in the well.

Discrete zone samples from multilevel wells were compared to a sample from a long-screened well. The long-screened well retains the chemical signature of the shallow, Ca-HCO_3, water. However, the multilevel well samples show that there are other flow zones that intersect the long-screened well which are not represented by the groundwater sample. Due to the effects of dilution and mixing, samples from long-screened intervals will obscure the presence of different flow zones and groundwater chemistries. This is especially true in fractured rocks, in which groundwater can flow through discrete zones that may not be well-connected to other zones. If a contaminated zone were to intersect a long-screened well, the contaminant concentrations could be mixed and diluted so that they were no longer detectable. In this situation, being able to identify the location, the hydraulic properties, and the concentrations of the contaminated zones through the use of multilevel wells would greatly expedite site characterization and remediation efforts.

6.2 Suggestions for Further Work

Field studies

This study was the first phase of a larger project being conducted at the West Bear Creek Valley field site. As such, the study was limited in scope, and there are many remaining questions to be resolved. The results of the bromide test and the lack of detection of significant concentrations of bromide in the well pairs suggest that the majority of the bromide may have diffused into the saprolite and/or shale matrix. Augering through the saprolite and taking samples for bromide analysis near the source well may help identify the bromide sink and will help to assess the importance of matrix diffusion in chemical transport at the site. In addition, analysis of the flow direction indicates that there are no monitoring wells that are along the direction of flow from the source well. Installing additional monitoring wells that are located along the direction of flow from the source well may be useful in future tracer testing at the site.

There are many questions that remain regarding the spatial connectivity of the flow zones. The degree of connectivity could be addressed by conducting small-scale slug or pump tests in the multilevel well sampling ports. A pressure monitoring system has been installed in the multilevel well sampling ports; this will provide a means by which fluctuations in the water levels in the flow zones can be measured. In addition, the permeability of the different sets of fractures (bed parallel, strike parallel, and strike perpendicular) should be examined both under natural flow and

pumping conditions.

Mineralogical and geochemical studies

The mineralogical characterization is based on analytical techniques (XRD, EDS) which are not the most appropriate for identifying the coatings present on the fracture surfaces. Additional work on better characterizing these coatings using HRTEM is highly recommended. The presence of gypsum in the shale has been postulated but not substantiated. Determining the presence or absence of gypsum would yield important information on the potential sources of sulfate to the groundwater. Analysis of sulfur isotopes in the groundwater would also help constrain the origin of the sulfur since gypsum and pyrite have distinct sulfur isotopic ratios. The plagioclase feldspar phase used in the modeling was albite, to provide an additional source of sodium; however, the distinction between albite, anorthite, and solid-solution phases, was not made. Identifying a more precise plagioclase composition would help to constrain the sources of sodium and calcium in the system. Cation exchange has been identified as being an important process for providing sodium to the groundwater. The presence of clay and oxide minerals in the matrix suggests that exchange is possible; however, additional studies focussed on evaluating the capacity of the shale to yield sodium should be conducted.

The possibility of bentonite interacting with the groundwater has been suggested.

This interaction could contribute sodium and sulfate to groundwater and could be resulting in erroneous interpretations of the spatial variability in groundwater chemistry at the site. To evaluate this effect, batch experiments between the bentonite and the Type 1 water should be conducted to assess if the resulting water composition can approximate the composition of the Type 2 water.

Additional sampling of the multilevel wells is recommended to assess temporal variability in the groundwater chemistry and to observe if the orientation of the hydrochemical facies changes over time. In this study, trends in the variability of the metal ions could not be addressed due to the presence of colloids in the groundwater samples. To assess the spatial and temporal variability in groundwater chemistry, changes in redox conditions should also be monitored. Filtering with smaller diameter filters (<0.45 microns) and measuring the dissolved oxygen in the multilevel wells may help to better understand redox variability.

The presence of the Type 2 water in the shallow groundwater system at the site has been attributed to deeper waters which are flowing upward to discharge. The chemistry of the water and the presence of upward vertical gradients at the site support this hypothesis; however, additional studies should be conducted to find other ways to identify if this Type 2 water is flowing up from depth. One way to demonstrate this is with dating techniques, including chlorofluorocarbons (CFCs).

Modeling studies

Mass balance models were used to examine the different hypothesis of the origin of the Type 3 waters. As previously discussed, mass balance models have significant limitations because they do not consider thermodynamics or kinetics. In addition, the solutions of mass balance models are not unique, and as such, are subject to a variety of interpretations. Reaction path models, which can simulate dissolution and precipitation of known amounts of minerals, would help in assessing the plausibility of mass transfer between groundwater and the surrounding rocks.

7. References cited

Appelo, C.A.J. and D. Postma. 1993. Geochemistry, Groundwater, and Pollution. Balkema Publishers, Rotterdam. 536 pp.

Bowser, C.J. and B.F. Jones. 1990. Geochemical constraints on groundwaters dominated by silicate hydrolysis: an interactive spreadsheet, mass balance approach. Chemical Geology, vol. 84, pp. 33-35.

Dustman, J., R. Davis, and T. Oothoudt. 1992. Soil, bedrock, and groundwater sampling using Rotasonic drilling techniques. In: Proceedings of the Sixth National Outdoor Action Conference on Aquifer Restoration, Ground Water Monitoring, and Geophysical Methods, May 11-13, 1992, Las Vegas, NV. Ground Water Management, Book 11, pp. 179-187.

Foreman, J.L. 1991. Petrologic and Geochemical Evidence for Water-Rock Interaction in the Mixed Carbonate-Siliciclastic Nolichucky Shale (Upper Cambrian) in East Tennessee, Ph.D. Dissertation. University of Tennessee-Knoxville. 227 pp.

Foster, M.D. 1950. The origin of high sodium bicarbonate waters in the Atlantic and Gulf Coast Plains. Geochimica et Cosmochimica Acta, vol. 1, pp. 33-48.

Freeze, R.A. and J.A. Cherry. 1979. Groundwater. Prentice Hall Publishers, Englewood Cliffs, NJ. 604 pp.

Fritz, S.J. 1994. A survey of charge-balance errors on published analyses of potable ground and surface water. Ground Water, vol. 32, no. 4, pp. 539-546.

Gierke, W.G., W.B. Lozier, and R. Pearson. 1988. Task 2, Well Logging and Geohydrologic Testing, Site Characterization and Groundwater Flow Computer Model Application, Vol. 1. Golder Associates, Inc., ORNL/Sub/30X-SA706C, Oak Ridge, TN.

Barrow, J.C. 1994. The resonant sonic drilling method: an innovative technology for environmental restoration programs. Ground Water Monitoring and Remediation, vol. 14, no. 2, pp. 153-160.

Goldstein, J.I., D.E. Newbury, P. Echlin, D.C. Joy, A.D. Romig, Jr., C.E. Lyman, C. Fiori, and E. Lifshin. 1992. Scanning Electron Microscopy and X-Ray Microanalysis: A Text for Biologists, Materials Scientists, and Geologists, second edition, Plenum Press, New York, NY. 820 pp.

Haase, C.S. and H.L. King. 1987. Controls on shallow groundwater composition in a geologically complex terrain near Oak Ridge, Tennessee. AGU Fall Meeting, EOS Supplement, vol. 68, no. 44, p. 1290.

Haase, C.S. 1992. Application of chemistry and geochemical modeling to the identification of groundwater flow systems with fractured bedrock. AGU Fall Meeting, EOS Supplement, vol. 73, no. 43, p. 189.

Harned, D.A. and C.C. Daniel III. 1989. The transition zone between bedrock and regolith: conduit for contamination? In: Daniel, C.C. III, R.K. White, and P.A. Stone (eds.) Proceedings of a Conference on Ground Water in the Piedmont of the Eastern United States, October 16-18, 1989, Charlotte, NC. pp. 336-348.

Hatcher, R.D., P.J. Lemiszki, R.B. Dreier, R.H. Ketelle, R.R. Lee, D.A. Leitzke, W.M. McMaster, J.L. Foreman, and S.Y. Lee. 1992. Status Report on the Geology of the Oak Ridge Reservation, Environmental Sciences Division Publication Pub. No. 3860, ORNL/TM-12074, Oak Ridge National Laboratory, Oak Ridge, TN. 244 pp.

Hem, J.D. 1985. Study and Interpretation of the Chemical Characteristics of Natural Water, third edition. U.S. Geological Survey Water-Supply Paper 2254, 263 pp.

Holdren, G.R., Jr. and R.A. Berner. 1979. Mechanism of feldspar weathering 1, Experimental studies. Geochimica et Cosmochimica Acta, vol. 43. pp. 1161-1171.

Hughes, R.E., D.M. Moore, and H.D. Glass. 1994. Qualitative and Quantitative Methods of Clay Minerals in Soils. In: Quantitative Methods in Soil Mineralogy. Soil Science Society of America (SSSA) Miscellaneous Publications, SSSA, Inc., Madison, WI. pp. 330-355.

Jenne, E.A., J.W. Ball, J.M. Burchard, D.V. Vivit, and J.H. Parks. 1980. Geochemical modeling: apparent solubility controls on Ba, Zn, Cd, Pb, and F in waters of the Missouri Tri-State mining area. In: D.D. Hemphill (ed.) Trace Substances in Environmental Health XIV. University of Missouri, Columbia, MO. pp. 353-361.

Lasaga, A.C. 1984. Chemical kinetics of water-rock interactions. Journal of Geophysical Research, vol. 89, no. B6. pp. 4009-4025.

Lee, R.R., R.H. Ketelle, J.M. Bownds, and T.A. Rizk. 1992. Aquifer analysis and modeling in a fractured, heterogeneous medium. Ground Water, vol. 30, no. 4, pp. 589-597.

Lee, S.Y., L.K. Hyder, and P.D. Alley. 1987. Mineralogical Characterization of Selected Shales in Support of Nuclear Waste Repository Studies: Progress Report. Environmental Sciences Division Pub. No. 2985, ORNL/TM-10567, Oak Ridge National Laboratory, Oak Ridge, TN. 36 pp.

Lee, S.Y., L.K. Hyder, and P.M. Baxter. 1989. Mineralogical Characterization of Selected Shales in Support of Nuclear Waste Repository Studies: Progress Report for October 1987-September 1988. Environmental Sciences Division Pub. No. 3225, ORNL/TM-10968, Oak Ridge National Laboratory, Oak Ridge, TN. 61 pp.

Macalady, D.L., D. Langmuir, T. Grundl, and A. Elzerman. 1990. Use of model-generated Fe(3+) ion activities to compute Eh and ferric oxyhydroxide solubilities in anaerobic systems. In: Melchior, D.C. and R.L. Bassett (eds.). Chemical Modeling of Aqueous Systems II, American Chemical Society, Washington, D.C., pp. 350-367.

Matthess, G. 1982. The Properties of Groundwater. J. Wiley and Sons. New York, NY. 406 pp.

Mazor, E. 1992. Interpretation of water-rock interactions in cases of mixing and undersaturation. In: Kharaka, Y.K. and A.S. Maest (eds.). Water-Rock Interaction, WRI-7, Volume 1: Low Temperature Environments. Balkema Publishers, Rotterdam. pp. 233-236.

McBride, M. 1994. Environmental Chemistry of Soils. Oxford University Press, Inc., New York, NY. 406 pp.

McKenzie, R.M. 1977. Manganese oxides and hydroxides. In: Dixon, J.B. and S.B. Weed (eds.). Minerals in Soil Environments. Soil Science Society of America, Inc., Madison, WI. pp. 181-192.

Moline, G.R. and M.E. Schreiber. 1995. Summary of FY94 Site Characterization and Installation of Multilevel Wells at a West Bear Creek Valley Research Site on the Oak Ridge Reservation. ORNL/TM-13029, Oak Ridge National Laboratory, Oak Ridge, TN.

Moore, G.K. 1988. Concepts of Groundwater Occurrence and Flow near the Oak Ridge National Lab, Tennessee. Environmental Sciences Division Pub. No. 3218, ORNL/TM-10969, Oak Ridge National Laboratory, Oak Ridge, TN.

Moore, G.K. and L.E. Toran. 1922. Supplement to a Hydrologic Framework for the Oak Ridge Reservation, Oak Ridge, Tennessee. Environmental Sciences Division Pub. No. 3982, ORNL/TM-12191, Oak Ridge National Laboratory, Oak Ridge, TN.

Moore, G.K. and S.C. Young, 1992. Identification of Groundwater-Producing Fractures by Using and Electromagnetic Borehole Flowmeter in Monitoring Wells on the Oak Ridge Reservation. ORNL/ER-91, Oak Ridge National Laboratory, Oak Ridge, TN.

Moses, C.O., D.K. Nordstrom, J.S. Herman, and A.L. Mills. 1987. Aqueous pyrite oxidation by dissolved oxygen and by ferric iron. Geochimica et Cosmochimica Acta, vol. 51. pp. 1561-1571.

National Atmospheric Deposition Program. 1994. NADP/NTN Annual Data Summary: Precipitation Chemistry in the United States, 1993. Natural Resource Ecology Laboratory, Colorado State University, Fort Collins, CO. 465 pp.

National Atmospheric Deposition Program (NRSP-3)/National Trends Network. 1994. NADP/NTN Coordination Office Natural Resource Ecology Laboratory, Colorado State University, Fort Collins, CO. 87 pp.

Nicholson, R.V., R.W. Gillham, and E.J. Reardon. 1988. Pyrite oxidation in carbonate-buffered solution: 1. Experimental kinetics. Geochimica et Cosmochimica Acta, vol. 52. pp. 1077-1085.

Nicholson, R.V., R.W. Gillham, and E.J. Reardon. 1990. Pyrite oxidation in carbonate-buffered solution: 2. Rate control by oxide coatings. Geochimica et Cosmochimica Acta, vol. 54. pp. 395-402.

Paillet, F.L., A.E. Hess and R.H. Morin. 1990. Estimation of the relative permeability distribution in fractured granitic rocks by means of vertical flow measurements in the Siblingen borehole, Switzerland. U.S. Geological Survey Water-Resources Investigations Report 90-4034, 24 pp.

Parkhurst, D.L., D.C. Thorstenson, and L.N. Plummer. 1980. PHREEQE - A Computer Program for Geochemical Calculations. U.S. Geological Survey Water Resources Investigations Report 80-96, 195 pp.

Phillips, D.H. 1988. Genesis of Soils from Ancient Alluvium, Maryville Limestone and Nolichucky Shale in East Tennessee. M.S. Thesis, University of Tennessee-Knoxville.

Pickens, J.F., J.A. Cherry, R.M. Coupland, G.E. Grisak, W.F. Merritt, and B.A. Risto. 1981. A multilevel device for ground-water sampling. Ground Water Monitoring Review, vol. 1, no. 2, pp. 48-51.

Plummer, L.N., E.C. Prestemon, and D.L. Parkhurst. 1991. An Interactive Code (NETPATH) For Modeling Net Geochemical Reactions Along a Flow Path. U.S. Geological Survey Water Resources Investigations Report 91-4078, 227 pp.

Plummer, L.N., B.F. Jones, and A.H. Truesdell. 1976. WATEQF - A FORTRAN IV Version of WATEQ, a Computer Program for Calculating Chemical Equilibrium of Natural Waters, U.S. Geological Survey Water Resources Investigations Report 76-13, 61 pp.

Rimstidt, J.D. and H.L. Barnes. 1980. The kinetics of silica-water reactions. Geochimica et Cosmochimica Acta, vol. 44. pp. 1683-1699.

Rizk, T.A. 1990. Groundwater Flow and Contaminant Transport in Geologic Media. Ph.D. Dissertation. North Carolina State University, Raleigh, NC. 257 pp.

Roberson, C.E., J.H. Feth, P.R. Seabar, and P. Anderson. 1963. Differences Between Field and Laboratory Determinations of pH, Alkalinity, and Specific Conductance of Natural Water. U.S. Geological Survey Professional Paper 475-C, pp. C212-C215.

Sanford, W.E., D.K. Solomon, and R.G. Shropshire. 1994. Noble gases as groundwater tracers in fractured saprolite. AGU Spring Meeting, EOS Supplement, vol. 75, no. 16, p. 147.

Schwertmann, U. and R.M. Taylor. 1977. Iron oxides. In: Dixon, J.B. and S.B. Weed. (eds.). Minerals in Soil Environments. Soil Science Society of America, Inc., Madison, WI. pp. 145-176.

Shevenell, L.A., G.K. Moore, and R.B. Dreier. 1994. Contaminant spread and flushing in fractured rocks near Oak Ridge, TN. Ground Water Monitoring and Remediation, vol. 14, no. 4, pp. 120-129.

Shapiro, A.M. and P.A. Hsieh. 1991. Research in Fractured Rock Hydrogeology: Characterizing Fluid Movement and Chemical Transport in Fractured Rock at the Mirror Lake Drainage Basin, New Hampshire. U.S. Geological Survey Toxic Substances Hydrology Program, Water Resources Investigations Report 91-4034, pp. 155-161.

Solomon, D.K., G.K. Moore, L.E. Toran, R.B. Dreier, and W.M. McMaster. 1992. Status Report: A Hydrologic Framework for the Oak Ridge Reservation. Environmental Sciences Division Pub. No. 3815, ORNL/TM-12026, Oak Ridge National Laboratory, Oak Ridge, TN. 60 pp.

Stumm, W. and J.J. Morgan. 1981. Aquatic Chemistry, second edition. Wiley-Interscience Publications, J. Wiley and Sons, Inc. New York, NY. 780 pp.

Toran, L.E., D.K. Solomon, W.M. McMaster, C.M. Morrisey. 1991. Matrix diffusion as a mechanism to explain recent tritium and old (14)C in groundwater from fractured sedimentary rocks. AGU EOS Transactions, vol. 72, no. 17, p. 111.

Von Damm, K.L. and A.J. VandenBrook. 1989. Geochemical Controls on Shale Groundwaters: Results of Reaction Path Modeling. Environmental Sciences Division Pub. No. 3173, ORNL/TM-10944, Oak Ridge National Laboratory, Oak Ridge, TN. 84 pp.

Welton, J.E. 1984. SEM Petrology Atlas. American Association of Petroleum Geologists, Tulsa, OK. 84 pp.

Williams, J.H. and R.W. Conger. 1990. Preliminary delineation of contaminated water-bearing fractures intersected by open-hole bedrock wells. Ground Water Monitoring Review, vol. 10, no. 3, pp. 118-126.

Wilson, M.J. 1987. X-Ray Powder Diffraction Methods. In: Wilson, M.J. (ed.). A Handbook of Determinative Methods in Clay Mineralogy. Blackie and Son, Ltd., London. 308 pp.

Appendix A: Monitoring well construction

JOB NO. 873-3512	PROJECT UMES / GW ASSES / SCV-ORM	WELL NO. GW-456/457	SHEET 1 OF 1
GA INSP. JBJ/WBL	DRILLING METHOD AIR/WATER ROTARY	GROUND ELEV. 842.7 FT	WATER DEPTH AS SHOWN
WEATHER SUNNY, CLEAR	DRILLING COMPANY HIGHLAND DRILLING	COLLAR ELEV. 844.86/845.31	DATE/TIME 12-9-87/1250
TEMP. 40 F	DRILL RIG INGERSOLL-RAND / DRILLER GARY	STARTED 1000/11-12-87 (TIME / DATE)	COMPLETED 1130/11-13-87 (TIME / DATE)

MATERIALS INVENTORY

WELL CASING 2 in. dia. 79.60 l.f.	WELL SCREEN 2 in. dia. 20.58 l.f.	BENTONITE SEAL PELLETS
CASING TYPE PVC	SCREEN TYPE MACHINE SLOTTED	INSTALLATION METHOD POURED
JOINT TYPE THREADED	SLOT SIZE 0.010 IN	FILTER PACK QTY. 11 3/4 BAGS
GROUT QUANTITY 135 GALLONS	CENTRALIZERS STAINLESS STEEL (2)	FILTER PACK TYPE SAND
GROUT TYPE WATER + TYPE 1 + BENT POWD	DRILLING MUD TYPE NONE	INSTALLATION METHOD POURED

DEPTH	SOIL/ROCK DESCRIPTION
0.0	GROUND SURFACE
	Reddish brown to tan, soft to moderately hard SAPROLITE
10.0	
19.4	
20.0	NOUCHUCKY SHALE Reddish brown to grayish black, unweathered SHALE and MUDSTONE; interbedded with gray to black, hard LIMESTONE
30.0	
40.0	
50.0	
60.0	
70.0	
70.0	BORING TERMINATED AT 70.0 FT.

WELL SKETCH

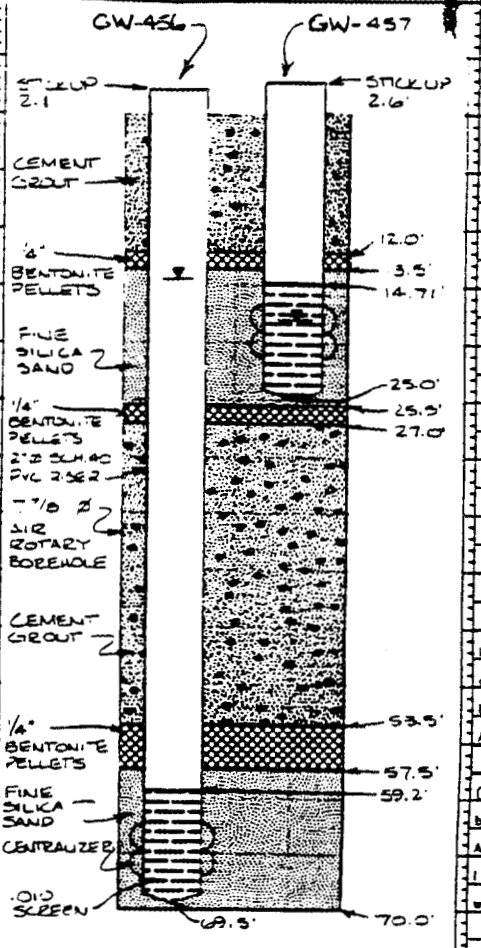

INSTALLATION NOTES

Sounded hole to 70.0 ft BGS. Added ~ 1/2 bag of sand, sounded sand to 69.5 ft. Installed:

screen + tip = 10.29 ft
6 joints at 9.95 ea = 59.99 ft
stickup = - 4.8 ft

69.50 ft

Added 4 bags of sand and sounded to 57.5 ft. Placed ~ 1 1/3 buckets of 1/4" pellets and sounded to 53.5 ft at 1230. 1500 added 60 gallons cement at ratio of 5 gal water/1 bag cement. Sounded grout (11-13-87) to 27 ft. Added ~ 1/3 bucket of 1/4" bentonite pellets. Sounded to 25.5 ft. Added ~ 1/4 bag of sand and sounded to 25 ft.

30.19 ft
- 5.19 stickup

25.0 ft

Installed: screen + tip = 10.29 ft and 2 joints at 9.95 each. Added 7 bags sand and sounded to 13.5 ft. Added ~ 3 1/2 buckets 1/4" bentonite pellets and sounded to 12 ft. Added 75 gallons of grout (1 bag Type 1 + 3 lbs bentonite powder + 5 gallons water).

See table 6.2 well development summary data.

WELL DEVELOPMENT NOTES

(Well Installation Notes Continued)

Appendix A: Monitoring well construction (con't)

JOB NO. 873-3812	PROJECT VOMFS / OW ASSES / BCV-OBM	WELL NO. GW-458/459	SHEET 1 OF 1
GA INSP. BJ	DRILLING METHOD AIR / WATER ROTARY	GROUND ELEV. 842.7 FT	WATER DEPTH AS SHOWN
WEATHER 50 F SUNNY	DRILLING COMPANY HIGHLAND DRILLING	COLLAR ELEV. 844.88/845.1	DATE/TIME 12-9-87/1243
TEMP. 50's	DRILL RIG INGERSOLL-RAND / DRILLER GARY	STARTED 1340/11-13-87 (TIME / DATE)	COMPLETED 1445/11-14-87 (TIME / DATE)

MATERIALS INVENTORY

WELL CASING 2 in. dia. 79.8 l.f.	WELL SCREEN 2 in. dia. 20.58 l.f.	BENTONITE SEAL 1/4" PELLETS
CASING TYPE PVC SCH 40	SCREEN TYPE .010 IN MACHINE SLOTTED	INSTALLATION METHOD POURED
JOINT TYPE THREADED	SLOT SIZE .010 IN	FILTER PACK QTY. 9 BAGS
GROUT QUANTITY 110 GALLONS	CENTRALIZERS STAINLESS STEEL (2)	FILTER PACK TYPE SAND
GROUT TYPE TYPE I CEMENT + BENT POWD	DRILLING MUD TYPE ------	INSTALLATION METHOD POURED

DEPTH	SOIL/ROCK DESCRIPTION
0.0	GROUND SURFACE
2.0	SAPROLITE
18.5	NOUCHUCKY SHALE Reddish-brown to grayish-black, unweathered SHALE and MUDSTONE; interbedded with gray to black, hard LIMESTONE
70.0	BORING TERMINATED AT 70.0 FT.

WELL SKETCH

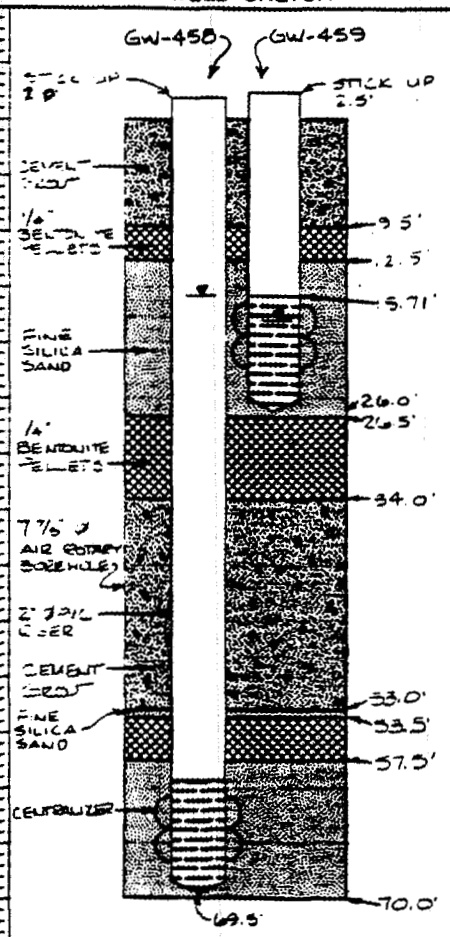

INSTALLATION NOTES

Sounded hole to 70.0 ft BGS. Added ~ 1/2 bag sand and sounded to 69.5 ft.
Installed: screen + tip = 10.29 ft
6 joints at 9.95 ea = 59.99 ft
stickup ~ 4.8 ft

69.90 ft

Added ~ 3 1/2 bags of sand and sounded to 55 ft (1445). Added another ~ 2/3 bucket bentonite pellets and sounded to 53.5 ft (1600)
Added ~ 1/2 bag sand and sounded to 53.0 ft. Added 80 gallons grout-bentonite powder mixture.
Sounded to 34.0 ft.
2 joints at 9.95 ft
19.90 ft
+ 10.29 ft

30.19 ft
stickup ~ 4.19 ft

26.00 ft

(0915) Added 8 buckets of 1/4"

WELL DEVELOPMENT NOTES

0915 Added 8 buckets of 1/4" bentonite pellets and sounded to 26.5 ft. Added 1/2 bag sand and sounded to 28.0 ft. Then installed 2 joints + screen + tip. Added 1 1/2 buckets of bentonite pellets and sounded to 9.5 ft.
1445 Began grouting, added 50 gallons grout-bentonite powder mixture.

Appendix A: Monitoring well construction (con't)

JOB NO 873-3512	PROJECT MMES / GW ASSES / [illegible]	WELL NO GW-460/461	SHEET 1 OF 1
DA INSP JBJ	DRILLING METHOD AIR / WATER ROTARY	GROUND ELEV 842.2 FT	WATER DEPTH AS SHOWN
WEATHER [illegible]	DRILLING COMPANY HIGHLAND DRILLING	COLLAR ELEV. 842.15/842.5	DATE/TIME 12-3-87/1248
TEMP [illegible] F	DRILL RIG INGERSOLL-RAND DRILLER GARY	STARTED 1030/11-16-87 (TIME / DATE)	COMPLETED 1530/11-17-87 (TIME / DATE)

MATERIALS INVENTORY

WELL CASING 2 in o.d. [illegible]	WELL SCREEN 2 in o.d. 20.59 ft	BENTONITE SEAL ~ 4 BUCKETS 1/4" PELLETS
CASING TYPE PVC	SCREEN TYPE MACHINE SLOTTED	INSTALLATION METHOD POURED
JOINT TYPE THREADED	SLOT SIZE .010 IN	FILTER PACK QTY 9 BAGS
GROUT QUANTITY [illegible] GALLONS	CENTRALIZERS STAINLESS STEEL (2)	FILTER PACK TYPE SAND
GROUT TYPE TYPE I W/ BENTONITE	DRILLING MUD TYPE -----	INSTALLATION METHOD POURED

DEPTH	SOIL/ROCK DESCRIPTION
0.0	GROUND SURFACE
	SAPROLITE
25.0	Competent rock at ~ 25.0 ft
	NOLICHUCKY SHALE
70.0	BORING TERMINATED AT 70.0 FT BGS.

WELL SKETCH

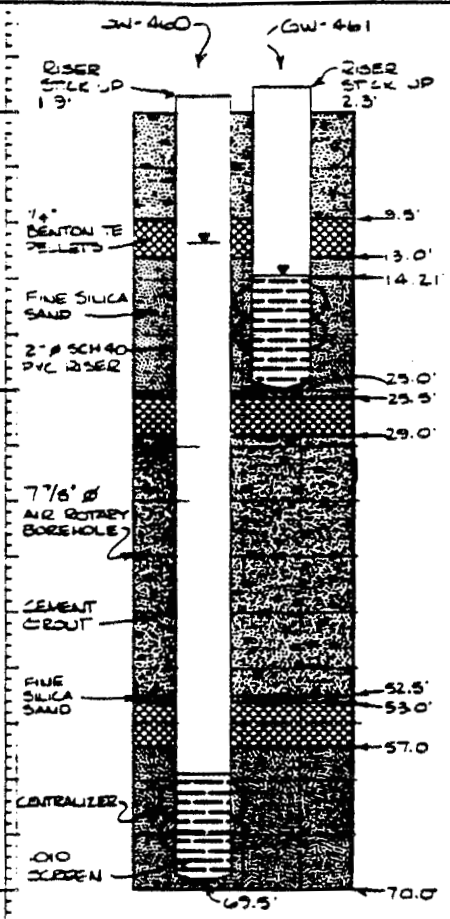

INSTALLATION NOTES

Sounded hole to 70.0 ft. Added ~ 1/2 bag sand and sounded to 69.5 ft.
Installed ~ 2 joints at 9.95 ft each
~ screen ~ tip at 10.29 ft
10.29 ft
stickup ~ .49 ft

69.50 ft
Added ~ 4 bags sand and sounded to 57.0 ft. Added ~ 1 1/2 buckets of 1/4" bentonite pellets and sounded to 53 ft. (1330)
Added ~ 1/2 bag sand and sounded to 52.5 ft.
1530 Added 60 gallons of grout-bentonite powder mixture. Sounded to 29.0 ft. Added 1 bucket bentonite pellets and sounded to 25.5 ft. (2035) Added ~ 1/2 bag sand and sounded to 25.0 ft. Added ~ 1 1/2 bags sand and sounded to 13.0 ft. Added 1 1/2 bucket bentonite pellets and sounded to 9.5 ft. Added 21 gallons grout-bentonite powder mixture. For angular well:

WELL DEVELOPMENT NOTES

For angular well installed:
screen ~ tip at 10.29 ft.
2 joints at 9.95 ft each
10.19 ft
stickup ~ 5.19 ft

15.30 ft

Appendix A: Monitoring well construction (con't)

JOB NO 471-3512	PROJECT MMES / GW ASSES / BCV-ORNL	WELL NO GW-462	SHEET 1 OF 1
GA INSP JBL	DRILLING METHOD AIR / WATER ROTARY	GROUND ELEV. 842.5 FT	WATER DEPTH 16.44 FT
WEATHER PT. CLOUDY	DRILLING COMPANY HIGHLAND	COLLAR ELEV. 843.1 FT	DATE/TIME 12-3-87/1751
TEMP 60's F	DRILL RIG INGERSOLL-RAND / DRILLER GARY	STARTED 1000/11-17-87 (TIME / DATE)	COMPLETED 1545/11-17-87 (TIME / DATE)

MATERIALS INVENTORY

WELL CASING 4 in dia 22 LF	WELL SCREEN 4 in dia. 50.05 LF	BENTONITE SEAL 2 BUCKETS 1/4" PELLETS
CASING TYPE PVC SCH 40	SCREEN TYPE MACHINE SLOTTED	INSTALLATION METHOD POURED
JOINT TYPE THREADED	SLOT SIZE 0.010 IN	FILTER PACK QTY. 16 1/2 BAGS
GROUT QUANTITY 40 GAL	CENTRALIZERS 1 (STAINLESS STEEL)	FILTER PACK TYPE 20/40 SAND
GROUT TYPE TYPE #1 BENTONITE	DRILLING MUD TYPE ---	INSTALLATION METHOD POURED

DEPTH	SOIL/ROCK DESCRIPTION
0.0	GROUND SURFACE
0.0	SAPROLITE
10.0	
20.0	
22.5	Competent rock at 22.5 ft
	NOLICHUCKY SHALE
30.0	
40.0	
50.0	
60.0	
70.0	BORING TERMINATED AT 70.0 FT.

WELL SKETCH

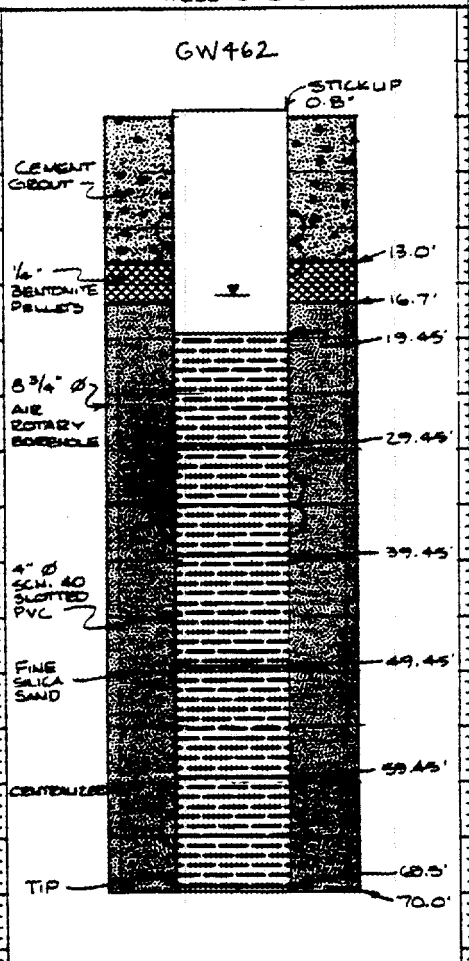

INSTALLATION NOTES

Added ~ 1/2 bag sand after sounding to 70 ft, then sounded to 69.5 ft

installed:

2 casing at 10 ft each = 20.0 ft
4 screens at 10.1 ft each = 40.0 ft
1 screen 10 = 10.05 ft
70.05 ft
stickup = - 0.55 ft
69.50 ft

Added ~ 16 bags 20/40 sand and sounded to 16.7 ft. Added 2 buckets 1/4" bentonite pellets and sounded to 13.0 ft. Grouted to surface (added ~ 40 gal) grout-bentonite powder mixture

WELL DEVELOPMENT NOTES

See table 6.2 well development summary data

Appendix A: Monitoring well construction (con't)

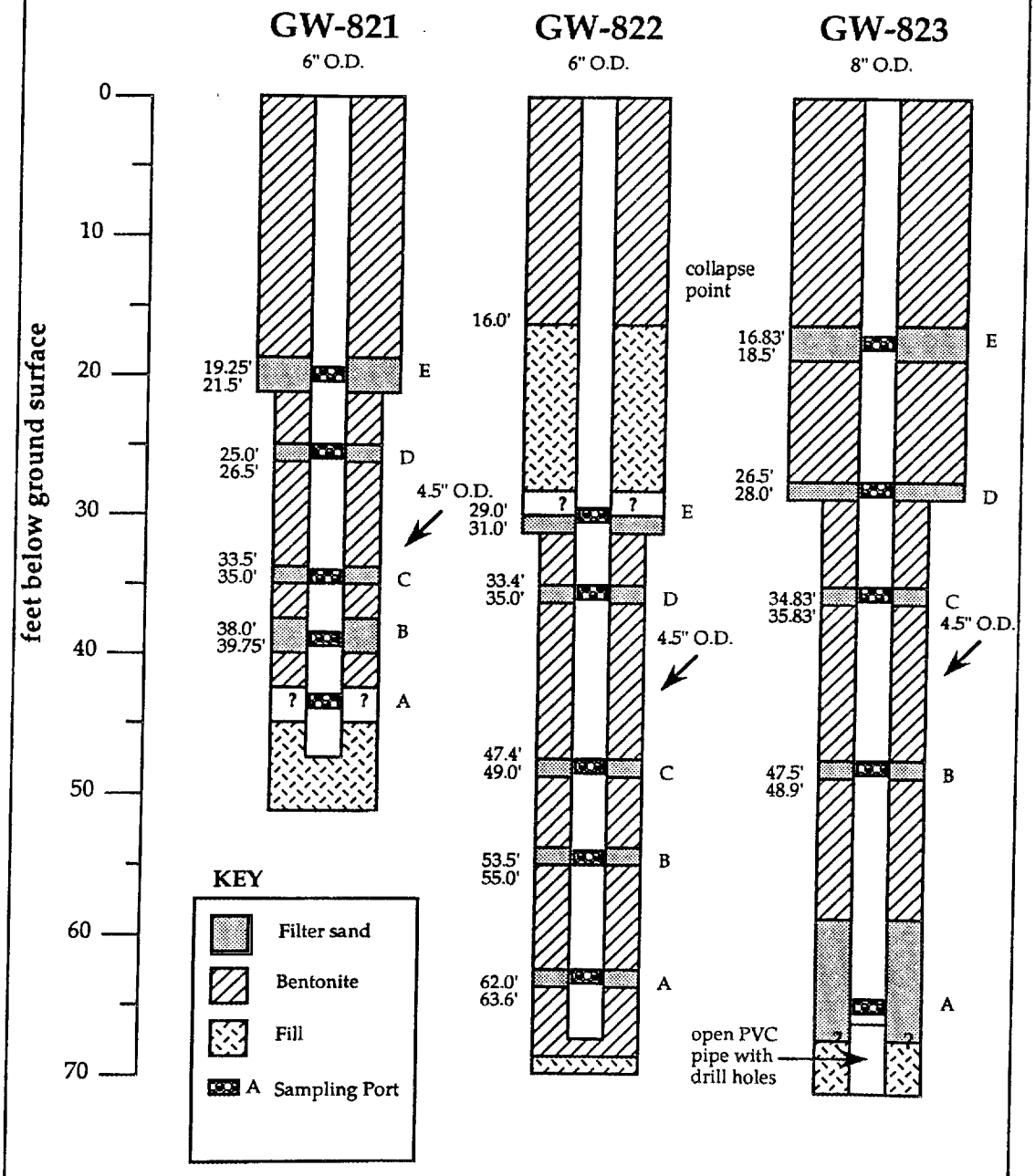

Appendix B: Water Elevation Data (feet AMSL)							
date	GW456	GW457	GW458	GW459	GW460	GW461	GW462
3/29/94	841.19	839.24	838.68		839.73	837.47	839.3
3/31/94	840.85	838.85	838.3	837.2	839.4	837.1	
4/3/94	840.2	837.75	837.45	836	838.65	836.23	837.75
4/8/94	840.94	838.75	838.3	836.75	840.4	837	838.72
4/9/94	840.55	838.23	837.82	836.32	838.99	836.59	838.2
4/11/94	841.44	840.68	839.06	838.83	840.07	837.9	839.67
4/13/94	841.85	840.05	839.46	839.03	840.34	838.37	840.01
4/15/94	841.06	838.79	838.42	836.79	839.37	837.3	838.77
4/18/94	841.03	838.74	838.43	836.73	839.32	837.31	838.75
4/20/94	840.16	837.74	837.58	835.99	838.5	836.49	837.74
4/22/94	839.45	837.03	836.92	835.46	837.88	835.91	837.02
4/25/94	838.45	836.1	835.99	834.73	836.99	835.09	836.11
4/27/94	837.84	835.49	835.43	834.24	837.11	836.81	835.5
4/29/94	837.66	835.26	835.25	834.03	836.28	834.32	835.27
5/4/94	837.24	834.97	834.87	833.93	835.98	834.03	834.96
5/10/94	836.55	834.18	834.11	832.89	835.3	833.11	834.19
5/13/94	836.13	833.8	833.67	832.46	834.86	832.69	833.8
5/17/94	835.75	833.45	833.34	832.09	834.54	832.35	833.4
5/20/94	835.4	833.1	832.99	831.74	834.14	831.96	833.1
5/23/94	834.8	832.58	832.4	831.2	833.52	831.4	832.42
5/27/94	834.52	832.3	832.29	831.18	833.28	831.24	832.22
5/31/94	834.24	832.14	831.95	830.75	833.08	830.95	832.13
6/2/94	834.04	831.89	831.69	830.54	832.82	830.68	831.9
6/6/94	833.74	831.52	831.14	830.2	832.52	831.28	831.6
6/8/94	833.7	831.5	831.3	830.1		830.24	831.5
6/10/94	833.58	831.48	831.18	830.62	832.5	830.4	831.44
6/13/94			831.65	830.52			831.86
6/15/94	833.71	831.61	831.43	830.19	832.65	830.36	831.6
6/17/94	833.64	831.48	831.3	829.99	832.53	830.21	831.5
6/20/94	833.4	831.22	830.98	829.74	832.26	829.88	831.21
6/22/94	833.25	831.04	830.82	829.6	832.1	829.68	831.04
6/24/94	833.22	830.98	830.76	829.54	832.02	829.58	830.98
6/27/94	833.98	832.52	832.1	833.48	833.28	831.6	832.5
6/29/94	834.54	832.7	832.46	831.92	833.62	831.5	832.72
7/1/94	834.12	831.58	831.44	831.54	832.66	831.02	831.62
7/4/94	833.6	830.8	830.66	830.42	831.96	830.22	830.8
7/6/94	833.32	830.47	830.31	829.96	831.66	829.88	830.48
7/8/94	833.06	830.37	830.25	829.68	831.48	829.78	830.4
7/11/94	832.84	830.56	830.08	829.45	831.26	829.54	830.56
7/13/94	832.82	829.91	829.82	829.48	831.18	829.36	829.94
7/15/94	832.8	830.08	829.96	829.94	831.34	829.56	830.1
7/18/94	833.78	831.7	831.5	831.8	832.72	831.18	831.68
7/20/94	833.6	831.06	830.9	830.74	832.24	830.48	831.02
7/22/94	833.46	830.67	830.5	830.16	831.96	830.1	830.66

Appendix B: Water Elevation Data (con't)							
date	GW456	GW457	GW458	GW459	GW460	GW461	GW462
7/25/94	833.08	830.12	829.95	829.56	831.48	829.52	830.12
7/27/94	833	830.22	830.04	830.4	831.42	829.6	830.22
7/29/94	833.52	831.3	831.1	831.4	832.4	830.76	831.3
8/1/94	833.24	830.52	830.32	830.04	831.78	829.92	830.52
8/3/94	832.98	830.08	829.88	829.6	831.4	829.48	830.08
8/5/94	833	830.21	829.98	830.52	831.4	829.6	830.2
8/8/94	832.99	830.14	829.96	829.74	831.45	829.55	830.1
8/10/94	832.76	829.8	829.57	829.34	831.14	829.18	829.72
8/12/94	832.52	829.5	829.32	829.04	830.87	828.91	829.5
8/15/94	832.68	830.46	830.26	831	831.42	829.98	830.46
8/17/94	833.02	830.45	830.24	830.12	831.7	829.9	830.44
8/19/94	832.78	829.93	829.71	829.5	831.28	829.36	829.91
8/22/94	833.41	831.33	831.07	831.56	832.34	830.8	831.32
8/24/94	833.32	830.66	830.43	830.4	831.92	830.1	830.66
8/26/94	833.74	830.24	830	829.72	831.58	829.64	830.24
8/29/94	832.84	829.78	829.54	829.24	831.18	829.16	829.78
8/31/94	832.58	829.48	829.25	828.96	830.81	828.86	829.34
9/2/94	832.5	829.52	829.31	829.2	830.78	828.93	829.55
9/7/94	832.15	829.1	828.9	828.76	830.38	828.48	828.95
9/9/94	831.98	828.96	828.78	828.7	830.2	828.28	828.75
9/18/94	832.66	831.12	830.89	831.99	831.75	830.66	831.1
9/21/94	832.9	829.5	829.93	829.87	831.39	829.58	830.2
10/11/94	831.91	829.31	829.3	829.05	830.61	828.51	829.1
10/14/94	831.88	829.06	829.04	828.5	830.45	828.17	829.04
10/18/94	831.61	828.69	828.66	827.79	830.1	827.79	828.65
10/21/94	831.69	828.82	828.82	828.44	830.51	827.98	828.84
10/25/94	831.58	828.7	828.67	827.74	830.33	827.83	828.72
11/1/94	831.27	828.24	828.22	827.44	829.94	827.36	828.25
11/4/94	831.37	830.96	831.4	827.56	830.18	828.6	829.89
11/8/94	831	828.07	828.04	827.33	829.69	827.3	828.08
11/11/94	831.38	829.14	829.19	829.26	830.33	828.47	829.18
11/22/94	831.04	827.99	828.04	827.15	829.74	827.14	828
11/25/94	830.94	827.9	827.93	827.1	829.62	827.09	827.91
11/29/94	833.12	831.78	831.72	831.94	832.45	830.82	831.85
12/2/94	833.51	831.13	831.08	830.16	832.17	830.07	830.34
12/13/94	835.69	833.11	833.06	832.75	834.52	832.22	833.12
12/16/94	835.45	832.62	832.58	831.74	834.13	831.72	832.63
12/20/94	835.26	832.41	832.35	831.48	833.95	831.52	832.39
1/3/95	834.47	831.45	831.46	829.95	833.13	830.51	831.44
1/10/95	837.04	834.04	833.94	833.62	835.64	833.09	834.03
1/13/95	838.13	835.11	834.93	834.74	836.77	834.06	835.08
1/17/95	840.34	837.63	837.12	836.75	838.78	836.16	837.47
1/20/95	839.85		836.48	835.68			836.76
1/27/95	838.55	835.07	834.9	833.87	836.83	833.92	835.02

Appendix B: Water Elevation Data (con't)							
date	GW456	GW457	GW458	GW459	GW460	GW461	GW462
1/31/95	839.92	836.86	836.51	835.62	838.36	835.43	836.77
2/3/95	838.37	836.1	835.83	834.82	837.79	834.79	836.04
2/7/95	838.82	835.57	835.38	834.4	837.38	834.37	835.52
2/10/95	838.43	835.16	835.01	833.99	836.87	834.07	835.12
2/14/95	837.7	834.47	834.38	833.41	836.18	833.5	834.46
2/17/95	840.48	837.96	837.47	837.46	839.08	836.52	837.84
2/21/95	839.78	836.59	836.24	835.33	838.15	835.24	836.42
2/24/95	838.89	835.67	835.43	834.48	837.3	834.48	835.56
2/28/95	838.82	836	835.68	835.73	837.48	834.89	836.88
3/3/95	839	835.93	835.62	834.89	837.46	834.75	835.81
3/7/95	839.55	836.55	837.22	835.65	838.03	835.32	836.42
3/10/95	840.53	837.87	837.33	836.73	838.95	836.48	837.67
3/13/95	839.71	836.66	836.33	835.38	838.03	835.45	836.52
3/16/95	838.86	835.85	835.63	834.69	837.3	834.83	835.76
3/21/95	839.56	835.98	835.7	835.62	837.25	835.02	835.86
3/31/95	837.22	834.37	834.3	833.44	835.8	833.6	834.36
4/6/95	837.87	835.82	836.54	833.7	831.13	830.14	833.78
4/18/95	835.68	833.07	833	832	834.42	832.3	833.04
4/21/95	836.01	833.77	833.62	833.81	834.9	833.06	833.7
4/24/95	836.47	833.97	833.88	833.34	835.26	833.15	833.93
5/1/95	835.77	833.25	833.07	832.16	834.47	832.35	833.12
5/5/95	836.62	833.98	833.85	833.19	835.3	833.13	833.94
5/8/95	836.28	833.48	833.37	832.48	834.87	832.64	833.44
5/17/95	838.06	835.6	835.4	834.57	837.1	834.56	835.52

Appendix B: Water elevation data (con't)

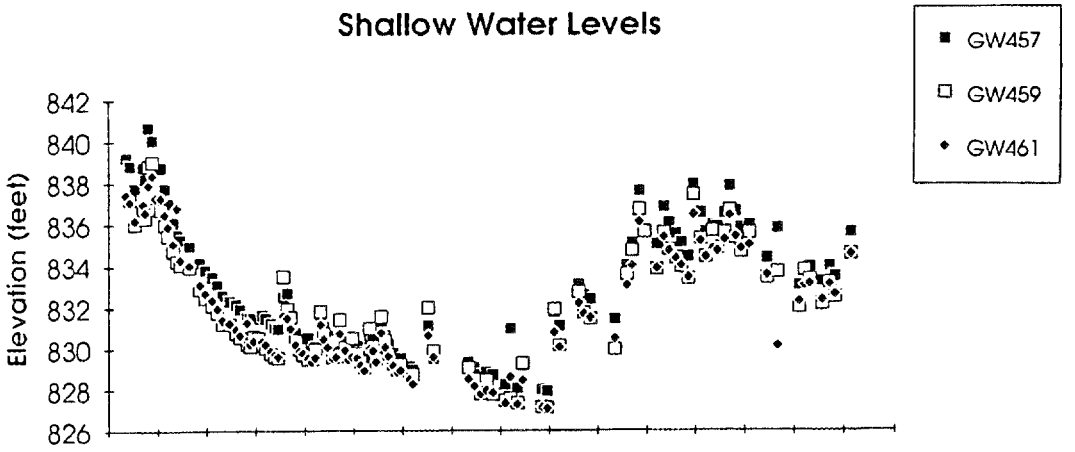

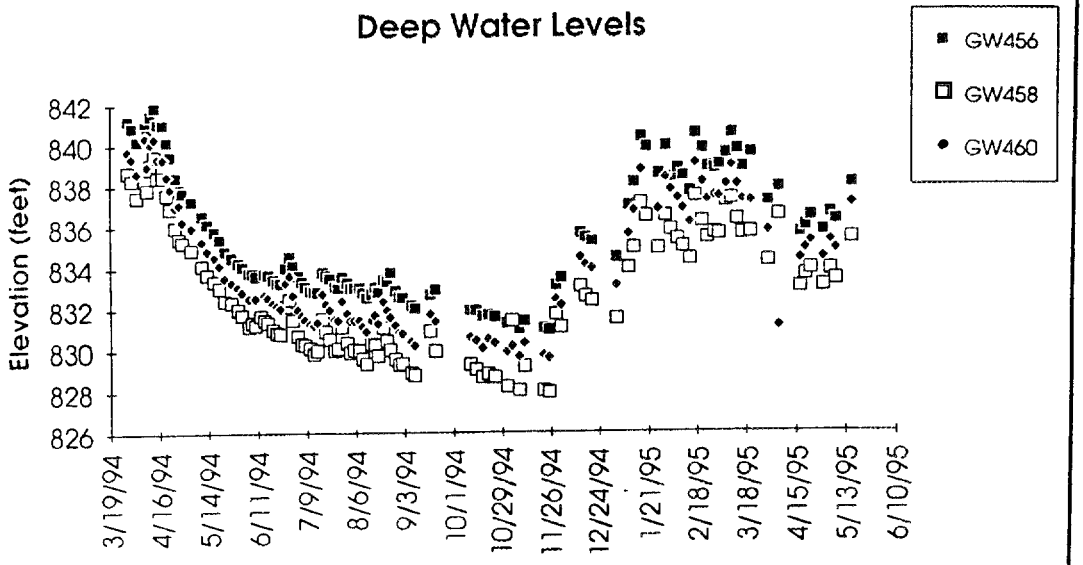

Appendix B: Water elevation data (con't)

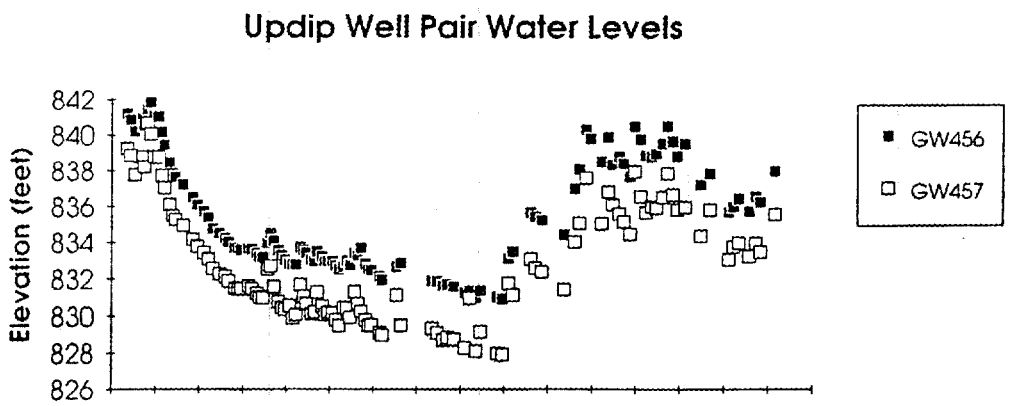

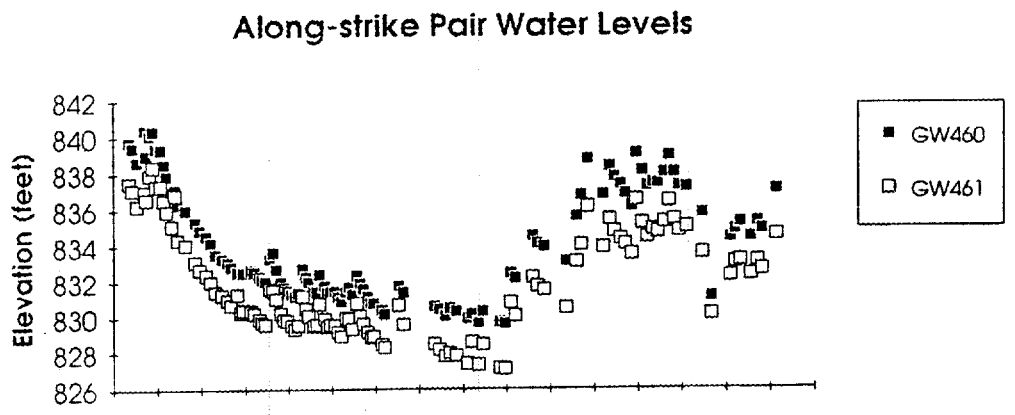

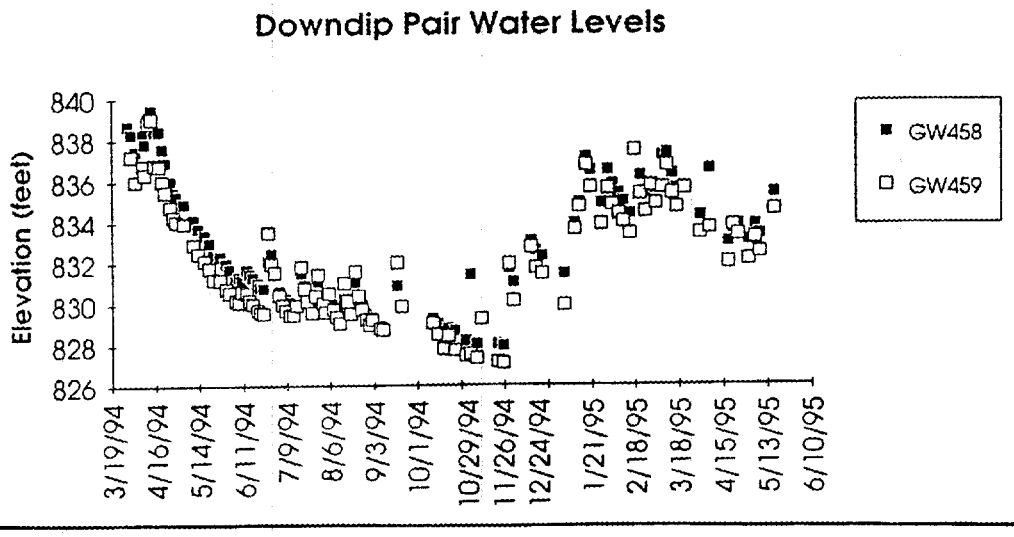

Appendix B: Precipitation Data, West Bear Creek Valley						
from Dr. W. Sanford						
Date	Rainfall (inches)	Rainfall (mm)		Date	Rainfall (inches)	Rainfall (mm)
3/29/94	0	0		5/10/94	0	0
3/30/94	0.334	8.5		5/11/94	0	0
3/31/94	0.055	1.4		5/12/94	0	0
4/1/94	0	0		5/13/94	0	0
4/2/94	0	0		5/14/94	0.09	2.3
4/3/94	0.25	6.4		5/15/94	0.48	12.2
4/4/94	0	0		5/16/94	0.004	0.1
4/5/94	1.4	35.6		5/17/94	0	0
4/6/94	0.348	8.8		5/18/94	0	0
4/7/94	0	0		5/19/94	0	0
4/8/94	0	0		5/20/94	0	0
4/9/94	0	0		5/21/94	0	0
4/10/94	1.95	49.5		5/22/94	0	0
4/11/94	0.6	15.2		5/23/94	0	0
4/12/94	2.146	54.5		5/24/94	0	0
4/13/94	0.028	0.7		5/25/94	0	0
4/14/94	0	0		5/26/94	0.79	20.1
4/15/94	2	50.8		5/27/94	0.004	0.1
4/16/94	0	0		5/28/94	0	0
4/17/94	0	0		5/29/94	0	0
4/18/94	0	0		5/30/94	0	0
4/19/94	0	0		5/31/94	0	0
4/20/94	0	0		6/1/94	0	0
4/21/94	0	0		6/2/94	0.21	5.3
4/22/94	0	0		6/3/94	0.106	2.7
4/23/94	0	0		6/4/94	0	0
4/24/94	0	0		6/5/94	0.004	0.1
4/25/94	0	0		6/6/94	0.154	3.9
4/26/94	0	0		6/7/94	0.35	8.9
4/27/94	0.225	5.7		6/8/94	0.276	7
4/28/94	0	0		6/9/94	0.366	9.3
4/29/94	0	0		6/10/94	0.685	17.4
4/30/94	0	0		6/11/94	0.004	0.1
5/1/94	0.275	7		6/12/94	0	0
5/2/94	0	0		6/13/94	0.346	8.8
5/3/94	0.85	21.6		6/14/94	0	0
5/4/94	0	0		6/15/94	0.15	3.8
5/5/94	0	0		6/16/94	0.008	0.2
5/6/94	0	0		6/17/94	0.213	5.4
5/7/94	0.2	5.1		6/18/94	0.008	0.2
5/8/94	0	0		6/19/94	0	0
5/9/94	0	0		6/20/94	0	0

Appendix B: Precipitation data (con't)

Date	Rainfall (inches)	Rainfall (mm)		Date	Rainfall (inches)	Rainfall (mm)
6/21/94	0	0		8/5/94	0.559	14.2
6/22/94	0	0		8/6/94	0	0
6/23/94	0	0		8/7/94	0	0
6/24/94	0.417	10.6		8/8/94	0	0
6/25/94	0	0		8/9/94	0	0
6/26/94	1.571	39.9		8/10/94	0	0
6/27/94	0.693	17.6		8/11/94	0	0
6/28/94	0.012	0.3		8/12/94	0	0
6/29/94	0	0		8/13/94	0	0
6/30/94	0	0		8/14/94	1.295	32.9
7/1/94	0	0		8/15/94	0	0
7/2/94	0	0		8/16/94	0.354	9
7/3/94	0	0		8/17/94	0.012	0.3
7/4/94	0	0		8/18/94	0	0
7/5/94	0.071	1.8		8/19/94	0.236	6
7/6/94	0.004	0.1		8/20/94	0.449	11.4
7/7/94	0	0		8/21/94	0.587	14.9
7/8/94	0.193	4.9		8/22/94	0	0
7/9/94	0.114	2.9		8/23/94	0	0
7/10/94	0.004	0.1		8/24/94	0	0
7/11/94	0.378	9.6		8/25/94	0	0
7/12/94	0.157	4		8/26/94	0	0
7/13/94	0.15	3.8		8/27/94	0	0
7/14/94	0.114	2.9		8/28/94	0	0
7/15/94	0.079	2		8/29/94	0.035	0.9
7/16/94	0.154	3.9		8/30/94	0	0
7/17/94	0.165	4.2		8/31/94	0.689	17.5
7/18/94	0.15	3.8		9/1/94	0.075	1.9
7/19/94	0.13	3.3		9/2/94	0.012	0.3
7/20/94	0.366	9.3		9/3/94	0	0
7/21/94	0.024	0.6		9/4/94	0	0
7/22/94	0.047	1.2		9/5/94	0.047	1.2
7/23/94	0	0		9/6/94	0.138	3.5
7/24/94	0	0		9/7/94	0.008	0.2
7/25/94	0	0		9/8/94	0	0
7/26/94	0.555	14.1		9/9/94	0	0
7/27/94	0.85	21.6		9/10/94	0	0
7/28/94	0.087	2.2		9/11/94	0	0
7/29/94	0	0		9/12/94	0	0
7/30/94	0	0		9/13/94	0	0
7/31/94	0.008	0.2		9/14/94	0	0
8/1/94	0.004	0.1		9/15/94	0	0
8/2/94	0.028	0.7		9/16/94	0	0
8/3/94	0.091	2.3		9/17/94	2.004	50.9
8/4/94	0.287	7.3		9/18/94	0.075	1.9

Appendix B: Precipitation data (con't)

Date	Rainfall (inches)	Rainfall (mm)		Date	Rainfall (inches)	Rainfall (mm)
9/19/94	0	0		11/3/94	0	0
9/20/94	0	0		11/4/94	0	0
9/21/94	0	0		11/5/94	0.055	1.4
9/22/94	0	0		11/6/94	0.039	1
9/23/94	0.472	12		11/7/94	0	0
9/24/94	0.13	3.3		11/8/94	0	0
9/25/94	0	0		11/9/94	0.736	18.7
9/26/94	0.083	2.1		11/10/94	0.146	3.7
9/27/94	0	0		11/11/94	0	0
9/28/94	0.008	0.2		11/12/94	0	0
9/29/94	0	0		11/13/94	0	0
9/30/94	0	0		11/14/94	0	0
10/1/94	0	0		11/15/94	0	0
10/2/94	0	0		11/16/94	0	0
10/3/94	0.024	0.6		11/17/94	0	0
10/4/94	0	0		11/18/94	0	0
10/5/94	0	0		11/19/94	0	0
10/6/94	0	0		11/20/94	0	0
10/7/94	0	0		11/21/94	0.063	1.6
10/8/94	0	0		11/22/94	0	0
10/9/94	1.004	25.5		11/23/94	0	0
10/10/94	0.008	0.2		11/24/94	0	0
10/11/94	0	0		11/25/94	0	0
10/12/94	0.252	6.4		11/26/94	0.177	4.5
10/13/94	0.043	1.1		11/27/94	1.441	36.6
10/14/94	0	0		11/28/94	1.244	31.6
10/15/94	0	0		11/29/94	0.004	0.1
10/16/94	0	0		11/30/94	0	0
10/17/94	0	0		12/1/94	0	0
10/18/94	0	0		12/2/94	0	0
10/19/94	0.492	12.5		12/3/94	0.106	2.7
10/20/94	0.004	0.1		12/4/94	0.591	15
10/21/94	0.008	0.2		12/5/94	0.22	5.6
10/22/94	0.197	5		12/6/94	0	0
10/23/94	0.004	0.1		12/7/94	0	0
10/24/94	0	0		12/8/94	0	0
10/25/94	0	0		12/9/94	0	0
10/26/94	0.02	0.5		12/10/94	1.559	39.6
10/27/94	0	0		12/11/94	0	0
10/28/94	0	0		12/12/94	0	0
10/29/94	0	0		12/13/94	0.008	0.2
10/30/94	0	0		12/14/94	0	0
10/31/94	0.189	4.8		12/15/94	0	0
11/1/94	0.02	0.5		12/16/94	0.264	6.7
11/2/94	0	0		12/17/94	0.138	3.5

Appendix B: Precipitation data (con't)

Date	Rainfall (inches)	Rainfall (mm)		Date	Rainfall (inches)	Rainfall (mm)
12/18/94	0	0		2/1/95	0	0
12/19/94	0	0		2/2/95	0.098	2.5
12/20/94	0	0		2/3/95	0.205	5.2
12/21/94	0.024	0.6		2/4/95	0.067	1.7
12/22/94	0.26	6.6		2/5/95	0	0
12/23/94	0	0		2/6/95	0	0
12/24/94	0	0		2/7/95	0.047	1.2
12/25/94	0	0		2/8/95	0	0
12/26/94	0	0		2/9/95	0.004	0.1
12/27/94	0	0		2/10/95	0.106	2.7
12/28/94	0	0		2/11/95	0	0
12/29/94	0	0		2/12/95	0.004	0.1
12/30/94	0.008	0.2		2/13/95	0	0
12/31/94	0.177	4.5		2/14/95	0.02	0.5
1/1/95	0.035	0.9		2/15/95	1.48	37.6
1/2/95	0	0		2/16/95	0.894	22.7
1/3/95	0	0		2/17/95	0.004	0.1
1/4/95	0	0		2/18/95	0.008	0.2
1/5/95	0	0		2/19/95	0.012	0.3
1/6/95	0.11	2.8		2/20/95	0	0
1/7/95	1.299	33		2/21/95	0.012	0.3
1/8/95	0	0		2/22/95	0	0
1/9/95	0	0		2/23/95	0.098	2.5
1/10/95	0	0		2/24/95	0.008	0.2
1/11/95	0.921	23.4		2/25/95	0	0
1/12/95	0.012	0.3		2/26/95	0	0
1/13/95	0	0		2/27/95	0.681	17.3
1/14/95	1.89	48		2/28/95	0.193	4.9
1/15/95	0.772	19.6		3/1/95	0	0
1/16/95	0.008	0.2		3/2/95	0	0
1/17/95	0	0		3/3/95	0.232	5.9
1/18/95	0	0		3/4/95	0.004	0.1
1/19/95	0.272	6.9		3/5/95	0.48	12.2
1/20/95	0.039	1		3/6/95	0.028	0.7
1/21/95	0	0		3/7/95	0.055	1.4
1/22/95	0	0		3/8/95	1.689	42.9
1/23/95	0	0		3/9/95	0	0
1/24/95	0	0		3/10/95	0	0
1/25/95	0	0		3/11/95	0	0
1/26/95	0	0		3/12/95	0	0
1/27/95	0.138	3.5		3/13/95	0	0
1/28/95	1.646	41.8		3/14/95	0	0
1/29/95	0.024	0.6		3/15/95	0	0
1/30/95	0.173	4.4		3/16/95	0	0
1/31/95	0	0		3/17/95	0	0

Appendix B: Precipitation data (con't)

Date	Rainfall (inches)	Rainfall (mm)		Date	Rainfall (inches)	Rainfall (mm)
3/18/95	0	0		5/2/95	0	0
3/19/95	0	0		5/3/95	0	0
3/20/95	1.016	25.8		5/4/95	0.016	0.4
3/21/95	0.004	0.1		5/5/95	0	0
3/22/95	0	0		5/6/95	0	0
3/23/95	0	0		5/7/95	0.008	0.2
3/24/95	0	0		5/8/95	0	0
3/25/95	0	0		5/9/95	1.941	49.3
3/26/95	0	0		5/10/95	0.713	18.1
3/27/95	0.256	6.5		5/11/95	0.004	0.1
3/28/95	0	0		5/12/95	0	0
3/29/95	0	0		5/13/95	0.055	1.4
3/30/95	0	0		5/14/95	0.709	18
3/31/95	0	0		5/15/95	0	0
4/1/95	0	0		5/16/95	0.169	4.3
4/2/95	0	0		5/17/95	0	0
4/3/95	0	0				
4/4/95	0	0				
4/5/95	0	0				
4/6/95	0	0				
4/7/95	0	0				
4/8/95	0	0				
4/9/95	0	0				
4/10/95	0	0				
4/11/95	0	0				
4/12/95	0.421	10.7				
4/13/95	0	0				
4/14/95	0	0				
4/15/95	0	0				
4/16/95	0	0				
4/17/95	0.445	11.3				
4/18/95	0	0				
4/19/95	0.146	3.7				
4/20/95	0.079	2				
4/21/95	0.949	24.1				
4/22/95	0	0				
4/23/95	0.362	9.2				
4/24/95	0	0				
4/25/95	0	0				
4/26/95	0	0				
4/27/95	0	0				
4/28/95	0	0				
4/29/95	0	0				
4/30/95	0.083	2.1				
5/1/95	1.276	32.4				

Appendix C: Gradient calculations

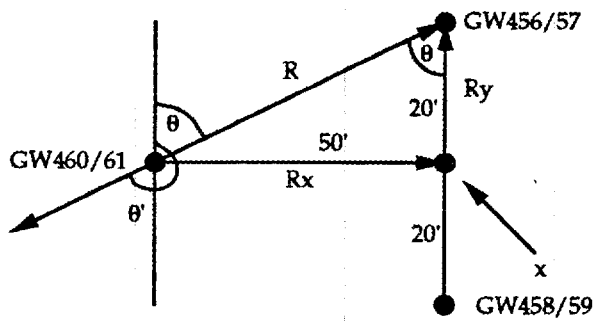

x = midpoint water level between updip and downdip well pair
x (shallow) = (GW456+GW458)/2
x (deep) = (GW457+GW459)/2

For the shallow wells, the gradient was calculated using water levels from GW457, GW459, and GW461:

$$R_x = \frac{(x - GW461)}{50'}$$

$$R_y = \frac{(GW457 - x)}{20'}$$

$$R = \sqrt{R_x^{\,2} + R_y^{\,2}}$$

$$\tan\theta = \frac{R_x}{R_y}$$

$$\theta = \arctan\left(\frac{R_x}{R_y}\right)$$

$$\theta' = \theta + 180$$

The deep gradient was calculated in the same way using water levels from GW456, GW458, and GW460.

	Shallow Wells							
Date	GW457	GW459	GW461	X	Rx	Ry	R	theta
3/31/94	838.85	837.2	837.1	838.03	0.0185	0.0412	0.04521	204.16
4/3/94	837.75	836	836.23	836.88	0.0129	0.0438	0.04561	196.43
4/8/94	838.75	836.75	837	837.75	0.015	0.05	0.0522	196.70
4/9/94	838.23	836.32	836.59	837.28	0.0137	0.0477	0.04968	196.01
4/11/94	840.68	838.83	837.9	839.76	0.0371	0.0462	0.05929	218.74
4/13/94	840.05	839.03	838.37	839.54	0.0234	0.0255	0.03461	222.54
4/15/94	838.79	836.79	837.3	837.79	0.0098	0.05	0.05095	191.09
4/18/94	838.74	836.73	837.31	837.74	0.0085	0.0502	0.05096	189.60
4/20/94	837.74	835.99	836.49	836.87	0.0075	0.0438	0.04439	189.73
4/22/94	837.03	835.46	835.91	836.25	0.0067	0.0392	0.03982	189.69
4/25/94	836.1	834.73	835.09	835.42	0.0065	0.0343	0.03486	190.75
4/27/94	835.49	834.24	836.81	834.87	-0.0389	0.0313	0.0499	128.78
4/29/94	835.26	834.03	834.32	834.65	0.0065	0.0308	0.03143	191.94
5/4/94	834.97	833.93	834.03	834.45	0.0084	0.026	0.02732	197.90
5/10/94	834.18	832.89	833.11	833.54	0.0085	0.0322	0.03335	194.77
5/13/94	833.8	832.46	832.69	833.13	0.0088	0.0335	0.03464	194.72
5/17/94	833.45	832.09	832.35	832.77	0.0084	0.034	0.03502	193.88
5/20/94	833.1	831.74	831.96	832.42	0.0092	0.034	0.03522	195.14
5/23/94	832.58	831.2	831.4	831.89	0.0098	0.0345	0.03586	195.86
5/27/94	832.3	831.18	831.24	831.74	0.01	0.028	0.02973	199.65
5/31/94	832.14	830.75	830.95	831.45	0.0099	0.0348	0.03613	195.90
6/2/94	831.89	830.54	830.68	831.22	0.0107	0.0338	0.03541	197.59
6/6/94	831.52	830.2	831.28	830.86	-0.0084	0.033	0.03405	165.72
6/8/94	831.5	830.1	830.24	830.80	0.0112	0.035	0.03675	197.74
6/15/94	831.61	830.19	830.36	830.90	0.0108	0.0355	0.03711	196.92
6/17/94	831.48	829.99	830.21	830.74	0.0105	0.0373	0.0387	195.74
6/20/94	831.22	829.74	829.88	830.48	0.012	0.037	0.0389	197.97
6/22/94	831.04	829.6	829.68	830.32	0.0128	0.036	0.03821	199.57
6/24/94	830.98	829.54	829.58	830.26	0.0136	0.036	0.03848	200.70
6/27/94	832.52	833.48	831.6	833.00	0.028	-0.024	0.03688	130.60
6/29/94	832.7	831.92	831.5	832.31	0.0162	0.0195	0.02535	219.72
7/1/94	831.58	831.54	831.02	831.56	0.0108	0.001	0.01085	264.71
7/4/94	830.8	830.42	830.22	830.61	0.0078	0.0095	0.01229	219.39
7/6/94	830.47	829.96	829.88	830.22	0.0067	0.0127	0.0144	207.72
7/8/94	830.37	829.68	829.78	830.03	0.0049	0.0173	0.01793	195.86
7/11/94	830.56	829.45	829.54	830.01	0.0093	0.0277	0.02927	198.53
7/13/94	829.91	829.48	829.36	829.70	0.0067	0.0108	0.01267	211.93
7/15/94	830.08	829.94	829.56	830.01	0.009	0.0035	0.00966	248.75
7/18/94	831.7	831.8	831.18	831.75	0.0114	-0.0025	0.01167	102.37
7/20/94	831.06	830.74	830.48	830.90	0.0084	0.008	0.0116	226.40
7/22/94	830.67	830.16	830.1	830.42	0.0063	0.0127	0.01422	206.29
7/25/94	830.12	829.56	829.52	829.84	0.0064	0.014	0.01539	204.57
7/27/94	830.22	830.4	829.6	830.31	0.0142	-0.0045	0.0149	107.58
7/29/94	831.3	831.4	830.76	831.35	0.0118	-0.0025	0.01206	101.96

Appendix C: Gradient calculations (con't)

Date	GW457	GW459	GW461	X	Rx	Ry	R	theta
8/1/94	830.52	830.04	829.92	830.28	0.0072	0.012	0.01399	210.96
8/3/94	830.08	829.6	829.48	829.84	0.0072	0.012	0.01399	210.96
8/5/94	830.21	830.52	829.6	830.37	0.0153	-0.0077	0.01715	116.86
8/8/94	830.14	829.74	829.55	829.94	0.0078	0.01	0.01268	217.95
8/10/94	829.8	829.34	829.18	829.57	0.0078	0.0115	0.0139	214.15
8/12/94	829.5	829.04	828.91	829.27	0.0072	0.0115	0.01357	212.05
8/15/94	830.46	831	829.98	830.73	0.015	-0.0135	0.02018	131.99
8/17/94	830.45	830.12	829.9	830.29	0.0077	0.0082	0.01129	223.03
8/19/94	829.93	829.5	829.36	829.72	0.0071	0.0108	0.01288	213.44
8/22/94	831.33	831.56	830.8	831.45	0.0129	-0.0057	0.01412	114.02
8/24/94	830.66	830.4	830.1	830.53	0.0086	0.0065	0.01078	232.92
8/26/94	830.24	829.72	829.64	829.98	0.0068	0.013	0.01467	207.61
8/29/94	829.78	829.24	829.16	829.51	0.007	0.0135	0.01521	207.41
8/31/94	829.48	828.96	828.86	829.22	0.0072	0.013	0.01486	208.98
9/2/94	829.52	829.2	828.93	829.36	0.0086	0.008	0.01175	227.07
9/7/94	829.1	828.76	828.48	828.93	0.009	0.0085	0.01238	226.64
9/9/94	828.96	828.7	828.28	828.83	0.011	0.0065	0.01278	239.42
9/18/94	831.12	831.99	830.66	831.56	0.0179	-0.0218	0.02817	140.55
9/21/94	829.5	829.87	829.58	829.69	0.0021	-0.0092	0.00949	167.21
10/11/94	829.31	829.05	828.51	829.18	0.0134	0.0065	0.01489	244.12
10/14/94	829.06	828.5	828.17	828.78	0.0122	0.014	0.01857	221.07
10/18/94	828.69	827.79	827.79	828.24	0.009	0.0225	0.02423	201.80
10/21/94	828.82	828.44	827.98	828.63	0.013	0.0095	0.0161	233.84
10/25/94	828.7	827.74	827.83	828.22	0.0078	0.024	0.02524	198.00
11/1/94	828.24	827.44	827.36	827.84	0.0096	0.02	0.02218	205.64
11/4/94	830.96	827.56	828.6	829.26	0.0132	0.085	0.08602	188.83
11/8/94	828.07	827.33	827.3	827.70	0.008	0.0185	0.02016	203.39
11/11/94	829.14	829.26	828.47	829.20	0.0146	-0.003	0.01491	101.61
11/22/94	827.99	827.15	827.14	827.57	0.0086	0.021	0.02269	202.27
11/25/94	827.9	827.1	827.09	827.50	0.0082	0.02	0.02162	202.29
11/29/94	831.78	831.94	830.82	831.86	0.0208	-0.004	0.02118	100.89
12/2/94	831.13	830.16	830.07	830.65	0.0115	0.0243	0.02684	205.37
12/13/94	833.11	832.75	832.22	832.93	0.0142	0.009	0.01681	237.63
12/16/94	832.62	831.74	831.72	832.18	0.0092	0.022	0.02385	202.69
12/20/94	832.41	831.48	831.52	831.95	0.0085	0.0233	0.02476	200.08
1/3/95	831.45	829.95	830.51	830.70	0.0038	0.0375	0.03769	185.79
1/10/95	834.04	833.62	833.09	833.83	0.0148	0.0105	0.01815	234.65
1/13/95	835.11	834.74	834.06	834.93	0.0173	0.0093	0.01962	241.87
1/17/95	837.63	836.75	836.16	837.19	0.0206	0.022	0.03014	223.12
1/31/95	836.86	835.62	835.43	836.24	0.0162	0.031	0.03498	207.59
2/3/95	836.1	834.82	834.79	835.46	0.0134	0.032	0.03469	202.72
2/7/95	835.57	834.4	834.37	834.99	0.0123	0.0293	0.03173	202.81
2/10/95	835.16	833.99	834.07	834.58	0.0101	0.0292	0.03094	199.05
2/14/95	834.47	833.41	833.5	833.94	0.0088	0.0265	0.02792	198.37
2/17/95	837.96	837.46	836.52	837.71	0.0238	0.0125	0.02688	242.29
2/21/95	836.59	835.33	835.24	835.96	0.0144	0.0315	0.03464	204.57

Appendix C: Gradient calculations (con't)

Date	GW457	GW459	GW461	X	Rx	Ry	R	theta
2/24/95	835.67	834.48	834.48	835.08	0.0119	0.0297	0.03204	201.80
2/28/95	836	835.73	834.89	835.87	0.0195	0.0067	0.02064	250.91
3/3/95	835.93	834.89	834.75	835.41	0.0132	0.026	0.02916	206.92
3/7/95	836.55	835.65	835.32	836.10	0.0156	0.0225	0.02738	214.73
3/10/95	837.87	836.73	836.48	837.30	0.0164	0.0285	0.03288	209.92
3/13/95	836.66	835.38	835.45	836.02	0.0114	0.032	0.03397	199.61
3/16/95	835.85	834.69	834.83	835.27	0.0088	0.029	0.03031	196.88
3/21/95	835.98	835.62	835.02	835.80	0.0156	0.009	0.01801	240.02
3/31/95	834.37	833.44	833.6	833.91	0.0061	0.0233	0.02404	194.70
4/6/95	835.82	833.7	830.14	834.76	0.0924	0.053	0.10652	240.16
4/18/95	833.07	832	832.3	832.54	0.0047	0.0267	0.02716	189.97
4/21/95	833.77	833.81	833.06	833.79	0.0146	-0.001	0.01463	93.92
4/24/95	833.97	833.34	833.15	833.66	0.0101	0.0158	0.01871	212.67
5/1/95	833.25	832.16	832.35	832.71	0.0071	0.0273	0.02816	194.60
5/5/95	833.98	833.19	833.13	833.59	0.0091	0.0197	0.02175	204.74
5/8/95	833.48	832.48	832.64	832.98	0.0068	0.025	0.02591	195.22
5/17/95	835.6	834.57	834.56	835.09	0.0105	0.0257	0.02781	202.18
average	832.829	831.989	831.841	832.41	0.0114	0.021	0.02388	208.41
avg 4/15-6/10/94	834.477	833.058	833.509	833.77	0.0052	0.0355	0.03583	188.30
avg 6/15-9/9/94	830.555	830.12	829.836	830.34	0.01	0.0109	0.0148	222.63
avg 9/9-11/25/94	829.033	828.423	828.197	828.73	0.0106	0.0152	0.01858	214.84
avg 11/29/94-3/13/9	835.03	834.137	833.885	834.58	0.014	0.0223	0.02635	212.06
avg 3/16-5/17/95	834.467	833.545	833.162	834.01	0.0169	0.023	0.02857	216.24

Appendix C: Gradient calculations (con't)

		DEEP WELLS						
Date	GW456	GW458	GW460	X	Rx	Ry	R	theta
3/31/94	841.19	838.68	839.73	839.94	0.0041	0.0628	0.0629	183.74
4/3/94	840.85	838.3	839.4	839.58	0.0035	0.0637	0.0638	183.14
4/8/94	840.2	837.45	838.65	838.83	0.0035	0.0688	0.0688	182.91
4/9/94	840.94	838.3	840.4	839.62	-0.0156	0.066	0.0678	166.7
4/11/94	840.55	837.82	838.99	839.19	0.0039	0.0683	0.0684	183.27
4/13/94	841.44	839.06	840.07	840.25	0.0036	0.0595	0.0596	183.46
4/15/94	841.85	839.46	840.34	840.66	0.0063	0.0598	0.0601	186.02
4/18/94	841.06	838.42	839.37	839.74	0.0074	0.066	0.0664	186.4
4/20/94	841.03	838.43	839.32	839.73	0.0082	0.065	0.0655	187.19
4/22/94	840.16	837.58	838.5	838.87	0.0074	0.0645	0.0649	186.54
4/25/94	839.45	836.92	837.88	838.19	0.0061	0.0633	0.0635	185.51
4/27/94	838.45	835.99	836.99	837.22	0.0046	0.0615	0.0617	184.28
4/29/94	837.84	835.43	837.11	836.64	-0.0095	0.0603	0.061	171.04
5/4/94	837.66	835.25	836.28	836.46	0.0035	0.0603	0.0604	183.32
5/10/94	837.24	834.87	835.98	836.06	0.0015	0.0592	0.0593	181.45
5/13/94	836.55	834.11	835.3	835.33	0.0006	0.061	0.061	180.56
5/17/94	836.13	833.67	834.86	834.90	0.0008	0.0615	0.0615	180.75
5/20/94	835.75	833.34	834.54	834.55	0.0001	0.0602	0.0603	180.1
5/23/94	835.4	832.99	834.14	834.20	0.0011	0.0603	0.0603	181.05
5/27/94	834.8	832.4	833.52	833.60	0.0016	0.06	0.06	181.53
5/31/94	834.52	832.29	833.28	833.41	0.0025	0.0558	0.0558	182.57
6/2/94	834.24	831.95	833.08	833.10	0.0003	0.0572	0.0573	180.3
6/6/94	834.04	831.69	832.82	832.87	0.0009	0.0587	0.0588	180.88
6/8/94	833.74	831.14	832.52	832.44	-0.0016	0.065	0.065	178.59
6/15/94	833.58	831.18	832.5	832.38	-0.0024	0.06	0.06	177.71
6/17/94	833.71	831.43	832.65	832.57	-0.0016	0.057	0.057	178.39
6/20/94	833.64	831.3	832.53	832.47	-0.0012	0.0585	0.0585	178.82
6/22/94	833.4	830.98	832.26	832.19	-0.0014	0.0605	0.0605	178.67
6/24/94	833.25	830.82	832.1	832.04	-0.0013	0.0607	0.0608	178.77
6/27/94	833.22	830.76	832.02	831.99	-0.0006	0.0615	0.0615	179.44
6/29/94	833.98	832.1	833.28	833.04	-0.0048	0.047	0.0472	174.17
7/1/94	834.54	832.46	833.62	833.50	-0.0024	0.052	0.0521	177.36
7/4/94	834.12	831.44	832.66	832.78	0.0024	0.067	0.067	182.05
7/6/94	833.6	830.66	831.96	832.13	0.0034	0.0735	0.0736	182.65
7/8/94	833.32	830.31	831.66	831.82	0.0031	0.0752	0.0753	182.36
7/11/94	833.06	830.25	831.48	831.66	0.0035	0.0702	0.0703	182.85
7/13/94	832.84	830.08	831.26	831.46	0.004	0.069	0.0691	183.32
7/15/94	832.82	829.82	831.18	831.32	0.0028	0.075	0.0751	182.14
7/18/94	832.8	829.96	831.34	831.38	0.0008	0.071	0.071	180.65
7/20/94	833.78	831.5	832.72	832.64	-0.0016	0.057	0.057	178.39
7/22/94	833.6	830.9	832.24	832.25	0.0002	0.0675	0.0675	180.17
7/25/94	833.46	830.5	831.96	831.98	0.0004	0.074	0.074	180.31
7/27/94	833.08	829.95	831.48	831.52	0.0007	0.0782	0.0783	180.51
7/29/94	833	830.04	831.42	831.52	0.002	0.074	0.074	181.55

Appendix C: Gradient calculations (con't)

Date	GW456	GW458	GW460	X	Rx	Ry	R	theta
8/1/94	833.52	831.1	832.4	832.31	-0.0018	0.0605	0.0605	178.3
8/3/94	833.24	830.32	831.78	831.78	0	0.073	0.073	180
8/5/94	832.98	829.88	831.4	831.43	0.0006	0.0775	0.0775	180.44
8/8/94	833	829.98	831.4	831.49	0.0018	0.0755	0.0755	181.37
8/10/94	832.99	829.96	831.45	831.48	0.0005	0.0757	0.0758	180.38
8/12/94	832.76	829.57	831.14	831.17	0.0005	0.0798	0.0798	180.36
8/15/94	832.52	829.32	830.87	830.92	0.001	0.08	0.08	180.72
8/17/94	832.68	830.26	831.42	831.47	0.001	0.0605	0.0605	180.95
8/19/94	833.02	830.24	831.7	831.63	-0.0014	0.0695	0.0695	178.85
8/22/94	832.78	829.71	831.28	831.25	-0.0007	0.0767	0.0768	179.48
8/24/94	833.41	831.07	832.34	832.24	-0.002	0.0585	0.0585	178.04
8/26/94	833.32	830.43	831.92	831.88	-0.0009	0.0723	0.0723	179.29
8/29/94	833.74	830	831.58	831.87	0.0058	0.0935	0.0937	183.55
8/31/94	832.84	829.54	831.18	831.19	0.0002	0.0825	0.0825	180.14
9/2/94	832.58	829.25	830.81	830.92	0.0021	0.0833	0.0833	181.44
9/7/94	832.5	829.31	830.78	830.91	0.0025	0.0798	0.0798	181.8
9/9/94	832.15	828.9	830.38	830.53	0.0029	0.0813	0.0813	182.04
9/18/94	831.98	828.78	830.2	830.38	0.0036	0.08	0.0801	182.58
9/21/94	832.66	830.89	831.75	831.78	0.0005	0.0442	0.0443	180.65
10/11/94	832.9	829.93	831.39	831.42	0.0005	0.0743	0.0743	180.39
10/14/94	831.91	829.3	830.61	830.61	-1E-04	0.0652	0.0653	179.91
10/18/94	831.88	829.04	830.45	830.46	0.0002	0.071	0.071	180.16
10/21/94	831.61	828.66	830.1	830.14	0.0007	0.0738	0.0738	180.54
10/25/94	831.69	828.82	830.51	830.26	-0.0051	0.0717	0.0719	175.93
11/1/94	831.58	828.67	830.33	830.13	-0.0041	0.0728	0.0729	176.77
11/4/94	831.27	828.22	829.94	829.75	-0.0039	0.0762	0.0763	177.07
11/8/94	831.37	831.4	830.18	831.39	0.0241	-7E-04	0.0241	91.782
11/11/94	831	828.04	829.69	829.52	-0.0034	0.074	0.0741	177.37
11/22/94	831.38	829.19	830.33	830.29	-0.0009	0.0547	0.0548	179.06
11/25/94	831.04	828.04	829.74	829.54	-0.004	0.075	0.0751	176.95
11/29/94	830.94	827.93	829.62	829.44	-0.0037	0.0753	0.0753	177.19
12/2/94	833.12	831.72	832.45	832.42	-0.0006	0.035	0.035	179.02
12/13/94	833.51	831.08	832.17	832.30	0.0025	0.0607	0.0608	182.36
12/16/94	835.69	833.06	834.52	834.38	-0.0029	0.0658	0.0658	177.47
12/20/94	835.45	832.58	834.13	834.02	-0.0023	0.0717	0.0718	178.16
1/3/95	835.26	832.35	833.95	833.81	-0.0029	0.0727	0.0728	177.72
1/10/95	834.47	831.46	833.13	832.97	-0.0033	0.0752	0.0753	177.49
1/13/95	837.04	833.94	835.64	835.49	-0.003	0.0775	0.0776	177.78
1/17/95	838.13	834.93	836.77	836.53	-0.0048	0.08	0.0801	176.57
1/31/95	838.55	834.9	836.83	836.73	-0.0021	0.0913	0.0913	178.68
2/3/95	839.92	836.51	838.36	838.22	-0.0029	0.0853	0.0853	178.05
2/7/95	838.37	835.83	837.79	837.10	-0.0138	0.0635	0.065	167.74
2/10/95	838.82	835.38	837.38	837.10	-0.0056	0.086	0.0862	176.27
2/14/95	838.43	835.01	836.87	836.72	-0.003	0.0855	0.0856	177.99
2/17/95	837.7	834.38	836.18	836.04	-0.0028	0.083	0.083	178.07
2/21/95	840.48	837.47	839.08	838.98	-0.0021	0.0752	0.0753	178.4

Appendix C: Gradient calculations (con't)

Date	GW456	GW458	GW460	X	Rx	Ry	R	theta
2/24/95	839.78	836.24	838.15	838.01	-0.0028	0.0885	0.0885	178.19
2/28/95	838.89	835.43	837.3	837.16	-0.0028	0.0865	0.0865	178.15
3/3/95	838.82	835.68	837.48	837.25	-0.0046	0.0785	0.0786	176.65
3/7/95	839	835.62	837.46	837.31	-0.003	0.0845	0.0846	177.97
3/10/95	839.55	837.22	838.03	838.39	0.0071	0.0582	0.0587	186.95
3/13/95	840.53	837.33	838.95	838.93	-0.0004	0.08	0.08	179.71
3/16/95	839.71	836.33	838.03	838.02	-0.0002	0.0845	0.0845	179.86
3/21/95	838.86	835.63	837.3	837.25	-0.0011	0.0808	0.0808	179.22
3/31/95	839.56	835.7	837.25	837.63	0.0076	0.0965	0.0968	184.5
4/6/95	837.22	834.3	835.8	835.76	-0.0008	0.073	0.073	179.37
4/18/95	837.87	836.54	831.13	837.21	0.1215	0.0333	0.126	254.7
4/21/95	835.68	833	834.42	834.34	-0.0016	0.067	0.067	178.63
4/24/95	836.01	833.62	834.9	834.82	-0.0017	0.0597	0.0598	178.37
5/1/95	836.47	833.88	835.26	835.18	-0.0017	0.0648	0.0648	178.5
5/5/95	835.77	833.07	834.47	834.42	-0.001	0.0675	0.0675	179.15
5/8/95	836.62	833.85	835.3	835.24	-0.0013	0.0692	0.0693	178.92
5/17/95	836.28	833.37	834.87	834.83	-0.0009	0.0727	0.0728	179.29
average	835.408	832.665	833.976	834.04	0.00121	0.0686	0.0686	181.01
avg 4/15-6/10/94	837.217	834.774	835.879	836.00	0.00232	0.0611	0.0611	182.18
avg 6/15-9/9/94	833.212	830.413	831.788	831.81	0.00049	0.07	0.07	180.4
avg 9/9-11/25/94	831.744	829.134	830.4	830.44	0.00079	0.0653	0.0653	180.69
avg 11/29/94-3/13/9	837.384	834.366	836.011	835.88	-0.0027	0.0755	0.0755	177.94
avg 3/16-5/17/95	837.277	834.481	835.339	835.88	0.0108	0.0699	0.0707	188.78

Appendix C: Flow direction calculations

	SHALLOW WELLS							
Date	GW457	GW459	GW461	X	Rx*8	Ry	R	theta
3/31/94	838.85	837.2	837.1	838.03	0.148	0.0412	0.15364	254.43
4/3/94	837.75	836	836.23	836.88	0.1032	0.0438	0.11209	247.03
4/8/94	838.75	836.75	837	837.75	0.12	0.05	0.13	247.38
4/9/94	838.23	836.32	836.59	837.28	0.1096	0.0477	0.11955	246.46
4/11/94	840.68	838.83	837.9	839.76	0.2968	0.0462	0.30038	261.14
4/13/94	840.05	839.03	838.37	839.54	0.1872	0.0255	0.18893	262.24
4/15/94	838.79	836.79	837.3	837.79	0.0784	0.05	0.09299	237.47
4/18/94	838.74	836.73	837.31	837.74	0.068	0.0502	0.08455	233.54
4/20/94	837.74	835.99	836.49	836.87	0.06	0.0438	0.07426	233.90
4/22/94	837.03	835.46	835.91	836.25	0.0536	0.0392	0.06643	233.79
4/25/94	836.1	834.73	835.09	835.42	0.052	0.0343	0.06227	236.63
4/27/94	835.49	834.24	836.81	834.87	-0.3112	0.0313	0.31277	95.73
4/29/94	835.26	834.03	834.32	834.65	0.052	0.0308	0.06041	239.40
5/4/94	834.97	833.93	834.03	834.45	0.0672	0.026	0.07205	248.85
5/10/94	834.18	832.89	833.11	833.54	0.068	0.0322	0.07526	244.63
5/13/94	833.8	832.46	832.69	833.13	0.0704	0.0335	0.07796	244.55
5/17/94	833.45	832.09	832.35	832.77	0.0672	0.034	0.07531	243.16
5/20/94	833.1	831.74	831.96	832.42	0.0736	0.034	0.08107	245.21
5/23/94	832.58	831.2	831.4	831.89	0.0784	0.0345	0.08566	246.25
5/27/94	832.3	831.18	831.24	831.74	0.08	0.028	0.08476	250.71
5/31/94	832.14	830.75	830.95	831.45	0.0792	0.0348	0.08649	246.31
6/2/94	831.89	830.54	830.68	831.22	0.0856	0.0338	0.09201	248.48
6/6/94	831.52	830.2	831.28	830.86	-0.0672	0.033	0.07487	116.15
6/8/94	831.5	830.1	830.24	830.80	0.0896	0.035	0.09619	248.66
6/15/94	831.61	830.19	830.36	830.90	0.0864	0.0355	0.09341	247.66
6/17/94	831.48	829.99	830.21	830.74	0.084	0.0373	0.09189	246.08
6/20/94	831.22	829.74	829.88	830.48	0.096	0.037	0.10288	248.92
6/22/94	831.04	829.6	829.68	830.32	0.1024	0.036	0.10854	250.63
6/24/94	830.98	829.54	829.58	830.26	0.1088	0.036	0.1146	251.69
6/27/94	832.52	833.48	831.6	833.00	0.224	-0.024	0.22528	96.12
6/29/94	832.7	831.92	831.5	832.31	0.1296	0.0195	0.13106	261.44
7/1/94	831.58	831.54	831.02	831.56	0.0864	0.001	0.08641	269.34
7/4/94	830.8	830.42	830.22	830.61	0.0624	0.0095	0.06312	261.34
7/6/94	830.47	829.96	829.88	830.22	0.0536	0.0127	0.0551	256.62
7/8/94	830.37	829.68	829.78	830.03	0.0392	0.0173	0.04283	246.25
7/11/94	830.56	829.45	829.54	830.01	0.0744	0.0277	0.07941	249.55
7/13/94	829.91	829.48	829.36	829.70	0.0536	0.0108	0.05467	258.66
7/15/94	830.08	829.94	829.56	830.01	0.072	0.0035	0.07209	267.22
7/18/94	831.7	831.8	831.18	831.75	0.0912	-0.002	0.09123	91.57
7/20/94	831.06	830.74	830.48	830.90	0.0672	0.008	0.06767	263.21
7/22/94	830.67	830.16	830.1	830.42	0.0504	0.0127	0.05199	255.80
7/25/94	830.12	829.56	829.52	829.84	0.0512	0.014	0.05308	254.71
7/27/94	830.22	830.4	829.6	830.31	0.1136	-0.004	0.11369	92.27

Appendix C: Flow direction calculations (con't)

Date	GW457	GW459	GW461	X	Rx*8	Ry	R	theta
7/29/94	831.3	831.4	830.76	831.35	0.0944	-0.002	0.09443	91.52
8/1/94	830.52	830.04	829.92	830.28	0.0576	0.012	0.05884	258.23
8/3/94	830.08	829.6	829.48	829.84	0.0576	0.012	0.05884	258.23
8/5/94	830.21	830.52	829.6	830.37	0.1224	-0.008	0.12265	93.62
8/8/94	830.14	829.74	829.55	829.94	0.0624	0.01	0.0632	260.90
8/10/94	829.8	829.34	829.18	829.57	0.0624	0.0115	0.06345	259.56
8/12/94	829.5	829.04	828.91	829.27	0.0576	0.0115	0.05874	258.71
8/15/94	830.46	831	829.98	830.73	0.12	-0.013	0.12076	96.42
8/17/94	830.45	830.12	829.9	830.29	0.0616	0.0082	0.06215	262.37
8/19/94	829.93	829.5	829.36	829.72	0.0568	0.0108	0.05781	259.28
8/22/94	831.33	831.56	830.8	831.45	0.1032	-0.006	0.10336	93.19
8/24/94	830.66	830.4	830.1	830.53	0.0688	0.0065	0.06911	264.60
8/26/94	830.24	829.72	829.64	829.98	0.0544	0.013	0.05593	256.56
8/29/94	829.78	829.24	829.16	829.51	0.056	0.0135	0.0576	256.45
8/31/94	829.48	828.96	828.86	829.22	0.0576	0.013	0.05905	257.28
9/2/94	829.52	829.2	828.93	829.36	0.0688	0.008	0.06926	263.37
9/7/94	829.1	828.76	828.48	828.93	0.072	0.0085	0.0725	263.27
9/9/94	828.96	828.7	828.28	828.83	0.088	0.0065	0.08824	265.78
9/18/94	831.12	831.99	830.66	831.56	0.1432	-0.022	0.14484	98.64
9/21/94	829.82	829.87	829.58	829.69	0.0168	-0.009	0.01918	118.84
10/11/94	829.31	829.05	828.51	829.18	0.1072	0.0065	0.1074	266.53
10/14/94	829.06	828.5	828.17	828.78	0.0976	0.014	0.0986	261.84
10/18/94	828.69	827.79	827.79	828.24	0.072	0.0225	0.07543	252.65
10/21/94	828.82	828.44	827.98	828.63	0.104	0.0095	0.10443	264.78
10/25/94	828.7	827.74	827.83	828.22	0.0624	0.024	0.06686	248.96
11/1/94	828.24	827.44	827.36	827.84	0.0768	0.02	0.07936	255.40
11/4/94	830.96	827.56	828.6	829.26	0.1056	0.085	0.13556	231.17
11/8/94	828.07	827.33	827.3	827.70	0.064	0.0185	0.06662	253.88
11/11/94	829.14	829.26	828.47	829.20	0.1168	-0.003	0.11684	91.47
11/22/94	827.99	827.15	827.14	827.57	0.0688	0.021	0.07193	253.03
11/25/94	827.9	827.1	827.09	827.50	0.0656	0.02	0.06858	253.04
11/29/94	831.78	831.94	830.82	831.86	0.1664	-0.004	0.16645	91.38
12/2/94	831.13	830.16	830.07	830.65	0.092	0.0243	0.09514	255.23
12/13/94	833.11	832.75	832.22	832.93	0.1136	0.009	0.11396	265.47
12/16/94	832.62	831.74	831.72	832.18	0.0736	0.022	0.07682	253.36
12/20/94	832.41	831.48	831.52	831.95	0.068	0.0233	0.07186	251.12
1/3/95	831.45	829.95	830.51	830.70	0.0304	0.0375	0.04827	219.03
1/10/95	834.04	833.62	833.09	833.83	0.1184	0.0105	0.11886	264.93
1/13/95	835.11	834.74	834.06	834.93	0.1384	0.0093	0.13871	266.18
1/17/95	837.63	836.75	836.16	837.19	0.1648	0.022	0.16626	262.40
1/31/95	836.86	835.62	835.43	836.24	0.1296	0.031	0.13326	256.55
2/3/95	836.1	834.82	834.79	835.46	0.1072	0.032	0.11187	253.38
2/7/95	835.57	834.4	834.37	834.99	0.0984	0.0293	0.10266	253.45
2/10/95	835.16	833.99	834.07	834.58	0.0808	0.0292	0.08593	250.10
2/14/95	834.47	833.41	833.5	833.94	0.0704	0.0265	0.07522	249.37
2/17/95	837.96	837.46	836.52	837.71	0.1904	0.0125	0.19081	266.24

Appendix C: Flow direction calculations (con't)

Date	GW457	GW459	GW461	X	Rx*8	Ry	R	theta
2/21/95	836.59	835.33	835.24	835.96	0.1152	0.0315	0.11943	254.71
2/24/95	835.67	834.48	834.48	835.08	0.0952	0.0297	0.09974	252.65
2/28/95	836	835.73	834.89	835.87	0.156	0.0067	0.15615	267.52
3/3/95	835.93	834.89	834.75	835.41	0.1056	0.026	0.10875	256.17
3/7/95	836.55	835.65	835.32	836.10	0.1248	0.0225	0.12681	259.78
3/10/95	837.87	836.73	836.48	837.30	0.1312	0.0285	0.13426	257.74
3/13/95	836.66	835.38	835.45	836.02	0.0912	0.032	0.09665	250.67
3/16/95	835.85	834.69	834.83	835.27	0.0704	0.029	0.07614	247.61
3/21/95	835.98	835.62	835.02	835.80	0.1248	0.009	0.12512	265.88
3/31/95	834.37	833.44	833.6	833.91	0.0488	0.0233	0.05406	244.53
4/6/95	835.82	833.7	830.14	834.76	0.7392	0.053	0.7411	265.90
4/18/95	833.07	832	832.3	832.54	0.0376	0.0267	0.04614	234.57
4/21/95	833.77	833.81	833.06	833.79	0.1168	-1E-03	0.1168	90.49
4/24/95	833.97	833.34	833.15	833.66	0.0808	0.0158	0.08232	258.97
5/1/95	833.25	832.16	832.35	832.71	0.0568	0.0273	0.063	244.37
5/5/95	833.98	833.19	833.13	833.59	0.0728	0.0197	0.07543	254.82
5/8/95	833.48	832.48	832.64	832.98	0.0544	0.025	0.05987	245.32
5/17/95	835.6	834.57	834.56	835.09	0.084	0.0257	0.08786	252.96
-								
average	832.829	831.989	831.841	832.41	0.0909	0.021	0.0933	256.99
avg 4/15-6/10/94	834.77	833.373	833.765	834.07	0.04905	0.0349	0.06022	234.54
avg 6/15-9/9/94	830.6	830.159	829.879	830.38	0.08	0.011	0.08075	262.16
avg 9/9-11/25/94	829.119	828.541	828.296	828.83	0.08537	0.0144	0.08658	260.41
avg 11/29/94-3/13/95	834.632	833.761	833.505	834.20	0.11073	0.0218	0.11285	258.87
avg 3/16-5/17/95	834.564	833.619	833.243	834.09	0.13578	0.0236	0.13782	260.13

		DEEP WELLS						
Date	GW456	GW458	GW460	X	Rx*8	Ry	R	theta
3/31/94	841.19	838.68	839.73	839.94	0.0328	0.0628	0.0708	207.60
4/3/94	840.85	838.3	839.4	839.58	0.028	0.0637	0.0696	203.71
4/8/94	840.2	837.45	838.65	838.83	0.028	0.0688	0.0742	202.16
4/9/94	840.94	838.3	840.4	839.62	-0.1248	0.066	0.1412	117.87
4/11/94	840.55	837.82	838.99	839.19	0.0312	0.0683	0.075	204.57
4/13/94	841.44	839.06	840.07	840.25	0.0288	0.0595	0.0661	205.83
4/15/94	841.85	839.46	840.34	840.66	0.0504	0.0598	0.0782	220.15
4/18/94	841.06	838.42	839.37	839.74	0.0592	0.066	0.0887	221.89
4/20/94	841.03	838.43	839.32	839.73	0.0656	0.065	0.0923	225.26
4/22/94	840.16	837.58	838.5	838.87	0.0592	0.0645	0.0875	222.55
4/25/94	839.45	836.92	837.88	838.19	0.0488	0.0633	0.0799	217.65
4/27/94	838.45	835.99	836.99	837.22	0.0368	0.0615	0.0717	210.90
4/29/94	837.84	835.43	837.11	836.64	-0.076	0.0603	0.097	128.41
5/4/94	837.66	835.25	836.28	836.46	0.028	0.0603	0.0664	204.93
5/10/94	837.24	834.87	835.98	836.06	0.012	0.0592	0.0605	191.45
5/13/94	836.55	834.11	835.3	835.33	0.0048	0.061	0.0612	184.50
5/17/94	836.13	833.67	834.86	834.90	0.0064	0.0615	0.0618	185.94
5/20/94	835.75	833.34	834.54	834.55	0.0008	0.0602	0.0603	180.76
5/23/94	835.4	832.99	834.14	834.20	0.0088	0.0603	0.0609	188.31
5/27/94	834.8	832.4	833.52	833.60	0.0128	0.06	0.0614	192.04
5/31/94	834.52	832.29	833.28	833.41	0.02	0.0558	0.0592	199.74
6/2/94	834.24	831.95	833.08	833.10	0.0024	0.0572	0.0573	182.40
6/6/94	834.04	831.69	832.82	832.87	0.0072	0.0587	0.0592	186.99
6/8/94	833.74	831.14	832.52	832.44	-0.0128	0.065	0.0662	168.86
6/15/94	833.58	831.18	832.5	832.38	-0.0192	0.06	0.063	162.26
6/17/94	833.71	831.43	832.65	832.57	-0.0128	0.057	0.0584	167.34
6/20/94	833.64	831.3	832.53	832.47	-0.0096	0.0585	0.0593	170.68
6/22/94	833.4	830.98	832.26	832.19	-0.0112	0.0605	0.0615	169.51
6/24/94	833.25	830.82	832.1	832.04	-0.0104	0.0607	0.0616	170.29
6/27/94	833.22	830.76	832.02	831.99	-0.0048	0.0615	0.0617	175.54
6/29/94	833.98	832.1	833.28	833.04	-0.0384	0.047	0.0607	140.75
7/1/94	834.54	832.46	833.62	833.50	-0.0192	0.052	0.0554	159.73
7/4/94	834.12	831.44	832.66	832.78	0.0192	0.067	0.0697	195.99
7/6/94	833.6	830.66	831.96	832.13	0.0272	0.0735	0.0784	200.31
7/8/94	833.32	830.31	831.66	831.82	0.0248	0.0752	0.0792	198.24
7/11/94	833.06	830.25	831.48	831.66	0.028	0.0702	0.0756	201.73
7/13/94	832.84	830.08	831.26	831.46	0.032	0.069	0.0761	204.88
7/15/94	832.82	829.82	831.18	831.32	0.0224	0.075	0.0783	196.63
7/18/94	832.8	829.96	831.34	831.38	0.0064	0.071	0.0713	185.15
7/20/94	833.78	831.5	832.72	832.64	-0.0128	0.057	0.0584	167.34
7/22/94	833.6	830.9	832.24	832.25	0.0016	0.0675	0.0675	181.36
7/25/94	833.46	830.5	831.96	831.98	0.0032	0.074	0.0741	182.48
7/27/94	833.08	829.95	831.48	831.52	0.0056	0.0782	0.0785	184.09

Appendix C: Flow direction calculations (con't)

Date	GW456	GW458	GW460	X	Rx*8	Ry	R	theta
7/29/94	833	830.04	831.42	831.52	0.016	0.074	0.0757	192.20
8/1/94	833.52	831.1	832.4	832.31	-0.0144	0.0605	0.0622	166.61
8/3/94	833.24	830.32	831.78	831.78	0	0.073	0.073	180.00
8/5/94	832.98	829.88	831.4	831.43	0.0048	0.0775	0.0776	183.54
8/8/94	833	829.98	831.4	831.49	0.0144	0.0755	0.0769	190.80
8/10/94	832.99	829.96	831.45	831.48	0.004	0.0757	0.0759	183.02
8/12/94	832.76	829.57	831.14	831.17	0.004	0.0798	0.0799	182.87
8/15/94	832.52	829.32	830.87	830.92	0.008	0.08	0.0804	185.71
8/17/94	832.68	830.26	831.42	831.47	0.008	0.0605	0.061	187.53
8/19/94	833.02	830.24	831.7	831.63	-0.0112	0.0695	0.0704	170.85
8/22/94	832.78	829.71	831.28	831.25	-0.0056	0.0767	0.077	175.83
8/24/94	833.41	831.07	832.34	832.24	-0.016	0.0585	0.0606	164.70
8/26/94	833.32	830.43	831.92	831.88	-0.0072	0.0723	0.0726	174.31
8/29/94	833.74	830	831.58	831.87	0.0464	0.0935	0.1044	206.39
8/31/94	832.84	829.54	831.18	831.19	0.0016	0.0825	0.0825	181.11
9/2/94	832.58	829.25	830.81	830.92	0.0168	0.0833	0.0849	191.41
9/7/94	832.5	829.31	830.78	830.91	0.02	0.0798	0.0822	194.08
9/9/94	832.15	828.9	830.38	830.53	0.0232	0.0813	0.0845	195.94
9/18/94	831.98	828.78	830.2	830.38	0.0288	0.08	0.085	199.80
9/21/94	832.66	830.89	831.75	831.78	0.004	0.0442	0.0444	185.17
10/11/94	832.9	829.93	831.39	831.42	0.004	0.0743	0.0744	183.08
10/14/94	831.91	829.3	830.61	830.61	-0.0008	0.0652	0.0653	179.30
10/18/94	831.88	829.04	830.45	830.46	0.0016	0.071	0.071	181.29
10/21/94	831.61	828.66	830.1	830.14	0.0056	0.0738	0.074	184.34
10/25/94	831.69	828.82	830.51	830.26	-0.0408	0.0717	0.0825	150.38
11/1/94	831.58	828.67	830.33	830.13	-0.0328	0.0728	0.0798	155.73
11/4/94	831.27	828.22	829.94	829.75	-0.0312	0.0762	0.0824	157.75
11/8/94	831.37	831.4	830.18	831.39	0.1928	-7E-04	0.1928	90.22
11/11/94	831	828.04	829.69	829.52	-0.0272	0.074	0.0788	159.82
11/22/94	831.38	829.19	830.33	830.29	-0.0072	0.0547	0.0552	172.51
11/25/94	831.04	828.04	829.74	829.54	-0.032	0.075	0.0815	156.89
11/29/94	830.94	827.93	829.62	829.44	-0.0296	0.0753	0.0809	158.53
12/2/94	833.12	831.72	832.45	832.42	-0.0048	0.035	0.0353	172.19
12/13/94	833.51	831.08	832.17	832.30	0.02	0.0607	0.064	198.22
12/16/94	835.69	833.06	834.52	834.38	-0.0232	0.0658	0.0697	160.56
12/20/94	835.45	832.58	834.13	834.02	-0.0184	0.0717	0.0741	165.62
1/3/95	835.26	832.35	833.95	833.81	-0.0232	0.0727	0.0764	162.31
1/10/95	834.47	831.46	833.13	832.97	-0.0264	0.0752	0.0797	160.67
1/13/95	837.04	833.94	835.64	835.49	-0.024	0.0775	0.0811	162.79
1/17/95	838.13	834.93	836.77	836.53	-0.0384	0.08	0.0887	154.36
1/31/95	838.55	834.9	836.83	836.73	-0.0168	0.0913	0.0928	169.57
2/3/95	839.92	836.51	838.36	838.22	-0.0232	0.0853	0.0884	164.78
2/7/95	838.37	835.83	837.79	837.10	-0.1104	0.0635	0.1274	119.91
2/10/95	838.82	835.38	837.38	837.10	-0.0448	0.086	0.097	152.48
2/14/95	838.43	835.01	836.87	836.72	-0.024	0.0855	0.0888	164.32
2/17/95	837.7	834.38	836.18	836.04	-0.0224	0.083	0.086	164.90

Appendix C: Flow direction calculations (con't)

Date	GW456	GW458	GW460	X	Rx*8	Ry	R	theta
2/21/95	840.48	837.47	839.08	838.98	-0.0168	0.0752	0.0771	167.41
2/24/95	839.78	836.24	838.15	838.01	-0.0224	0.0885	0.0913	165.80
2/28/95	838.89	835.43	837.3	837.16	-0.0224	0.0865	0.0894	165.48
3/3/95	838.82	835.68	837.48	837.25	-0.0368	0.0785	0.0867	154.88
3/7/95	839	835.62	837.46	837.31	-0.024	0.0845	0.0878	164.14
3/10/95	839.55	837.22	838.03	838.39	0.0568	0.0582	0.0814	224.28
3/13/95	840.53	837.33	838.95	838.93	-0.0032	0.08	0.0801	177.71
3/16/95	839.71	836.33	838.03	838.02	-0.0016	0.0845	0.0845	178.92
3/21/95	838.86	835.63	837.3	837.25	-0.0088	0.0808	0.0812	173.78
3/31/95	839.56	835.7	837.25	837.63	0.0608	0.0965	0.1141	212.21
4/6/95	837.22	834.3	835.8	835.76	-0.0064	0.073	0.0733	174.99
4/18/95	837.87	836.54	831.13	837.21	0.972	0.0333	0.9726	268.04
4/21/95	835.68	833	834.42	834.34	-0.0128	0.067	0.0682	169.18
4/24/95	836.01	833.62	834.9	834.82	-0.0136	0.0597	0.0613	167.18
5/1/95	836.47	833.88	835.26	835.18	-0.0136	0.0648	0.0662	168.14
5/5/95	835.77	833.07	834.47	834.42	-0.008	0.0675	0.068	173.24
5/8/95	836.62	833.85	835.3	835.24	-0.0104	0.0692	0.07	171.46
5/17/95	836.28	833.37	834.87	834.83	-0.0072	0.0727	0.0731	174.35
average	835.408	832.665	833.976	834.04	0.00972	0.0686	0.0693	188.07
avg 4/15-6/10/94	837.439	834.999	836.1	836.22	0.01912	0.061	0.0639	197.40
avg 6/15-9/9/94	833.241	830.455	831.827	831.85	0.00338	0.0697	0.0697	182.78
avg 9/9-11/25/94	831.849	829.225	830.474	830.54	0.01	0.0656	0.0663	188.67
avg 11/29/94-3/13/95	836.953	833.944	835.592	835.45	-0.0231	0.0752	0.0787	162.96
avg 3/16-5/17/95	837.664	834.841	835.71	836.25	0.08676	0.0706	0.1118	230.88

Appendix D: Helium Data														
			Area Counts								C/Co			
DATE	456	457	458	459	460	461	462	Ave C0	456	457	458	459	460	461
25-Mar							20900	20900						
3-Apr	0	0	1.6	0	8.3	0	59052	39976	0	0	0	0	0	0
5-Apr	6.4	0	0	0	0	0	63071	47674	1E-04	0	0	0	0	0
8-Apr	0	33	0	0	0	0	87593	57654	0	6E-04	0	0	0	0
11-Apr	0	0	0	0	0	0		57654	0	0	0	0	0	0
13-Apr	0	9.5	46.8	0	6.1	5.1	117217	69567	0	1E-04	0	0	0	0
15-Apr	0	0	12.2	0	0	4	114811	77107	0	0	0	0	0	0
18-Apr	1	0	0	0	0	0	156182	88404	1E-05	0	0	0	0	0
20-Apr	0	0		0	0	0	74580	86676	0	0		0	0	0
22-Apr	0	0	7.8	0	0	0	140234	92627	0	0	0	0	0	0
25-Apr	0		8.5	0	0	0	132772	96641	0		0	0	0	0
27-Apr	9.4	36.9	0	0	0	0	120108	98775	1E-04	4E-04	0	0	0	0
29-Apr	0	11.7	0	0	0	0		98775	0	1E-04	0	0	0	0
4-May	0	0	0	0	0	10.5	82740	97438	0	0	0	0	0	0
10-May	0	0	0	0	0	0	109407	98359	0	0	0	0	0	0
13-May	0	8.6	0	0	0	0	87989	97618	0	9E-05	0	0	0	0
17-May	0	0	0	0	7.3	4.7	35490	93476	0	0	0	0	0	0
20-May	4.2	0	0	0	15.4	116		93476	4E-05	0	0	0	0	0
23-May	0	0	0	0	10.8	16.3		93476	0	0	0	0	0	0
27-May	0	7.9	0	0	0	230	49642	90737	0	9E-05	0	0	0	0
31-May	0		0	0		367		90737	0		0	0		0
2-Jun	0	0	0	0	35.9	371	36085	87522	0	0	0	0	0	0
6-Jun	0	0	0	0	33.3		36714	84699	0	0	0	0	0	
8-Jun		0	0	0	22.9	169	71908	84026		0	0	0	0	0
10-Jun	0	0	0	7.2	41.4		143926	87021	0	0	0	0	0	
13-Jun			0	0	0	420	40403	84801			0	0	0	0
15-Jun	36	0	0	0	0	751	69579	84109	4E-04	0	0	0	0	0.01
17-Jun	28	0	0	0		634		84109	3E-04	0	0	0		0.01
20-Jun	27	0	0	0	0	843	39041	82150	3E-04	0	0	0	0	0.01
22-Jun	9.8	0	0	0	112	574	117819	83636	1E-04	0	0	0	0	0.01
24-Jun	9	0	0	0	0	0	7980	80610	1E-04	0	0	0	0	
27-Jun		0	0	0	79	754	141912	82968		0	0	0	0	0.01
4-Jul	8	20	0	10	155		121444	84393	9E-05	2E-04	0	0	0	
6-Jul	10	8	0	0	42			84393	1E-04	9E-05	0	0	0	
8-Jul	9	27	0	0	66	836	102148	85027	1E-04	3E-04	0	0	0	0.01
11-Jul	0	8	0	0	70	259	120800	86260	0	9E-05	0	0	0	0
13-Jul		0	0	0	121	415	34401	84532		0	0	0	0	0
15-Jul	0		0		204	1300	140253	86329	0		0		0	0.02
18-Jul	0	7	0	0		1348	130286	87703	0	8E-05	0	0		0.02
20-Jul	0	0	0	0	196	978	2705	85127	0	0	0	0	0	0.01
22-Jul	0	0	0	0	154	749	21929	83268	0	0	0	0	0	0.01
25-Jul	0	0	0	0	200	1431	72014	82947	0	0	0	0	0	0.02
27-Jul	0	0	0	0	199	868		82947	0	0	0	0	0	0.01
29-Jul	0	6	0	0			107938	83641	0	7E-05	0	0	0	0
1-Aug	0	0	0	0		1560		83641	0	0	0	0	0	0.02
3-Aug	0		0	0	213	1389	56576	82909	0	0	0	0	0	0.02
5-Aug	0	5.9	0	0	484		36503	81688	0	7E-05	0	0	0.01	0
8-Aug	0	0	0	0		1540	56647	81046	0	0	0	0	0	0.02
10-Aug	0	0	0	0	367	1483	61007	80545	0	0	0	0	0	0.02
12-Aug	0	0	0	0	259	304		80545	0	0	0	0	0	0
15-Aug	0	7.1	0	0	264	3571	215228	83830	0	8E-05	0	0	0	0.04
17-Aug	0	8.5	0	0	278	1750	221968	87119	0	1E-04	0	0	0	0.02
19-Aug	0	0			276	2016	193146	89585	0	0	0	0	0	0.02
22-Aug	0	0	0	0	281	2237		89585	0	0	0	0	0	0.02

Appendix E: Bromide Source Concentration				
date	time (day)	C (ppm)	C/C0	-ln(C/C0)
11-Apr-94	0	15200	1.00E+00	0.000
13-Apr-94	2	550	3.62E-02	3.319
15-Apr-94	4	115	7.57E-03	4.884
18-Apr-94	7	37.7	2.48E-03	5.999
20-Apr-94	9	28.1	1.85E-03	6.293
22-Apr-94	11	23.2	1.53E-03	6.485
25-Apr-94	14	17.8	1.17E-03	6.750
27-Apr-94	16	16.5	1.09E-03	6.826
29-Apr-94	18	10.6	6.97E-04	7.268
4-May-94	23	5.23	3.44E-04	7.975
10-May-94	29	8.03	5.28E-04	7.546
17-May-94	36	5.89	3.88E-04	7.856
20-May-94	39	6.59	4.34E-04	7.743
31-May-94	40	4.39	2.89E-04	8.150
2-Jun-94	42	3.9	2.57E-04	8.268
6-Jun-94	46	5.14	3.38E-04	7.992
15-Jun-94	55	3.85	2.53E-04	8.281
17-Jun-94	57	5.63	3.70E-04	7.901
20-Jun-94	60	4.18	2.75E-04	8.199
22-Jun-94	62	4.83	3.22E-04	8.041
24-Jun-94	64	7.11	4.74E-04	7.654
27-Jun-94	67	6.13	4.09E-04	7.803
1-Jul-94	71	3.61	2.41E-04	8.332
12-Jul-94	82	3.13	2.09E-04	8.475
15-Jul-94	85	3.22	2.15E-04	8.446
18-Jul-94	88	1.94	1.29E-04	8.953
21-Jul-94	91	9.68	6.45E-04	7.346
25-Jul-94	95	4.09	2.73E-04	8.207
27-Jul-94	97	4.55	3.03E-04	8.101
29-Jul-94	99	3.29	2.19E-04	8.425
1-Aug-94	102	2.23	1.49E-04	8.814
3-Aug-94	104	3.4	2.27E-04	8.392
9-Aug-94	110	2.32	1.55E-04	8.774
11-Aug-94	112	2.19	1.46E-04	8.832
15-Aug-94	116	1.7	1.13E-04	9.085
17-Aug-94	118	1.91	1.27E-04	8.969
19-Aug-94	120	2.34	1.56E-04	8.766
23-Aug-94	124	0.819	5.46E-05	9.815

Appendix F: Core logs

Core log for GW821

Interval: 0-5'	Length: 2.6'	Estimated interval: 2.4-5'

Top 0.3': dark brown, organic soil, twigs.
Rest: Dark yellowish orange (10YR6/6) to moderate yellowish brown (10YR4/2), dry, crumbly, weathered silty clay/sand. Saprolite-shale structures apparent.

Interval: 5-10' (pushed w/H20)	Length: 2.9'	Estimated interval: 7.1-10'

Same color as above, clay-rich silty sand, some weathered pebbles, STAINED, moist.

Interval: 10-15'	Length: 3'	Estimated interval: 12-15'

Same as above, but darker brown at bottom of interval, very rubbly. Dry and crumbly. Heavily STAINED. Lighter tan when cut.

Interval: 15-17'	Length: 1.2'	Estimated interval: 15.8-17'

Lost top half of core.
16-17': dusky yellow (5Y6/4) to light olive brown (5Y6/6) silty sand. Very WEATHERED but no staining apparent. Shaly bedding. Dry.

Interval: 17-18'	Length: 1'	Estimated interval: 17-18'

Light olive brown (5Y5/6) silty sand matrix, dry and crumbly, with dark grey (N3) weathered shale fragments. Some Fe stained fragments at ~17.5'. Mn-oxide coatings observed. FE STAINED and WEATHERED observed throughout entire interval. Difficult to see because fragments covered in soil.

**********WATER AT 18'**********

Interval: 18-20.5'	Length: 2.5'	Estimated interval: 18-20.5'

18-19.5': Dark brown silt, WET, with fragments of heavily Fe-stained shale.
*19': Larger pieces of rock, HEAVILY FE STAINED
19.5-20.5': Dark grey (N3), busted up shale, very dry, some indurated pieces, some weathered. No significant Fe staining.

Interval: 20.5-22'	Length: 2.5	Estimated interval: 20.5-22'

Top 1' (slough): brown silt-clay, moist, covering weathered shale fragments.
20.5-22': Dark grey (N3) fine-grained shale, dry, very powdery. Some larger pieces. No significant Fe staining, except for shale piece at 22' which has FE STAINING and green alterations.

Interval: 22-23'	Length: 13"	Estimated interval: 22-23'

22-22.7': Brown, clay-covered weathered shale. Soft but retains shaly structure. Calcite veins observed, some in-situ weathering, heavily FE STAINED weathering rinds on fragments. One competent piece at 22', rest of interval is very clay-rich and soft. Clay is moist.
22.7-23': Grey, extremely weathered shale. No competent pieces, very crumbly, dry.

Interval: 23-25'	Length: 2'	Estimated interval: 23-25'

23-24': Dark grey (N3) fine-grained shale, very busted up, dry. Mostly small fragments, a few larger pieces.
*24': FE STAINED shale; green alterations observed in this zone.
24-25': Lighter grey powder on shale fragments. FE STAINING observed on many of the fragments. Most fragments less than 2" in length. A few larger pieces, one with significant FE STAINING..

**********WET DRILLING BEGINS AT 25'**********

Interval: 25-30'	Length: ~3'	Estimated interval: 27-30'

Top 1": FE STAINED calcite/shale. Green alteration product on shale.
27--27.5': oolite with some BLACK STAINING. Minor Fe staining on top.
27.5-28.7': Dark grey (N3) shale, mostly small fragments, very blocky. Minor calcite veining. No Fe staining.
28.7-30': Clay-rich dark grey shale, no fragments. Looks like weathered in situ. Extremely soft and crumbly.

Interval: 30-35'	Length: 2.8'	Estimated interval: 32.2-35'

32.2-32.7': Dark grey (N3) shale, many Fe stained fragments, some associated with calcite vein. Small to medium size fragments.
32.7-34.2': Dark grey weathered shale with MAJOR FE STAINING, very tiny fragments of shale.

Appendix F: Core logs (con't)

34.2-35': oolite with calcite veins. Large (2" length) core pieces. Upper few inches are weathered.

Interval: 35-40'	Length: ~3.5'	Estimated interval: 36.5-40'

36.5-37.5': oolite, large pieces (3" long core) with cross-cutting calcite veins.
*37-37.5': SIGNIFICANT FE STAINING ALONG SIDES OF OOLITE -VERTICAL FRACTURE.
37.5-38': Dark grey (N3) shale, SIGNIF. FE STAINING MANY PIECES - likely part of same fracture.
38-38.5': Dark grey clay-rich shale, in-situ weathering, soft. Some larger shale pieces in clay.
38.5-40': crumbly, dark grey weathered and fissile shale. In-situ calcite vein weathering. Some small fragments.
40': 3" core of dark grey shale, FE STAINED on one face.

Interval: 40-45'	Length: 3.2'	Estimated interval: 41.8'-45'

41.8-42.5': Brownish grey (5YR4/1) shale, some heavily STAINED Fe CALCITE vein pieces in shale. One larger (2" or so) piece, rest small fragments. Fragment of oolite but don't know placement.
42.5-42.7': Larger pieces of dark greenish grey shale, calcite growth along sides.
42.7-43.2': Clay-rich weathered, dark greenish grey shale. Very soft, some larger fragments but they break/crumble when handled.
43.2-45': Dark grey crumbly clay/shale. Calcite vein weathered in site. No larger pieces.

Interval: 45-48'	Length: 2.7'	Estimated interval: 45.3-48'

45.3-46': oolite with green alteration product (glauconite??) on surface. Some thin, white, cross-cutting calcite veins. Some larger core pieces.
46-46.2': Dark greenish grey fine-grained shale, thin pieces. No Fe staining.
46.2-46.4': Dark grey clay-rich fissile shale, thin shaly bedding.
46.4-47.4': Dark greenish grey clay-rich shale, larger pieces than above.
47.4-50': Dark grey fissile shale, no pieces.

Interval: 48-50'	Length: 18"	Estimated interval: ??

**Slough discarded
~1.5' of small to medium size fragments of mostly dark grey (N3) fine-grained shale. Some pieces of dark greenish grey (5G4/1) shale in top 6". Small pieces of calcite vein in top 6", slight Fe staining but hard to tell placement. Calcite growth along shale facies elongated. Some red mineral grains (hematite??) and black minerals grains(Mn oxide??) observed.
Bottom piece: shale/carbonate interlayered, few " thick, 3" long.

Appendix F: Core logs (con't)

Core log for GW822

Interval: 0-3'	Length: 3'	Estimated interval: 0-3'

0-0.5': Dark brown soil with organic matter, leaves, and twigs.
0.5-3': Dark yellowish orange (10YR6/6) to light brown (5YR6/6) silty sand, dry, crumbly, weathered saprolite, shaly bedding and clay structure preserved. Very weathered, strong reddish color.

Interval: 3-5'	Length: 2'	Estimated interval: 3-5'

3-4': dark organic and stained silt, some leaves, twigs, heavy staining of rock fragments.
4-5': 4 pieces of saprolite core, heavy staining within saprolite.

Interval: 5-7'	Length: 2.25'	Estimated interval: ~5-7'

Same as above; heavily stained silt, clay, fine sand/ saprolite.
5-6': crumbly
6-7': cohesive cores, with heavy staining on surfaces and on inside.

Interval: 7-9'	Length: 1.7'	Estimated interval: 7.3-9'

7.3-8.6': crumbly, heavily stained and weathered shale, all competent rock fragments are carbonate. wavy shaly bedding preserved.
8.6-9': greenish gray shale/saprolite core, interlayed with dark brown silt/clay

Interval: 9-11'	Length: ~34"	Estimated interval: 9-11'

9-10': dark yellowish orange (10YR6/6) to moderate yellowish brown (10YR5/4) silt and clay, dry and crumbly, no rock fragments, VERY HEAVY STAINING AT ~9'.
10-11': larger cores of saprolite, same color as above.
* heavy staining throughout this interval

Interval: 11-13'	Length: 28"	Estimated interval: 11-13'

Top 4": brown soil rubble (slough)
11-13': same color as above, very weathered saprolite, significant Fe staining and weathering throughout. Core pieces are 3-4" in length. Hard to distinguish specific flow zones but most heavily stained at ~11.5'. Slightly moist and crumbly.

Appendix F: Core logs (con't)

Interval: 13-14'	Length: 2'	Estimated interval: 13-14'

Top 1.3': silty sand, same color as above, moist and crumbly with blocky fragments of stained shale.
Bottom 0.7': saprolite core, less orange tint, more olive color than above, significant Fe staining throughout.

Interval: 14-15'	Length: 1'	Estimated interval: 14-15'

14-14.5': shale/saprolite moderate to dark yellowish brown with olive tint, similar to 17-19' saprolite, slightly moist, crumbly. Heavily stained surfaces on greenish-gray shale.
14.5-15': more competent saprolite core.

Interval: 15-16'	Length: ~2'	Estimated interval: 15-16'

15-15.5': grayish orange powder covering medium to large size shale pieces with HEAVY FE STAINING. Significant staining on shale surfaces throughout interval. DRY!!
15.5-16': very pale orange powder (lighter than above), appears to be same rock type as above.

Interval: 16-17'	Length: 13"	Estimated interval: 16-17'

16-16.3': dark brown silty clay
16.3-16.4': grey silt layer, small twigs
16.4-16.8': moderate yellowish brown (10YR5/4) silty sand, some clay, moderate staining on oolite piece at 16.8', many small twigs.
16.8-17': moderate yellowish brown to light olive gray (5Y5/2), piece of heavily stained oolite at 17'.

Interval: 17-19'	Length: 2'	Estimated interval: 17-19'

WET!!!
17-18.3': very wet brown silt/clay/fine sand, very mushy, with disks of carbonate. Carbonate surfaces NOT stained.
18.3-19': very weathered/stained greenish gray shale/saprolite. moist, not as wet as above. HEAVY Fe staining along horizontal places at 18.5'
18.5-20': weathered but NO significant staining.

Interval: 19-21'	Length: 2.5'	Estimated interval: 19-21'

WET!!!!!!!!
19-20.5': greenish gray shale fragments, some heavily dark oxide stained, in

moderate yellowish brown silty clay matrix. Most shale very soft, few more indurated pieces. MAJOR FLOW ZONE.
20.5-21': same as above but more orange staining.

Interval: 21-22	Length: 1'	Estimated interval: 21-22'

21-21.3': brown silty clay with large, dark grey piece of carbonate.
21.3-21.5': large dark grey carbonate piece.
21.5-22': moderate olive brown (5Y4/4) saprolite, same as below, moist clay, shale fragments have heavy dark oxide staining. mostly clay, less fragments than above.

Interval: 22-23'	Length: 18"	Estimated interval: ~22-23'

Top 4": dark brown silty clay with shale fragments (slough)
22-23': same color as below but more moist, very crumbly, weathered saprolite, staining within saprolite cores and pieces. Some greenish gray shale fragments, most HEAVILY STAINED with dark oxide.

Interval: 23-24'	Length: 18"	Estimated interval: 23-24'

DRY!!!
Top 6": brown silty clay (slough)
23-23.25': moderate to light olive brown weathered saprolite, no shale.
23.25-23.75': same as above but shale fragments present, silty clay, very crumbly , shale indurated but very fragmented. greenish grey shale. small-medium size fragments. moderate dark oxide staining on some shale fragments. can't tell if/where fracture zone occurs.
23.75-24': same as above but no shale.

Interval: 24-27'	Length: ~2'	Estimated interval: 25-27'

EXTREMELY WET!!!!!!
25-26': moderate yellowish brown (10YR5/4) to dark yellowish brown (10YR4/2) silty sand to silty clay with small shale fragments. Shale fragments are HEAVILY STAINED with Fe and Mn oxides. Appears to be MAJOR FLOW ZONE!!!!
26--26.5': Light olive gray (5Y5/2) silty clay with greenish gray shale fragments. WET. Shale fragments are HEAVILY STAINED with Fe and Mn oxides.
26.5-27': same as top interval.

Interval: 27-31'	Length: 3'	Estimated interval: 28-31'

28-29.5': Dark yellowish brown (10 YR 4/2) to dusky brown (5YR2/2) silty clay, WET, top few inches has few fragments of shale.

~28.5' and 29: dark yellowish orange (10YR6/6) clay layers, very fine-grained, WET, sandwiched between thin, black, coarser-grained layers.
~29': darker, coarser-grained layer, inches thick, some orange discoloration.
29-29.5': dark yellowish brown (10YR4/2), same as top interval, with fragments of shale which have significant STAINING.
29.5-31': Light olive gray (5Y5/2) saprolite disks, clay-rich weathered shale. shaly bedding. fragments of greenish gray shale within clay have dark STAINING. DRY and crumbly; minor Fe staining on surfaces of disks.

**********BEDROCK AT 31' (?)**********

Interval: 31-32'	Length: 14"	Estimated interval: 31-32'

31-32': Dark grey (N3) weathered shale and clay. Shale in fragments, a few larger pieces at bottom of core. Clay very crumbly, moist. Shale appears to be weathered in-situ to clay; clay retains shaly bedding characteristics. Some thin brown silty clay interlayers at ~31.2' and ~31.4'.
* Moderate to heavy Fe staining on shale/clay at ~31'

Interval: 32-33'	Length: 1'	Estimated interval: 32-33'

Dark brown clay at top and covering sides of top portion of core.
32-33': dark grey (N3) shale and clay. Clay is crumbly but very cohesive. Some yellow and brown alteration within clay (weathering products?) but small-scale. Three disks of shale present, very indurated, no Fe staining observed. A few smaller shale fragments. Does not appear to be significant flow zone.

**********BEGIN DRILLING WITH WATER AT 33 FEET**********

Interval: 33-35'	Length': 2'	Estimated interval: 33-35'

33-33.75': Dark to medium grey shale with reddish carbonate interlayers, some internal deformation observed. Large pink calcite vein with large crystals, elongated. Slight Fe staining at bottom of this zone. Medium size (<2" long) fragments.
33.75-34.25': clay-rich weathered shale, soft, fissile. Reddish brown interlayers. Some shale fragments in clay.
34.25': calcite vein/carbonate layer, competent.
34.25-35': clay-rich weathered shale, same as above. Solid pieces are predominantly carbonate. Carbonate fragments at bottom.
No significant Fe staining in this interval.

Interval: 35-40'	Length: 3.25'	Estimated interval: 36.75-40'

*Slough discarded
36.75-38.25': Dark grey shale with lighter reddish grey carbonate intervals (brownish grey 5YR4/1). Large pink calcite vein, slightly Fe stained at top. Thinner white calcite cross cutting veins, many perpendicular to bedding. Nice laminations on some pieces. Some larger (few" length) pieces.
Carbonate layer (not sure about placement), with coarse-grained Mn oxide coating. Elongated crystals, intraclasts.
38.25-39.25': pulverized shale, some larger pieces retrieved, rest (slough) discarded.
39.25': oolite
39.25-40': clay-rich fissile shale and shale pieces. Very weathered, fissile, soft. Looks natural.
40': Oolite
No Fe staining observed in this interval

Interval: 40-45'	Length: 3.25'	Estimated interval: 42-45'

42-43.50': Dark grey (N3) shale with brownish grey (5YR4/1) carbonate intervals. Horizontal bedding visible in shale and carbonate. Carbonate intervals up to 1" thick. oolite layer at ~42.25', coarse-grained. Thin white calcite veins, both cross-cutting and bed parallel. Some larger pieces. No Fe staining. Pieces seem to break along shale, not along carbonate.
43.5-43.75': fissile shale, mostly tiny pieces.
43.75': few inches of dusky yellowish brown (10YR2/2) shale.
43.75-44': coarse-grained brownish gray (5YR4/1) oolite, small black minerals, shale intraclasts, calcite veins. FE staining on shale (bed parallel) and on side, microfolding structures observed.
44-45': clay-rich shale, very weathered and fissile. Most incorporated in clay. Clay looks natural, clay structures observed, iron staining, in situ weathering of calcite veins. More competent pieces have carbonate layers. Moderate Fe staining, esp. in zone right below oolite. shale very fissile, clay-rich.

Interval: 45-50'	Length: 2.7'	Estimated interval: 47.3-50'

47.3-48.3': predominantly medium to dark grey (N4/N3) shale, well indurated, with light carbonate intervals. One carbonate piece has coarse-grained infilling. Cross-cutting think white calcite veins, most perpendicular to bedding, lots of shale fragments. No Fe staining.
48.3-48.6': lighter brownish grey (5YR6/1) oolite with thin calcite veins ~ 45 deg dip to vertical axis. Oxide covering on side of larger piece. FE staining with weathered pits, parallel to calcite veins.
48.6-50': clay-covered fissile shale, very soft and weathered. Medium to dark

Appendix F: Core logs (con't)

grey (N4/N3) some in situ weathering of calcite vein, some staining in clay. Clay looks natural.

Interval: 50-55'	Length: 3'	Estimated interval: 52-55'

52-54': Medium to dark grey (N4/N3) shale fragments, well indurated, most pieces 1/2" in length. Oolite with Mn oxides staining at top. some pieces of shale have structures that look like slickensides. Carbonate interlayers, some oolite pieces. Some larger shale pieces. No significant. Fe staining.
54-55': fissile, clay-rich, small shale fragments. Sign. Fe staining at 54'.

Interval: 55-60'	Length: 2.6'	Estimated interval: 57.4-60'

57.4-58.4': dark grey (N3) fine-grained shale, well indurated, with cross-cutting thin white calcite veins and few thicker pink veins. FE staining on several pieces but hard to tell placement. Calcite elongation.
58.4-59.1': fissile shale, mostly tiny pieces, brownish black (5YR2/1) with pieces of brownish grey (5YR4/1) to brownish black medium grained carbonate with some elongated crystals. Small black minerals. calcite veins, some with green alteration product.
59.1-60': dark greenish grey (4G4/1) to brownish grey/black (5YR4/1 to 5YR2/1) shale, tiny pieces. THIS INTERVAL DISCARDED.

Interval: 60-65'	Length: 2.5'	Estimated interval: 62.5-65'

62.5-64': oolite, brownish grey (5YR4/1) to medium dark grey (N4) many thin cross-cutting white calcite veins, green shale intraclast/vein, glauconite (??) on oolite surface. stylolitic piece (sampled). large core piece (6").
64-64.25': med to dark grey (N4/N3) shale, some thin carbonate intervals. pink calcite vein, looks bed parallel. Bottom piece has small black minerals (Mn ox?)
64.25-64.75': oolite, same as top interval, heavy Fe staining on small pieces. Mn oxide.
64.75-65': HEAVILY FE STAINED shale, original core clay covered. Mostly small pieces, clay discarded.

Interval: 65-70'	Length: 2.25'	Estimated interval: 67.75-70'

67.75-68': HEAVILY FE STAINED calcite veins, elongated crystal growth, in shale. some carbonate layers up to 1/4" thick. Shale fine-grained, shaly bedding but well indurated. medium to dark grey, carbonate intervals brownish grey (5YR4/1).

Appendix F: Core logs (con't)

68-69': predominantly shale with carbonate interlayers. calcite with preferred elongation on many surfaces.
69-69.5': oolite with thin white cross cutting calcite veins, black mineral on surface. shale intraclasts, iron staining along rinds. Some Fe staining along veins.
69.5-70': Very fissile shale, clay-covered, few larger pieces.

Core log for GW823

Interval: 0-3'	Length: 3'	Estimated interval: 0-3'

0-0.5': dark brown organic clay soil, twigs.
0.5-1': dark yellowish orange (10YR6/6) to moderate yellowish brown (10YR5/4) clay core.
1-3': same color as above, dry and crumbly, clay/silt/fine sand, shaly bedding/weathering structures observed.

Interval: 3-5' (pushed w/H2O)	Length: 2'	Estimated interval: 3-5'

3-4': same as above, moderate yellowish brown (10YR5/4) silty sand, crumbly, few pieces of stained shale.
4-5': same as above, but consolidated core, laminations and weathering structures observed.

Interval: 5-7'	Length: 2'	Estimated interval: 5-7'

Top 3" dark grey/black, organic smell, some twigs.
5-6': moderate yellowish brown saprolite, WET (probably from above interval pushed out with water). Heavily stained, very few small shale fragments.
6-7': dry and crumbly.

Interval: 7-9'	Length: 2'	Estimated interval: 7-9'

7-8.4': olive gray (5Y3/2) silty sand with dark red/black staining, dry, crumbly.
8.4-9': same as above but more reddish staining.

Interval: 9-11' (pushed w/H2O)	Length: 3'	Estimated interval: 9-11'

9-11': same as above but consolidated core (5 pieces), weathered, moist to wet, no competent pieces, heavily stained.

**********WATER at ~11'.5**********

Interval: 11-13'	Length: 2.5'	Estimated interval: 11?-13'

WET!!!!!
top 6": brown clay (slough)
11-11.5': dusky yellowish brown (10YR2/2) clay and shale fragments.
11.5-13': dark brown silty MUSH; WET, some staining, many shale pieces.
12': Large (4") piece of heavily STAINED shale!!

Appendix F: Core logs (con't)

Interval: 13-15'	Length: 1.7'	Estimated interval: 13.3-15'

13.3-13.8': dark brown silty MUSH, WET
13.8-14.3': grayish olive (10Y4/2) weathered shale/clay, top 13.8-13.9 WET (brown clay); rest is moist in crumbly grayish olive clay. Shale fragments stained.
14.3-15': grayish olive weathered shale core, not as heavily stained as above, moist.

Interval: 15-20'	Length: 3'	Estimated interval: 17?-20'

Top 1': dark brown WET silty mush
1-2': greenish grey shale/saprolite, fissile, moist to wet, weathered, some pieces.
2-3': MAJOR STAINING, reddish brown saprolite, very weathered and stained, DRY.

Interval: 20-21'	Length: 18"	Estimated interval: 20-21'

20-21': moist to wet saprolite, same as below, crumbly, moist, no large rock pieces, very heavy dark staining.

Interval: 21-22.5'	Length: 3'	Estimated interval: 21-22.5'

21-22.5': moderate to dark yellowish brown, same as below, dry, crumbly saprolite. Heavily stained competent shale pieces.

Interval: 22.5-23.5'	Length: 2'	Estimated interval: 22.5-23.5'

Very HEAVILY STAINED AND WEATHERED!
Same as below, dark brown silty sand/clay with shale fragments.
22-22.5': Heavily stained shale, many large pieces.
22.5-23': mostly weathered, less competent.

Interval: 23.5-24.5'	Length: 1.7'	Estimated interval: 23.5-24.5'

Top 6": brown clay (slough)
23.5-23.75': heavily weathered and stained shale pieces in clay, saprolite.
23.75-24.25': slightly moist, crumbly, darker than below. HEAVILY STAINED weathered shale. some small pieces of competent shale.
24.25'-25': consolidated weathered shale/saprolite, can see shaly bedding structures.

Interval: 24.5-25'	Length: 1.3'	Estimated interval: 24.5-25'

Top 0.7': brown clay with shale fragments (slough?), moist.
24.5-24.6': consolidated weathered shale/clay (saprolite), staining.

24.6-25': dark yellowish brown, dry, crumbly, silty sand with weathered shale pieces (saprolite), no competent shale, all extremely weathered.

**********TOP OF BEDROCK: 25' ??????**********

Interval: 25-26'	Length: 1.5'	Estimated interval: 25-26'

Top 6": dark grey weathered shale covered by brown silty clay, soft, no staining.
25-26': same as below, dark yellowish brown to light olive grey, dry and crumbly, dark grey shale pieces with weathering rinds, staining on many pieces, no specific zone of staining. no competent shale, all extremely weathered.

Interval: 26-27'	Length: 1.5'	Estimated interval: 26-27'

Top 6": brown clay with shale fragments (slough?)
26-26.5': dark yellowish brown (10YR4/2) to light olive gray (5Y5/2), dry, crumbly silty sand with pieces of heavily weathered shale. some pieces heavily stained, can't tell placement of staining.
26.5-27': same as above but lighter, more pale yellowish brown (10YR6/2)
27': competent piece of shale, moderate staining.

**********WET DRILLING BEGINS AT 27'**********

Interval: 27-35'	Length: ~3'	Estimated interval: ??

**SLOUGH DISCARDED
Top 2": weathered, Fe stained calcite vein.
0-~2': dark grey shale, some calcite veining, indurated, LARGE PIECE. carbonate intervals. HEAVY FE STAINING at 1'.
2-~2.75': oolite, small shale intraclasts, stylolite features., black minerals.
2.75-3': shale, no veining. Medium size (few " length, 1/2" thick) pieces.

Interval: 35-40'	Length: 3.25'	Estimated interval: 36.75-40'

36.75-37.75': oolite, yellow mineralization ~37'. Mica(?) and black minerals observed, shale intraclasts. Black staining on some pieces.
37.75-38.75': shale, some large 1/2" length pieces. FE stained zone at ~38'. most pieces medium size. Burrow structures (?) . Fe staining along calcite vein. Thin white cross-cutting calcite veins.
38.75-40': clay-rich zone, much Fe staining in clay.

Interval: 40-45'	Length: 3'	Estimated interval: 42-45'

42-43': oolite, some calcite veins, one vein lined with black mineral (stylolitic), larger pieces , up to 2-3" in length.
43-44': HEAVILY STAINED SHALE, medium size pieces with carbonate

Appendix F: Core logs (con't)

interlayers.
44-45': clay-rich shale, mostly clay. some small shale pieces.

Interval: 45-49'	Length: 1' (48-49')	Estimated interval: 48-49'

48-48.5': small pieces of stained and unstained shale, bits of oolite.
48.5-49': oolite with shale intraclasts, looks stylolitic. oolite breaks along these planes of weakness. Major FE staining along shale stylolite. FE STAINING IN THIS INTERVAL

Interval: 49-54' "top"	Length: 2'	Estimated interval: 49-51'

49-49.25': oolite with thin white cross-cutting veins; dark staining on side. Some dark stained pieces between 49 and 49.5'; can't tell placement.
49.25-51': dark grey shale and carbonate interlayer pieces, no clay. Several stained pieces at ~50.3', but hard to tell placement. More stained pieces at 50.5'; part of same fracture?

Interval: 49-54' "bottom"	Length: 3'	Estimated interval: 51-54'

51-54': small pieces of shale; rest is weathered clay-rich shale.

Interval: 54-65' "top"	Length: 1.5'	Estimated interval: ??

Oolite carbonate interval, one large pink calcite vein, black minerals, one red mineral (hematite?), elongated calcite crystals. Some shale pieces at bottom.

Interval: 54-65' "bottom"	Length: 3'	Estimated interval: ??

top 1': dark grey shale pieces, some up to 3" long, no staining observed in silt/clay.
1-1.5': dark grey fissile weathered shale in clay matrix, no staining.
1.5-2': greenish grey shale, fissile, weathered shale in clay, some larger pieces. no staining, weathered calcite vein.
2.25-2.5': dark grey, very clay-rich , small pieces of shale
2.5-2.75': dark grey and fissile
2.75-3': dark grey shale/clay with pieces.
***no staining observed, but very weathered.

Interval: 65-70' "top"	Length: 1' (~4' original)	Estimated interval:??

Mostly broken up shale, small pieces, soft, shaly bedding. Iron stained pieces at top. Some oolite pieces; not sure about placement.
**SLOUGH DISCARDED

Interval: 65-70' "bottom"	Length: 1.5' (~4' original)	Estimated interval: ??

**SLOUGH DISCARDED
Top 6": 2" long disk of oolite, veining and shale intraclasts/stylolite.
middle 6": dark grey shale, same as "top" interval, very soft, calcite at bottom of one piece.
next 6": clay-rich shale, mostly clay. shale structure seen when broken, very crumbly, fissile, soft.
bottom 2": oolite.

Appendix G: Flowmeter data

GW821 Ambient Test									Injection-Ambient				
	depth	volts	Q (L/min	std dev	head	adj V	adj Q		Qa	Da	Qi	Di	Qi-Qa
time	18	-0.278	0.001	0.002	3.7	0.000	0.000		0.000	18	0.000	18	0.000
7:52:09	45.8	-0.279	0.001	0.004	3.71	-0.001	0.000		0.000	45.8	0.006	47	
8:01:54	43.9	-0.276	0.002	0.003	3.73	0.002	0.001		0.001	43.9	0.003	45.8	0.004
8:06:42	42	-0.278	0.001	0.002	3.72	0.000	0.000		0.000	42	0.012	43.9	0.011
8:13:35	40.1	-0.271	0.004	0.001	3.71	0.007	0.003		0.003	40.1	0.000	42	0.000
8:18:06	38	-0.271	0.004	0.002	3.71	0.007	0.003		0.003	38	0.013	40	0.010
8:24:25	36	-0.262	0.008	0.004	3.72	0.016	0.007		0.009	37	0.002	38	-0.001
8:36:19	34	-0.268	0.005	0.003	3.71	0.010	0.005		0.007	36	0.001	37	-0.008
8:41:00	37	-0.259	0.009	0.006	3.72	0.019	0.009		0.008	35	0.008	36	0.001
8:48:16	35	-0.26	0.009	0.002	3.73	0.018	0.008		0.005	34	0.022	35	0.014
8:53:06	32	-0.262	0.008	0.002	3.7	0.016	0.007		0.006	33	0.007	34	0.002
8:57:16	30	-0.266	0.006	0.001	3.7	0.012	0.005		0.007	32	0.011	33	0.005
9:00:26	33	-0.264	0.007	0.003	3.71	0.014	0.006		0.005	30	-0.014	32	-0.021
9:03:29	30	-0.266	0.006	0.002	3.68	0.012	0.005		0.004	28	0.010	30	0.004
9:06:42	28	-0.269	0.005	0.004	3.7	0.009	0.004		0.004	27.5	0.006	28	0.001
9:10:35	26	-0.229	0.023	0.002	3.7	0.049	0.022		0.023	27	0.010	27.5	0.006
9:13:46	27	-0.227	0.024	0.004	3.71	0.051	0.023		0.022	26	0.016	27	-0.007
9:17:06	27.5	-0.27	0.004	0.004	3.71	0.008	0.004		0.020	25	0.018	26	-0.004
9:21:21	25	-0.233	0.021	0.002	3.7	0.045	0.020		0.019	24	0.021	25	0.001
9:24:46	24	-0.235	0.02	0.002	3.71	0.043	0.019		0.024	23	0.028	24	0.009
9:29:16	23	-0.225	0.025	0.002	3.7	0.053	0.024				0.024	23	0.000
9:32:16											-0.351	18	-0.351
GW821 Injection Test													
	depth	volts	Q (L/min	std dev	head	adj V	adj Q						
time	18	-0.292	0.003	0.003	3.74	-0.300	0.000						
11:35:08	45.8	-0.285	0.007	0.004	4.38	-0.293	0.003						
11:57:07	43.9	-0.265	0.016	0.002	4.38	-0.273	0.012						
12:02:57	40	-0.263	0.017	0.008	4.38	-0.271	0.013						
13:00:37	38	-0.287	0.006	0.002	4.37	-0.295	0.002						
13:17:16	37	-0.291	0.004	0.004	4.39	-0.299	0.001						
13:31:57	36	-0.274	0.012	0.003	4.38	-0.282	0.008						
13:37:51	34	-0.277	0.01	0.003	4.37	-0.285	0.007						
13:50:21	33	-0.268	0.014	0.006	4.38	-0.276	0.011						
13:54:41	32	-0.323	-0.01	0.008	4.38	-0.331	-0.014						
14:03:24	30	-0.271	0.013	0.004	4.39	-0.279	0.010						
14:10:51	28	-0.28	0.009	0.007	4.39	-0.288	0.006						
14:22:36	27	-0.257	0.02	0.003	4.39	-0.265	0.016						
14:26:41	26	-0.252	0.021	0.005	4.38	-0.260	0.018						
14:30:26	25	-0.246	0.024	0.004	4.38	-0.254	0.021						
14:34:38	24	-0.23	0.031	0.007	4.36	-0.238	0.028						
14:47:51	23	-0.24	0.027	0.003	4.39	-0.248	0.024						
14:52:58	27.5	-0.271	0.013	0.003	4.39	-0.279	0.010						
15:03:51	35	-0.244	0.025	0.005	4.38	-0.252	0.022						
15:17:26	42	-0.293	0.003	0.005	4.37	-0.301	0.000	Interce	0.1348				
15:26:31	18	-1.074	-0.348	0.014	4.36	-1.082	-0.351	x1	0.4495				
15:36:21	47	-0.28	0.009	0.002	4.37	-0.288	0.006						

Appendix G: Flowmeter data (con't)

GW822 Ambient Test									Injection-Ambient				
time	depth	volts	Q (L/min	std dev	head	adj V	adj Q		Qa	Da	Qi	Di	Qi-Qa
7:08:03	17.76	-0.189	-0.085	0.007	8.02	0.000	0.000		-0.023	68	-0.003	68.1	0.020
7:28:00	68	-0.251	-0.113	0.002	8.03	-0.052	-0.023		-0.022	66	-0.011	66	0.010
7:42:39	66	-0.255	-0.115	0.001	8.08	-0.048	-0.022		-0.022	64	-0.010	64	0.011
7:52:38	64	-0.26	-0.117	0.001	8.09	-0.048	-0.022		0.006	62	0.010	62	0.004
7:59:41	62	-0.202	-0.091	0.003	8.08	0.014	0.006		-0.016	60	-0.009	60	0.008
8:05:52	60	-0.255	-0.115	0.001	8.07	-0.036	-0.016		0.014	58	-0.015	58	-0.029
8:11:07	58	-0.191	-0.086	0.002	8.08	0.030	0.014		0.068	56	-0.130	57	-0.130
8:16:24	56	-0.074	-0.033	0.002	8.09	0.150	0.068		0.079	54	-0.164	56	-0.232
8:20:51	54	-0.051	-0.023	0.003	8.09	0.176	0.079		0.072	52	-0.156	54	-0.235
8:24:51	52	-0.07	-0.032	0.002	8.09	0.159	0.072		0.012	50	-0.143	52	-0.215
8:28:58	50	-0.204	-0.092	0.001	8.08	0.027	0.012		0.090	49.5	-0.152	51	-0.222
8:38:55	48	-0.043	-0.019	0.001	8.09	0.193	0.087		0.089	49	-0.099	50	-0.111
8:49:36	49	-0.045	-0.02	0.002	8.09	0.197	0.089		0.087	48	-0.162	49	-0.251
8:56:47	49.5	-0.045	-0.02	0.002	8.09	0.200	0.090		0.091	47	-0.160	48	-0.247
9:31:37	47	-0.062	-0.028	0.002	8	0.201	0.091		0.040	46	-0.150	47	-0.241
9:36:18	46	-0.177	-0.08	0.003	7.99	0.088	0.040		0.127	44	-0.002	46	-0.042
10:49:35	23.13	-0.308	-0.139	0.007	8.09	0.000	0.000		0.102	42	-0.149	44	-0.276
11:31:49	23.1	-0.303	-0.004	0.002	8.08	0.000	0.000		0.116	40	-0.149	42	-0.250
11:45:32	44	-0.029	0.119	0.018	8.12	0.282	0.127		0.118	38	-0.187	40	-0.302
11:53:00	42	-0.089	0.092	0.019	8.2	0.225	0.102		0.118	36	-0.170	38	-0.289
11:56:08	40	-0.059	0.106	0.002	8.17	0.257	0.116		0.119	34	-0.147	36	-0.265
12:02:19	38	-0.057	0.106	0.027	8.16	0.262	0.118	0.03	0.000	23.1	-0.126	34	-0.245
12:09:30	36	-0.077	0.098	0.004	8.09	0.262	0.118	0:50:45			-0.556	23	-0.556
12:15:10	34	-0.063	0.104	0.002	8.11	0.263	0.119						
12:22:34	23.1	-0.333	-0.018	0.006	8.11	0.000	0.000						
GW822 Injection test													
time	depth	volts	Q (L/min	std dev	head	adj V	adj Q						
8:54:46	23	-0.241	-0.004	0.003	8.01	-0.232	0.000						
9:10:23	68	-0.253	-0.01	0.002	8.5	-0.244	-0.005						
9:53:08	68.1	-0.248	-0.007	0.008	8.76	-0.239	-0.003						
10:05:40	66	-0.266	-0.015	0.006	8.76	-0.257	-0.011						
10:13:29	64	-0.264	-0.014	0.002	8.73	-0.255	-0.010						
10:19:01	62	-0.218	0.006	0.002	8.73	-0.209	0.010						
10:34:06	60	-0.26	-0.013	0.002	8.75	-0.251	-0.009						
10:46:03	58	-0.274	-0.019	0.004	8.76	-0.265	-0.015						
11:02:20	57	-0.53	-0.134	0.03	8.75	-0.521	-0.130						
11:09:11	56	-0.605	-0.168	0.002	8.76	-0.596	-0.164						
11:17:57	54	-0.586	-0.159	0.005	8.76	-0.577	-0.156						
11:26:18	52	-0.558	-0.147	0.005	8.75	-0.549	-0.143						
11:30:59	51	-0.578	-0.156	0.003	8.75	-0.569	-0.152						
11:37:53	50	-0.461	-0.103	0.005	8.75	-0.452	-0.099						
11:44:05	49	-0.6	-0.166	0.003	8.75	-0.591	-0.162						
11:54:16	48	-0.595	-0.163	0.005	8.76	-0.586	-0.160						
12:03:22	47	-0.573	-0.153	0.002	8.74	-0.564	-0.150						
12:07:39	46	-0.245	-0.006	0.001	8.75	-0.236	-0.002						
12:15:23	44	-0.572	-0.153	0.003	8.75	-0.563	-0.149						
12:22:23	42	-0.57	-0.152	0.004	8.74	-0.561	-0.149						
13:18:02	23	-0.3	-0.032	0.002	8.24	-0.228	0.000						
13:39:04	40	-0.715	-0.219	0.001	8.75	-0.643	-0.187	b1	0.105				
13:45:47	38	-0.679	-0.203	0.002	8.75	-0.607	-0.170	m1	0.451				
13:56:48	36	-0.627	-0.179	0.002	8.75	-0.555	-0.147						
14:03:22	34	-0.581	-0.159	0.002	8.75	-0.509	-0.126	b2	0.103				
14:15:10	23	-1.537	-0.589	0.01	8.75	-1.465	-0.556	m2	0.450				

GW823 Ambient Test			z1= -0.263	z2= -0.3					Injection-Ambient			
time	depth	volts	Q (L/min)	std dev	head	adj V	adj Q		Qa	Da	Ql	Dl	Ql-Qa
8:28:28	18	-0.273	-0.005	0.003	2.58	-0.26	0.000		0.000	18.1	0.000	18	0.000
8:45:35	60	-0.277	-0.007	0.003	2.6	-0.27	-0.002		-0.002	60	-0.002	59.8	0.000
8:47:55	58	-0.287	-0.011	0.004	2.57	-0.28	-0.007		-0.007	58	0.000	58.2	0.007
8:52:32	56	-0.275	-0.006	0.002	2.58	-0.27	-0.001		-0.001	56	0.007	56	0.009
8:55:49	54	-0.254	0.004	0.002	2.59	-0.24	0.008		0.008	54	0.004	54.1	-0.005
9:02:25	52	-0.271	-0.004	0.002	2.58	-0.26	0.001		0.001	52	-0.002	52	-0.002
9:12:10	51	-0.279	-0.008	0.006	2.58	-0.27	-0.003		0.030	46.2	-0.319	46	-0.349
13:07:55	18	-0.293	0.003	0.003	2.55	-0.3	0.000		0.028	44	-0.298	44	-0.326
13:18:11	46	-0.262	0.017	0.013	2.57	-0.27	0.014		0.025	42	-0.360	42	-0.385
13:24:10	46.1	-0.236	0.029	0.013	2.57	-0.24	0.026		0.028	40	-0.356	40	-0.383
13:26:50	46.2	-0.226	0.034	0.009	2.56	-0.23	0.030		0.014	38	-0.179	38	-0.193
13:44:18	38	-0.261	0.018	0.006	2.58	-0.27	0.014		0.022	36	-0.240	36	-0.261
13:52:38	36	-0.245	0.025	0.008	2.56	-0.25	0.022		0.023	34	-0.193	34	-0.216
13:57:25	34	-0.243	0.026	0.007	2.57	-0.25	0.023		0.029	32	-0.253	32	-0.282
14:02:35	32	-0.229	0.032	0.007	2.57	-0.24	0.029		0.032	30	-0.239	30	-0.271
14:06:48	30	-0.222	0.035	0.005	2.57	-0.23	0.032		0.018	28	-0.158	28	-0.176
14:16:26	28	-0.253	0.021	0.006	2.52	-0.26	0.018						
14:24:03	44	-0.231	0.031	0.005	2.58	-0.24	0.028						
14:33:34	42	-0.238	0.028	0.002	2.6	-0.25	0.025						
14:38:19	40	-0.232	0.031	0.003	2.59	-0.24	0.028						
14:58:45	18	-0.307	-0.003	0.013	2.59	-0.31	-0.006						
15:08:08	18.1	-0.293	0.003	0.008	2.6	-0.3	0.000						
GW823 InjectionTest			z1= -0.272	z2= -0.3									
time	depth	volts	Q (L/min)	std dev	head	adj V	adj Q						
8:20:20	18	-0.268	0.002	0.003	2.65	-0.27	0.000						
8:40:05	59.8	-0.273	-0.001	0.003	3.25	-0.28	-0.002						
9:03:00	58	-0.272	0	0.008	3.24	-0.28	-0.002						
9:19:21	56	-0.252	0.009	0.006	3.25	-0.26	0.007						
9:26:15	54	-0.258	0.007	0.003	3.24	-0.26	0.005						
9:28:56	54.1	-0.26	0.005	0.002	3.25	-0.26	0.004						
10:03:19	52	-0.272	0	0.007	3.24	-0.28	-0.002						
10:59:27	18	-0.29	-0.008	0.004	2.76	-0.29	-0.010						
13:35:00	18	-0.293	0.003	0.004	2.62	-0.3	0.000						
13:55:40	46	-1.002	-0.316	0.009	3.24	-1.01	-0.319						
14:10:38	44	-0.956	-0.295	0.005	3.23	-0.96	-0.298						
14:28:44	42	-1.094	-0.357	0.004	3.25	-1.1	-0.360						
14:34:49	40	-1.084	-0.353	0.003	3.24	-1.09	-0.356						
14:45:24	38	-0.69	-0.175	0.005	3.24	-0.7	-0.179						
15:22:34	36	-0.826	-0.237	0.003	3.25	-0.83	-0.240						
15:29:42	34	-0.723	-0.19	0.003	3.24	-0.73	-0.193						
15:36:44	32	-0.856	-0.25	0.003	3.24	-0.86	-0.253						
15:45:19	30	-0.825	-0.236	0.003	3.25	-0.83	-0.239						
16:08:50	28	-0.645	-0.155	0.006	3.24	-0.65	-0.158						
17:01:00	58.2	-0.293	0.003	0.01	2.78	-0.3	0.000						

Appendix H: Point dilution data

GW821: 24-26.5

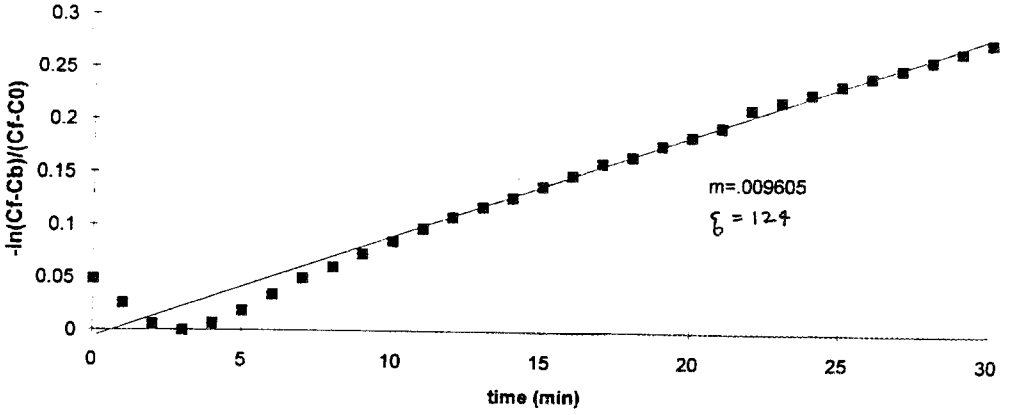

GW821: 26-28.5

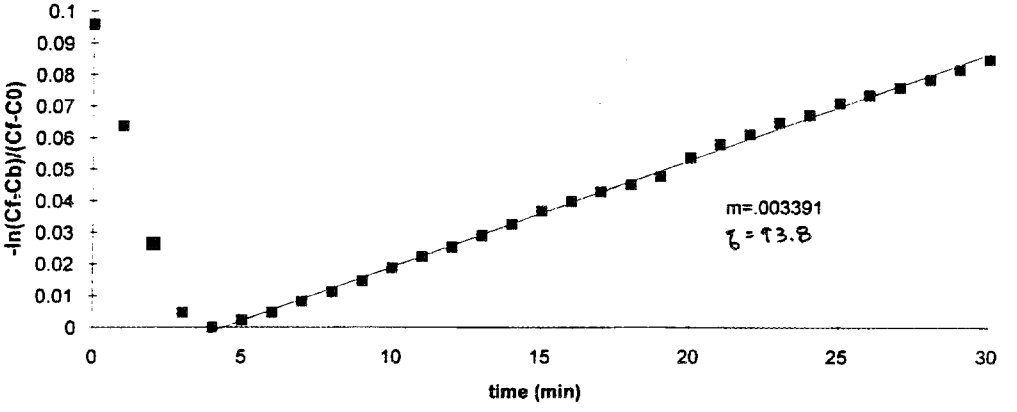

GW821: ~~26-28.5~~ 25-30.5

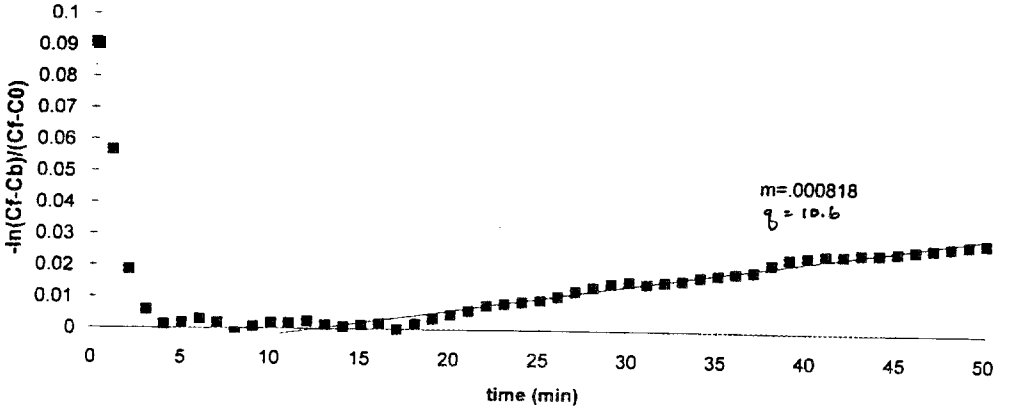

Appendix H: Point dilution data (con't)

GW821: 30-32.5

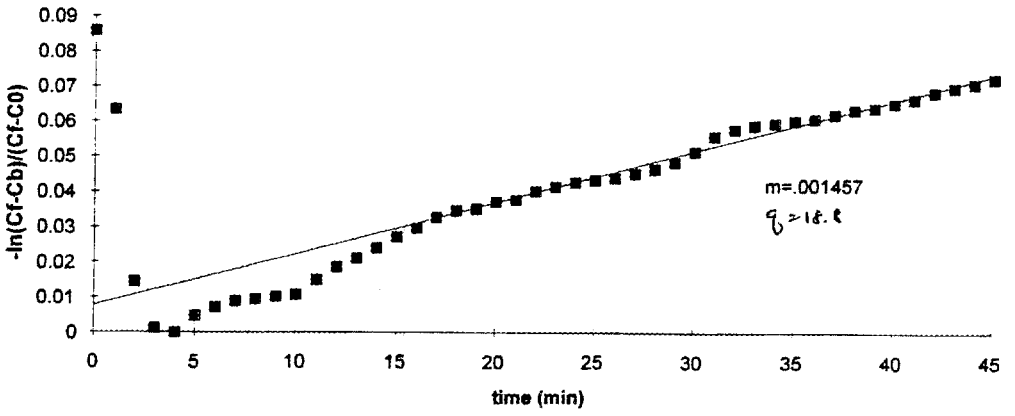

GW821: 32-34.5

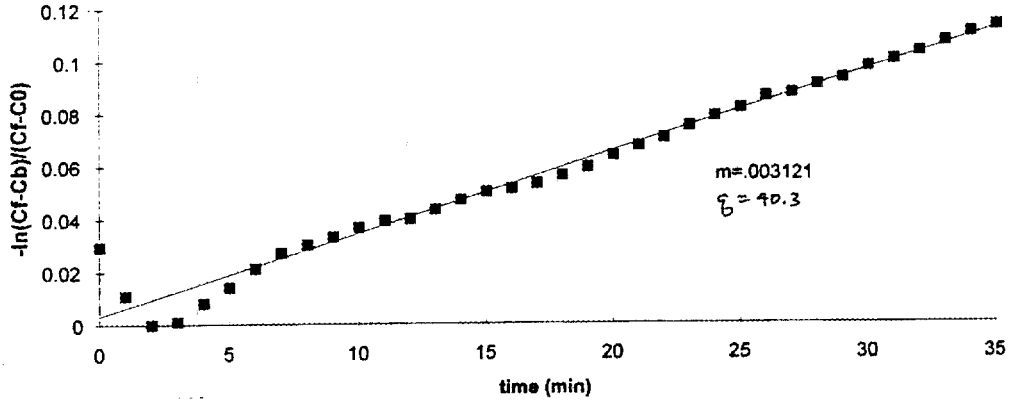

GW821: 34-36.5

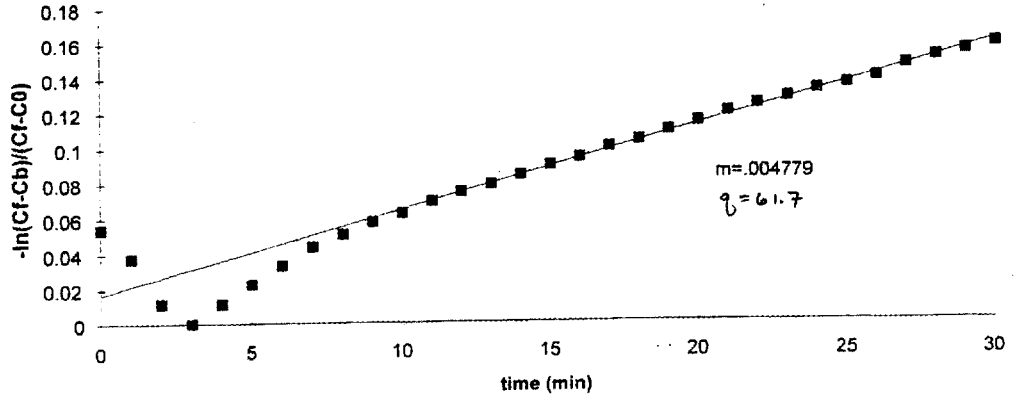

Appendix H: Point dilution data (con't)

GW821: 36-38.5

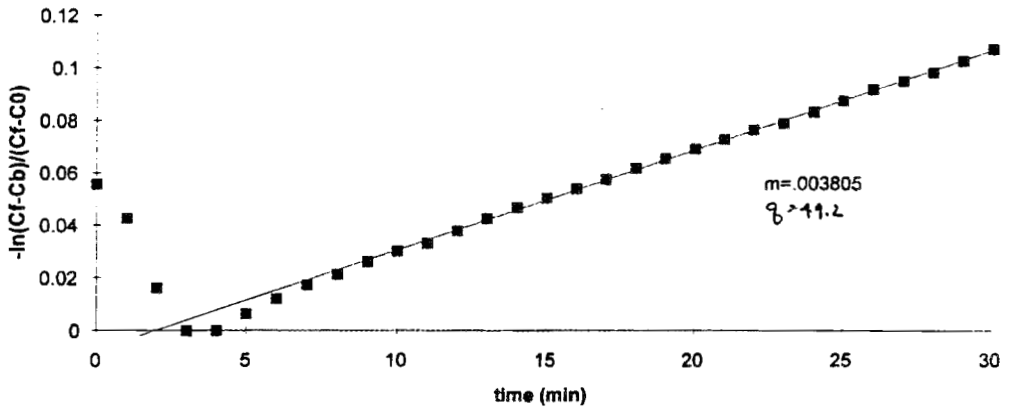

GW821: 38-40.5

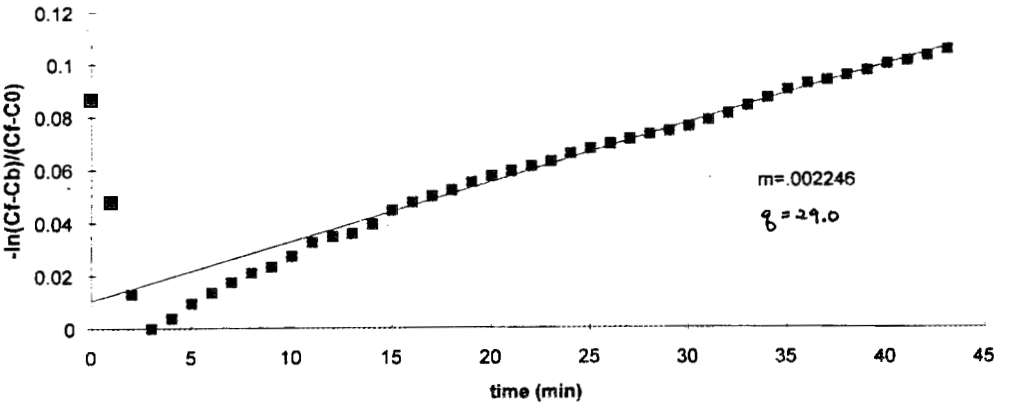

GW821: 38-40.5

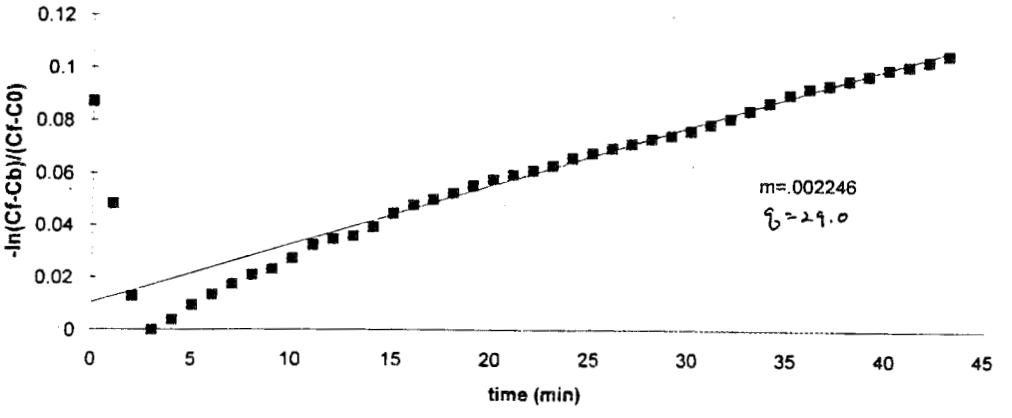

Appendix H: Point dilution data (con't)

GW822 #17

34-36.5'

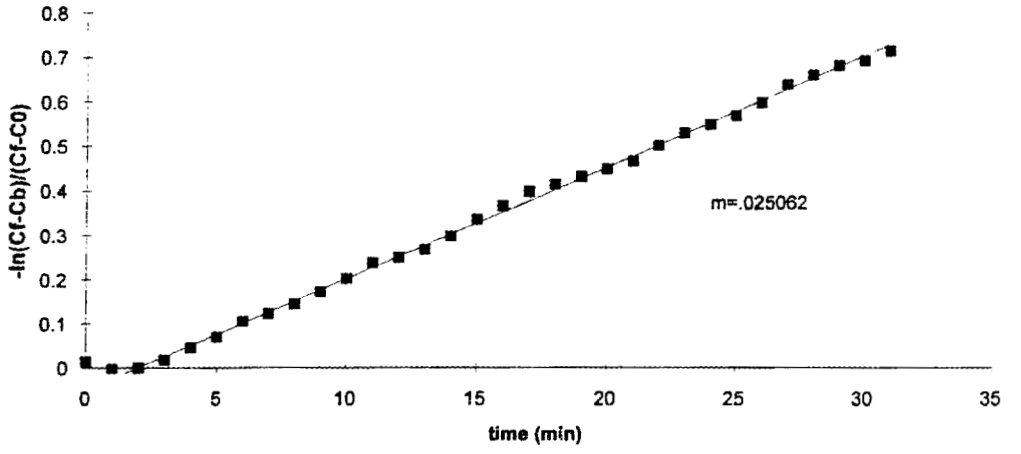

GW822 #16

36-38.5'

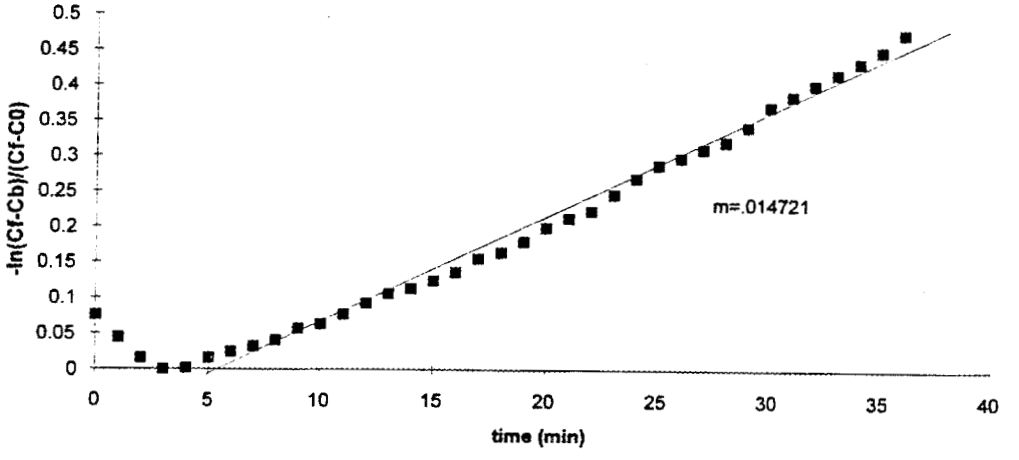

GW822 #15

38-40.5'

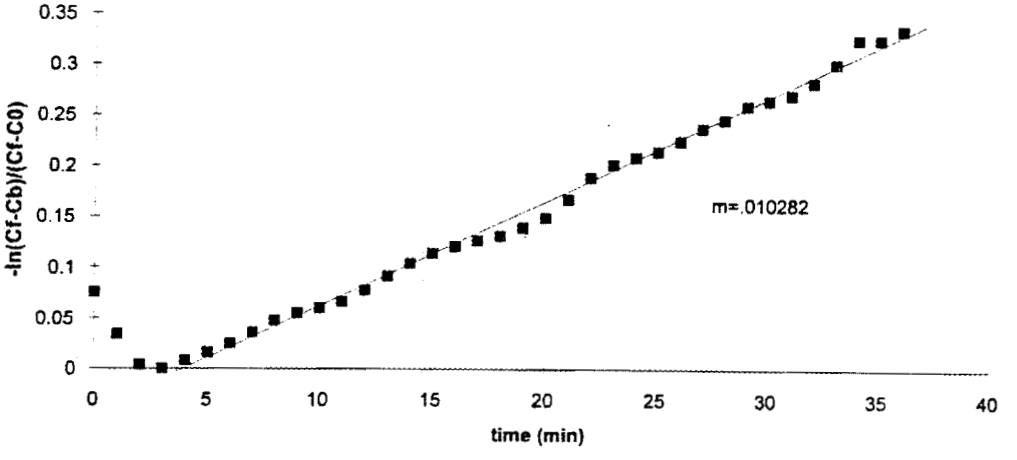

GW822 #14

40 - 42.5'

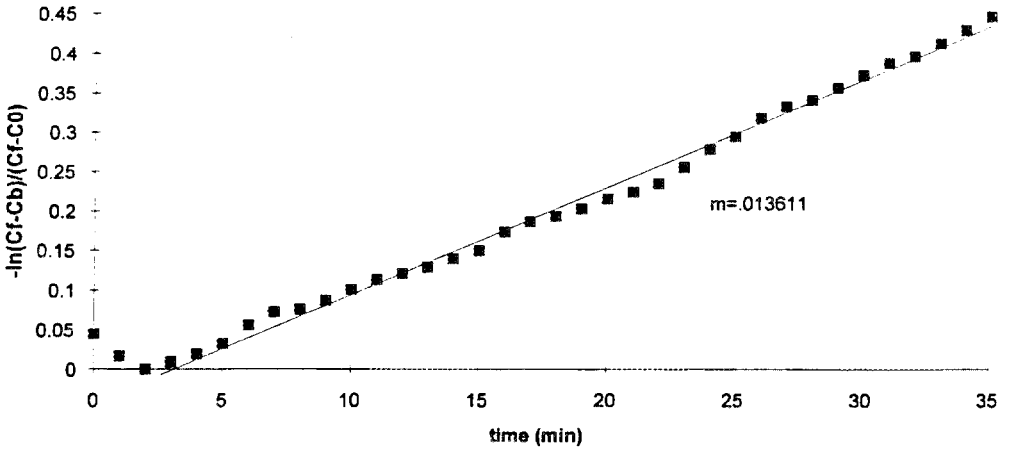

GW822 #13

42 - 44.5'

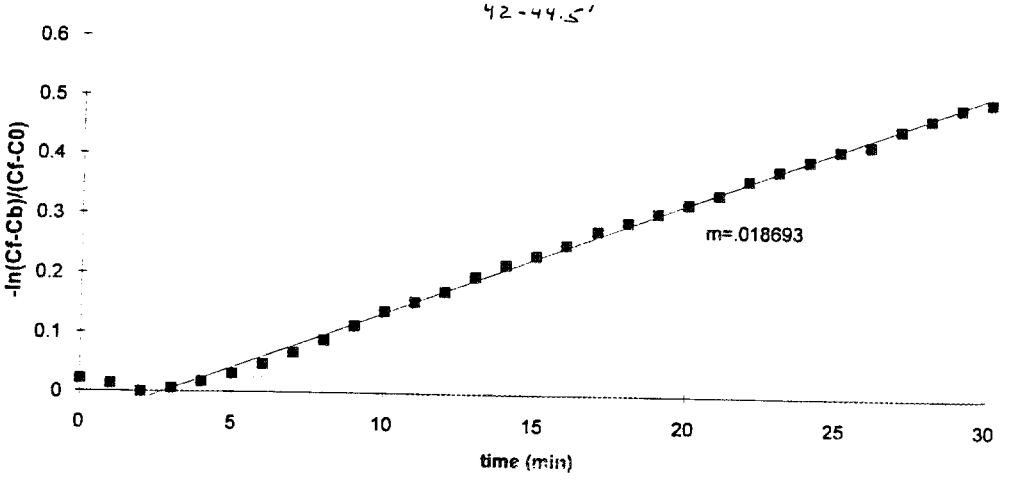

GW822 #12

44 - 46.5'

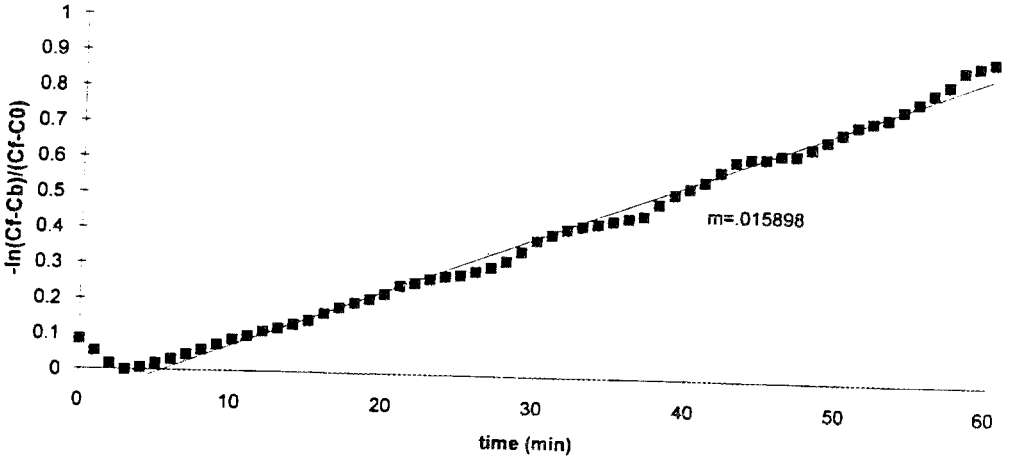

Appendix H: Point dilution data (con't)

GW822 #11

46 - 48.5'

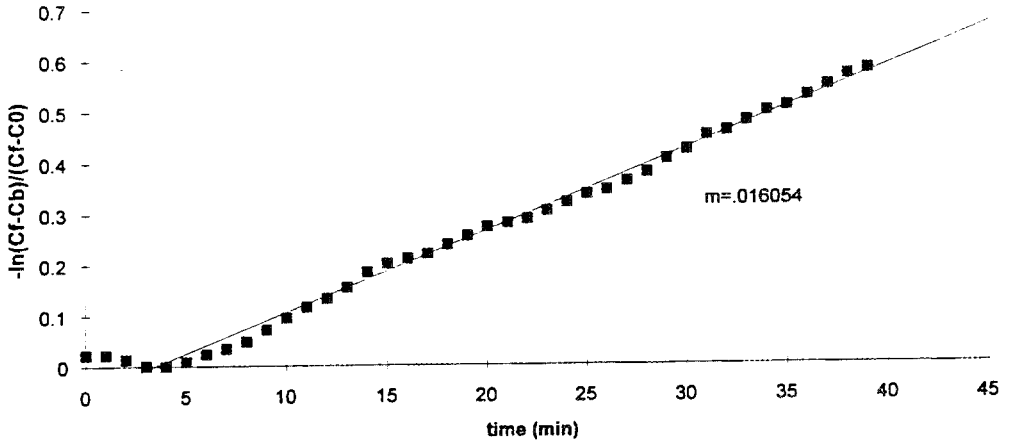

GW822 #10

48 - 50.5'

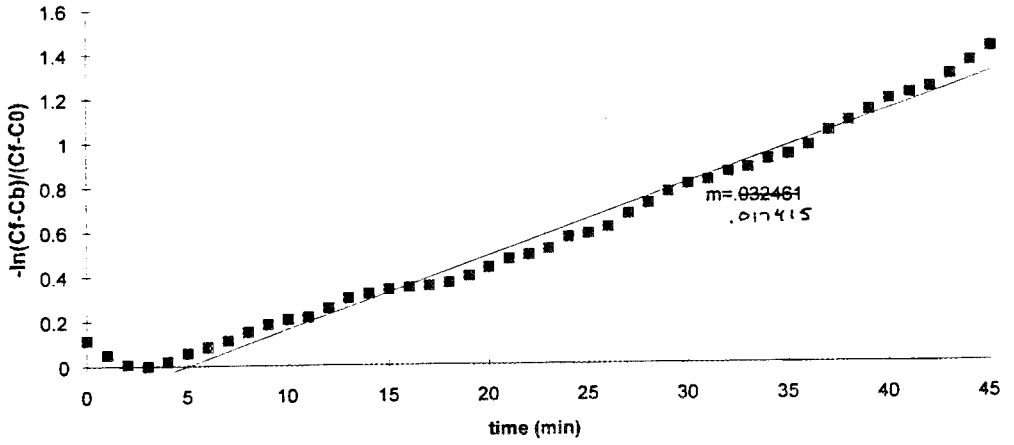

GW822 #9

50 - 52.5'

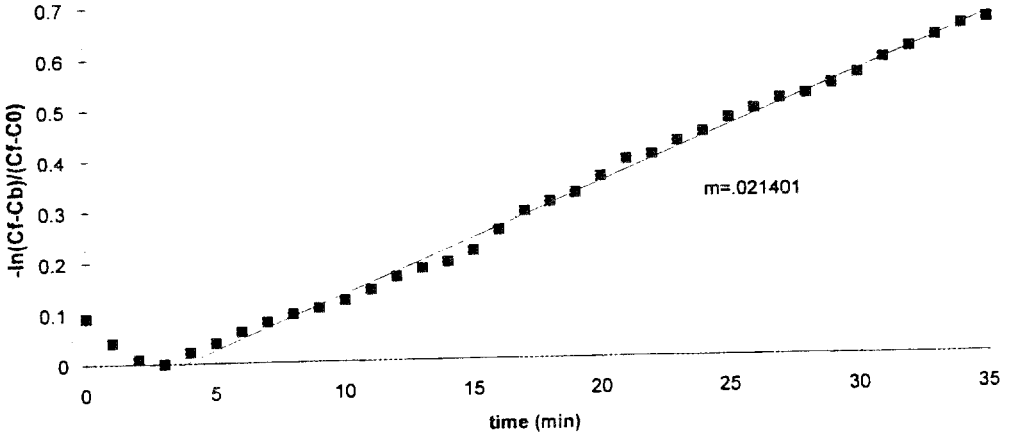

Appendix H: Point dilution data (con't)

GW822 #8

52 - 54.5'

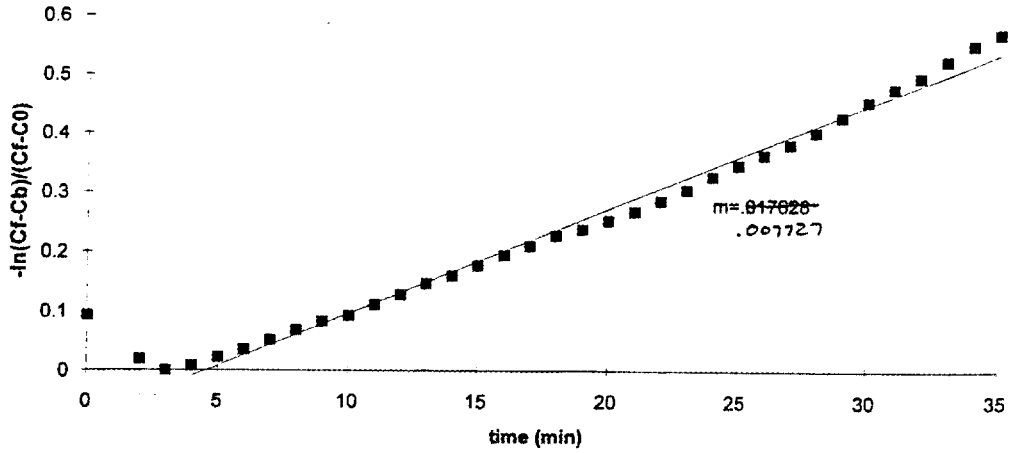

GW822 #7

54 - 56.5'

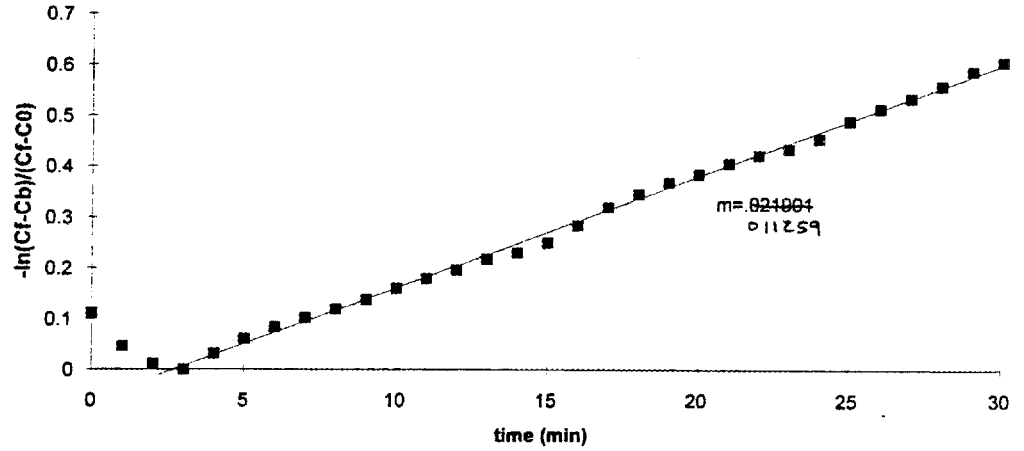

GW822 #6

56 - 58.5'

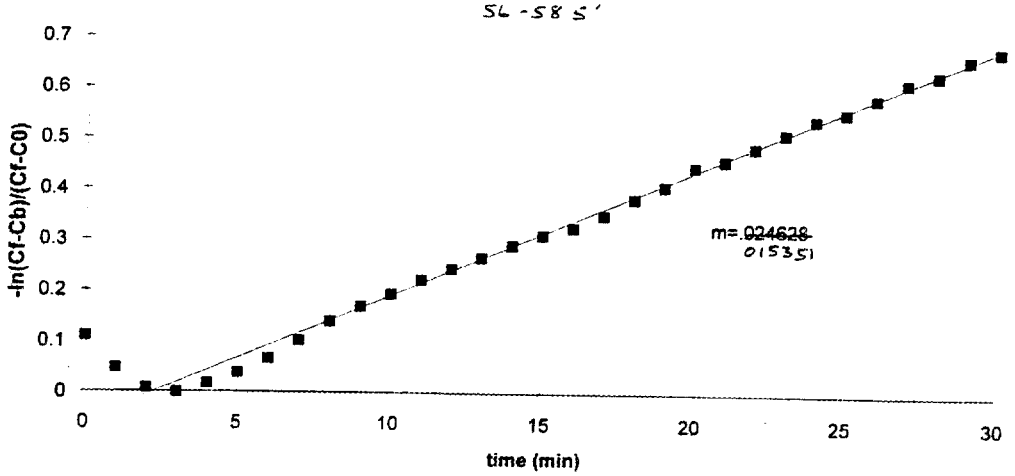

GW822 #5

58-60.5'

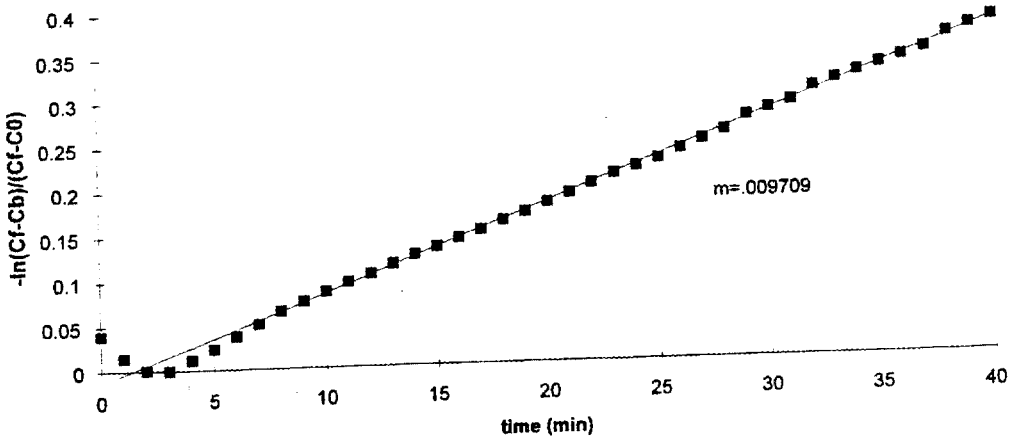

GW822 #4

60-62.5'

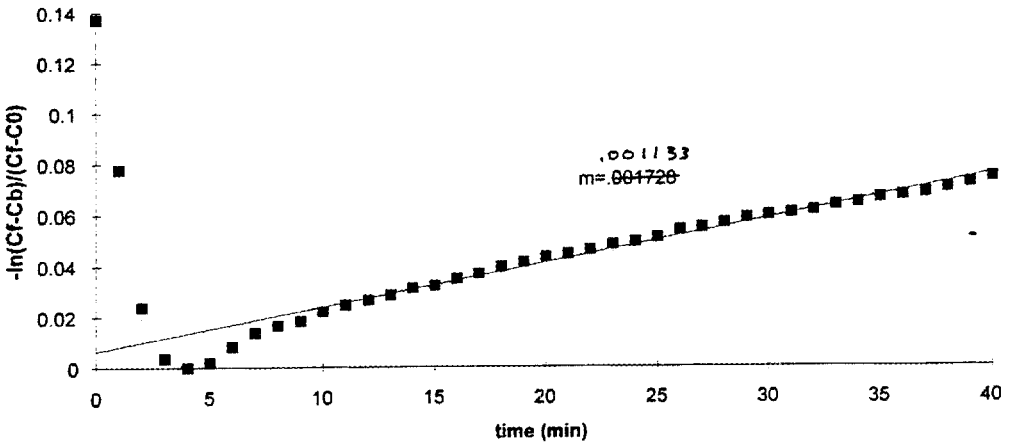

GW822 #3

62-64.5'

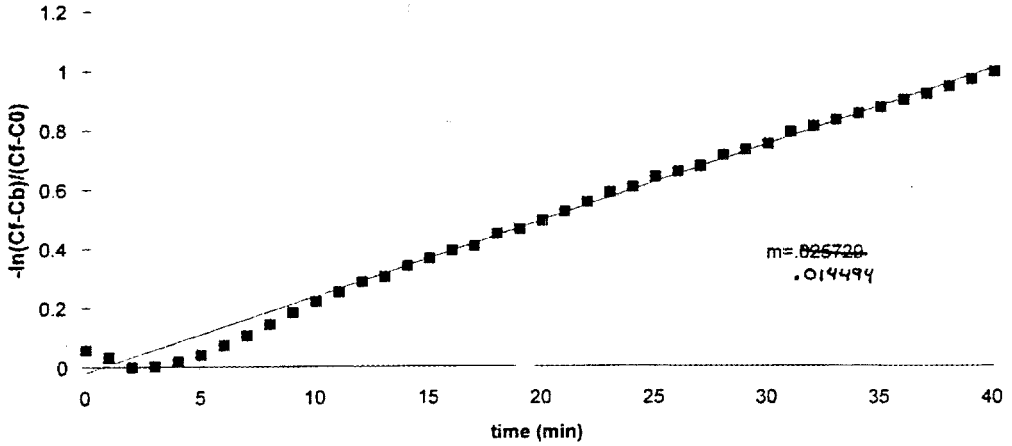

Appendix H: Point dilution data (con't)

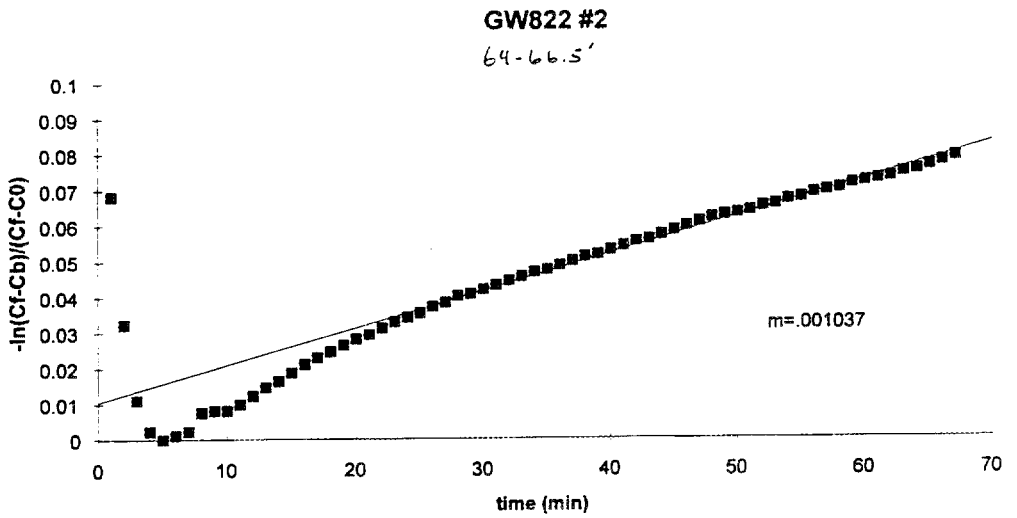

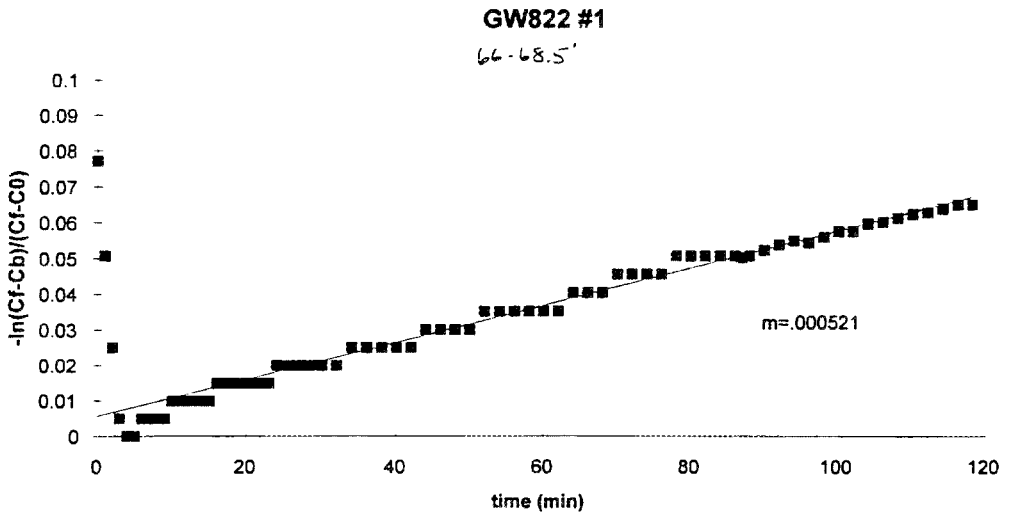

Appendix H: Point dilution data (con't)

GW823: 28-30.5

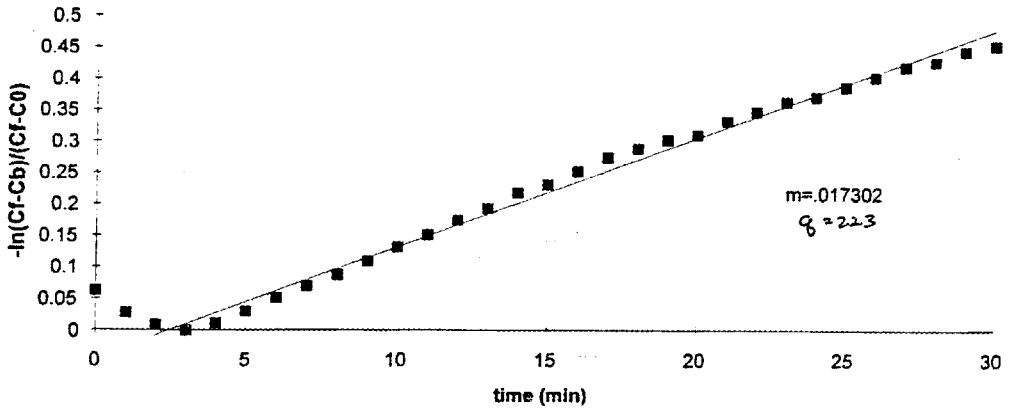

GW823: 28-30.5
(Late time fit)

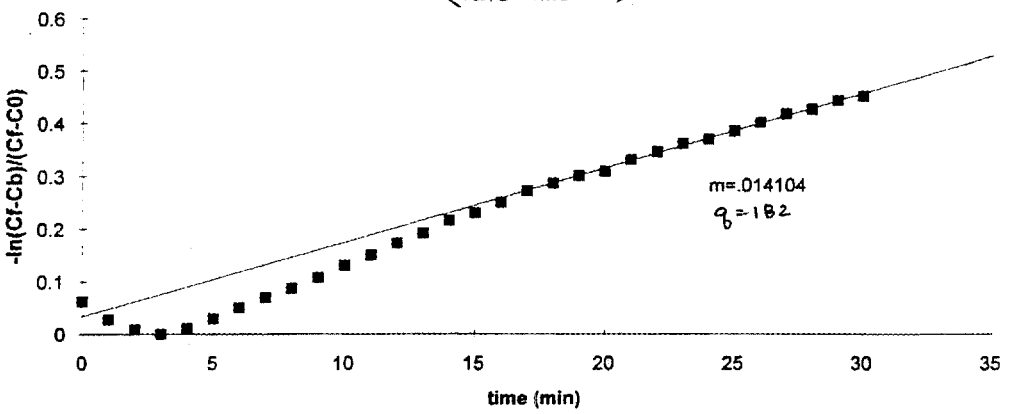

GW823: 30-32.5

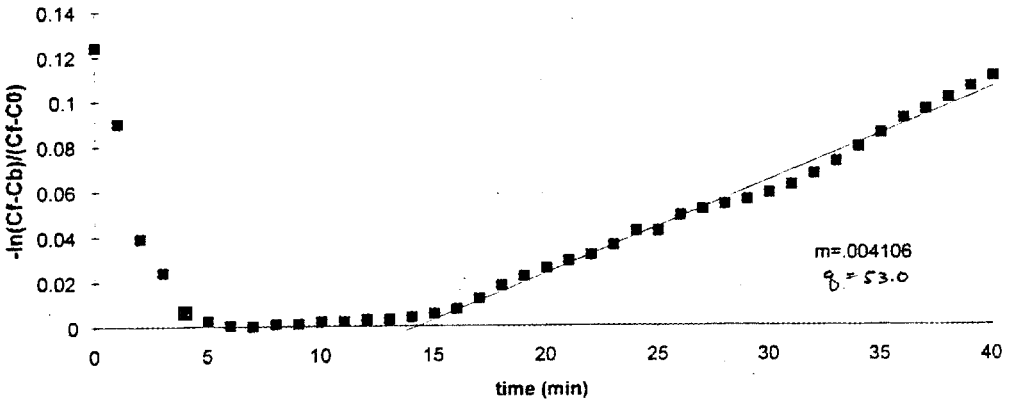

Appendix H: Point dilution data (con't)

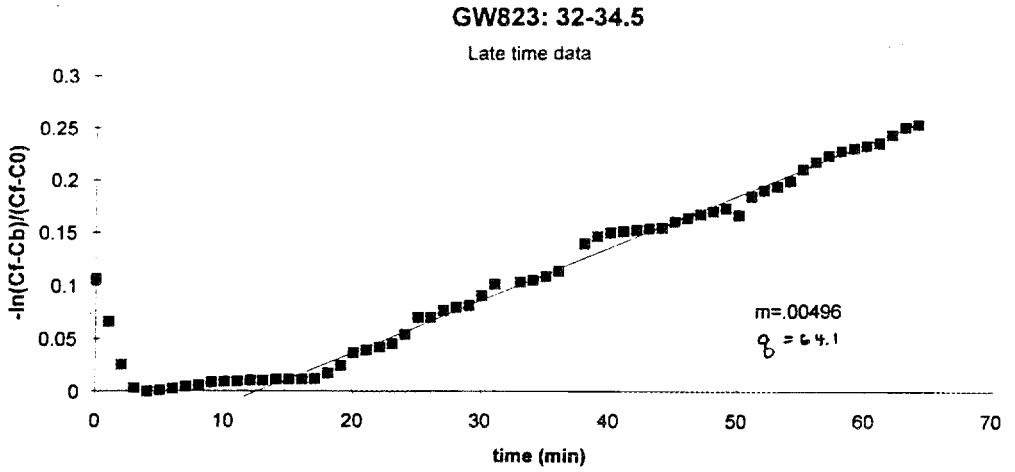

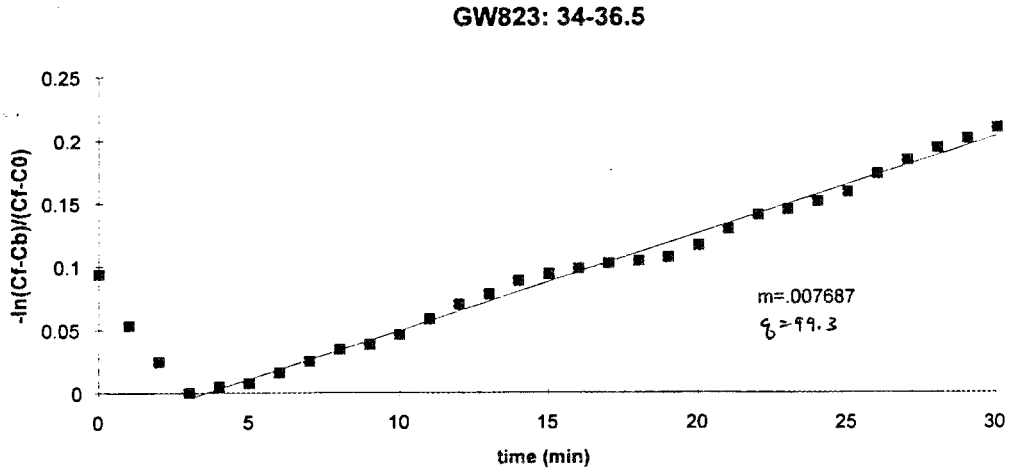

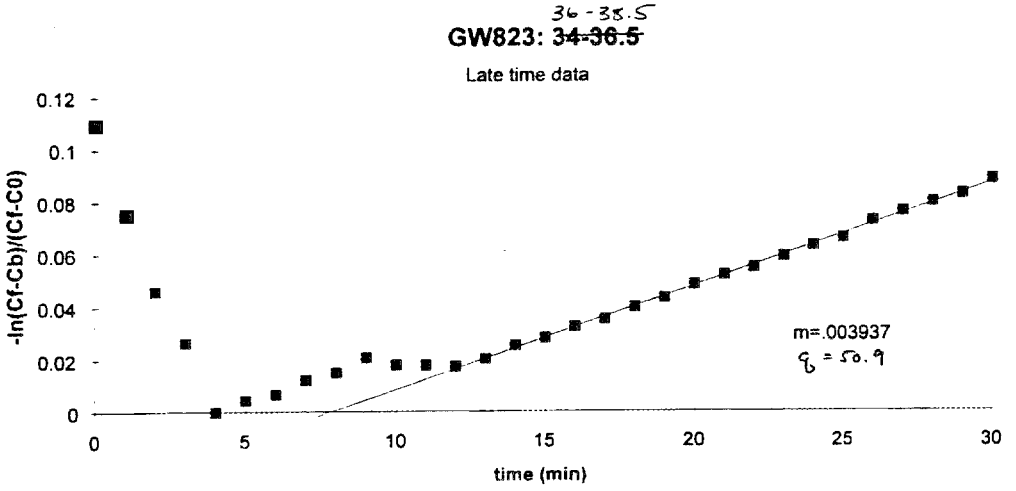

Appendix H: Point dilution data (con't)

GW823: 38-40.5

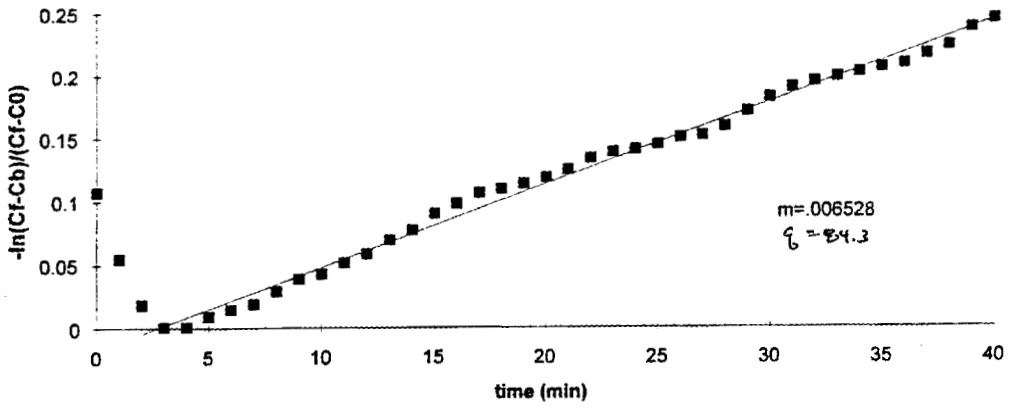

GW823: 40-42.5

Late time data

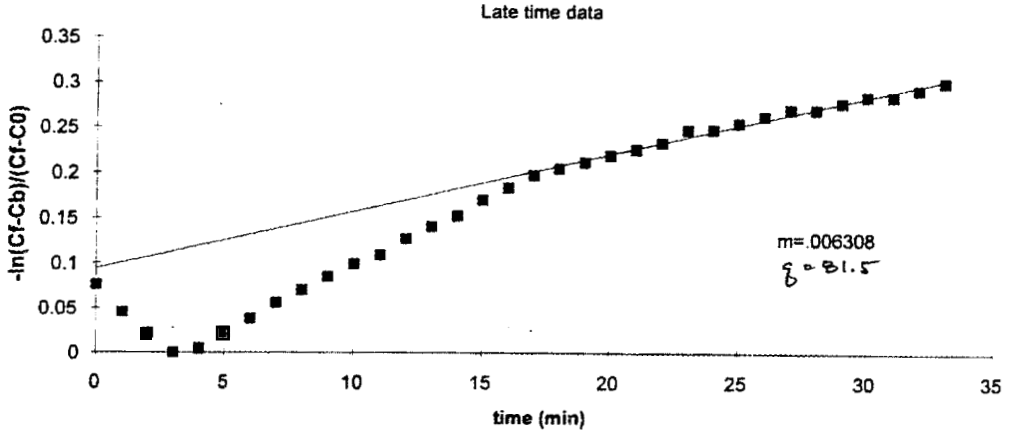

GW823: 42-44.5

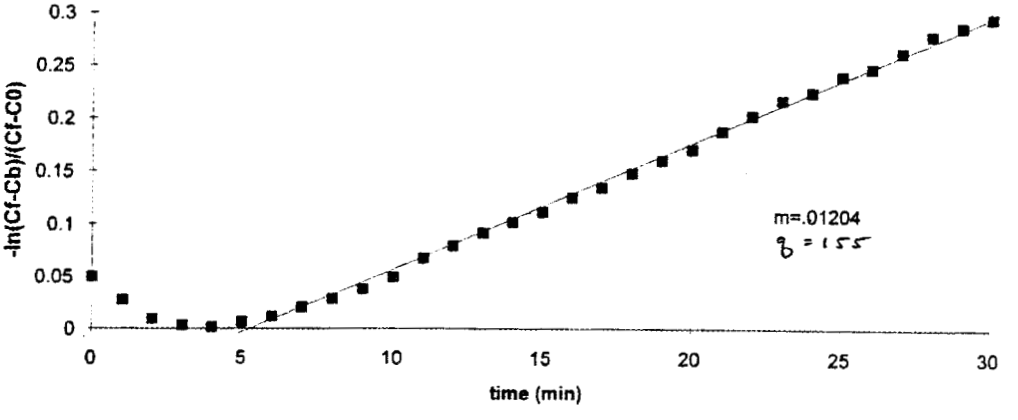

Appendix H: Point dilution data (con't)

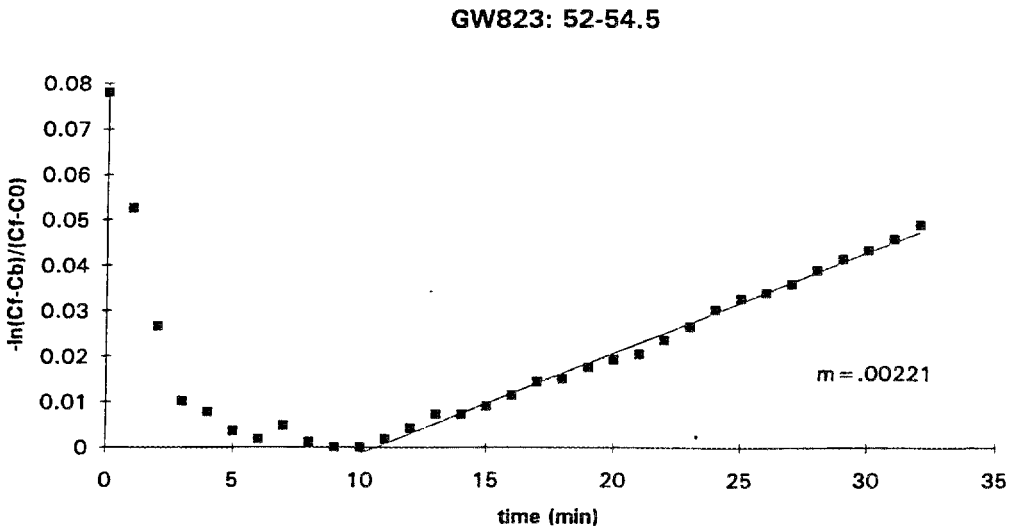

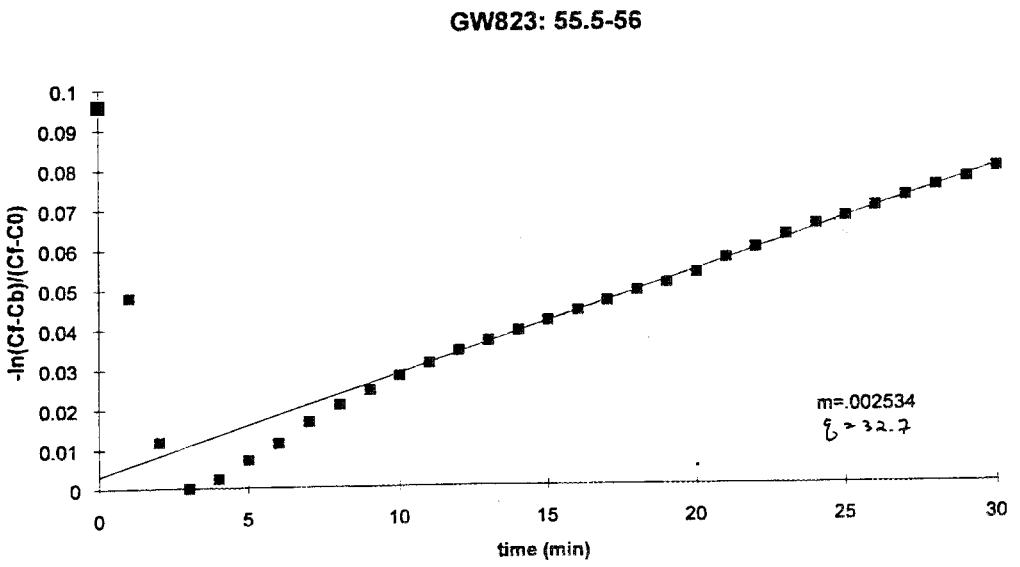

Appendix I: Geochemistry data

Packer and pore water samples

Well	Sample Date	depth feet	pH	Alk.	Est. % HCO3	HCO3 (mg/L)	CO3 (mg/L)	Br (mg/L)	Cl (mg/L)	F (mg/L)	NO3 (mg/L)	PO4 (mg/L)	SO4 (mg/L)
GW82115		24.00	8.27	172.9	100%	210.80	0.00	0.015	0.765		0	0	5.85
GW82115RC		24.00	8.27	172.9	100%	210.80	0.00	0.015	0.765		0	0	5.85
GW82116		25.50	8.16	171.8	100%	209.46	0.00	0	0.783		0.04	0	6.11
GW82116RA		25.50	8.16	171.8	100%	209.46	0.00	0.061	0.888		0	0	6.09
GW82117		27.40	7.99	171.6	100%	209.22	0.00	0	0.836		0	0	6.2
GW82118		28.60	8.02	173.1	100%	211.05	0.00	0	1.002		0	0	6.14
GW82119		30.20	8.02	176.9	100%	215.68	0.00	0	0.969		0	0	6.21
GW82120		32.20	8.08	174.6	100%	212.87	0.00	0	1.276		0	0	6.11
GW82121		33.00	8.00	176.3	100%	214.95	0.00	0	1.29		0	0	6.08
GW82121RA		33.00	8.00	176.3	100%	214.95	0.00	0	0.92		0	0	6.07
GW82122		35.20	8.09	172.9	100%	210.80	0.00	0	0.879		0	0	6.3
GW82123		37.00	8.04	172.4	100%	210.19	0.00	0	0.949		0	0.078	6.17
GW82124		39.00	7.93	181.1	100%	220.80	0.00	0	0.962		0	0	6.17
GW82214		33.30	8.01	173.5	100%	211.53	0.00	0.352	1.243		0	0	6.64
GW82201		34.60	8.00	181.9	99%	219.56	1.09	0.376	1.114		0.03	0	6.78
GW82201RA		34.60	8.00	181.9	99%	219.56	1.09	0.335	1.067		0	0	6.69
GW82202		37.70	7.97	180	100%	219.46	0.00	0.341	0.951		0.05	0	6.52
GW82203		41.00	8.01	184.5	100%	224.95	0.00	0.35	1.015		0.09	0	6.57
GW82204		42.70	8.21	177.3	100%	216.17	0.00	0.339	0.889		0.05	0	6.55
GW82205		45.00	8.18	175.1	100%	213.48	0.00	0.346	1.177		0	0	6.46
GW82205RC		45.00	8.18	175.1	100%	213.48	0.00	0.346	1.177		0	0	6.46
GW82206		47.00	8.17	180.5	100%	220.07	0.00	0.345	0.929		0.07	0	6.55
GW82206RA		47.00	8.17	180.5	100%	220.07	0.00	0.336	0.978		0.07	0	6.61
GW82207		48.70	8.14	202.7	100%	247.13	0.00	0.328	1.026		0.04	0	6.51
GW82208		51.30	8.26	173	100%	210.92	0.00	0.324	0.942		0.08	0	6.51
GW82209		53.00	8.04	174	100%	212.14	0.00	0.3	0.943		0.05	0	6.52
GW82213		55.50	8.10	174.1	100%	212.27	0.00	0.308	0.969		0.08	0	6.76
GW82210		57.20	7.98	176.2	100%	214.83	0.00	0.284	0.906		0.04	0	6.49
GW82211		61.00	8.02	179.4	100%	218.73	0.00	0.233	1		0.05	0	6.54

Notes: RA=replicate anion analysis, RC=replicate cation analysis

Appendix I: Geochemistry data (con't)

Packer and pore water samples

Well	Sample Date	depth feet	pH	Alk.	Est. % HCO3	HCO3 (mg/L)	CO3 (mg/L)	Br (mg/L)	Cl (mg/L)	F (mg/L)	NO3 (mg/L)	PO4 (mg/L)	SO4 (mg/L)
GW82211RA		61.00	8.02	179.4	100%	218.73	0.00	0.221	1.003		0.05	0	6.25
GW82212		63.20	7.99	177.1	100%	215.92	0.00	0.204	1.002		0.04	0	6.35
GW82325		27.70	7.84	172.8	100%	210.68	0.00	1.44	1.059		0	0	6.33
GW82325RC		27.70	7.84	172.8	100%	210.68	0.00	1.44	1.059		0	0	6.33
GW82326		29.00	7.78	178.6	100%	217.75	0.00	1.454	1.066		0	0	6.28
GW82326RA		29.00	7.78	178.6	100%	217.75	0.00	1.441	1.104		0	0	6.25
GW82327		32.00	7.85	223.1	100%	272.01	0.00	1.413	1.119		0	0	6.32
GW82328		34.90	7.82	178.7	100%	217.87	0.00	1.428	0.973		0	0	5.99
GW82329		36.00	7.82	179.2	100%	218.48	0.00	1.4	1.061		0	0	6.09
GW82330		37.00	7.89	180	100%	219.46	0.00	1.398	1.31		0	0	5.94
GW82331		39.00	7.84	172.5	100%	210.31	0.00	1.391	0.892		0	0	5.93
GW82331RA		39.00	7.84	172.5	100%	210.31	0.00	1.427	0.984		0	0	6.12
GW82332		42.00	8.00	172.4	100%	210.19	0.00	1.439	0.93		0.01	0	6.08
GW82333		43.10	7.98	175.1	100%	213.48	0.00	1.408	0.948		0	0	6.09
GW82335		51.20	8.02	177.6	100%	216.53	0.00	1.292	0.987		0	0.119	6.13
GW82335RC		51.20	8.02	177.6	100%	216.53	0.00	1.292	0.987		0	0.119	6.13
GW82334		55.10	7.99	179.5	100%	218.85	0.00	1.167	0.908		0.03	0	6.18
PW82202		16.00	7.89	289.8	100%	353.33	0.00	0.885	72.76		0	0.118	103
PW82202RA		16.00	7.89	289.8	100%	353.33	0.00	0.84	68.27		0	0.116	97.3
PW82203		16.00	8.00	152.2	100%	185.56	0.00	0.793	65.24		0	0.133	64.2
PW82203RA		16.00	8.00	152.2	100%	185.56	0.00	0.809	66.96		0	0.069	65.4
PW82204		25.00	8.06	145.4	100%	177.27	0.00	0.117	8.79		0	0	20.1
PW82204RA		25.00	8.06	145.4	100%	177.27	0.00	0.112	9.515		0	0.139	20.3
PW82205		25.00	8.08	132.6	100%	161.67	0.00	0.109	9.613		0	0.044	20.9
PW82205RA		25.00	8.08	132.6	100%	161.67	0.00	0.116	9.571		0	0.233	21
PW82306		18.00	5.54	2.8	100%	3.41	0.00	0.391	83.5		0.22	0.082	18.9
PW82306RA		18.00	5.54	2.8	100%	3.41	0.00	0.145	21.18		0.19	0.063	13.2

Notes: RA=replicate anion analysis, RC=replicate cation analysis

Appendix I: Geochemistry data (con't)

Packer and pore water samples (con't)

Well	Al (mg/L)	Sb (mg/L)	P (mg/L)	Ba (mg/L)	Be (mg/L)	B (mg/L)	Cd (mg/L)	Ca (mg/L)	Cr (mg/L)	Co (mg/L)
GW82115	0.95	< 0.05	< 0.3	0.26	< 0.001	< 0.08	< 0.005	58	0.0041	< 0.004
GW82115RC	0.94	< 0.05	< 0.3	0.26	< 0.001	< 0.08	< 0.005	58	0.005	0.004
GW82116	0.58	< 0.05	< 0.3	0.27	< 0.001	< 0.08	< 0.005	55	< 0.004	< 0.004
GW82116RA	1.58	< 1.05	< 0.3	0.27	< 1.001	< 1.08	< 0.005	55	< 1.004	< 1.004
GW82117	0.47	< 0.05	< 0.3	0.27	< 0.001	< 0.08	< 0.005	55	< 0.004	< 0.004
GW82118	0.52	< 0.05	0.32	0.29	< 0.001	< 0.08	< 0.005	56	< 0.004	0.005
GW82119	0.49	< 0.05	0.31	0.29	< 0.001	< 0.08	< 0.005	55	< 0.004	< 0.004
GW82120	1.1	< 0.05	0.4	0.34	< 0.001	< 0.08	< 0.005	58	0.019	0.006
GW82121	3.3	< 0.05	0.37	0.51	< 0.001	< 0.08	< 0.005	67	0.0077	0.006
GW82121RA	4.3	< 0.05	0.37	0.51	< 1.001	< 1.08	< 0.005	67	0.0077	0.006
GW82122	2.6	< 0.05	0.37	0.49	< 0.001	< 0.08	< 0.005	62	0.0078	0.009
GW82123	2.1	< 0.05	0.32	0.44	< 0.001	< 0.08	< 0.005	60	0.0082	0.006
GW82124	1.4	< 0.05	0.31	0.41	< 0.001	< 0.08	< 0.005	58	0.0042	< 0.004
GW82214	1.3	< 0.05	< 0.3	0.43	< 0.001	< 0.08	< 0.005	65	0.0044	< 0.004
GW82201	0.49	< 0.05	< 0.3	0.4	< 0.001	< 0.08	< 0.005	60	< 0.004	< 0.004
GW82201RA	1.49	< 1.05	< 0.3	0.4	< 1.001	< 1.08	< 0.005	60	< 1.004	< 1.004
GW82202	0.17	< 0.05	< 0.3	0.37	< 0.001	< 0.08	< 0.005	58	< 0.004	< 0.004
GW82203	0.61	< 0.05	< 0.3	0.39	< 0.001	< 0.08	< 0.005	60	0.05	< 0.004
GW82204	0.09	< 0.05	< 0.3	0.35	< 0.001	< 0.08	< 0.005	48	0.0082	< 0.004
GW82205	0.33	< 0.05	< 0.3	0.38	< 0.001	< 0.08	< 0.005	60	< 0.004	< 0.004
GW82205RC	0.33	< 0.05	< 0.3	0.38	< 0.001	< 0.08	< 0.005	60	< 0.004	< 0.004
GW82206	0.17	< 0.05	< 0.3	0.37	< 0.001	< 0.08	< 0.005	58	0.0041	< 0.004
GW82206RA	1.17	< 1.05	< 0.3	0.37	< 1.001	< 1.08	< 0.005	58	1.0041	< 1.004
GW82207	0.27	< 0.05	< 0.3	0.37	< 0.001	< 0.08	< 0.005	58	< 0.004	< 0.004
GW82208	< 0.05	< 0.05	< 0.3	0.37	< 0.001	< 0.08	< 0.005	50	< 0.004	< 0.004
GW82209	0.074	< 0.05	< 0.3	0.38	< 0.001	< 0.08	< 0.005	50	< 0.004	< 0.004
GW82213	0.98	< 0.05	< 0.3	0.42	< 0.001	< 0.08	< 0.005	61	< 0.004	< 0.004
GW82210	0.37	< 0.05	< 0.3	0.41	< 0.001	< 0.08	< 0.005	57	< 0.004	< 0.004
GW82211	2.5	< 0.05	< 0.3	0.56	< 0.001	< 0.08	< 0.005	73	0.0091	< 0.004

Notes: RA=replicate anion analysis, RC=replicate cation analysis

Appendix I: Geochemistry data (con't)

Packer and pore water samples (con't)

Well	Al (mg/L)	Sb (mg/L)	P (mg/L)	Ba (mg/L)	Be (mg/L)	B (mg/L)	Cd (mg/L)	Ca (mg/L)	Cr (mg/L)	Co (mg/L)
GW82211RA	3.5	< 1.05	< 0.3	0.56	< 1.001	< 1.08	< 0.005	73	1.0091	< 0.004
GW82212	1.6	< 0.05	< 0.3	0.54	< 0.001	< 0.08	< 0.005	61	0.0051	< 0.004
GW82325	1.7	< 0.05	0.59	0.39	< 0.001	< 0.08	< 0.005	110	0.0041	0.008
GW82325RC	1.6	< 0.05	0.59	0.38	< 0.001	< 0.08	< 0.005	110	0.0042	0.006
GW82326	4.5	< 0.05	0.35	0.5	0.001	< 0.08	< 0.005	76	0.0085	0.014
GW82326RA	5.5	< 0.05	0.35	0.5	0.001	< 1.08	< 0.005	76	0.0085	0.014
GW82327	0.72	< 0.05	< 0.3	0.29	< 0.001	< 0.08	< 0.005	59	< 0.004	< 0.004
GW82328	0.32	< 0.05	< 0.3	0.27	< 0.001	< 0.08	< 0.005	59	< 0.004	< 0.004
GW82329	0.55	< 0.05	< 0.3	0.27	< 0.001	< 0.08	< 0.005	59	0.0053	< 0.004
GW82330	0.71	< 0.05	< 0.3	0.29	< 0.001	< 0.08	< 0.005	59	< 0.004	< 0.004
GW82331	0.45	< 0.05	< 0.3	0.28	< 0.001	< 0.08	< 0.005	62	< 0.004	0.004
GW82331RA	1.45	< 1.05	< 0.3	0.28	< 1.001	< 1.08	< 0.005	62	< 0.004	0.004
GW82332	0.64	< 0.05	< 0.3	0.3	< 0.001	< 0.08	< 0.005	62	< 0.004	< 0.004
GW82333	0.37	< 0.05	< 0.3	0.29	< 0.001	< 0.08	< 0.005	61	< 0.004	< 0.004
GW82335	3.4	< 0.05	0.4	0.61	< 0.001	< 0.08	< 0.005	70	0.0056	0.010
GW82335RC	3.4	< 0.05	0.42	0.61	< 0.001	< 0.08	< 0.005	71	0.0061	0.010
GW82334	3.6	< 0.05	0.38	0.78	< 0.001	< 0.08	< 0.005	74	0.0055	0.120
PW82202	6.8	< 0.05	0.49	0.38	0.001	< 0.08	< 0.005	260	0.032	0.011
PW82202RA	7.8	< 0.05	0.49	0.38	0.001	< 1.08	< 0.005	260	0.032	0.011
PW82203	2.5	< 0.05	< 0.3	0.15	< 0.001	< 0.08	< 0.005	99	0.0097	< 0.004
PW82203RA	3.5	< 1.05	< 0.3	0.15	< 1.001	< 1.08	< 0.005	99	1.0097	< 1.004
PW82204	7.9	< 0.05	< 0.3	0.34	0.001	< 0.08	< 0.005	68	0.032	0.016
PW82204RA	8.9	< 1.05	< 0.3	0.34	0.001	< 1.08	< 0.005	68	0.032	0.016
PW82205	17	< 0.05	0.36	0.65	0.002	< 0.08	< 0.005	65	0.073	0.033
PW82205RA	18	< 0.05	0.36	0.65	0.002	< 1.08	< 0.005	65	0.073	0.033
PW82306	0.53	< 0.05	< 0.3	0.02	< 0.001	< 0.08	< 0.005	1.9	< 0.004	< 0.004
PW82306RA	1.53	< 1.05	< 0.3	0.02	< 1.001	< 1.08	< 0.005	1.9	< 1.004	< 1.004

Notes: RA=replicate anion analysis, RC=replicate cation analysis

Appendix I: Geochemistry data (con't)

Packer and pore water samples (con't)

Well	Cu (mg/L)	Fe (mg/L)	Pb (mg/L)	Mg (mg/L)	Mn (mg/L)	Mo (mg/L)	Ni (mg/L)	K (mg/L)	Se (mg/L)	Si (mg/L)	Ag (mg/L)
GW82115	< 0.007	2.2	< 0.05	8.3	0.25	< 0.04	< 0.01	< 2	< 0.005	9.2	< 0.005
GW82115RC	< 0.007	2.2	< 0.05	8.2	0.25	< 0.04	< 0.01	2.2	< 0.005	9.1	< 0.005
GW82116	< 0.007	2.3	< 0.05	8.2	0.32	< 0.04	< 0.01	< 2	< 0.005	8.6	< 0.005
GW82116RA	< 0.007	2.3	< 0.05	8.2	0.32	< 1.04	< 1.01	< 3	< 0.005	8.6	< 0.005
GW82117	< 0.007	1.6	< 0.05	8.4	0.32	< 0.04	< 0.01	2.3	< 0.005	8.6	< 0.005
GW82118	< 0.007	2.1	< 0.05	8.5	0.35	< 0.04	< 0.01	2.2	< 0.005	8.7	< 0.005
GW82119	< 0.007	1.7	< 0.05	8.5	0.36	< 0.04	< 0.01	< 2	< 0.005	8.6	< 0.005
GW82120	< 0.007	3.6	< 0.05	9	0.48	< 0.04	< 0.01	< 2	< 0.005	9.4	< 0.005
GW82121	0.01	7.8	< 0.05	10	0.87	< 0.04	< 0.01	3.1	< 0.005	12	< 0.005
GW82121RA	0.01	7.8	< 0.05	10	0.87	< 1.04	< 0.01	3.1	< 0.005	12	< 0.005
GW82122	< 0.007	9.8	< 0.05	9.8	1	< 0.04	< 0.01	2.5	< 0.005	11	< 0.005
GW82123	< 0.007	6.7	< 0.05	9.7	0.78	< 0.04	< 0.01	2.5	< 0.005	11	< 0.005
GW82124	< 0.007	4.1	< 0.05	9.6	0.66	< 0.04	< 0.01	2.7	< 0.005	9.8	< 0.005
GW82214	< 0.007	5.9	< 0.05	9	0.28	< 0.04	< 0.01	2	< 0.05	10	< 0.005
GW82201	< 0.007	2.1	< 0.05	8	0.16	< 0.04	< 0.01	< 2	< 0.05	9.8	< 0.005
GW82201RA	< 0.007	2.1	< 0.05	8	0.16	< 1.04	< 1.01	< 3	< 0.05	9.8	< 0.005
GW82202	< 0.007	0.96	< 0.05	7.7	0.14	< 0.04	< 0.01	< 2	< 0.05	9.2	< 0.005
GW82203	< 0.007	2.3	< 0.05	8	0.16	< 0.04	0.03	< 2	< 0.05	9.8	< 0.005
GW82204	< 0.007	0.58	< 0.05	7.1	0.12	< 0.04	< 0.01	< 2	< 0.05	8.6	< 0.005
GW82205	< 0.007	1.6	< 0.05	7.8	0.15	< 0.04	< 0.01	< 2	< 0.05	9.4	< 0.005
GW82205RC	< 0.007	1.6	< 0.05	7.7	0.15	< 0.04	< 0.01	< 2	< 0.05	9.4	< 0.005
GW82206	< 0.007	0.91	< 0.05	7.6	0.14	< 0.04	< 0.01	< 2	< 0.05	9.2	< 0.005
GW82206RA	< 0.007	0.91	< 0.05	7.6	0.14	< 1.04	< 1.01	< 3	< 0.05	9.2	< 0.005
GW82207	< 0.007	0.9	< 0.05	7.7	0.15	< 0.04	< 0.01	< 2	< 0.05	9.3	< 0.005
GW82208	< 0.007	0.2	< 0.05	7.6	0.13	< 0.04	< 0.01	< 2	< 0.05	9.2	< 0.005
GW82209	< 0.007	0.47	< 0.05	7.6	0.13	< 0.04	< 0.01	< 2	< 0.05	8.8	< 0.005
GW82213	< 0.007	2.5	< 0.05	8.9	0.19	< 0.04	0.01	< 2	< 0.05	10	< 0.005
GW82210	< 0.007	1.3	< 0.05	8.1	0.15	< 0.04	< 0.01	2.1	< 0.05	9	< 0.005
GW82211	0.009	6.1	< 0.05	10	0.34	< 0.04	< 0.01	2.7	< 0.05	11	< 0.005

Appendix I: Geochemistry data (con't)

Packer and pore water samples (con't)

Well	Cu (mg/L)	Fe (mg/L)	Pb (mg/L)	Mg (mg/L)	Mn (mg/L)	Mo (mg/L)	Ni (mg/L)	K (mg/L)	Se (mg/L)	Si (mg/L)	Ag (mg/L)
GW82211RA	0.009	6.1	< 0.05	10	0.34	< 1.04	< 0.01	2.7	< 0.05	11	< 0.005
GW82212	< 0.007	3.5	< 0.05	10	0.22	< 0.04	< 0.01	2.3	< 0.005	11	< 0.005
GW82325	< 0.007	6.8	< 0.05	8.7	1.2	< 0.04	< 0.01	3.1	< 0.005	9.6	< 0.005
GW82325RC	< 0.007	6.7	< 0.05	8.6	1.2	< 0.04	< 0.01	2.6	< 0.005	9.5	< 0.005
GW82326	0.009	11	< 0.05	9.9	0.8	< 0.04	< 0.01	2.4	< 0.005	14	< 0.005
GW82326RA	0.009	11	< 0.05	9.9	0.8	< 1.04	< 0.01	2.4	< 0.005	14	< 0.005
GW82327	< 0.007	3.4	< 0.05	7.6	0.49	< 0.04	< 0.01	< 2	< 0.005	8.8	< 0.005
GW82328	< 0.007	2.2	< 0.05	7.4	0.44	< 0.04	< 0.01	< 2	< 0.005	8.8	< 0.005
GW82329	< 0.007	2.6	< 0.05	7.5	0.45	< 0.04	< 0.01	< 2	< 0.05	9	< 0.005
GW82330	< 0.007	6.2	< 0.05	7.5	0.48	< 0.04	< 0.01	< 2	< 0.05	9.3	< 0.005
GW82331	< 0.007	2.9	< 0.05	7.8	0.45	< 0.04	< 0.01	< 2	< 0.05	9.3	< 0.005
GW82331RA	< 0.007	2.9	< 0.05	7.8	0.45	< 1.04	< 1.01	< 3	< 0.05	9.3	< 0.005
GW82332	< 0.007	3.7	< 0.05	7.9	0.48	< 0.04	< 0.01	< 2	< 0.05	9.6	< 0.005
GW82333	< 0.007	202	< 0.05	7.7	0.45	< 0.04	< 0.01	< 2	< 0.05	9.1	< 0.005
GW82335	0.015	16	< 0.05	9.5	1.6	< 0.04	< 0.01	2.5	< 0.05	14	< 0.005
GW82335RC	0.016	16	< 0.05	9.6	1.6	< 0.04	< 0.01	3.1	< 0.05	14	< 0.005
GW82334	0.018	14	< 0.05	10	2.3	< 0.04	< 0.01	3.1	< 0.05	14	< 0.005
PW82202	0.008	11	0.087	12	3	< 0.04	0.02	7.4	< 0.05	15	< 0.005
PW82202RA	0.008	11	0.087	12	3	< 1.04	0.02	7.4	< 0.05	15	< 0.005
PW82203	< 0.007	3.3	< 0.05	8.6	1.4	< 0.04	< 0.01	6.5	< 0.05	6.8	< 0.005
PW82203RA	< 0.007	3.3	< 0.05	8.6	1.4	< 1.04	< 0.01	6.5	< 0.05	6.8	< 0.005
PW82204	0.011	11	< 0.05	5	1.6	< 0.04	0.01	4	< 0.05	17	0.014
PW82204RA	0.011	11	< 0.05	5	1.6	< 1.04	0.01	4	< 0.05	17	0.014
PW82205	0.018	23	< 0.05	8.2	2.9	< 0.04	0.05	5.4	< 0.05	32	0.008
PW82205RA	0.018	23	< 0.05	8.2	2.9	< 1.04	0.05	5.4	< 0.05	32	0.008
PW82306	< 0.007	0.83	< 0.05	0.34	0.12	< 0.04	< 0.01	< 2	< 0.05	5.6	< 0.005
PW82306RA	< 0.007	0.83	< 0.05	0.34	0.12	< 1.04	< 1.01	< 3	< 0.05	5.6	< 0.005

Notes: RA=replicate anion analysis, RC=replicate cation analysis

Appendix I: Geochemistry data (con't)

Packer and pore water samples (con't)

Well	Na (mg/L)	Sr (mg/L)	Li (mg/L)	V (mg/L)	Zn (mg/L)	pH	Temp (deg C)	Cond. (umho/cm)	Turb. (ppm)
GW82115	6.3	0.37	0.014	0.0029	0.140			339.0	
GW82115RC	6.2	0.37	0.014	0.0029	0.130				
GW82116	6.5	0.41	0.014	0.0029	0.240			340.0	
GW82116RA	6.5	0.41	0.014	0.0029	0.240				
GW82117	6.8	0.43	0.014	0.0034	0.300			344.0	
GW82118	6.8	0.44	0.013	0.0035	0.250			345.0	
GW82119	7	0.45	0.013	< 0.002	0.220			346.0	
GW82120	7.2	0.47	0.015	0.0043	0.260			345.0	
GW82121	7.1	0.5	0.021	0.0098	0.310			347.0	
GW82121RA	7.1	0.5	0.021	0.0098	0.310				
GW82122	7.1	0.5	0.019	0.0087	0.610			345.0	
GW82123	7.3	0.51	0.017	0.0066	0.410				
GW82124	7.9	0.53	0.016	0.0056	0.480			347.0	
GW82214	6.6	0.46	0.014	0.0047	0.590			348.0	
GW82201	6.5	0.45	0.012	0.0023	0.280			311.0	
GW82201RA	6.5	0.45	0.012	0.0023	0.280				
GW82202	6.5	0.45	0.012	< 0.002	0.270			344.0	
GW82203	6.7	0.45	0.013	0.0035	0.190			341.0	
GW82204	6.1	0.41	0.01	< 0.002	0.100			315.0	
GW82205	6.5	0.45	0.012	0.0025	0.140			342.0	
GW82205RC	6.5	0.45	0.013	0.0035	0.140				
GW82206	6.6	0.45	0.012	< 0.002	0.130			342.0	
GW82206RA	6.6	0.45	0.012	< 0.002	0.130				
GW82207	6.6	0.44	0.012	< 0.002	0.140			341.0	
GW82208	6.9	0.48	0.012	0.0021	0.092			339.0	
GW82209	6.9	0.47	0.012	< 0.002	0.150			334.0	
GW82213	7	0.5	0.014	0.0023	0.510			338.0	
GW82210	7	0.53	0.013	< 0.002	0.140			336.0	
GW82211	8.2	0.66	0.019	0.0069	0.380			328.0	

Notes: RA=replicate anion analysis, RC=replicate cation analysis

Appendix I: Geochemistry data (con't)

Packer and pore water samples (con't)

Well	Na (mg/L)	Sr (mg/L)	Li (mg/L)	V (mg/L)	Zn (mg/L)	pH	Temp (deg C)	Cond. (umho/cm)	Turb. (ppm)
GW82211RA	8.2	0.66	0.019	0.0069	0.380				
GW82212	8.9	0.68	0.017	0.0034	0.100			344.0	
GW82325	6.4	0.45	0.015	0.0066	0.240			326.0	
GW82325RC	6	0.44	0.014	0.0061	0.240				
GW82326	6.2	0.39	0.021	0.011	0.400			350.0	
GW82326RA	6.2	0.39	0.021	0.011	0.400				
GW82327	6.3	0.37	0.013	0.004	0.190			315.0	
GW82328	6.4	0.37	0.011	0.0025	0.130			349.0	
GW82329	6.2	0.37	0.011	0.0026	0.170			349.0	
GW82330	6.4	0.37	0.012	0.0036	0.310			352.0	
GW82331	6.7	0.39	0.013	0.0027	0.140			350.0	
GW82331RA	6.7	0.39	0.013	0.0027	0.140				
GW82332	6.9	0.4	0.013	0.0023	0.190			335	
GW82333	6.9	0.39	0.012	< 0.002	0.120			332	
GW82335	7.9	0.45	0.019	0.012	0.720			345	
GW82335RC	7.8	0.45	0.02	0.013	0.720				
GW82334	9.1	0.49	0.02	0.011	0.580			339	
PW82202	21	0.52	0.013	0.016	0.037				
PW82202RA	21	0.52	0.013	0.016	0.037				
PW82203	17	0.19	< 0.005	0.0075	0.095				
PW82203RA	17	0.19	< 1.005	0.0075	0.095				
PW82204	3.5	0.13	0.012	0.012	0.056				
PW82204RA	3.5	0.13	0.012	0.012	0.056				
PW82205	3.3	0.13	0.023	0.025	0.084				
PW82205RA	3.3	0.13	0.023	0.025	0.084				
PW82306	1.2	0.005	< 0.005	< 0.002	0.014				
PW82306RA	1.2	0.005	< 1.005	0.002	0.014				

Notes: RA=replicate anion analysis, RC=replicate cation analysis

Multilevel well samples

Appendix I: Geochemistry data (con't)

Well	Sample Date	depth	pH	Alk.	Est. % HCO3	HCO3 (mg/L)	CO3 (mg/L)	Br (mg/L)	Cl (mg/L)	F (mg/L)	NO3 (mg/L)	PO4 (mg/L)	SO4 (mg/L)
GW462	1/25/95	20-70	7.58	186	100%	226.77	0.00	0.35	0.85	< 0.1	< 0.1	< 0.5	6.8
GW821A	1/24/95	45.50	8.37	190.1	100%	231.77	0.00	< 0.1	3.1	0.1	1.6	< 0.5	30
GW821B	1/24/95	38.50	8.12	200.6	100%	244.57	0.00	< 0.1	1.5	< 0.1	1.9	< 0.5	45
GW821C	1/24/95	34.00	7.99	195.6	100%	238.48	0.00	< 0.1	1.5	< 0.1	1.3	< 0.5	31
GW821CRA	1/24/95	34.00	7.99	195.6	100%	238.48	0.00	< 0.1	1.4	< 0.1	1.2	< 0.5	31
GW821D	1/24/95	25.50	7.82	175.6	100%	214.09	0.00	< 0.1	1.1	0.12	< 0.1	< 0.5	7.3
GW821DD	1/24/95	25.50	7.82	173.3	100%	211.29	0.00	< 0.1	0.92	< 0.1	0.32	< 0.5	6.6
GW821E	1/24/95	20.00	7.86	151.2	100%	184.35	0.00	< 0.1	0.94	< 0.1	0.55	< 0.5	6.9
GW821ERC	1/24/95	20.00	7.86	151.2	100%	184.35	0.00	< 0.1	0.94	< 0.1	0.55	< 0.5	6.9
GW822A	1/24/95	65.00	7.76	179.2	100%	218.48	0.00	< 0.1	0.82	< 0.1	< 0.1	< 0.5	11
GW822ARC	1/24/95	65.00	7.76	179.2	100%	218.48	0.00	< 0.1	0.82	< 0.1	< 0.1	< 0.5	11
GW822AD	1/24/95	65.00	7.71	183.3	100%	223.48	0.00	< 0.1	0.83	< 0.1	< 0.1	< 0.5	10
GW822B	1/24/95	54.00	7.77	191.4	100%	233.36	0.00	< 0.1	1	< 0.1	0.51	< 0.5	20
GW822C	1/25/95	48.50	8.04	216.4	100%	263.84	0.00	0.14	3.7	< 0.1	0.9	< 0.5	110
GW822D	1/24/95	34.00	7.85	204.5	100%	249.33	0.00	< 0.1	1.5	< 0.1	0.57	< 0.5	41
GW822DRA	1/24/95	34.00	7.85	204.5	100%	249.33	0.00	< 0.1	1.4	< 0.1	0.58	< 0.5	41
GW822E	1/24/95	29.50	8.28	183.3	100%	223.48	0.00	4.7	1	< 0.1	0.32	< 0.5	6.9
GW823A	1/25/95	65.50		198.1	100%	241.53	0.00	< 0.1	1.3	0.17	0.36	< 0.5	11
GW823AD	1/25/95	65.50	8.01	198.1	100%	241.53	0.00	< 0.1	1.3	0.17	0.37	< 0.5	11
GW823B	1/23/95	48.00	7.75	185.6	100%	226.29	0.00	0.34	1	0.1	0.33	< 0.5	11
GW823C	1/23/95	35.50	7.86	225.6	100%	275.05	0.00	0.42	2.9	< 0.1	0.56	< 0.5	28
GW823CRA	1/23/95	35.50	7.86	225.6	100%	275.05	0.00	0.41	2.9	< 0.1	0.56	< 0.5	28
GW823D	1/23/95	27.00	7.71	270.3	100%	329.55	0.00	1.8	5.5	< 0.1	< 0.1	< 0.5	170
GW823DRC	1/23/95	27.00	7.76	270.3	100%	329.55	0.00	1.8	5.5	< 0.1	< 0.1	< 0.5	170

Notes: RA=replicate anion analysis, RC=replicate cation analysis, D=duplicate sample

Appendix I: Geochemistry data (con't)

Multilevel well samples (con't)

Well	Al (mg/L)	Sb (mg/L)	P (mg/L)	Ba (mg/L)	Be (mg/L)	B (mg/L)	Cd (mg/L)	Ca (mg/L)	Cr (mg/L)	Co (mg/L)
GW462	< 0.05	< 0.05	< 0.3	0.46	< 0.001	< 0.08	< 0.005	52	< 0.004	< 0.004
GW821A	2.5	< 0.05	< 0.3	0.18	< 0.001	< 0.08	< 0.005	28	< 0.004	< 0.004
GW821B	1.8	< 0.05	< 0.3	0.17	< 0.001	< 0.08	< 0.005	29	< 0.004	< 0.004
GW821C	3.8	< 0.05	< 0.3	0.23	< 0.001	< 0.08	< 0.005	41	< 0.004	< 0.004
GW821CRA	3.8	< 0.05	< 0.3	0.23	< 0.001	< 0.08	< 0.005	41	< 0.004	< 0.004
GW821D	0.73	< 0.05	< 0.3	0.21	< 0.001	< 0.08	< 0.005	56	< 0.004	< 0.004
GW821DD	< 0.05	< 0.05	< 0.3	0.02	< 0.001	< 0.08	< 0.005	55	< 0.004	< 0.004
GW821E	< 0.05	< 0.05	< 0.3	0.14	< 0.001	< 0.08	< 0.005	47	< 0.004	< 0.004
GW821ERC	< 0.05	< 0.05	< 0.3	0.14	< 0.001	< 0.08	< 0.005	47	< 0.004	< 0.004
GW822A	0.16	< 0.05	< 0.3	0.4	< 0.001	< 0.08	< 0.005	43	< 0.004	< 0.004
GW822ARC	1.7	< 0.05	< 0.3	0.4	< 0.001	< 0.08	< 0.005	43	< 0.004	< 0.004
GW822AD	0.15	< 0.05	< 0.3	0.4	< 0.001	< 0.08	< 0.005	43	< 0.004	< 0.004
GW822B	0.053	< 0.05	< 0.3	0.36	< 0.001	< 0.08	< 0.005	51	< 0.004	< 0.004
GW822C	0.053	< 0.05	< 0.3	0.16	< 0.001	< 0.08	< 0.005	49	< 0.004	< 0.004
GW822D	0.19	< 0.05	< 0.3	0.37	< 0.001	< 0.08	< 0.005	58	< 0.004	< 0.004
GW822DRA	0.19	< 0.05	< 0.3	0.37	< 0.001	< 0.08	< 0.005	58	< 0.004	< 0.004
GW822E	< 0.05	< 0.05	< 0.3	0.21	< 0.001	< 0.08	< 0.005	62	< 0.004	< 0.004
GW823A	0.76	< 0.05	< 0.3	0.17	< 0.001	< 0.08	< 0.005	38	< 0.004	< 0.004
GW823AD	< 0.05	< 0.05	< 0.3	0.19	< 0.001	< 0.08	< 0.005	46	< 0.004	< 0.004
GW823B	< 0.05	< 0.05	< 0.3	0.11	< 0.001	< 0.08	< 0.005	51	< 0.004	< 0.004
GW823C	1.9	< 0.05	< 0.3	0.15	< 0.001	< 0.08	< 0.005	55	< 0.004	< 0.004
GW823CRA	1.9	< 0.05	< 0.3	0.15	< 0.001	< 0.08	< 0.005	55	< 0.004	< 0.004
GW823D	0.96	< 0.05	< 0.3	0.21	< 0.001	< 0.08	< 0.005	61	< 0.004	< 0.004
GW823DRC	1.3	< 0.05	< 0.3	0.21	< 0.001	< 0.08	< 0.005	59	< 0.004	< 0.004

Notes: RA=replicate anion analysis, RC=replicate cation analysis, D=duplicate sample

Multilevel well samples (con't) **Appendix I: Geochemistry data (con't)**

Well	Cu (mg/L)	Fe (mg/L)	Pb (mg/L)	Mg (mg/L)	Mn (mg/L)	Mo (mg/L)	Ni (mg/L)	K (mg/L)	Se (mg/L)	Si (mg/L)	Ag (mg/L)
GW462	< 0.01	0.21	< 0.05	9.4	0.28	< 0.04	< 0.01	2.4	< 0.05	9.4	< 0.005
GW821A	< 0.01	1.2	< 0.05	6.5	0.85	< 0.04	< 0.01	3.1	< 0.05	13	< 0.005
GW821B	< 0.01	0.62	< 0.05	7	0.51	< 0.04	< 0.01	2.2	< 0.05	13	< 0.005
GW821C	< 0.01	1.5	< 0.05	7.6	0.84	< 0.04	< 0.01	< 2	< 0.05	17	< 0.005
GW821CRA	< 0.01	1.5	< 0.05	7.6	0.84	< 0.04	< 0.01	< 2	< 0.05	17	< 0.005
GW821D	< 0.01	0.43	< 0.05	7.1	0.35	< 0.04	< 0.01	< 2	< 0.05	9.3	< 0.005
GW821DD	< 0.01	< 0.05	< 0.05	7	0.31	< 0.04	< 0.01	< 2	< 0.05	7.8	< 0.005
GW821E	< 0.01	< 0.05	< 0.05	5.9	0.36	< 0.04	< 0.01	< 2	< 0.05	7.3	< 0.005
GW821ERC	< 0.01	< 0.05	< 0.05	5.9	0.36	< 0.04	< 0.01	< 2	< 0.05	7.3	< 0.005
GW822A	< 0.01	0.31	< 0.05	9.6	0.16	< 0.04	< 0.01	2.9	< 0.05	9.6	< 0.005
GW822ARC	< 0.01	0.32	< 0.05	9.6	0.16	< 0.04	< 0.01	2.8	< 0.05	9.6	< 0.005
GW822AD	< 0.01	0.31	< 0.05	9.5	0.16	< 0.04	< 0.01	2.8	< 0.05	9.5	< 0.005
GW822B	< 0.01	< 0.05	< 0.05	9	0.1	< 0.04	< 0.01	< 2	< 0.05	8.9	< 0.005
GW822C	< 0.01	0.07	< 0.05	7.7	0.63	< 0.04	< 0.01	3.2	< 0.05	7.7	< 0.005
GW822D	< 0.01	0.19	< 0.05	9.4	0.17	< 0.04	< 0.01	2.4	< 0.05	10	< 0.005
GW822DRA	< 0.01	0.19	< 0.05	9.4	0.17	< 0.04	< 0.01	2.4	< 0.05	10	< 0.005
GW822E	< 0.01	< 0.05	< 0.05	6.1	0.021	< 0.04	< 0.01	< 2	< 0.05	7.1	< 0.005
GW823A	< 0.01	0.43	< 0.05	6.1	1.8	< 0.04	< 0.01	< 2	< 0.05	6.9	< 0.005
GW823AD	< 0.01	< 0.05	< 0.05	7.3	2.1	< 0.04	< 0.01	< 2	< 0.05	6.7	< 0.005
GW823B	< 0.01	< 0.05	< 0.05	6.2	0.3	< 0.04	< 0.01	< 2	< 0.05	7.6	< 0.005
GW823C	< 0.01	0.84	< 0.05	6.8	0.54	< 0.04	< 0.01	2.2	< 0.05	11	< 0.005
GW823CRA	< 0.01	0.84	< 0.05	6.8	0.54	< 0.04	< 0.01	2.2	< 0.05	11	< 0.005
GW823D	< 0.01	0.76	< 0.05	7.1	5.8	< 0.04	< 0.01	< 2	< 0.05	8.2	< 0.005
GW823DRC	< 0.01	0.9	< 0.05	7.1	5.8	< 0.04	< 0.01	2.4	< 0.05	9	< 0.005

Notes: RA=replicate anion analysis, RC=replicate cation analysis, D=duplicate sample

Appendix I: Geochemistry data (con't)

Multilevel well samples (con't)

Well	Na (mg/L)	Sr (mg/L)	Li (mg/L)	V (mg/L)	Zn (mg/L)	pH	Temp (deg C)	Cond. (umho/cm)	Turb. (ppm)
GW462	8.5	0.67	0.011	< 0.002	0.007	7.5	11.9	0.07	172
GW821A	60	1.2	0.016	< 0.002	0.038	7.9	7.7	0.1	140
GW821B	68	0.98	0.016	< 0.002	0.010	7.6	7.2	0.17	100
GW821C	47	1	0.013	< 0.002	0.015	7.5	6.9	0.1	400
GW821CRA	47	1	0.013	< 0.002	0.015	7.5	6.9	0.1	400
GW821D	7.4	0.65	0.01	< 0.002	0.007	7.6	5.6	0.01	330
GW821DD	7.4	0.56	0.012	< 0.002	0.006	7.6	5.6	0.01	330
GW821E	6.8	0.21	0.008	< 0.002	< 0.005	7.7	5.6	0.04	140
GW821ERC	6.8	0.21	0.007	< 0.002	< 0.005	7.7	5.6	0.04	140
GW822A	18	0.82	0.014	< 0.002	0.010	7.5	10	0.04	210
GW822ARC	18	0.82	0.013	< 0.002	0.010	7.5	10	0.04	210
GW822AD	18	0.81	0.013	< 0.002	0.010	7.5	10	0.04	210
GW822B	21	0.67	0.016	< 0.002	0.012	7.3	7.5	0.04	190
GW822C	82	0.94	0.026	< 0.002	0.070	7.5	3.6	0.03	200
GW822D	33	0.57	0.001	< 0.002	0.001	7.4	4.9	0.07	130
GW822DRA	33	0.57	0.001	< 0.002	0.001	7.4	4.9	0.07	130
GW822E	5	0.36	0.006	< 0.002	0.011	7.4	11.2	0.05	60
GW823A	24	1.1	0.006	< 0.002	0.027	8.1	5.7	0.05	310
GW823AD	29	0.53	0.006	< 0.002	0.008	8.1	5.7	0.05	310
GW823B	19	0.46	0.007	< 0.002	0.006	7.4	10.9	0.06	195
GW823C	46	1.3	0.007	< 0.002	0.010	7.3	9.7	0.17	270
GW823CRA	46	1.3	0.007	< 0.002	0.010	7.3	9.7	0.17	270
GW823D	120	1.7	< 0.005	< 0.002	0.008	7.2	10.1	0.51	330
GW823DRC	120	1.7	< 0.005	< 0.002	0.009	7.2	10.1	0.51	330

Notes: RA=replicate anion analysis, RC=replicate cation analysis, D=duplicate sampl

Appendix J: GW821 Packer Major Ions

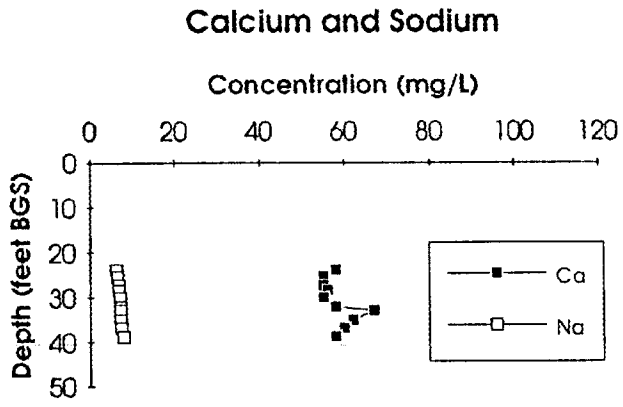

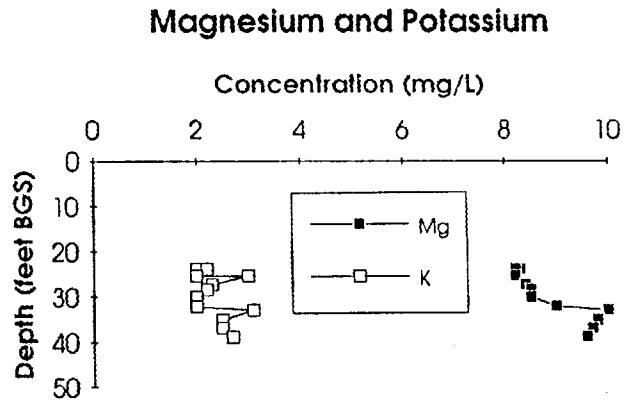

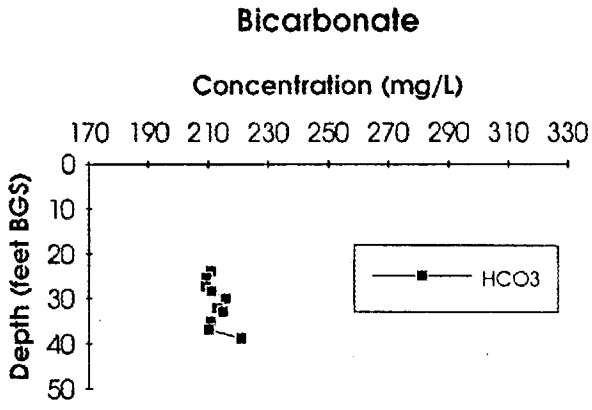

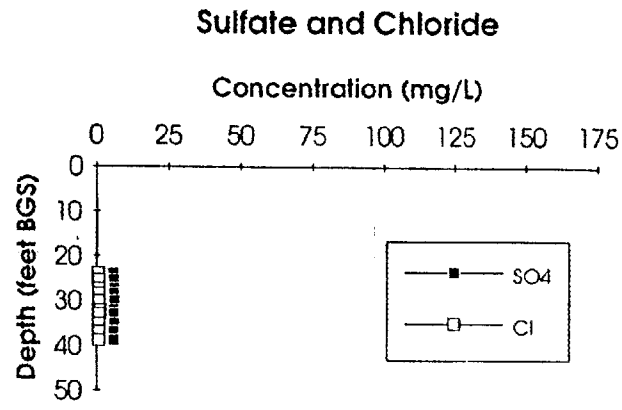

Appendix J: GW822 Packer Major Ions

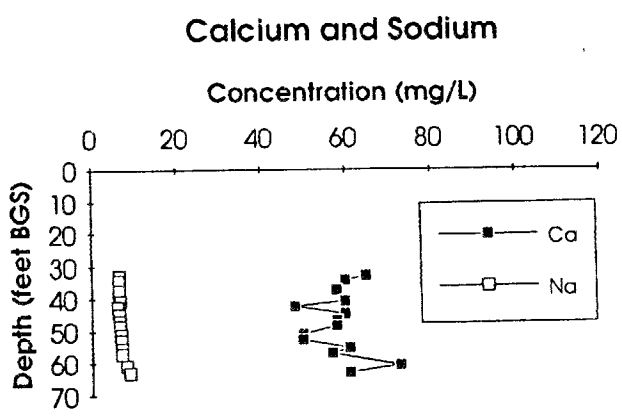

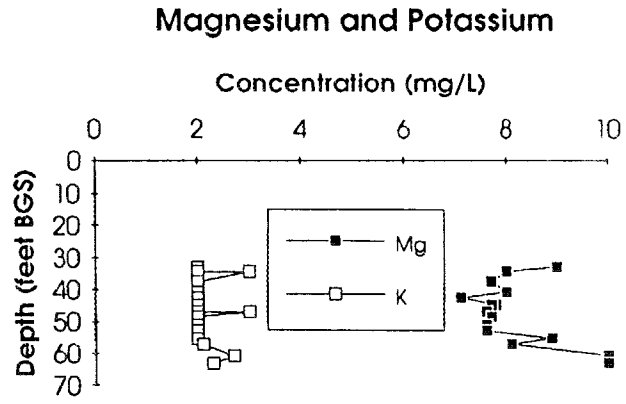

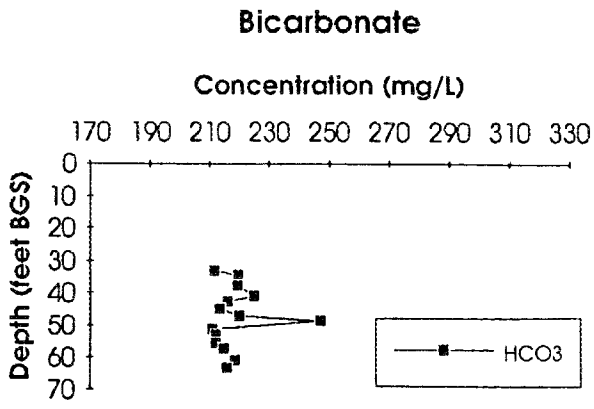

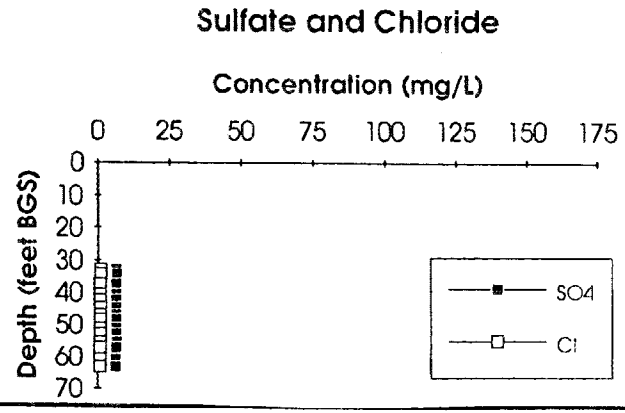

Appendix J: GW823 Packer Major Ions

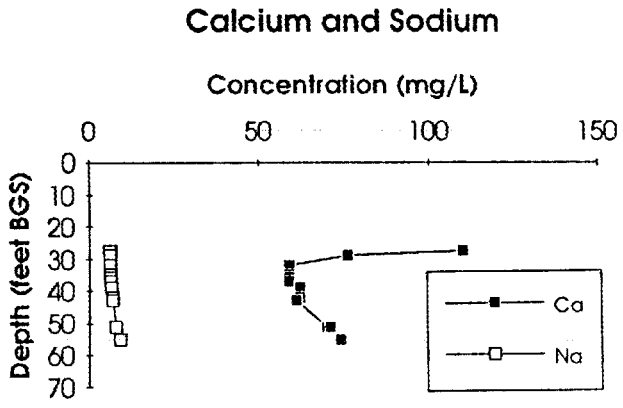

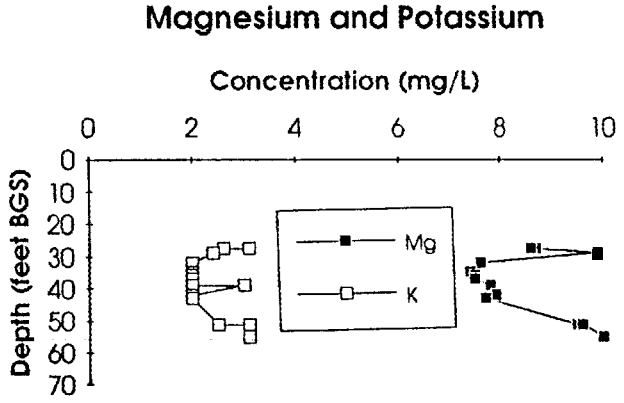

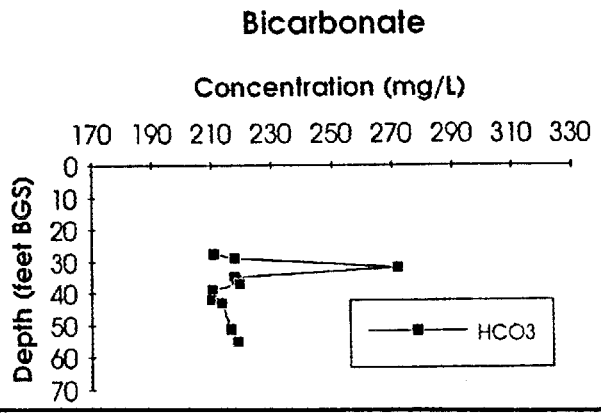

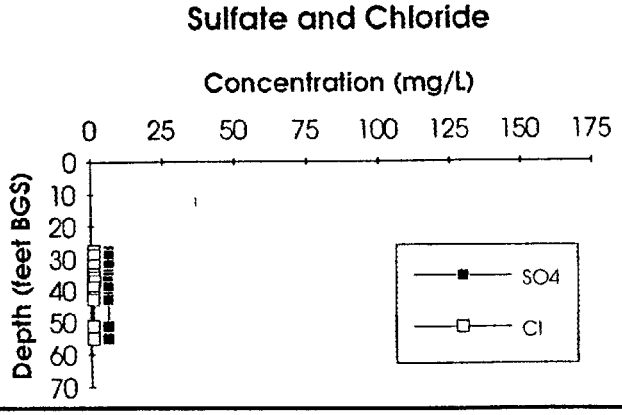

Appendix J: GW821 Packer Minor Ions

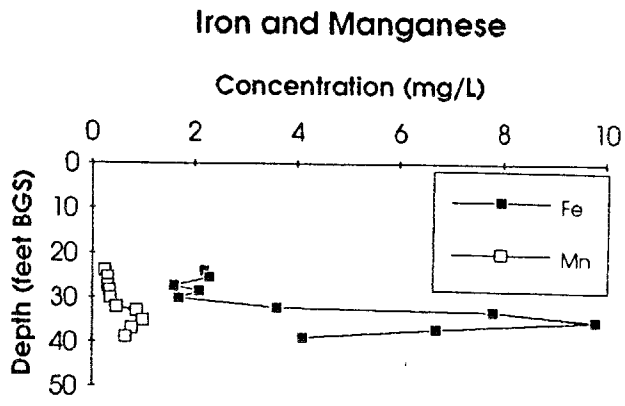

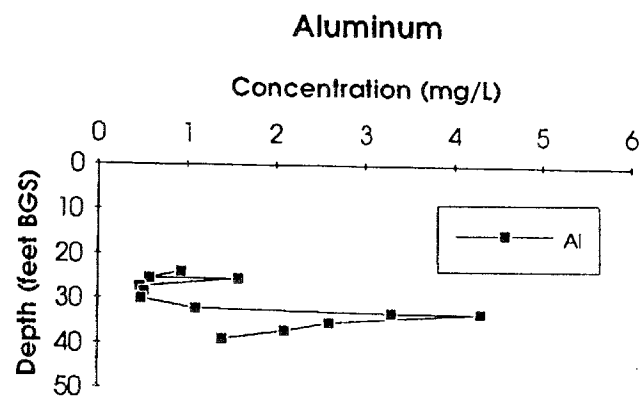

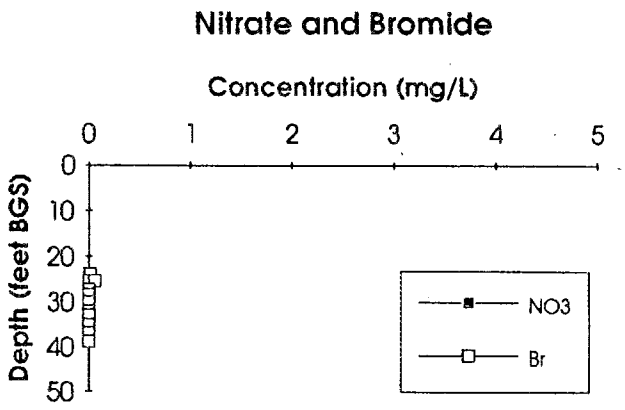

Appendix J: GW822 Packer Minor Ions

Iron and Manganese

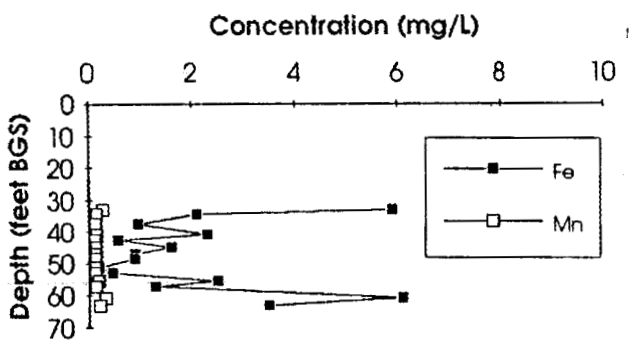

Aluminum

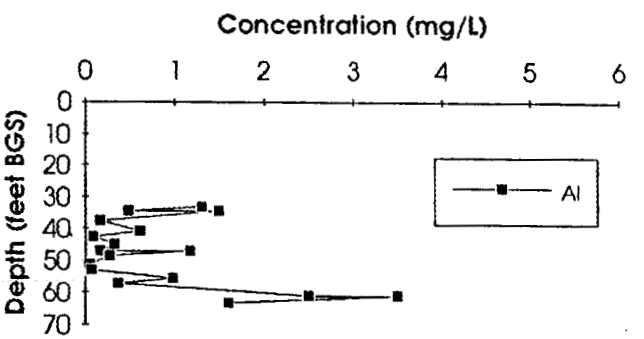

Nitrate and Bromide

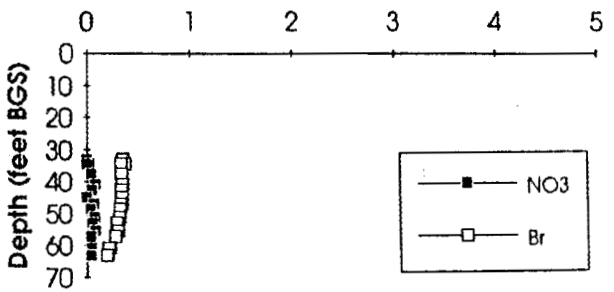

Appendix J: GW823 Packer Minor Ions

Iron and Manganese

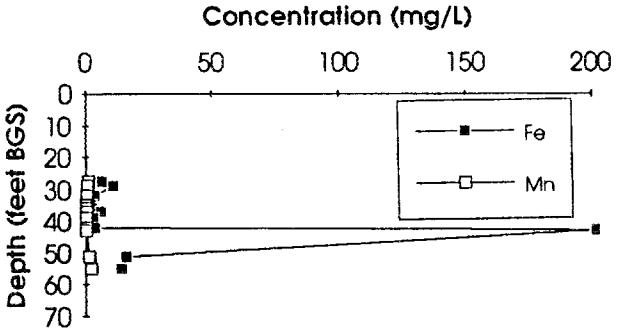

Aluminum

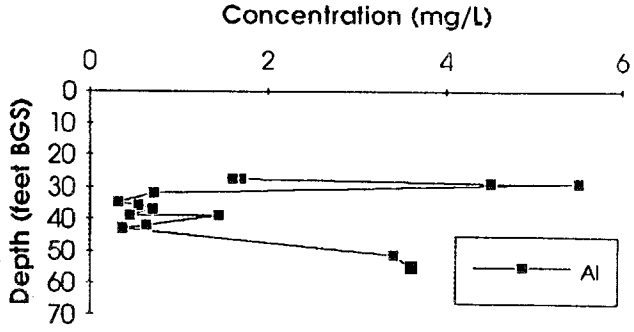

Nitrate and Bromide

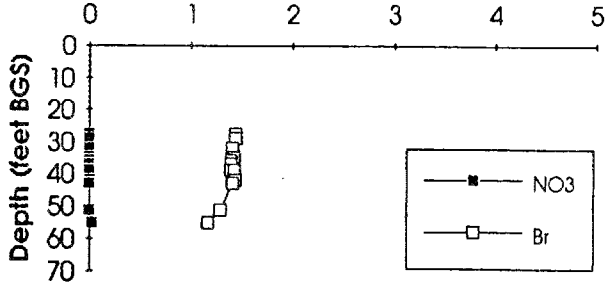

Appendix K:
PHREEQE Input File—GW821, field pH and D.O. of 3 mg/l

```
000010000  0 0      0.0
ELEMENTS
C       15  61.017

SOLUTION 1
GW821A, USE ALKALINITY (HCO3-) FOR C
11 15 2        7.9  11.94        7.7 1.0
  4     28.00  5      6.50  6     60.00  7      3.10  8      1.20
  9     0.085  15  231.7700  14       3.1  16      30.0  17       1.6
 13      13.0
END

000010000  0 0      0.0
ELEMENTS
C       15  61.017

SOLUTION 1
GW821B, USE ALKALINITY (HCO3-) FOR C
11 15 2        7.6  12.24        7.2 1.0
  4     29.00  5      7.00  6     68.00  7      2.20  8      0.62
  9     0.510  15  244.5700  14       1.5  16      45.  17       1.9
 13      13.0
END

000010000  0 0      0.0
ELEMENTS
C       15  61.017

SOLUTION 1
GW821C, USE ALKALINITY (HCO3-) FOR C
11 15 2        7.5  12.34        6.9 1.0
  4       41  5      7.6  6      47.  7      0.00  8      1.50
  9     0.840  15    238.48  14       1.5  16      31.  17       1.3
 13       17
END

000010000  0 0      0.0
ELEMENTS
C       15  61.017

SOLUTION 1
GW821D, USE ALKALINITY (HCO3-) FOR C
11 15 2        7.6  12.24        10. 1.0
```

```
 4      56.  5      7.1  6      7.4  7      0.00  8      0.43
 9    0.350  15    214.09  14      1.1  16      7.3  17      0.0
 13      9.3
END

000010000  0 0      0.0
ELEMENTS
C       15  61.017

SOLUTION 1
GW821E, USE ALKALINITY (HCO3-) FOR C
11 15 2        7.7  12.14        10. 1.0
 4      47.  5      5.9  6      6.8  7      0.00  8      0.05
 9    0.360  15    184.35  14      0.94  16      6.9  17      0.55
 13      7.3
END
```

PHREEQE Input File—GW822, FIELD PH, D.O. 3mg/l

```
000010000  0 0      0.0
ELEMENTS
C       15  61.017

SOLUTION 1
GW822A, USE ALKALINITY (HCO3-) FOR C
11 15 2        7.50  12.34        10. 1.0
 4      43  5      9.6  6      18  7      2.9  8      .31
 9      .16  15    218.48  14      .82  16      11.0  17      0.0
 13      9.6
END

000010000  0 0      0.0
ELEMENTS
C       15  61.017

SOLUTION 1
GW822B, USE ALKALINITY (HCO3-) FOR C
11 15 2        7.30  12.54        7.5 1.0
 4      51.  5      9.0  6      21.  7      0.  8      0.05
 9      0.1  15    233.36  14      1.0  16      20.  17      .51
 13      8.9
END

000010000  0 0      0.0
ELEMENTS
```

```
C       15  61.017

SOLUTION 1
GW822C, USE ALKALINITY (HCO3-) FOR C
11 15 2       7.50  12.24        3.6 1.0
  4      49.  5      7.7  6      82.  7      3.2  8      0.07
  9     0.63  15    263.84  14      3.7  16      110.  17      0.9
 13      7.7
END

000010000  0 0      0.0
ELEMENTS
C       15  61.017

SOLUTION 1
GW822D, USE ALKALINITY (HCO3-) FOR C
11 15 2       7.40  12.44        4.9 1.0
  4      58.  5      9.4  6      33.  7      2.4  8      0.19
  9     0.17  15    249.33  14      1.5  16      41.  17      0.57
 13      10.
END

000010000  0 0      0.0
ELEMENTS
C       15  61.017

SOLUTION 1
GW822E, USE ALKALINITY (HCO3-) FOR C
11 15 2       7.40  12.44        11.2 1.0
  4      62.  5      6.1  6      5.0  7      0.00  8      0.05
  9    0.021  15    223.48  14      1.0  16      6.9  17      0.32
 13      7.1
END
```

PHREEQE Input File—GW823 FIELD PH, D.O. 3 mg/l

```
000010000  0 0      0.0
ELEMENTS
C       15  61.017

SOLUTION 1
GW823A, USE ALKALINITY (HCO3-) FOR C
11 15 2       8.10  11.74        5.7 1.0
  4      38.  5      6.1  6      24  7      0.0  8      .43
  9      1.8  15    241.53  14      1.3  16      11.0  17      0.36
```

```
 13      6.9
END

000010000  0 0      0.0
ELEMENTS
C       15  61.017

SOLUTION 1
GW823B, USE ALKALINITY (HCO3-) FOR C
11 15 2       7.40  12.44       10.9 1.0
  4      51.  5      6.2  6      19.  7      0.  8      0.05
  9      0.3  15    226.29  14      1.0  16      11.  17      0.33
 13      7.6
END

000010000  0 0      0.0
ELEMENTS
C       15  61.017

SOLUTION 1
GW823C, USE ALKALINITY (HCO3-) FOR C
11 15 2       7.30  12.54       9.7 1.0
  4      55.  5      6.8  6      46.  7      2.2  8      0.84
  9      0.54  15    275.05  14      2.9  16      28.  17      0.56
 13      11.
END

000010000  0 0      0.0
ELEMENTS
C       15  61.017

SOLUTION 1
GW823D, USE ALKALINITY (HCO3-) FOR C
11 15 2       7.20  12.64       9.7 1.0
  4      61.  5      7.1  6      120.  7      0.0  8      0.76
  9      5.8  15    329.55  14      5.5  16      170.  17      0.00
 13      8.2
END
```

Appendix K:
PHREEQE Input File: Conservative Mixing Types 1 and 2 waters--> Type 3?


```
000010100  0 0
ELEMENTS
C       15   61.0171

SOLUTION 1
Type 1 water - 822E
11 15 2       7.40  12.44       11.2 1.0
  4      62.  5      6.1  6      5.0  7      0.00  8      0.05
  9    0.021  15    223.48  14      1.0  16      6.9  17      0.32
 13      7.1
MIXING with type 2 water - 823D
001011100  1 0
ELEMENTS
C       15   100.

SOLUTION 2
GW823D (Type 2), USE ALKALINITY (HCO3-) FOR C
11 15 2       7.20  12.64       9.7 1.0
  4      61.  5      7.1  6      120.  7      0.0  8      0.76
  9      5.8  15    329.55  14      5.5  16      170.  17      0.00
 13      8.2
STEPS
    0.7
END
```

Appendix L: U.W. and Field Sample Numbers

		where referenced		
U.W. Sample#	**Field Sample #**	**Tables**	**Figures**	
U.W. 1786/1	821-14	Table 4-2	Fig. 4-1	
U.W. 1786/2	821-10	Table 4-3		
U.W. 1786/3	821-2R	Table 4-4		
U.W. 1786/4	821-2G	Table 4-5		
U.W. 1786/5	821-5	Table 4-6		
U.W. 1786/6	822-14	Table 4-7		
U.W. 1786/7	822-18	Table 4-8		
U.W. 1786/8	822-1	Table 4-9		
U.W. 1786/9	822-3grey	Table 4-10		
U.W. 1786/10	822-2blk	Table 4-11		
U.W. 1786/11	822-13	Table 4-12		
U.W. 1786/12	822-2	Table 4-13	Fig. 4-1	Fig. 4-6
U.W. 1786/13	823-7	Table 4-14		
U.W. 1786/14	823-6	Table 4-15	Fig. 4-7	
U.W. 1786/15	823-23	Table 4-16		
U.W. 1786/16	823-9	Table 4-17		
U.W. 1786/17	823-20	Table 4-18	Fig. 4-1	
U.W. 1786/18	823-22a	Table 4-19		
U.W. 1786/19	823-22b	Table 4-20		
U.W. 1786/20	823-1	Table 4-21	Fig. 4-5	
U.W. 1786/21	823-3	Table 4-22	Fig. 4-1	